

# **The role of SDCCAG3 in Apoptosis & Ciliogenesis**



The  
University  
Of  
Sheffield.

By:

**Shruti Sharma**

A thesis submitted in partial fulfilment of the requirements for the  
degree of

Doctor of Philosophy

The University of Sheffield

Faculty of Science

Department of Biomedical Science

**September 2016**

## Abstract

Serologically defined colon cancer antigen-3 (SDCCAG3) is a coiled-coil domain containing protein that has been implicated in various cellular processes such as endosomal sorting, vesicular trafficking, and cytokinesis. The current study has identified two novel roles of SDCCAG3 i.e. regulation of Fas mediated apoptosis and ciliogenesis.

This study demonstrates that SDCCAG3 is involved in post-endocytic sorting of Fas receptors (a type I transmembrane receptor involved in apoptotic signalling). Depletion of SDCCAG3 by RNA interference led to a delay in transitioning of internalized Fas receptors from early to late endosomes/lysosomes, which resulted in an increased surface population of Fas receptors and consequently increased apoptotic signalling. Further in depth analysis revealed a defect in the intraluminal vesicle sorting of Fas receptors in the absence of SDCCAG3. Dysbindin, a cytosolic protein known to link proteins with the ESCRT machinery, was found to be involved with SDCCAG3 in sorting of Fas receptors for lysosomal degradation. This study also proposes the plausible complex formation between SDCCAG3 and a known negative regulator of Fas receptors, PTPN13, at the early/sorting endosomes. In conclusion, this study identified a novel role of SDCCAG3 in negative regulation of apoptotic signalling.

Current research also defines a role of SDCCAG3 in ciliogenesis. Unpublished data from the Erdmann lab suggested a direct interaction between SDCCAG3 and intraflagellar transport protein-88 (IFT88), a central protein involved in ciliogenesis and ciliary trafficking (Yu, unpublished data). Similar to IFT88, SDCCAG3 was also found to localize at the basal body, regulate cilia formation and ciliary length in IMCD3 cells in this study. Additionally, depletion of SDCCAG3 affected localization of a transmembrane protein called Polycystin-2 and not Rab8 to cilia. Defects in Polycystin-2 trafficking to cilia have been linked to polycystic kidney disorder in numerous studies. Thus, this study establishes SDCCAG3 as a novel ciliary protein involved in ciliogenesis and trafficking.

## Acknowledgement

I would like to express my sincere gratitude to my supervisor Dr. Kai Erdmann for his unwavering support and guidance over the last few years. He knew exactly when and how to push me. His infectious enthusiasm and constructive criticism helped me immensely in carrying out this work successfully. Thank you for your critical opinions that have helped in revising and shaping this thesis.

I would also like to acknowledge the help and support of my advisors Professor Kathryn Ayscough and Dr. Louise Robson throughout my PhD. Special thanks to Dr. Andrew Peden for not only helping me with constructs, antibodies, reagents, protocols used in this study but also with his valuable comments and feedback on my work.

Sincere thanks to my colleague/collaborator in this study- Fangyan Yu for all her help and support in carrying out this work. Agnieszka and Zainab, I cannot thank you two enough for all your love, support, coffee, cake and pizzas in these last four years. I would like to acknowledge all the help and advice that I have received from all the people on the D-floor (Florey Building). Thank you guys!

Just like my life, this work also would not have been easy without my husband, Shrey. I would like to acknowledge his contribution towards the analysis of intraluminal sorting of receptors. He wrote the MS excel VBA code for calculating the middle fluorescence intensity in the intraluminal vesicles (appendix I).

Finally, I want to thank my family, particularly my parents, for supporting me emotionally, financially and giving me an opportunity to fulfil my ambitions. I am grateful to my wonderful parents-in-law for their constant love and support throughout my PhD.

Thank you very much, everyone!

## **Declaration**

I declare that the work presented in this thesis is my own composition and has been carried out by myself unless otherwise stated. I confirm that this work was done while in candidature for a research degree at The University of Sheffield. None of this work has been published before submission.

Figures and consulted work from other publishers have been clearly acknowledged. Where I have quoted from the work of others, the source is always given. I have acknowledged all main sources of help.

Where the thesis is based on work done by others, I have described it clearly in the introduction sections and did not present it as my results. Where the work was done in collaboration, I have acknowledged clearly exactly what was done by others and what I have contributed myself.

Shruti Sharma

September 2016

# Table of Contents

<b>List of figures</b> .....	- 3 -
<b>Abbreviation</b> .....	- 6 -
<b>1 Introduction</b> .....	- 8 -
1.1 Intracellular trafficking.....	- 8 -
1.1.1 Trafficking pathways of cell surface receptors .....	- 9 -
1.1.2 Endosomal sorting of cell surface receptors .....	- 12 -
1.1.3 Transport of surface receptors to MVB/Lysosome .....	- 17 -
1.1.4 Endosomal sorting defects in human diseases .....	- 20 -
1.2 Programmed cell death or Apoptosis .....	- 21 -
1.2.1 Death Receptors .....	- 22 -
1.2.2 Fas receptor mediated apoptosis .....	- 23 -
1.2.3 Types of apoptotic signalling .....	- 27 -
1.2.4 Caspase.....	- 28 -
1.2.5 Apoptotic signalling in cancer progression.....	- 30 -
1.3 Regulation of apoptosis by PTPN13 .....	- 30 -
1.3.1 Protein tyrosine phosphatase, non-receptor type-13 .....	- 30 -
1.3.2 Negative regulation of apoptotic signalling by PTPN13 .....	- 31 -
1.4 SDCCAG3.....	- 34 -
1.4.1 SDCCAG3 interacts with PTPN13 .....	- 34 -
1.4.2 SDCCAG3 in endocytic trafficking .....	- 35 -
1.5 Trafficking in the primary cilium .....	- 36 -
1.5.1 The structure of cilia .....	- 36 -
1.5.2 Ciliary trafficking pathways.....	- 38 -
1.5.3 Trafficking defects in ciliopathies.....	- 39 -
<b>AIMS</b> .....	- 41 -
<b>2 Materials and Methods</b> .....	- 42 -
2.1 Materials .....	- 42 -
2.1.1 Chemicals and reagents.....	- 42 -
2.1.2 Commercial Kits .....	- 43 -
2.1.3 Primary Antibodies .....	- 43 -
2.1.4 Secondary Antibodies .....	- 44 -
2.1.5 Biological Material.....	- 45 -
2.1.6 Buffers and Solutions.....	- 45 -
2.1.7 Primers .....	- 46 -
2.1.8 siRNA.....	- 46 -
2.1.9 Constructs.....	- 47 -
2.2 Methods .....	- 47 -
2.2.1 Bacteria procedures .....	- 47 -
2.2.2 Mammalian Cell Culture.....	- 48 -
	- 0 -

2.2.3	DNA manipulation .....	- 48 -
2.2.4	Polymerase Chain reaction.....	- 50 -
2.2.5	Protein Methods .....	- 53 -
2.2.6	Flow cytometry .....	- 55 -
2.2.7	Immunocytochemistry.....	- 56 -
2.2.8	Statistical analysis .....	- 56 -
2.2.9	Assays .....	- 56 -
<b>3</b>	<b>Role of SDCCAG3 in Fas receptor trafficking .....</b>	<b>- 61 -</b>
3.1	Introduction .....	- 61 -
3.2	Aim.....	- 61 -
3.3	Results .....	- 62 -
3.3.1	Knockdown of SDCCAG3 increased cell surface levels of FasR ..	- 62 -
3.3.2	SDCCAG3 KD did not affect the transcriptional activity of FasR .	- 74 -
3.3.3	SDCCAG3 KD did not alter the rate of internalization of FasR ....	- 77 -
3.3.4	Effect on the basal level of overexpressed Fas receptors upon SDCCAG3 knockdown.....	- 79 -
3.3.5	SDCCAG3 co-localizes with internalized Fas receptors and sorts them into Late Endosomes/Lysosomes.....	- 82 -
<b>4</b>	<b>Molecular mechanism of FasR sorting by SDCCAG3 .....</b>	<b>- 90 -</b>
4.1	Introduction .....	- 90 -
4.2	Aim.....	- 90 -
4.3	Results .....	- 91 -
4.3.1	Depletion of SDCCAG3 delays sorting of Fas receptors into ILVs-	91 -
4.3.2	Molecular machineries involved in sorting Fas receptors.....	- 103 -
<b>5</b>	<b>Role of SDCCAG3 in apoptotic signalling.....</b>	<b>- 112 -</b>
5.1	Introduction .....	- 112 -
5.2	Aim.....	- 114 -
5.3	Results .....	- 115 -
5.3.1	Depletion of SDCCAG3 increases the rate of caspase 8 cleavage-	115 -
5.3.2	SDCCAG3 is cleaved upon activation of Fas mediated apoptosis-	116 -
5.4	Analysis of PTPN13 localization with Fas receptors .....	- 119 -
5.4.1	PTPN13 co-localized with internalized Fas receptors .....	- 119 -
5.4.2	PTPN13 and Fas receptors co-localize in the early endosomes....	- 120 -
<b>6</b>	<b>Discussion .....</b>	<b>- 122 -</b>
6.1	SDCCAG3 regulates post-endocytic trafficking of FasR .....	- 122 -
6.2	SDCCAG3 co-localizes with FasR in early endosomes and regulates their sorting towards late endosome/lysosome .....	- 125 -
6.3	SDCCAG3 mediates endosome-to-lysosome sorting of Fas receptors via Dysbindin-HRS axis.....	- 128 -
6.4	SDCCAG3 is a novel negative regulator of Fas mediated apoptosis...	- 131 -
6.5	Does SDCCAG3 form a complex with PTPN13 to regulate trafficking of Fas receptors and apoptotic signalling?.....	- 133 -
6.6	Proposed model for SDCCAG3 mediated regulation of apoptosis.....	- 134 -

<b>7</b>	<b>SDCCAG3 in ciliogenesis</b> .....	- 136 -
7.1	Introduction .....	- 136 -
7.2	Aim .....	- 137 -
7.3	Results .....	- 138 -
7.3.1	Localization of transiently expressed SDCCAG3 in cilia.....	- 138 -
7.3.2	SDCCAG3 localization to centrosome is not dependent on IFT88.....	- 140 -
7.3.3	SDCCAG3 depletion impairs ciliogenesis.....	- 141 -
7.3.4	Rescue of ciliogenesis defect upon SDCCAG3 re-expression .....	- 142 -
7.3.5	SDCCAG3 and IFT88 function in the same pathway.....	- 144 -
7.3.6	Depletion of SDCCAG3 impairs trafficking of Polycystin-2 .....	- 145 -
7.3.7	Rescue of Polycystin-2 trafficking with EGFP-SDCCAG3 .....	- 147 -
7.3.8	Depletion of SDCAAG3 does not alter Rab8 trafficking to cilia .	- 148 -
<b>7.4</b>	<b>Discussion</b> .....	- 150 -
7.4.1	SDCCAG3 localizes to cilia .....	- 150 -
7.4.2	Regulation of cilia formation and length by SDCCAG3 .....	- 150 -
7.4.3	SDCCAG3 regulates trafficking of ciliary cargo.....	- 152 -
7.5	SDCCAG3 at the crossroads .....	- 153 -
7.5.1	Cell cycle and ciliogenesis .....	- 153 -
7.5.2	Endocytic trafficking and ciliogenesis .....	- 153 -
7.5.3	Ciliogenesis and Apoptosis .....	- 154 -
<b>8</b>	<b>Summary and future perspectives</b> .....	- 155 -
8.1	Overview of the role of SDCCAG3 in FasR trafficking and apoptosis-	155 -
8.2	SDCCAG3 and PTPN13 in apoptosis: future perspectives.....	- 156 -
8.3	Overview of the role of SDCCAG3 in ciliogenesis .....	- 157 -
8.4	Concluding remarks .....	- 157 -
<b>Appendix I</b> .....		- 159 -
<b>Bibliography</b> .....		- 161 -

## List of figures

<b>Figure 1.1:</b> The exocytic pathways.....	-10-
<b>Figure 1.2:</b> The endocytic pathways.....	-11-
<b>Figure 1.3:</b> Illustrative presentation of proposed tubular endosomal network (TEN).....	-14-
<b>Figure 1.4:</b> Proposed model for intraluminal vesicle formation by ESCRT complexes.....	-19-
<b>Figure 1.5:</b> Schematic representation of death receptors.....	-23-
<b>Figure 1.6:</b> Modular structure of Fas receptor.....	-24-
<b>Figure 1.7:</b> In silico modelling of FasR-FasL complex.....	-26-
<b>Figure 1.8:</b> Proposed model for FasR compartmentalization and signalling.....	-27-
<b>Figure 1.9:</b> Modular structure of PTPN13.....	-31-
<b>Figure 1.10:</b> Proposed model of regulation of apoptosis by PTPN13.....	-33-
<b>Figure 1.11:</b> Modular structure of serologically defined colon cancer antigen....	-34-
<b>Figure 1.12:</b> The structure of cilia.....	-37-
<b>Figure 1.13:</b> Polarized vesicle trafficking during ciliogenesis.....	-38-
<b>Figure 1.14:</b> Modes of trafficking defects in ciliopathies.....	-40-
<b>Figure 2.1:</b> Calculation of $\Delta\text{act}$ value.....	-52-
<b>Figure 3.1:</b> Immunofluorescence analysis of antibodies against Fas receptors in HeLa cells.....	-63-
<b>Figure 3.2:</b> Microscopic analysis of FasR surface levels upon SDCCAG3 knockdown in HeLa cells.....	-64-
<b>Figure 3.3:</b> Validation of Fas antibodies for Flow cytometry.....	-65-
<b>Figure 3.4:</b> Immunoblot analysis of the knockdown efficiency of SDCCAG3....	-66-
<b>Figure 3.5:</b> Flow cytometry analysis of FasR cell surface levels.....	-67-
<b>Figure 3.6:</b> Optimization of cell surface biotinylation.....	-68-
<b>Figure 3.7:</b> Validation of anti-Fas C-20 antibody for immunoblotting.....	-69-
<b>Figure 3.8:</b> Analysis of FasR levels by cell surface biotinylation upon SDCCAG3 knockdown.....	-70-
<b>Figure 3.9:</b> Rescue of cell surface levels of FasR upon SDCCAG3 knockdown...-	-72-
<b>Figure 3.10:</b> Analysis of FasR levels upon SDCCAG3 knockdown in HCT116 cells.....	-73-
<b>Figure 3.11:</b> Flow cytometry analysis for Fas receptor levels in HCT116.....	-74-
<b>Figure 3.12:</b> Analysis of mRNA levels of <i>Fas</i> upon SDCCAG3 depletion.....	-75-
<b>Figure 3.13:</b> Optimization of qRT-PCR.....	-76-
<b>Figure 3.14:</b> Relative mRNA levels of <i>Fas</i> receptors by qRT-PCR.....	-77-
<b>Figure 3.15:</b> Flow cytometry analysis of the rate of trafficking of Fas receptors...-	-78-
<b>Figure 3.16:</b> Trafficking of FasR upon stimulation with a non-agonistic antibody.....	-79-
<b>Figure 3.17:</b> The modular structure of Fas receptor construct.....	-79-

<b>Figure 3.18:</b> Surface expression of EGFP-SDCCAG3.....	-80-
<b>Figure 3.19:</b> Effect of SDCCAG3 depletion on basal levels of EGFP-SDCCAG3.....	-81-
<b>Figure 3.20:</b> Rate of degradation of EGFP-SDCCAG3.....	-82-
<b>Figure 3.21:</b> Analysis of co-localization between internalized FasR and SDCCAG3.....	-83-
<b>Figure 3.22:</b> Quantification of co-localization between internalized FasR and SDCCAG3.....	-84-
<b>Figure 3.23:</b> Subcellular localization of internalized FasR and SDCCAG3 in early endosomes.....	-85-
<b>Figure 3.24:</b> Effect of SDCCAG3 depletion on subcellular localization of internalized FasR upon stimulation.....	-87-
<b>Figure 3.25:</b> Effect of SDCCAG3 depletion on subcellular localization of internalized FasR at steady-state.....	-89-
<b>Figure 4.1:</b> The enlarged endosomes.....	-91-
<b>Figure 4.2:</b> Intraluminal vesicle sorting of internalized FasR upon stimulation....	-93-
<b>Figure 4.3:</b> Structured illumination microscopic analysis of ILV sorting of stimulated FasR.....	-95-
<b>Figure 4.4:</b> Intraluminal sorting of FasR at steady state after after 4 hours of uptake.....	-97-
<b>Figure 4.5:</b> Intraluminal sorting of FasR at steady state after after 4 hours of uptake.....	-98-
<b>Figure 4.6:</b> Intraluminal vesicle sorting of Transferrin receptors.....	-100-
<b>Figure 4.7:</b> Intraluminal vesicle sorting of EGF receptors.....	-102-
<b>Figure 4.8:</b> Immunoblot analysis of interaction between SDCCAG3 and Dysbindin.....	-103-
<b>Figure 4.9:</b> Localization of SDCCAG3 on the limiting membrane of the enlarged endosomes.....	-104-
<b>Figure 4.10:</b> Immunofluorescence analysis of dysbindin, HRS and SDCCAG3 localization on the limiting membrane of the enlarged endosomes.....	-106-
<b>Figure 4.11:</b> Flow cytometry analysis of surface levels of FasR upon depletion of dysbindin, HRS and SDCCAG3.....	-108-
<b>Figure 4.12:</b> Intraluminal sorting of stimulated FasR upon depletion of dysbindin and HRS.....	-110-
<b>Figure 5.1:</b> Cell viability analysis of HeLa cells.....	-112-
<b>Figure 5.2:</b> SDCCAG3 is cleaved upon activation of FasR.....	-114-
<b>Figure 5.3:</b> Immunoblot analysis of Caspase 8 in HeLa cells.....	-115-
<b>Figure 5.4:</b> Immunoblot analysis of caspase 8 cleavage in HCT116.....	-116-
<b>Figure 5.5:</b> Coomassie blue staining of recombinant SDCCAG3.....	-117-
<b>Figure 5.6:</b> SDCCAG3 is a substrate of caspase 6.....	-118-
<b>Figure 5.7:</b> Analysis of cleavage pattern of SDCCAG3.....	-119-
<b>Figure 5.8:</b> PTPN13 co-localizes with internalized FasR.....	-120-

<b>Figure 5.9:</b> PTPN13 localizes with internalized FasR in early/sorting endosomes.....	-121-
<b>Figure 6.1:</b> Predicted model for SDCCAG3 mediated sorting of FasR .....	-130-
<b>Figure 6.2:</b> Hypothetical model of regulation of apoptotic signalling by SDCCAG3.....	-135-
<b>Figure 7.1:</b> SDCCAG3 interacts with intraflagellar transport protein-88.....	-136-
<b>Figure 7.2:</b> Localization of transient EGFP-SDCCAG3 expression constructs in IMCD3 cells.....	-139-
<b>Figure 7.3:</b> SDCCAG3 is recruited to centrosomes independently of IFT88.....	-140-
<b>Figure 7.4:</b> Depletion of SDCCAG3 impairs ciliogenesis.....	-141-
<b>Figure 7.5:</b> Depletion of SDCCAG3 decreases length of cilia.....	-142-
<b>Figure 7.6:</b> Rescue of ciliogenesis defect by transient expression of SDCCAG3.....	-143-
<b>Figure 7.7:</b> Rescue of cilia length upon expression of EGFP-SDCCAG3.....	-144-
<b>Figure 7.8:</b> SDCCAG3 coordinate with IFT88 in the same pathway.....	-145-
<b>Figure 7.9:</b> Depletion of SDCCAG3 disrupts trafficking of Polycystin-2.....	-146-
<b>Figure 7.10:</b> Rescue of trafficking defects in Polycystin-2 to cilia.....	-147-
<b>Figure 7.11:</b> SDCCAG3 does not regulate trafficking of Rab8 to cilia.....	-149-

## Abbreviation

**AICD**- Activation induced cell death  
**BLOC-1**-Biogenesis of lysosome-related organelle complex-1  
**CCVs**- Clathrin coated vesicles  
**CIE**- Clathrin independent endocytosis  
**CME**- Clathrin mediated endocytosis  
**CRD**- Cysteine rich domain  
**DED**- Death effector domain  
**DMEM**- Dulbecco's Modified Eagle Medium  
**DISC**- Death inducing signalling complex  
**DR**- Death receptors  
**ECD**- Extracellular domain  
**E.coli**- *Escherichia coli*  
**EE**- Early endosomes  
**EEA-1**- Early endosome antigen-1  
**ERC**- Endocytic recycling compartment  
**ESCRT**- Endosomal sorting complex required for transport  
**g**- grams  
**FADD**- Fas associated death domain  
**HRS**- Hepatocyte growth factor regulated tyrosine kinase substrate  
**IC**- Intermediate compartment  
**IFT**- Intraflagellar transport  
**ILV**-Intraluminal vesicle  
**LE**- Late endosome  
**LAMP-1**- Lysosomal associated membrane protein-1  
**MOTC**- Microtubule organizing centre  
**MOMP**-Mitochondrial outer membrane permeabilisation  
**MAPK**- Mitogen activated protein kinases  
**PLAD**- Pre-ligand binding assembly domain  
**PTPN13**- Protein tyrosine phosphatase, non-receptor type 13  
**PTM**- Post translational modifications  
**SE**- Sorting Endosomes

**SDCCAG3**- Serologically defined colon cancer antigen-3  
**SPOTS**- Signalling protein oligomerization transduction structures  
**STAM**- Signal-transducing adaptor molecule  
**TRADD**- TNFRSF1A associated via death domain  
**TNFRSF**-Tumour necrosis factor receptor superfamily  
**TRAILR1**- TNF related apoptosis inducing ligand receptor-1  
**TEN**- Tubular endosomal network  
**TGN**- Trans Golgi network  
**UIM**- Ubiquitin interaction motif  
**VHS**-Vps27, HRS, STAM  
**μ**- micro (prefix)

# **1 Introduction**

## **1.1 Intracellular trafficking**

All cells are enclosed in a membrane which isolates the inside of a cell from its surroundings, therefore creating a barrier that needs to be overcome for communication. Cells need to communicate with each other and their environment to carry out various physiological processes for growth and survival. They communicate through cell surface receptors which are present on the surface and bind with extracellular signalling molecules to induce signal transduction. For instance, growth factors and stem cells factors bind to receptor tyrosine kinases (RTKs) that span the plasma membrane and undergo conformational changes to activate downstream signalling cascade upon ligand binding. This RTK-Ras signalling cascade is crucial for various developmental processes, such as regulation of cell proliferation, differentiation, and promotion of cell survival [1]. Similarly, another signalling receptor called prolactin receptor (PRLR) is present on the surface of mammary gland cells and binds to prolactin and growth hormone (GH) to initiate JAK/STAT signalling pathway for upregulating casein gene for milk production [2]. Integrins are also well studied receptors that have been implicated in bi-directional signalling between cell, and extra-cellular matrix for cell growth, division, and differentiation. Hence, surface representation of transmembrane receptors is an obvious prerequisite for the cell to carry out their normal functions.

Receptors are transported to the surface via vesicular transport in which proteins are synthesised in the cytosol and packed into secretory vesicles to fuse with the plasma membrane. Upon ligand activation, these receptors are internalized from the cell environment and travel inside via various endocytic pathways. The two types of major intracellular trafficking pathways (exocytosis and endocytosis) operate continuously to support cellular survival and homeostasis. The fate of cell surface receptors upon internalization and deregulation of endocytosis in human diseases has been discussed in detail later in this section.

### 1.1.1 Trafficking pathways of cell surface receptors

Primary pathways involved in shuttling surface receptors in and out of the cell are exocytic and endocytic pathways. The exocytic pathway exports surface receptors from the endoplasmic reticulum (ER) through Golgi to the plasma membrane (PM) or from endosomes to PM. In the ER and Golgi, many surface receptors undergo post-translational modifications by the addition of sugar and lipid moieties and are packed into vesicles formed at the *trans*-Golgi which later fuse with the PM. Hence, two important steps in this pathway are ER-to-cis Golgi and *trans*-Golgi-to-PM. The characteristics of the vesicles involved in these two types of routes vary. ER-to-cis Golgi transition occurs via intermediate compartment (IC) which is packed with vesicles and tubules. This transition is highly regulated as multiple pieces of evidence suggest that surface receptors undergo a ‘quality check’ before exiting ER [3]. During intra-Golgi transport, receptors packed in vesicles are passed through the three Golgi cisternae by moving the vesicles forward and resident proteins backwards between the Golgi cisternae[4]. However, two other types of models have also been proposed to explain the intra-Golgi transport-‘The cisternal maturation’ model and ‘The Rapid partitioning’ model. The first model suggests that cisternae, packed with surface receptors, mature by fusing with retrograde vesicles arising from older cisternae. In the rapid partitioning model, Golgi enzymes are distributed differentially throughout the cisternae and the cargo moves at an exponential rate proportional to their total abundance in the Golgi[4]. After passing through Golgi, cargo proteins are sorted to recycling endosomes or plasma membrane in a network of tubular structures derived from *trans*-Golgi cisternae, known as the *trans*-Golgi network (TGN). In polarized epithelial cells, different types of sorting signals have been characterized for apical (like *O*- and *N*-glycosylation) and basolateral sorting (like tyrosine based motifs- NPXY or YXX $\phi$  and di-leucine motifs- [DE]XXXL[LI] or DXXLL). These signals are recognized by coat adaptors like AP1 and AP3, and GGAs that help in TGN to PM transport by recruiting clathrin on cargo laden tubular domains of TGN[5, 6].

In the endocytic pathway, cell surface receptors are internalized from the plasma membrane by either clathrin dependent or independent routes (like caveolae or raft mediated) into early endosomes where they are sorted further into recycling or late

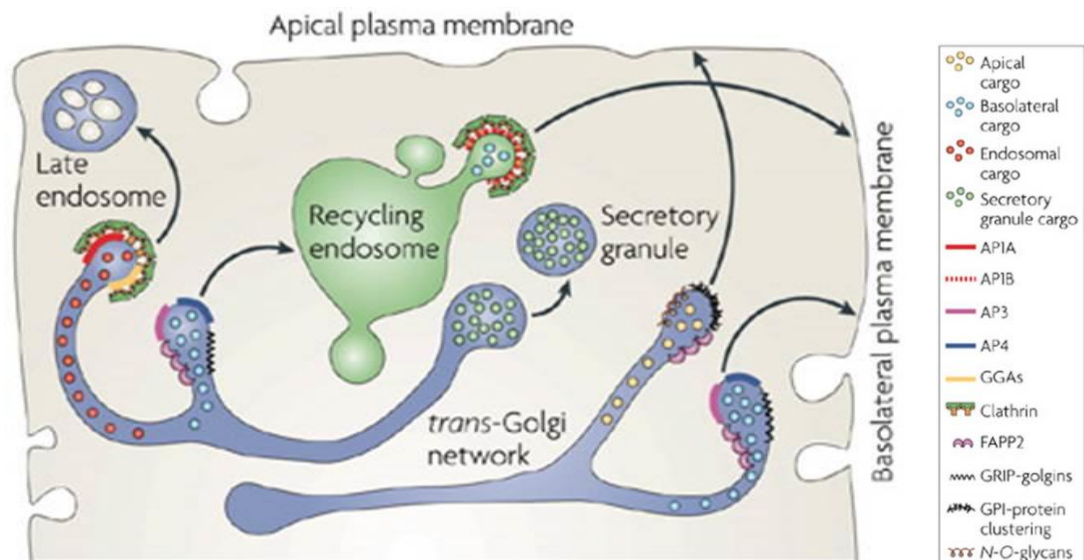


**Figure 1.1: The exocytic pathways.** They are involved in the transport of surface receptors from endosomes or biosynthetic machinery to the plasma membrane. The *trans*-Golgi network originates from *cis*-Golgi cisternae and consists of tubular networks that sort cargo to different destinations like plasma membrane, recycling endosomes or late endosomes. Surface receptors that are newly synthesised or have been transported from the endosomes to TGN are returned to the plasma membrane unless destined for lysosomal degradation via exocytic pathways. In a polarized epithelial cell, different sorting mechanisms operate based on specific signals for apical (e.g. glycosyl phosphatidylinositol (GPI)-anchored proteins) or basolateral targeting of surface receptors. Clathrin coated vesicles are generated from the tubular structures of TGN involving different types of adaptor proteins. AP1A and GGAs recognise signals for late endosomal trafficking while AP1B, AP3, and AP4 have been implicated in basolateral trafficking of some receptors. (Figure adopted from De Matteis and Luini, 2008 [6]).

endosomes. Cargo destined for degradation is transferred to the lysosome which is the primary degradation site for internalized proteins. Clathrin mediated endocytosis (CME) is the most common route for internalizing most of the signalling family receptors such as RTKs like epidermal growth factor receptors (EGFR) and GPCRs like  $\beta$ 2-androgenic receptors ( $\beta$ 2AR). However, some GPCRs, RTKs and other receptors like TGF $\beta$ , Wnt and Notch also undergo clathrin independent endocytosis (CIE) [7]. Receptors undergoing CME can be recruited directly into clathrin coated pits via adaptor proteins like AP2 that interacts with tyrosine and di-leucine motifs in the cytoplasmic domains of some receptors [8]. Maturing clathrin coated pits at the plasma membrane are budded into vesicles, called clathrin coated vesicles (CCVs) by the action of a mechanochemical enzyme, dynamin which is recruited by curvature sensing-BAR domain containing proteins like amphiphysin, endophilin,

and sorting nexin 9 (SNX9) [9]. Following scission, CCVs are transported into the cytoplasm where the vesicles are uncoated and fused with early endosomes. Subsequently, signalling of ligand bound activated receptors is either sustained or attenuated inside the endosomes.

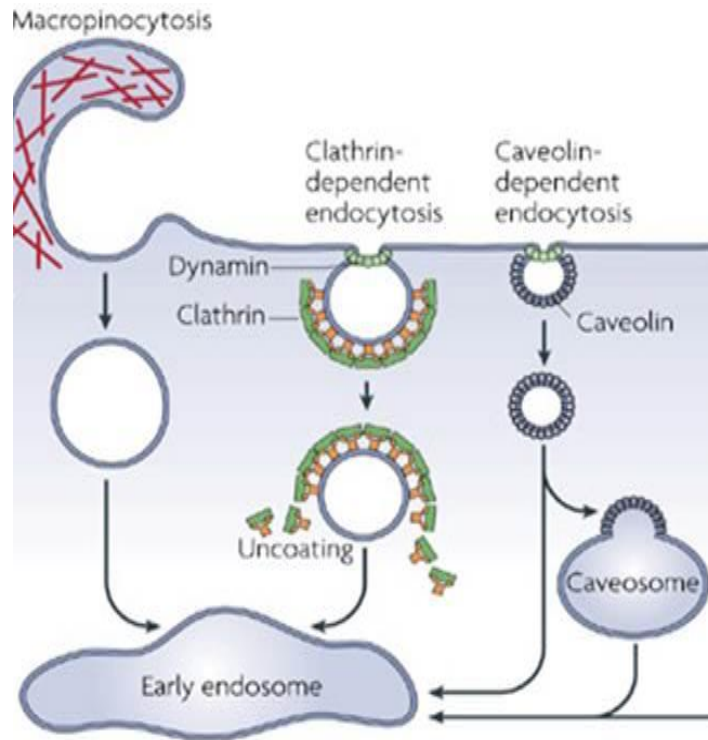


**Figure 1.2: The endocytic pathway** consists of various routes for entry of cargo like fluid phase uptake by micropinocytosis, clathrin dependent, and independent pathways. Most of the signalling receptors are known to internalize by clathrin mediated endocytosis while some receptors internalize via clathrin independent but dynamin dependent pathway using caveolins. All these routes lead to internalization of surface receptors into early endosomes. (Figure adopted from McMahon and Boucrot, 2011) [9].

Receptor mediated internalization is an important mechanism to terminate signalling mediated by the ligand bound receptors. Endocytosis of activated receptors can affect the strength and duration of signalling by physically eliminating or limiting the number of receptors available to the ligand at the surface. For instance, endocytosis of EGFR inhibits PLC $\gamma$ 1 and phosphoinositide 3-kinase (PI3K) signalling due to the absence of their lipid substrate, PtdIns(4,5)P<sub>2</sub> in endosomes [10]. However, numerous studies also support endosomal signalling largely categorized into two groups: signalling that occurs exclusively in endosomes, for which receptor mediated endocytosis is imperative and signalling that occurs both in endosomes and at the plasma membrane [7]. EGFR, for example, remain in their

ligand bound, active (phosphorylated) state until late stages of endocytosis as demonstrated by the presence of downstream RTK signalling components in the endosomes allowing continuous signalling of internalized EGFR [11]. It was also shown that in some cases complete activation of ERK1 and ERK2 required endocytosis because of the availability of MAPK scaffold complex, MEK partner-1 (MP1)-p14 complex, which is docked to the endosomal membrane via p18 adaptor protein and aids in phosphorylating ERK1 [12]. EGFR are also known to act through specialized signalling endosomes that are decorated with Rab5 and its two adaptors, APPL1 and 2 [7].

Following endocytosis, sorting of activated receptors back to the plasma membrane can reinitiate the signalling or delivery to the lysosomes can terminate the signalling process. Thus, post-endocytic sorting is another crucial event that decides the fate of receptors and their signalling process.

### **1.1.2 Endosomal sorting of cell surface receptors**

Within minutes of internalization, sorting of cargo in early endosomes is initialized. Early endosomes are highly dynamic, undergo homotypic fusion and are composed of complex pleomorphic structures containing both large vesicles and thin tubular extensions [13]. The limiting membrane of EE contains many subdomains that are not only structurally but also functionally distinct owing to different proteins residing on these subdomains. One of the most crucial residents of early endosomes is Rab 5 which is generated in its active GTP-bound form by Rabex-5. Rab5 recruits numerous effectors on the early endosomes that carry out various functions. PtdIns(3) kinase/hVPS34 is amongst the earliest set of effectors of Rab5 at EE which is required for generation of PtdIns(3)P, the most abundant phosphoinositide in the EE membrane. PtdIns(3)P imparts compartment identity to the EE and help in recruiting other Rab 5 effectors such as early endosomal antigen-1 (EEA-1) and sorting nexins (SNXs) [13]. The fusion events are mediated by a specialised set of membrane proteins called SNAREs (soluble N-ethylmaleimide-sensitive factor attachment protein receptors) such as syntaxin6 and syntaxin13, vit1a and VAMP4 that constitute the core machinery for EE fusion [14]. EEA-1 directly interacts with

syntaxin6 and syntaxin13 and localizes them to EE [15, 16]. Newly formed endosomes laden with cargo, fuse with one another and with pre-existing sorting endosomes which are vesicular structures with a pH of ~6.0 in their lumen. The endosome maturation model suggests that sorting endosomes accept incoming endosomes for only some time before translocating along the microtubules from the cell periphery towards the microtubule organizing centre (MOTC) [17]. Subsequently, their lumens become more acidic which leads to uncoupling of the ligands from their respective receptors. Therefore, endocytic sorting is initiated in the maturing sorting endosomes where surface receptors destined for recycling are segregated into tubular membranes that are pinched off and fused either with endocytic recycling compartments (ERC) or delivered directly to the plasma membrane. In contrast, surface receptors that contain lysosomal targeting information are separated out and delivered to late endosomes/lysosomes or remain in the EE which mature into lysosomes (according to the endosomal maturation model). In fact, there is now a growing appreciation of the notion that early and late endosomes are just stages of a continuum representing distinct membrane domains of an evolving sorting endosome also referred to as tubular endosomal network (TEN) [18]. This view supports the following ideas- firstly, endocytic recycling compartment (ERC) is not a separate compartment but rather a subdomain of TEN. Secondly, TEN represents a hub where many sorting machineries associate on different subdomains to sort cargo from endosome to TGN, lysosomes or PM.

**Sorting for recycling**-Surface receptors such as transferrin are sorted at EE to the plasma membrane via two major recycling pathways-‘fast’ and ‘slow’ [19]. The process of endosomal sorting for recycling has been described as the “geometry-based sorting” where membranes containing receptors like transferrin are pinched off from narrow tubular structures since the surface-area-to-volume ratio of tubules is larger than that of vesicular part of the sorting endosomes [19]. It has been described rather as a pre-sorting step where receptors destined for recycling are delivered directly to the plasma membrane. Multiple evidence show that upon internalization, transferrin is enriched more in static early endosomes which are only Rab5 positive rather than dynamic early endosomes that are both Rab5/Rab7 positive and hosts other receptors like EGFR [20]. Many GTPase regulators have been implicated in

directing transferrin towards recycling compartments like Rab4 by supporting tubular formations. Alternatively, transferrin can be trafficked to slow endocytic recycling compartment (ERC) in Rab4/Rab11 dependent manner [13, 21].

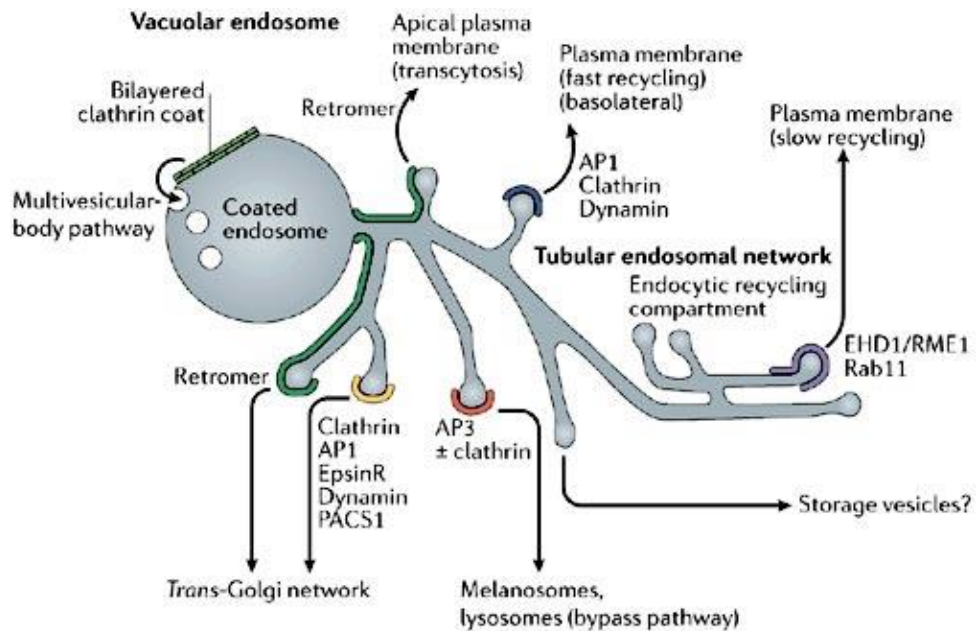


**Figure 1.3 Illustrative presentation of proposed tubular endosomal network (TEN)** consisting of a vacuolar region connected to dense tubular endosomes. The vacuolar region is coated with ‘bilayered’ clathrin coats and Hrs to recruit ESCRT machinery for sorting out cargo into the degradative pathway. Vacuolar endosome subsequently mature into late endosomes. The tubular network has specific subdomains occupied by different sorting devices such as retromer for TGN trafficking or direct recycling to apical membrane in polarized cells. Clathrin and its associated proteins like AP1 and dynamin are also involved in transport to TGN and fast recycling to the plasma membrane (basolateral) in polarized cells. A slow recycling route has been shown to be regulated by RME-1/EHD1 complex along with Rab11. AP3 has also been implicated in the transport of cargo vesicles to lysosomes or to melanosomes in pigmented cells. Other proteins like phosphofurin acidic-cluster-sorting protein-1 (PACS-1) and EpsinR are involved in retrograde transport to TGN [18].

A study also suggested that effectors of Rab4 such as Rabaptin-5/Rabex-5 bind to  $\gamma$ 1-adaptin subunit of AP1 and prevent the association of clathrin with it in order to prevent budding of vesicles from the endosomes thereby promoting transport of transferrin to ERC compartments [22]. An associate of Rabaptin-5/Rabex-5 complex, Rabenosyn-5, could potentially act as a linker between Rab4 complex and

Eps15 homology domain (EHD1) on ERC membranes as depletion of Rabenosyn-5 led to the accumulation of transferrin in an EEA-1 positive EE compartment [23]. Receptor mediated endocytosis/Eps15 homologue domain (RME-1/EHD) proteins family regulate recycling of transferrin from ERC compartments through actin regulators like Arf6 [24]. Other Rabs like Rab35, Rab22 and Rab8 have also been implicated in controlling transferrin recycling by various groups in different cell lines [25]. Another family of proteins that have been implicated in sorting is sorting nexins (SNX). Cullen and co-workers demonstrated that sorting nexin-4 (SNX4) regulates sorting of transferrin to recycling compartments since siRNA mediated depletion of SNX4 missorted transferrin receptors to lysosomal compartment. They hypothesized that SNX4 might mediate sorting via its association with kidney and brain expressed protein (KIBRA) that binds to dynein, a motor protein responsible for membrane tubulation [26].

**Retromer mediated sorting-** Retromer complex is an evolutionarily conserved unit that plays a vital role in the endosome-to-TGN retrieval of cargo. In higher eukaryotes, it consists of two main components- the cargo selective complex and membrane bending SNX-Bar dimer [27]. The cargo selective complex (CSC) is made up of Vps35, Vps26 and Vps29 proteins and the SNX component is made up of SNX1 or SNX2 and SNX5 or SNX6 in humans [18]. Cozier et al., demonstrated that SNX component is recruited to the endosomes by PtdIns(3)P that binds to the phox homology domain (PX) in all SNX proteins [28]. The CSC has been shown to be recruited to the endosomes by direct interaction of SNX3 and Rab7a with Vps35 [29]. The observation that SNX3 are known to present on early endosomes and Rab7a on late endosomes suggests that retromer is present in distinct microdomains of maturing/sorting endosomes that are positive for both SNX3 and Rab7a. Recent studies have also shown an association of WASH complex in retromer sorting complex by direct interaction between FAM21 (a WASH complex) and Vps35 [30, 31]. WASH complex is responsible for activation of Arp2/3, a nucleation promotion factor (NPF) that generates actin filaments on endosomes. Association of WASH complex gives mechanistic details into retromer mediated sorting as promotion of F-actin nucleation owing to WASH complex can explain segregation of endosomal domains and scission of endosomal domains by recruiting dynamin-2 [32]. Growing

number of evidence support the role of WASH complex in the recycling of receptors like EGFR in MEFs [33], glucose transporter-1 Glut-1 and CD28 in T-cells [34]. Inhibition of actin polymerisation by specific drugs resulted in defects in endosomal sorting and maturation [29]. A recent study elucidated the role of the SNX27-retromer-WASH complex that is responsible for sorting multiple receptors from the endosomes-to-cell surface. Silencing of Vps35 or SNX27 resulted in missorting of receptors into lysosomes for degradation [35]. Knockdown of WASH has also been shown to disrupt recycling of transferrin and integrin  $\alpha 5\beta 1$  receptors [36]. Therefore, retromer-WASH complex mediate sorting of receptors to both TGN and PM while WASH can mediate sorting of proteins into TGN, cell surface or lysosomes (discussed later).

**Sorting for degradation-** Surface receptors that are destined for lysosomal degradation contain distinct sorting signals like dileucine based [DE]XXXL[LI] peptide that aids in their rapid internalization and endo-lysosomal targeting e.g. CD4, GLUT4 etc [5]. A post-translational modification like ubiquitination is also a well-studied signal for receptor internalization and lysosomal sorting. Receptors can be subjected to diverse modes of ubiquitination such as monoubiquitination, multiple monoubiquitination, and polyubiquitination. The attachment of ubiquitin generally occurs in three sequential steps by ubiquitin activating (E1), ubiquitin conjugating (E2) and ubiquitin ligating (E3) enzymes. Their actions can be reversed by deubiquitinating enzymes (DUBs). Ubiquitin modifications are recognized by proteins containing ubiquitin-binding domains (UBDs) [37]. Some of these ubiquitin binding proteins reside at the limiting membranes of the sorting endosomes and participate in directing ubiquitinated surface receptors to the multivesicular bodies (MVBs). For example:

**HRS** (hepatocyte growth factor-regulated tyrosine kinase substrate) is an 115 kDa protein containing FYVE domain that interacts with phosphatidylinositol 3-phosphate [PtdIns3P] and aids in its recruitment to the endosomal membrane. HRS contains one double sided ubiquitin interaction motif (UIM) and one VHS (Vps27, HRS, and STAM) domain which help in recognizing the ubiquitinated cargo. It is a component of the endosomal sorting complex required for transport (ESCRT-0). Other members of ESCRT-0 complex like STAM (signal transducing adaptor

molecule) also contain a UIM and VHS domain for sorting [38]. Recent studies suggested a complex assembly that contains many UBDs collectively and mediates ILV sorting. A number of other proteins such as Esp15b contain two UIMs, forms a complex with HRS and STAM to mediate sorting of EGFR [39]. A Few studies have also reported ubiquitin independent sorting by HRS via hydrophobic amino acid cluster in interleukin-2 receptor  $\beta$  (IL-2R $\beta$ ) and interleukin-4 receptor  $\alpha$  (IL-4R $\alpha$ ) [40].

### **1.1.3 Transport of surface receptors to MVB/Lysosome**

In the sorting endosomes, most of the membrane material is recycled but as described above, the sorting of membrane proteins for degradation requires stringent selection. Endosomal sorting complex required for transport (ESCRT-0) initiates the multivesicular body (MVB) formation pathway. It is recruited by the cargo in the EE/sorting endosome, which further helps in recruiting flat clathrin coats on the endosomal membrane and helps in clustering specific cargo destined for degradation in the microdomains of the limiting membrane [41, 42]. Subsequently, ESCRT I and II complexes are also recruited at these microdomains that help in membrane deformation and budding to form intraluminal vesicles (ILVs). ESCRT I consists of proteins such as TSG101, Vps28, Vps37 and ubiquitin associated protein-1 (UBAP1) while ESCRT-II consists of Vps36, Vps22, and two Vps25 molecules. The membrane deforms into a bud and multiple pieces of evidence suggest that ESCRT I and II localize to the neck of this budding vesicle to stabilize it [38]. Once the bud is created, ESCRT III complex is recruited to carry out the membrane scission. The core subunits of ESCRT III consist of Vps20, Snf7, Vps24, and Vps2. It assembles transiently and recruits deubiquitination enzymes in order to recycle ubiquitin before sorting forming ILVs [41]. Several models have been proposed to understand how vesicles bud exactly into the endosomes. On the basis of the available data so far, it has been proposed that subunits of ESCRT III complex such as Vps20 and Snf7 are recruited and polymerized at the tip of the neck. It then recruits deubiquitinases such as AMSH (associated molecule with the SH3 domain of STAM) or USP8 (ubiquitin specific protease 8) for cargo deubiquitination. ESCRT III complex subunits coordinate to stabilize and constrict the neck of the vesicle in an energy driven

process which is provided by recruitment of type I AAA-ATPase Vps4 to release the vesicle from the limiting membrane. It also disassembles and recycles the ESCRT III complex after the vesicle is released [38, 41]. Formation of ILVs in vacuolar domains of the early endosomes containing transmembrane proteins destined for degradation gives rise to multi vesicular bodies (MVBs). According to the endosome maturation model, this vacuolar domain of EEs which is a Rab5/Rab7 hybrid separate out from the tubular endosomes by an unknown mechanism. This marks the beginning of a late endosome (LE) compartment. As the late endosome matures, it shifts to the perinuclear area, fuses with lysosomes, drops its pH and acquire lysosomal characteristics [17]. The presence of V-ATPases in the vacuolar domains of EEs enriches them in the newly formed LEs which results in an initial drop in the pH by 0.5 units in LEs [43]. Mature LEs have numerous ILVs (up to 30 or more depending on the cell type), pH ranges between 6.0-4.9 and their limiting membrane get enriched in lysosomal associated membrane protein-1 (LAMP-1) [44]. Later upon fusion with the lysosomes, the pH drops further to 4.5-5. Movement of mature LEs towards lysosomes in the perinuclear area is mediated by minus end directed, dynein-dependent motor [45].

In summary, this section described the basic pathways underpinning the transport of surface receptors which regulate their signalling and in turn determine cellular fate. Defects in these pathways or mutation in the components of trafficking pathways has been reported in several human diseases.

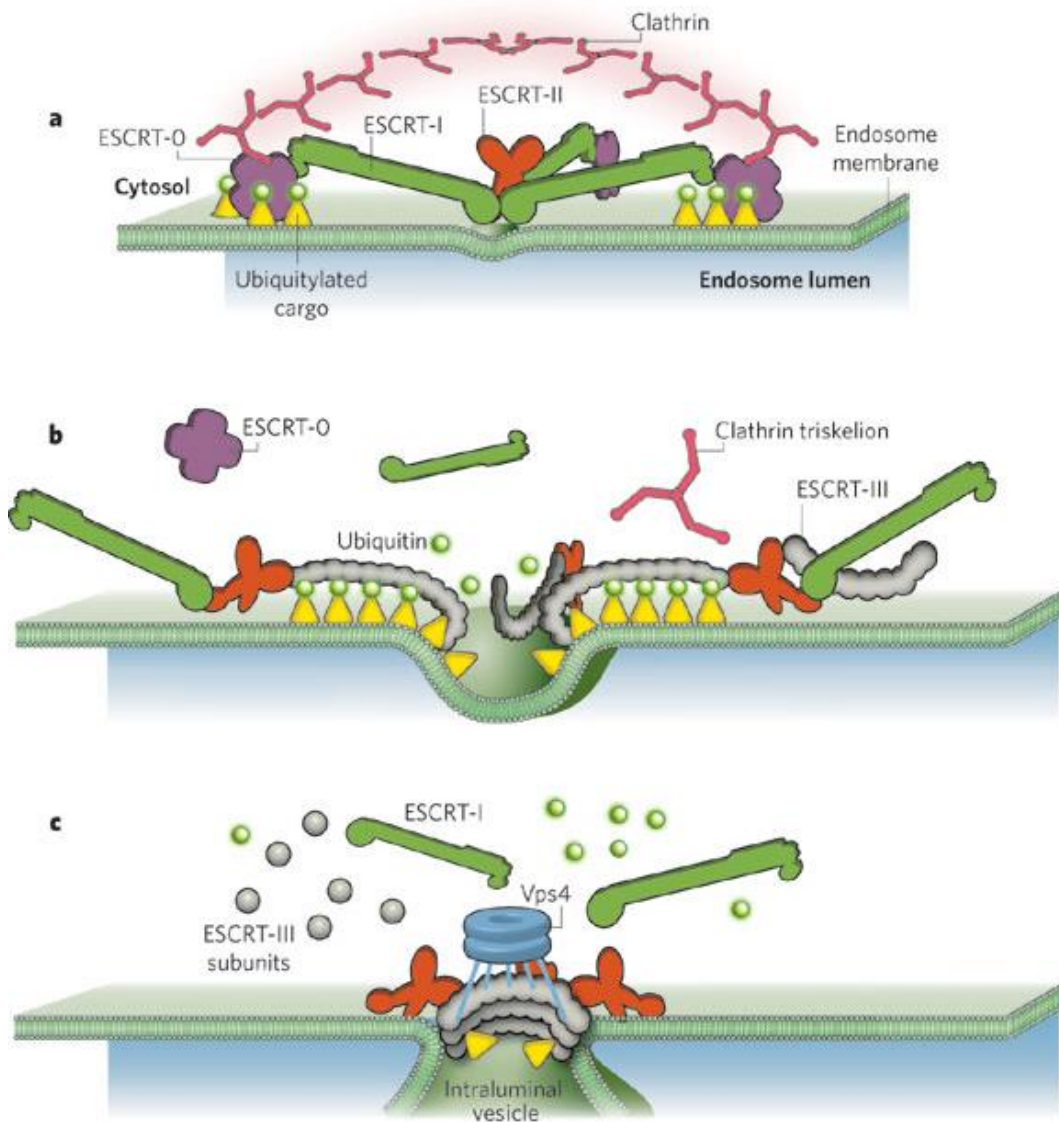


**Figure 1.4: Proposed model for intraluminal vesicle formation by ESCRT complexes.**

(a) Transmembrane proteins undergo post-translational modifications such as ubiquitination to mediate their sorting into ILVs. ESCRT-0 complex binds to the ubiquitinated cargo and to clathrin which further recruits ESCRT I and II into specialized microdomains of the endosomal membrane. (b) Next step is to deform the membrane to form an invagination into the endosome. ESCRT I and II have been shown to concentrate on the neck of the budding vesicle and initiate membrane deformation. They recruit ESCRT III complex that is formed transiently into spiral-shaped filaments to concentrate and stabilize cargo into the intraluminal vesicle. At this step, deubiquitinases are recruited by ESCRT III and ubiquitin is recycled back while the diffusion of cargo out of the vesicle is restricted by ESCRT III filaments. (c) Deformation is followed by membrane abscission. ESCRT III filaments continue to form the bud and subsequently, recruit Vps4 which helps in abscission of the neck and release of the intraluminal vesicle as well as disassembly of ESCRT III complex [41].

#### **1.1.4 Endosomal sorting defects in human diseases**

Both recycling and degradation of signalling receptors on the surface are tightly regulated to maintain cellular homeostasis. Defects in the sorting of surface receptors towards either of these pathways create an imbalance in signalling leading to diseases. As described before the retromer complex mediates sorting of several transmembrane receptors towards TGN and PM. Defects in retromer have been linked to growing number of neurodegenerative diseases [46]. For instance, haploinsufficiency of a retromer component called Vps35 in mice has been implicated in the defective sorting of amyloid precursor protein (APP) leading to its delay in endosome-to-TGN transition [47, 48]. Abnormal cleavage of APP is a well-known hallmark of Alzheimer's disease [49]. Another mutation in Vps35 gene, D620N, has been linked to Parkinson's disease [50]. A study by Cullen and co-workers demonstrated that this mutation in Vps35 resulted in decreased affinity for FAM21 and WASH complex from the retromer resulting in defects in endosome-to-TGN transport of CI-MPR [51]. Another recent study demonstrated an interaction between VPS35 and dopamine receptor D1 (DRD1) such that loss of VPS35 decreased cell surface levels of these receptors [52]. Loss of dopamine neurons in brain substantia nigra region leads to Parkinson's disease [53].

Disruption of endosome-to-lysosomal sorting pathway has also been linked to various diseases. For example, Hermansky-Pudlak syndrome (HPS) which is characterised by defects in four complexes such as adaptor protein -3 (AP-3) and the biogenesis of lysosome-related organelles complexes (BLOC-1 to 3) implicated in trafficking from endosomes to lysosomes or melanosomes, or synaptic vesicles. Therefore, it is characterized by hypopigmentation, platelet dysfunction, and other neurological defects [54-57] . A BLOC-1 component such as dysbindin has been shown to describe post-endocytic sorting of GPCRs [58, 59]. Downregulation of dysbindin leads to mislocalization of these receptors from the lysosomes to the cell surface which results in altered signalling. This study specifically focuses on the altered trafficking of one particular receptor called Fas receptor involved in apoptotic signalling. Cancer cells have been often reported to exhibit no or very little surface expression of Fas receptors leading to cells evading apoptosis. Therefore, further sections discuss apoptosis and Fas receptor trafficking in detail.

## 1.2 Programmed cell death or Apoptosis

During the process of growth and development of embryo or tissues, some cells die selectively while others survive. One of the signalling mechanisms in cells that control the process of cell death during such events is called programmed cell death or apoptosis (derived from ancient Greek-“apo”-off, “ptosis”-falling). It is a tightly regulated physiological process that leads to morphological changes in the cell such as rounding up, blebbing, cellular shrinkage and finally DNA fragmentation leading to cell death. Apoptosis can be differentiated from other types of cell death mechanisms based on the signalling pathway and mechanism of inducing cell death. For instance, Necrosis, another form of cell death is often elicited by external cues such as injury and trauma. In contrast to apoptosis, there is minimal chromatin condensation during necrosis; the plasma membrane is ruptured due to organelle swelling as opposed to cellular shrinkage in apoptosis [60].

Apoptosis is a vital component of our immune surveillance; defects in apoptotic signalling are known to cause autoimmune disorders and diseases like cancer. The immune system uses apoptosis during the selection process to eliminate those lymphocytes that are autoreactive to self-antigens or those that do not recognize foreign antigens. When a foreign antigen is recognized by T-cells, they undergo clonal expansion to produce effector cells in a typical immune response. T-cells are resistant to apoptotic signalling during the expansion phase but become sensitive via activation induced cell death (AICD) during the decline of the immune response. Memory T-cells are also resistant to apoptosis [61, 62].

The signalling mechanism of apoptosis has been characterized into two: intrinsic and extrinsic signalling pathways [63-65]. The intrinsic pathway can be activated by external stress such as UV rays and  $\gamma$ -irradiation or internal factors such as oxidative stress. It is executed by a Bcl-2 family of proteins containing orchestration of many cytosolic proteins that are either pro- or anti-apoptotic. In short, apoptotic signals lead to oligomerization of two of the Bcl-2 family members,- Bax and Bak, that can the insert themselves into the mitochondrial membrane. This causes mitochondrial outer membrane permeabilisation (MOMP) releasing its contents into cytoplasm like cytochrome-c which then binds to apoptotic protease-activating factor 1 (Apaf-1) in

the cytosol. Apaf-1 further recruits procaspase 9, an initiator caspase that further activates caspase 3/7. Caspases (cysteine-aspartic proteases) are a class of enzymes that carry out the actual process of apoptosis. The complex created by cytochrome c, Apaf-1 and procaspase 9 is called as 'apoptosome'. The Extrinsic pathway of apoptosis is carried out by a set of transmembrane receptors called death receptors (DR) that respond to death inducing ligands to carry out apoptotic signalling [66].

### **1.2.1 Death Receptors**

Receptors characterized by a homologous sequence of 87 amino acids called death domain (DM) in their cytoplasmic tail are known as death receptors. They belong to the tumour necrosis factor receptors (TNFR) superfamily that contains receptors against cytokines collectively called tumour necrosis factors (TNFs) [62, 63, 66]. TNF receptors exhibit extracellular cysteine rich domains that aid in binding cytokines. Death receptors carry out signal transduction for apoptotic or non-apoptotic pathway upon binding to their ligands. Death receptors in TNF superfamily are namely- TNFR (tumour necrosis factor receptor), Fas receptor also known as CD95 or Apo-1, TRAIL-R1 (TNF related apoptosis inducing ligand receptor-1), TRAIL-R2 (TNF related apoptosis inducing receptor-2). Another common feature of these death receptors is the recruitment of adaptor proteins to their cytoplasmic death domains upon activation by their ligand and formation of death inducing signalling complex (DISC) which recruits and cleaves procaspase 8. However, it should be noted that only TNFR and FASR are known to recruit adaptors called TRADD (TNFR associated death domain) and FADD (Fas associated death domain) respectively and adaptor proteins for TRAIL-R1 and TRAIL-R2 are still unknown [63]. Another group of death receptors in TNF superfamily consists of TNFR-1, DR5 (also known as KILLER, TRICK2), DR6 (also known as CD358), ectodysplasin A2 receptor (XEDAR) and nerve growth factor receptor (NGFR). These receptors do not form DISC signalling platforms upon activation by their ligand, instead, they use different downstream signalling molecules for apoptotic or non-apoptotic signalling [63]. For example, DR6 recruit TRADD to its death domain to activate NF- $\kappa$ B and MAPK8/JNK signalling to induce apoptosis in thymus, spleen, and white blood cells [67].

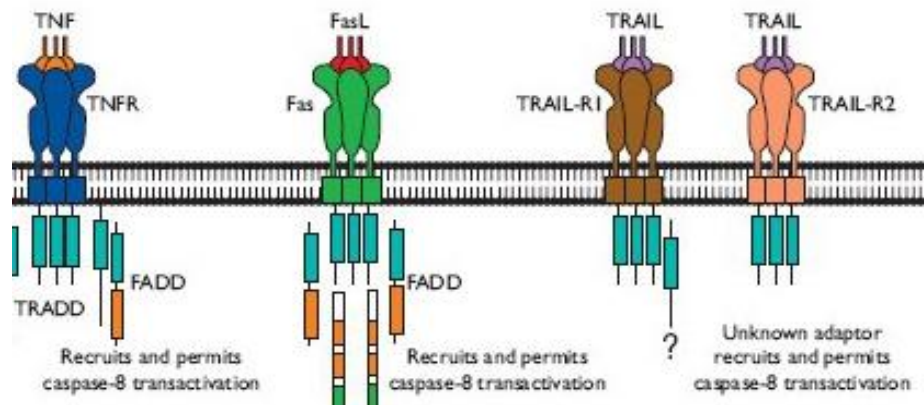


**Figure 1.5: Schematic representation of death receptors** belonging to the Tumour necrosis factor receptor superfamily. All the death receptors exhibit some common features like an extracellular domain for recognizing death inducing ligands, a transmembrane domain and a cytoplasmic domain containing death domain that recruits adaptor proteins like TRADD in the case of TNF-R1 and FADD in the case of FasR (Image adopted from Apoptosis Cell membrane receptors-Death receptors, [www.abdserotec.com](http://www.abdserotec.com)).

### 1.2.2 Fas receptor mediated apoptosis

Fas or CD95 receptors mediated apoptotic signalling is one the most extensively studied pathways. *Fas* gene has been suggested to code 18 different proteins out of which variant 1 encodes for full length Fas receptor consisting of 335aa long protein. While variant 2 lacks exon 6 that encodes for the transmembrane domain thereby producing a soluble receptor and variant 3 has shorter c-terminus encoding for a 220aa long protein [68]. So far 6 different soluble Fas receptors have been described but their precise function and signalling are not well known. Fas receptors are a type I transmembrane glycoprotein with three cysteine rich extracellular domains (CRD). Binding to Fas ligand is mediated by CRD 2 and the first loop of CRD3 [62, 69]. Many studies have suggested that Fas receptors exist as an associated trimer on the cell surface mediated by pre-ligand association domain (PLAD) [70, 71]. A transmembrane domain enables plasma membrane localization and an intracellular death domain of ~80aa executes apoptotic signalling for these receptors. C-terminus region contains a peptide (SLV) that interacts with a negative regulator of Fas signalling called Fas associated phosphatase (FAP-1) [72, 73]. This interaction exists only in the human Fas receptors, pointing towards a specialized mode of regulation that has been discussed in detail later.

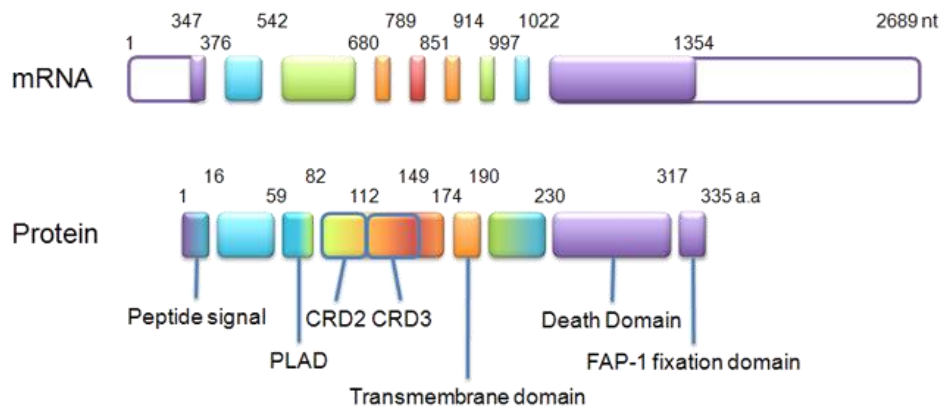


**Figure 1.6: Modular structure of Fas receptor.** Fas receptor is a 335 amino acid long type I transmembrane glycoprotein. The upper panel shows the structure of mRNA coding for full length Fas receptor in humans. The lower panel shows different domains of Fas receptors as described in the figure. The N-terminal region contains a signal peptide followed by a pre-ligand assembly domain (PLAD) and cysteine rich domains (CRD). The cytoplasmic domain contains an 87 amino acid long death domain followed by C-terminal FAP-1 (Fas associated phosphatase-1) binding domain. Figure adopted from Atlas of Genetics and Cytogenetics in Oncology [68].

Post-translational modifications (PTMs) of Fas receptor have been described in many studies out of which N-glycosylation is the best characterized [74]. It is known that addition of variable oligosaccharides chains increases the molecular weight of Fas receptor from up to 54kDa [75]. Inhibition of glycosylation or its enzymatic removal from the Fas receptors did not affect their surface expression levels but increased the apoptotic sensitivity of cells [75]. IFN $\gamma$  treatment was shown to increase the amount of N-glycosylated form of Fas receptors and also increased surface expression levels of FasR leading to increased apoptotic sensitivity [76]. Palmitoylation of FasR has also been described before [77, 78]. A recent study demonstrated that FasR palmitoylation by palmitoyl acyltransferase DHHC7 (aspartate-histidine-histidine-cysteine) regulates the stability of Fas by preventing its lysosomal degradation [79]. Silencing of DHHC7 led to decreased expression levels of Fas receptors thereby affecting apoptotic signalling as well [79]. Previously, a role of palmitoylation in the formation of stable DISC has also been reported [77]. Fas receptors have been shown to be phosphorylated in PLAD domain in the extracellular region and some potential sites in the death domain (intercellular region) have also been described [80]. Phosphorylation at tyrosine 291 in human FasR has been implicated in mediating internalization of activated receptors and

signalling. PMTs of Fas receptor occur in ER compartments of all cells from where they are transported to the cell surface, however, surface expression levels of Fas receptors vary in different cell lines. It is not clear whether different PMTs contribute to the differences in the surface expression levels of Fas receptors in different cell lines.

As mentioned before, Fas and TNF receptors might exist as pre-associated trimers on the cell surface and upon binding to their ligand undergo conformational changes to expose their cytoplasmic death domains to aid homotypic interactions between death domains of other receptors and adaptor proteins [71]. FADD, Fas associated death domain, are adaptor proteins that are known to be recruited to the activated receptors by their death domains within seconds. The N-terminus region of FADD contains death effector domain (DED) that rapidly recruits procaspase 8 by binding to DED domains embedded in procaspase 8, which is then cleaved to produce active caspase 8 molecules that act in a positive feedback loop enabling assembly of DISC [62-64, 68]. The presence of Fas aggregates upon receptor activation has been demonstrated for various cell lines in multiple studies. Evidence from most of the studies points towards the existence of Fas aggregates upon activation in specialized areas of plasma membrane called lipid rafts. These rafts are rich in cholesterol and sphingolipid; they are less fluidic and highly ordered, and biochemical purification of Fas aggregates showed that they were present in detergent resistant distinct domains of PM [81-83]. The event of partitioning Fas aggregates into lipid rafts has been shown to be actin dependent and is supported by the study that implicated ezrin to be the adaptor protein linking Fas receptors to the actin cytoskeleton [84].

Palmitoylation was also shown to be involved in lipid raft partitioning of Fas aggregates [77]. Fluorescent microscopy can detect these aggregates, often called as 'signalling protein oligomerization transduction structures' (SPOTS) [85]. Fas aggregates, DISC formation or activation of caspase 8 has been described as one of the early events in Fas mediated apoptosis that take place within 5 to 10 minutes of receptor activation [64, 82].

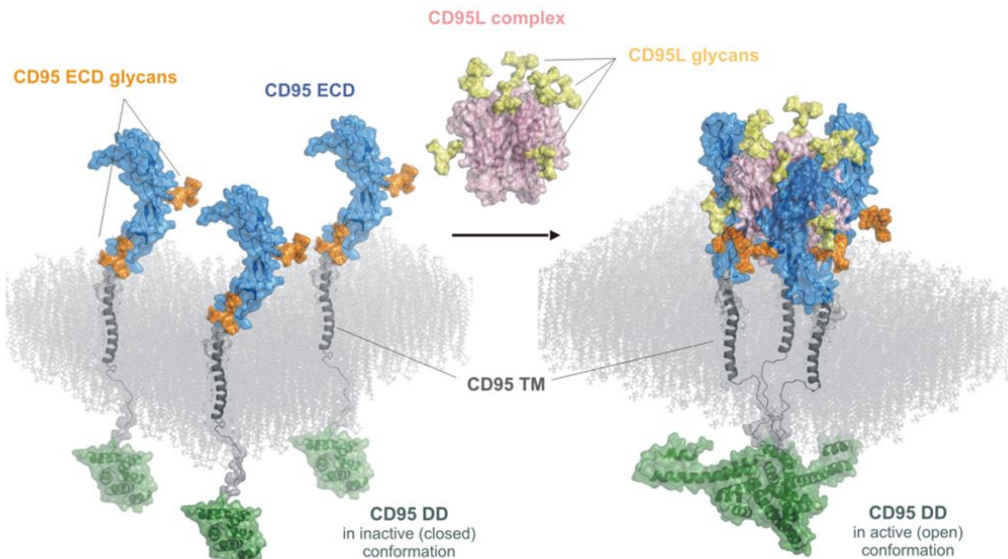
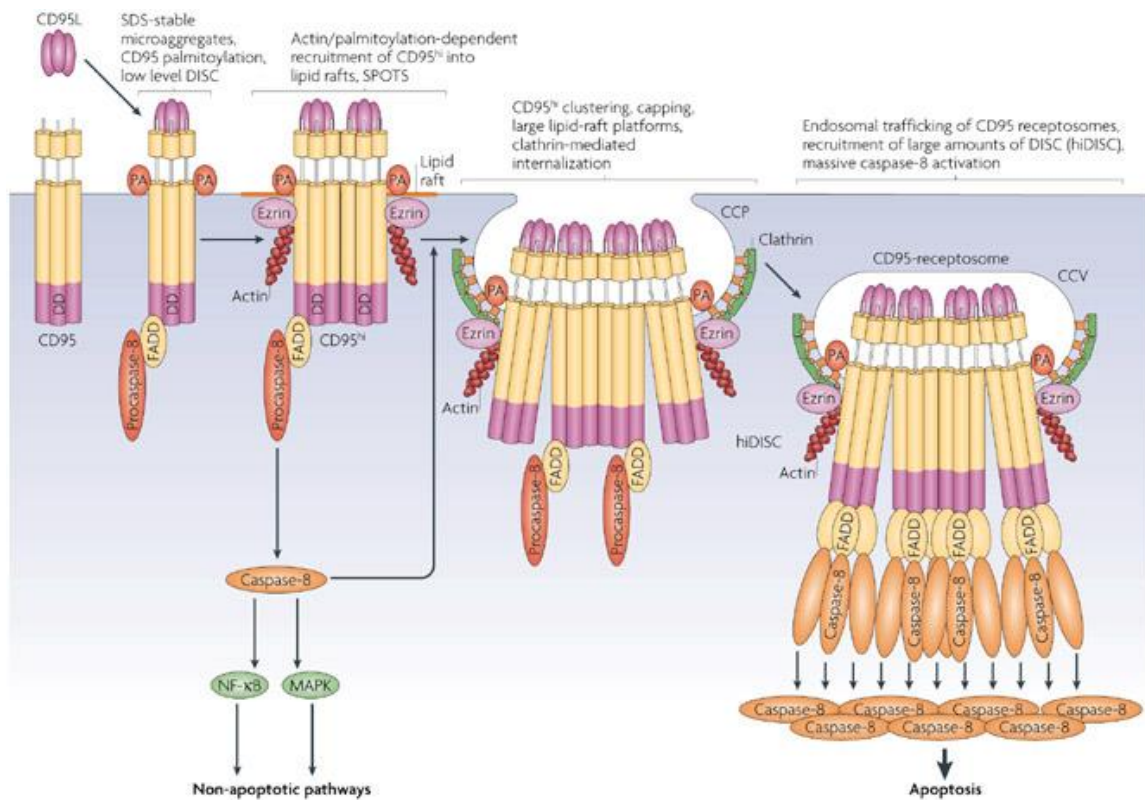


**Figure 1.7: In silico modelling of FasR-FasL complex.** Modelling of FasR or CD95 showing predicted sites for glycan attachment on the extracellular domain (ECD). The trimer of Fas ligand (or CD95L) also contains predicted glycan sites binds to FasR and engages them in a homotrimer formation. This brings intracellular death domains of these Fas receptors in association with each other resulting in an active conformation of the death domains. Figure adopted from Shatnyeva et.al. 2011[74].

Microscopic and sub-cellular fractionation analyses of Fas aggregates have revealed that they undergo internalization into endocytic vesicles positive for Rab4, EEA-1, and cathepsin D [82, 86]. Clathrin mediated endocytosis has been implicated as the major internalization route for Fas receptors [86]. Strong evidence suggests that internalization of Fas aggregates is a pre-requisite for effective DISC formation. Inhibition of internalization blocked proper DISC formation and inhibited apoptotic signalling [82]. Internalization of FasR has been shown in response to both crosslinking agonistic antibodies and recombinant soluble Fas ligand. Co-culturing cells together with cells expressing membrane bound Fas ligand, representing a more accurate physiological scenario, induced internalization of FasR [86]. However, in contrasting studies, the formation of Fas aggregates and their internalization were observed only in case of agonistic antibodies and not recombinant soluble Fas ligand. Inability to aggregate FasR did not alter the rate or extent of apoptotic signalling induced by soluble Fas ligand suggesting that formation of Fas aggregates might be a unique property of agonistic antibodies [87].



Nature Reviews | Molecular Cell Biology

**Figure 1.8: Proposed model for FasR compartmentalization and signalling.** Fas receptors exist as pre-associated trimers on PM which rapidly form SDS-stable microaggregates upon ligand binding. Post translational modification of FasR like palmitoylation and association with ezrin enables translocation of these aggregates into lipid rafts on PM. At this stage, FasR microaggregates are referred to as ‘signalling protein oligomerization transduction structures (SPOTS), recruit moderate levels of Fas associated death domain (FADD) adaptor and caspase 8 which can onset non-apoptotic signalling through activation of mitogen-activated protein kinase (MAPK) and the transcription factor nuclear factor- $\kappa$ B (NF- $\kappa$ B). Within 15 minutes of activation of FasR, they are internalized into clathrin coated vesicles via CME where they form high molecular weight structures and recruit high levels of DISC components, FADD and caspase 8. At this stage, FasR are able to mediate non-apoptotic signalling via caspase cascade [83].

### 1.2.3 Types of apoptotic signalling

Different cell types respond differently to the stimulation of Fas receptors by its ligand. This variation has been addressed by different researchers over the past few years. The consensus view seems to be that cells undergoing apoptosis can be categorized into two types: Type I and II. Many studies support the claim that difference between the two cell types does not lie in the sensitivity towards the

ligand but the intracellular signalling pathways that are used to induce apoptosis. In simple terms, it can be explained as type I cells that undergo extrinsic pathways and type II cells that undergo intrinsic pathways to induce apoptosis [64]. A Few studies argued that differences in the apoptotic pathways do not represent the physiological scenario and exist in tissue culture cells due to artificial stimulation by antibodies that induce aggregation [87]. This argument was refuted by the studies using transgenic mouse models expressing Bcl-2, an apoptotic regulator that protect from mitochondrial disruption by inhibiting pro-apoptotic protein (Bax and Bak) as mentioned before [88]. In such a mouse model, Peripheral T cells were sensitive to Fas ligand stimulation while hepatocytes were insensitive suggesting that T-cells were type I cell in which apoptotic signalling did not require mitochondria whereas hepatocytes were type II cells that required mitochondria. Therefore hepatocytes became insensitive to apoptosis upon overexpression of a mitochondrial protection factor [89]. Along a similar line, another mouse model deficient for Bid (a pro apoptotic protein required for inserting Bax into the mitochondrial membrane to disrupt it) turned hepatocytes insensitive towards apoptosis but did not affect the sensitivity of thymocytes as they do not require a mitochondrial pathway to induce apoptosis [90]. Therefore, these studies provided confirmatory evidence that our tissues undergo either type I (extrinsic) or type II (intrinsic) apoptotic signalling.

Additionally, there are overwhelming pieces of evidence suggesting that pre-association of FasR on PM, lipid-raft partitioning, SPOT formation, DISC assembly and internalization of Fas receptor aggregates are features of type I cells and that these events are not observed in type II cells [83, 91]. Disruption of actin filaments by Latrunculin A did not inhibit apoptosis in type II cells like Jukart T cells and CEM lymphoblasts but affected the apoptotic signalling in type I cells [92]. This data reinforces the significance of internalization and compartmentalization of FasR in apoptotic signalling in type I cells.

#### **1.2.4 Caspase**

Caspases are a family of protease enzymes that play an essential role in apoptotic signalling. Inhibition of caspase activities by their peptide inhibitors such as zVAD-

fmk (benzyloxycarbonyl-Val-Ala-Asp(OMe)-fluoromethylketone) inhibits apoptotic signalling. They have a cysteine protease activity and cleave at C-terminus of an aspartic acid within their target proteins [93]. Caspases are present as non-apoptotic proenzymes that get activated once cleaved into a larger and a smaller fragment. They are activated by either mutual processing or autocatalysis, or both. In the apoptotic pathway, caspases are classified into two distinct classes-initiator caspases and executioner caspases [94]. Upon activation of Fas receptors, initiator caspases like caspase 8 and 9 are activated depending upon the type of apoptotic signalling pathway. In type I cells or extrinsic pathway, recruitment of DISC is followed by recruitment of caspase 8 that in turn activates executioner caspases like caspase -3,-7,-6. Once activated, executioner caspases can cleave other executioner or initiator caspases creating a positive feedback circuit. In type II cells, the initiator caspase is caspase 9 which is recruited and activated by APAF-1 upon cytochrome c release during mitochondrial stress. Activated caspase 8 also plays a role in type II signalling by cleaving pro apoptotic protein Bid into truncated Bid (tBid) that is capable of inducing mitochondrial outer membrane permeabilisation [64, 93, 95-97].

Executioner caspases (-3,-6,-7) are highly homologous caspases. They carry out the actual process of apoptosis in the late stages where they cleave their substrates resulting in nuclear and cytoskeleton fragmentation. Studies using transgenic mice lacking caspase 3 activities have revealed that caspase 3 is an important player in membrane blebbing, DNA degradation, and nuclear fragmentation [98]. Caspase 3 has been shown to trigger caspase 6 upon stimulation with Fas ligand in Jukart cells [94]. Caspase 7 engages in the induction of apoptotic signalling in a different manner than caspase -3 and -6. The activity of caspase 7 has been shown to be not redundant with caspase 3 and a study also showed that caspase 7 was able to also compensate for some of the biochemical activities mediated by caspase 3 during Fas signalling [99]. In summary, the activity of caspases is a crucial event during apoptotic signalling capable of executing multiple biochemical events simultaneously resulting in the generation of a wide range of morphological changes in the cell.

### **1.2.5 Apoptotic signalling in cancer progression**

Immune cells like CD8<sup>+</sup> cytotoxic lymphocyte (CTLs) and CD4<sup>+</sup> cytolytic effector T-cells use Fas receptor mediated apoptosis to eliminate pre-cancerous cells or cancerous cells by infiltrating the tumour site[100]. Very often cancer cells develop resistance to Fas mediated apoptosis through various mechanisms like- blocking of apoptotic signalling at the DISC level by reduced expression of DISC components (FADD and caspase 8) [101, 102] or via increased expression levels of apoptotic inhibitors like c-FLIP [103]. Alterations in the expression levels of Bcl-2 family members to promote tumour survival have also been reported as one of survival tactics used by the cancer cells [104]. Direct modulation of surface expression levels of Fas is another survival mechanism adopted by cancer cells. Surface expression of Fas receptors is a pre-requisite for induction of apoptosis but many reported cancer cells are able to escape immune surveillance cells by lowering down the surface expression levels of Fas receptors [100]. Several studies showed a correlation between decreased surface levels of Fas receptors and increased expression levels of its negative regulator called Fas associated phosphatase (FAP-1) also known as protein tyrosine phosphatase 13 (PTPN13) [105, 106]. PTPN13 has no or very low constitutive expression levels in the pancreas but high expression level has been reported in pancreatic cancer cells that correlated with decreased sensitivity to apoptosis [107, 108]. FAP-1 or PTPN13 has been reported to bind directly to Fas receptors [72]. The inverse correlation between PTPN13 expression and Fas receptor surface levels suggest a defect in the intracellular trafficking of the Fas receptors as the total protein or mRNA levels of FasR are not affected by PTPN13.

## **1.3 Regulation of apoptosis by PTPN13**

### **1.3.1 Protein tyrosine phosphatase, non-receptor type-13**

Cellular equilibrium of protein tyrosine phosphorylation by protein tyrosine kinases and dephosphorylation by protein tyrosine phosphatases is an important homeostasis event; defects in protein tyrosine phosphatase have been involved in signalling defects causing diseases. PTPN13 (protein tyrosine phosphatase, non-receptor type 13) alias FAP-1 and PTPL1 is the largest phosphatase from the family of non-

receptor type phosphatases characterized by the presence of a C-terminus phosphatase domain [109]. It is around 270kDa in size and contains multiple domains [110]. The N-terminus of PTPN13 has a KIND (kinase noncatalytic C-lobe) domain. Not much is known about the function of this domain in PTPN13 but has been suggested to mediate protein-protein interactions not identified yet [111]. KIND domain is followed by a FERM (Four-point-one/Ezrin/Radixin/Moesin) domain. This domain binds to PtdIns(4,5)P<sub>2</sub> and therefore mediates plasma membrane localization of PTPN13 [112]. It has also been suggested to connect PTPN13 to the actin cytoskeleton by binding to F-actin [113]. PTPN13 contain 5 PDZ (PSD-95/*Drosophila* discs large/Zonula occludence) domains that are involved in protein-protein interactions. Owing to five PDZ domains, PTPN13 interacts with a large number of proteins and is therefore involved in several kinds of signalling pathways [109]. PDZ mediated interactions of PTPN13 with actin regulators suggests a role of PTPN13 in actin modulation. For example, PDZ 2 domain interacts with a tumour suppressor APC (adenomatous polyposis coli protein) involved in cell adhesion regulation through  $\beta$ -catenin [114]; secondly, PDZ 3 domain interacts with PRK2 (protein kinase C-related kinase 2), a rho effector kinase involved in apical junction formation, cell-cell adhesion, and actin cytoskeleton regulation [115]. Also, there is now overwhelming evidence to support the involvement of PTPN13 in cancer both as a tumour suppressor and promoter [110].



**Figure 1.9: Modular structure of PTPN13.** PTPN13 contains multiple domains such as N-terminus KIND (kinase noncatalytic C-lobe) domain followed by FERM (Four-point-one/Ezrin/Radixin/Moesin) domain, 5 PDZ domains, and a C-terminus phosphatase domain [109]

### 1.3.2 Negative regulation of apoptotic signalling by PTPN13

As mentioned in the previous section, PTPN13 has been implicated in negative regulation of FasR surface levels. FasR was shown to interact with PDZ 2 or PDZ 4 domain of PTPN13 via its C-terminus ‘SLV’ motif [72]. This interaction exists only in humans as the mouse homologue does not contain PTPN13 binding motif [116].

Several lines of evidence show that expression levels of PTPN13 regulate Fas mediated apoptotic signalling. Overexpression of PTPN13 reduced the sensitivity of pancreatic, liver and colon cancer cells towards apoptosis induced by either Fas ligand or agonistic anti-Fas antibodies as determined by cell viability assays, annexin v labelling, and analysis of PARP cleavage [73, 105-108, 117, 118]. Regulation of Fas mediated apoptosis was shown to be specifically controlled by PTPN13 in the following studies: (i) Introduction of a synthetic peptide against PTPN13 binding 'SLV' motif of FasR enhanced apoptosis. The synthetic peptide was suggested to block the interaction between PTPN13 and FasR through competitive binding [73], (ii) Cell viability was decreased in a dose dependent manner upon treatment with orthovanadate which blocks the tyrosine phosphatase activity suggesting that PTPN13 might be controlling FasR by dephosphorylating a tyrosine residue in FasR [107]. (iii) In glioma cells, an increase in phosphorylation at tyrosine 275 in the cytoplasmic DD of FasR was observed upon treatment with Fas ligand. PTPN13 was also co-immunoprecipitated with endogenous FasR upon activation. However, a point mutation in tyrosine 275 resulted in increased cell surface levels of FasR and decreased association with PTPN13 [119]. Therefore, this data supported the idea that PTPN13 dephosphorylates the cytoplasmic tail of FasR in complex with its ligand at the cell surface to block apoptotic signalling. Phosphorylation of Fas receptor has therefore been implicated in internalization of FasR [117]. Thus, it could be hypothesised that dephosphorylation by PTPN13 might block the intracellular trafficking of FasR either from Golgi-to-PM or endosome-to-PM alternatively; PTPN13 might also enhance internalization of FasR or interfere in the recycling pathway of FasR. A study reported the localization of PTPN13 with  $\beta$ -COP in the Golgi and the staining was found to be Brefeldin A sensitive [107].

In 2010, Schickel et. al., proposed a molecular mechanism to explain the correlation between increased expression of PTPN13 in cancer cells and downregulation of surface levels of FasR to escape apoptosis. They demonstrated that microRNA, mir200c which is an inhibitor of epithelial-mesenchymal-transition (EMT) transcriptional factors ZEB1 and ZEB2, targets PTPN13 and regulate its levels by translational repression. The expression level of PTPN13 correlated with the levels of mesenchymal markers like vimentin, fibronectin, and N-cadherin. Upon

transfection with mir200c, cancer cell lines like CAKI-1, HeyA8, and ACHN that displayed mesenchymal features altered their morphological characteristics to more epithelial like in addition to increased sensitivity towards apoptosis. The difference in the sensitivity towards Fas-mediated apoptosis upon transfection with mir200c was observed only upon triggering extrinsic apoptotic pathway and not the intrinsic pathway (that involves mitochondrial disintegration) suggesting a direct role of PTPN13 in regulating apoptosis in cancer cells [117].

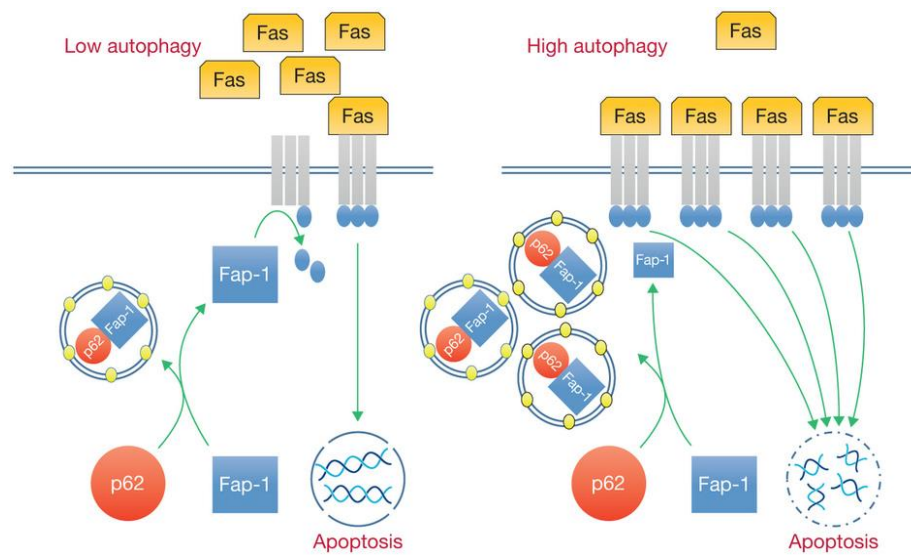


**Figure 1.10: Proposed model of regulation of apoptosis by PTPN13.** Basal autophagic flux within a population regulates PTPN13 protein levels thereby controlling FasR surface levels and apoptotic signalling [120]

A recent study proposed yet another molecular mechanism by which PTPN13 might regulate Fas mediated apoptosis. They suggested that upon stimulation with Fas ligand in type I cells, autophagy adaptor protein p62 interacts with PTPN13 to target it for lysosomal degradation and increase cell surface levels of FasR to induce apoptosis. They also demonstrated that cancer cells under normal tissue culture conditions have either high or low basal levels of autophagic flux in their population. Sensitization of type I cells towards extrinsic apoptosis was seen only during high autophagy flux [121].

## 1.4 SDCCAG3

Serologically defined colon cancer antigen 3 (SDCCAG3) was first isolated from cDNA expression libraries obtained from human colon cancer patients [122]. It is a 435aa long, 45kDa protein although it has four different splicing variants. It contains a coiled-coil domain but no catalytic activity has been assigned to it [123, 124]. Immunoblot analysis of SDCCAG3 revealed that it is extensively phosphorylated as multiple bands corresponding to SDCCAG3 were detected around 55kDa in HeLa cells [123]. A recent study showed a high level of expression of SDCCAG3 in mouse testis although it was found to be expressed in other tissues as well such as liver, thymus, lung, heart, small intestine and kidney. The study also described tissue distribution of SDCCAG3 in the seminiferous epithelium in the testis, at the base of the crypts in the small intestine and in the pancreatic islets [125].



**Figure 1.11: Modular structure of serologically defined colon cancer antigen.** SDCCAG3 consist of 435 amino acids containing a coiled-coil domain towards the C-terminus [123].

### 1.4.1 SDCCAG3 interacts with PTPN13

The N-terminus region of SDCCAG3 has been shown to interact with the FERM domain of PTPN13 and both the proteins have been shown to co-localize at the midbody. However, localization of SDCCAG3 to the midbody at the end of cytokinesis was not dependent on PTPN13 [123]. Both the proteins have been implicated in the regulation of cytokinesis [113], however, the mechanism behind this regulation still remains elusive. A correlation was observed between the expression levels of SDCCAG3 and multinucleated cells phenotype. PTPN13 and SDCCAG3 were also proposed to act together as a complex to regulate cytokinesis since silencing of both SDCCAG3 and PTPN13 give rise to a multinucleate phenotype which is not affected any further upon simultaneous knockdown of both the proteins. SDCCAG3 was found to interact with ARF GTPase-activating protein GIT1. Alterations in the expression levels of GIT-1 also correlated with the number of multinucleated cells in the same manner as SDCCAG3. This suggested a role of GIT-1 in SDCCAG3 mediated regulation of cytokinesis [123]. GIT-1 has been

implicated in negative regulation of Arf-6 [126], a known regulator of trafficking and cytokinesis [127]. Recently, SDCCAG3 was identified as an Arf-6 interacting protein via yeast-two hybrid screening. Overexpression of a mutant version lacking Arf-6 binding region in SDCCAG3 failed to localize at the midbody. Therefore, the formation of a hypothetical complex between SDCCAG3, GIT-1 and Arf6 was suggested where SDCCAG3 was proposed to act as a scaffold to regulate the activity of Arf6 via GIT-1[125]. However, further research is required to understand the functional relevance of the interaction between PTPN13 and SDCCAG3 in the regulation of cytokinesis.

#### **1.4.2 SDCCAG3 in endocytic trafficking**

Immunofluorescence analysis with an antibody against SDCCAG3 revealed its partial co-localization with EEA-1 and transferrin suggesting that SDCCAG3 was involved in early/recycling endosomal trafficking [123]. Another study confirmed this data and suggested that SDCCAG3 might be recruited to the endosomes owing to its interaction and co-localization with Vps35, a component of the retromer complex [35]. Later, it was shown that interaction of SDCCAG3 with Vps35 was mediated by FAM21/WASH complex [51]. SDCCAG3 has also been implicated in the sorting of some retromer dependent cargo like Glut-1[35]. It was also shown to regulate surface representation of tumour necrosis factor receptor-1 (TNFR1) [124]. Therefore, multiple pieces of evidence suggest that SDCCAG3 plays a role in vesicular trafficking.

## 1.5 Trafficking in the primary cilium

### 1.5.1 The structure of cilia

Primary cilia are specialized organelles projecting out into the extracellular space from the plasma membrane in almost every type of cells in a human body. They are evolutionarily conserved structures and are referred to as ‘cell’s antennae’. They sense chemical, light and mechanical stimuli along with regulating fluid flow like mucus or cerebrospinal fluid [128]. They serve important roles in various development and homeostasis pathways like sonic hedgehog and Wnt signalling pathways [129]. It is now well established that defects in cilia give rise to a wide range of human disorders collectively called as ciliopathies [130]. Cilia can be divided into two classes called primary and motile cilia. Motile cilia are found on the epithelial cell of the trachea, oviduct etc. where they beat in a wave like motion to control fluid flow. On the other hand, the primary cilium is immotile and is found on the apical surface of most epithelial cells [131].

The core structure of the primary cilium is called ‘axoneme’ which is composed of nine parallel doublet microtubule bundles in (9+0) arrangement. These microtubules arise from a structure beneath the plasma membrane called ‘basal body’. It is derived from mother centriole that acts as microtubule organising centres (MOTC) and forms a foundation for a cilium in mature cells [132]. Cilia are assembled during the G1 phase of the cell cycle when basal bodies (formed either from pre-existing or *de novo* centrioles) dock onto the ‘actin-rich cortex’ in the plasma membrane. Afterwards, basal bodies nucleate to give rise to axoneme that elongates and protrudes out of the plasma membrane. The region of the basal body where microtubules begin to form the outer doublet of the axoneme is called as ‘transition zone’. The region of the plasma membrane that invaginates at the base of the cilia is called as ‘ciliary pocket’ [132]. Cilia are highly dynamic structures with an active transport system since they require continuous supply of proteins synthesised in the cytoplasm to grow and function. These transport systems maintain the length of cilia by both retrograde and anterograde transport of proteins long the length of the cilia [129].

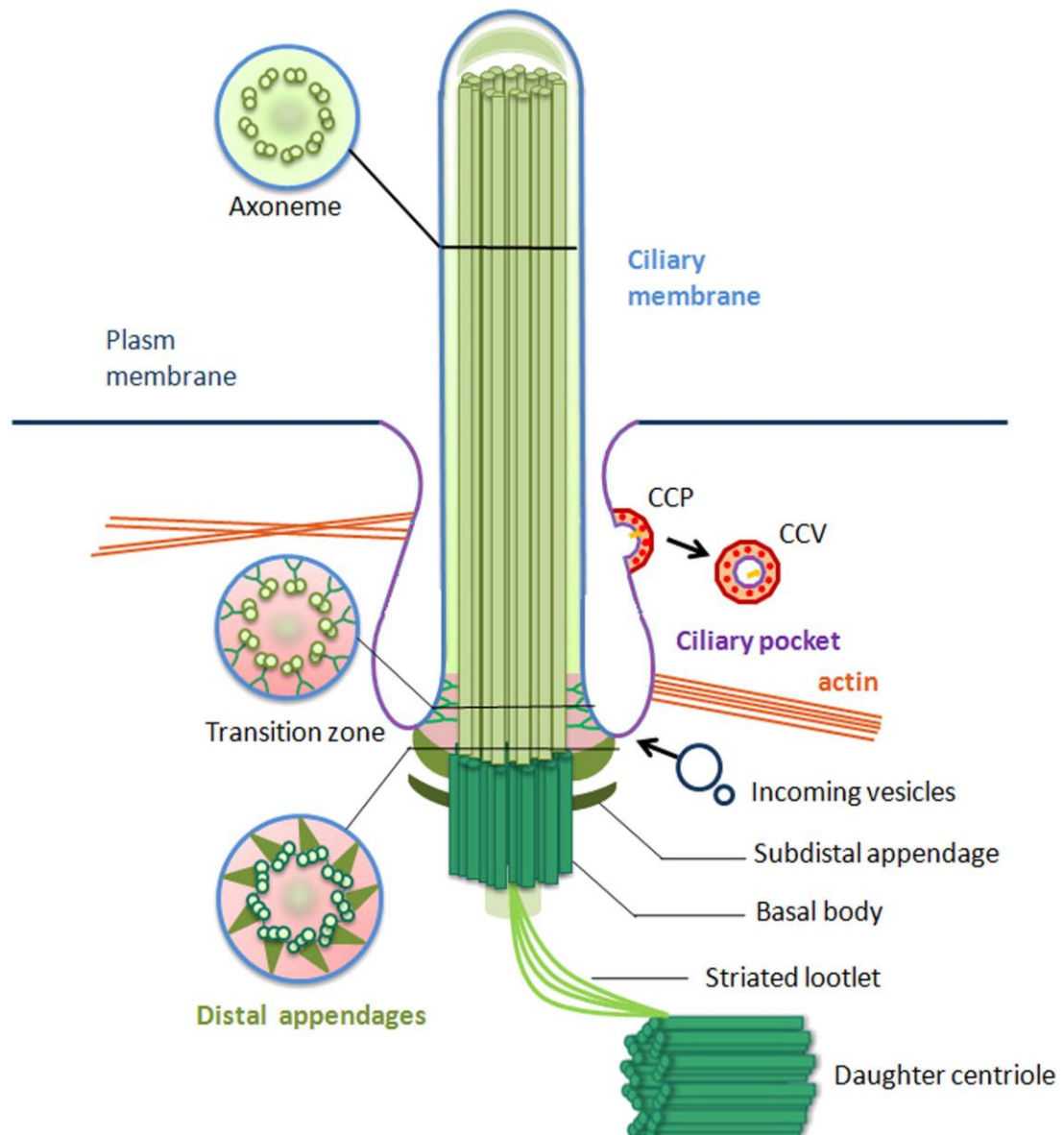
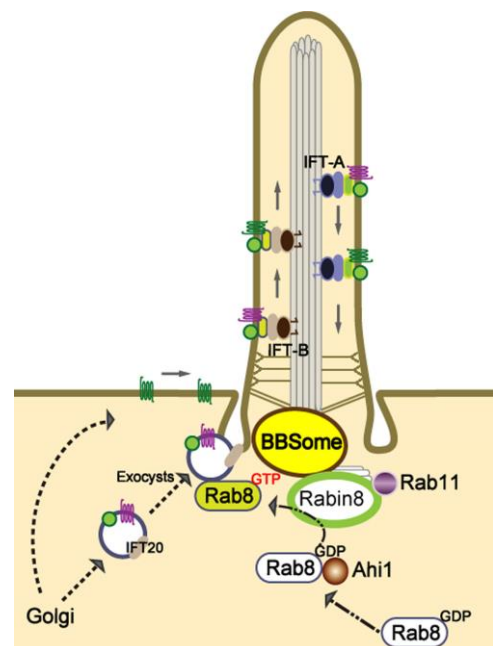


**Figure 1.12: The structure of cilia:** Illustration of the primary cilium structure showing cross sectional view of the microtubule arrangement (9+0) in the axoneme making the ciliary skeleton. Axoneme is covered by a ciliary membrane. The region of cilia in contact with the plasma membrane is called the transition zone. It connects the axoneme with the base of the cilia called as the basal body. Basal body is made up of the mother and daughter centrioles that migrate below the surface of the cell to assemble cilia during interphase. Distal appendages arise from the basal body and connect to the ciliary pocket. Ciliary pocket has been suggested to be the site of endocytosis where clathrin coated vesicles (CCV) fuse with the ciliary membrane. It might also be the site for docking incoming vesicles from the Golgi region. Growing cilia are assembled by proteins transported by via polarized vesicular transport. Actin helps in maintaining the shape and orientation of the growing cilia [133].

### 1.5.2 Ciliary trafficking pathways

The existence of active transport systems like polarized vesicle trafficking and intraflagellar transport (IFT) has been described in many studies that deliver proteins to and fro from the primary cilium. The transition zone (TZ) between the basal body and the axoneme serves as a barrier that impedes diffusion of lipids and proteins above a certain molecular weight and control selective entry/exit of the cargo through structures called transition fibres. Proteins like CEP20 are TZ components that have been described to restrict the entry of non-ciliary proteins [134, 135]. To aid in the selection of ciliary proteins, many ciliary targeting sequences (CTS) have been described, for example, polycystin-2 receptor possesses an N-terminal RVxP motif [136]. Other than motifs, PTMs like palmitoylation and myristoylation also aid in the sorting of protein to cilia [129, 137]. Ras superfamily members like Rabs along with Arl/Arf proteins have been described in polarized vesicle trafficking to cilia [138]. Rab8, a master regulator of cilia trafficking, is recruited to the basal body where it interacts with Rabin 8 to get activated [129]. Rabin 8 (a nucleotide exchange factor for Rab8) is recruited to the centrosome during initiation of ciliogenesis by Bardet-Biedl-Syndrome (BBS) protein-1, part of a larger BBSome complex that is involved in vesicle transport from Golgi-to-basal body-to cilia [139]. Rab11, a recycling regulator, is also known to regulate the accumulation of Rabin 8 at the centrosome in turn regulating Rab8 activity during ciliogenesis [140]. Transport of ciliary cargo from Golgi-to-basal body has also been described by conserved complexes called exocysts [141]. For instance Sec 10, an exocyst component, has been implicated in trafficking of IFT88 (intraflagellar transport protein 88) to the cilium [142].

**Figure 1.13: Polarized vesicle trafficking during ciliogenesis.** Cilia are enriched with receptors and proteins synthesised in the cytoplasm and transported from Golgi-to-PM from where they can be sorted into cilia. Alternatively, vesicles arising from the Golgi can be transported to the basal body by Rab proteins, IFT20 or exocysts[129].



The highly conserved IFT system consists of two main complexes namely IFT complex A and IFT complex B. Ciliary proteins associate with IFT-B which mediates anterograde transport towards the tip of the cilium through molecular motors like kinesin-2. In contrast, IFT-A is involved in retrograde transport of protein from cilia to the cilium base through dynein-2 [129, 143]. A well-studied component of IFT-B complex, IFT88 or Polaris has been shown to be important for cilia assembly and cargo transport [144]. Depletion of *IFT88* in mice led to reduced and shortened cilia [145]. IFT complexes are also important in mediating cilia dependent signalling. For instance, depletion of *IFT88* in mice studies showed loss of ventral neuronal cell types and polydactyly which resembled phenotypes observed with reduced sonic hedgehog signalling [129, 143, 146]. Another component of IFT-B complex called IFT20 localizes to Golgi via GMAP20 (Golgi anchoring protein). Loss of IFT20 interfered with transport of a transmembrane protein polycystin-2 to cilia leading to development of polycystic kidney disorder [147]. Therefore, defects in polarized transport system of ciliary trafficking can lead to development of ciliopathies.

### **1.5.3 Trafficking defects in ciliopathies**

Ciliopathies can be loosely classified into two main types- renal and multi-organ ciliopathies [148]. Renal ciliopathies include polycystic kidney disease in which defective trafficking of transmembrane receptors like polycystin-1, 2 or fibrocystin to cilia has been implicated in pathogenesis of this disease [130, 149] (figure 1.14, b). Multi-organ ciliopathies include diseases like Bardet-Biedl syndrome (BBS) which leads to multi-organ defects including renal abnormalities, obesity, polydactyly etc. It is caused due to mutation in genes that are a part of BBSome complex which mediates ciliary trafficking at the basal body, IFT particles turnover etc.[148] Another multi-organ disease, Lowe syndrome, results in defects in ciliogenesis overall leading to mental retardation, renal abnormalities and cataracts [150, 151]. It is caused by mutations in the gene *OCRL1* (Oculo-Cerebro-Renal syndrome of Lowe). *OCRL1* has been shown to interact with Rab8 and many other effectors that have been implicated in sorting and delivery of ciliary cargo from Golgi or endosomes [152, 153].

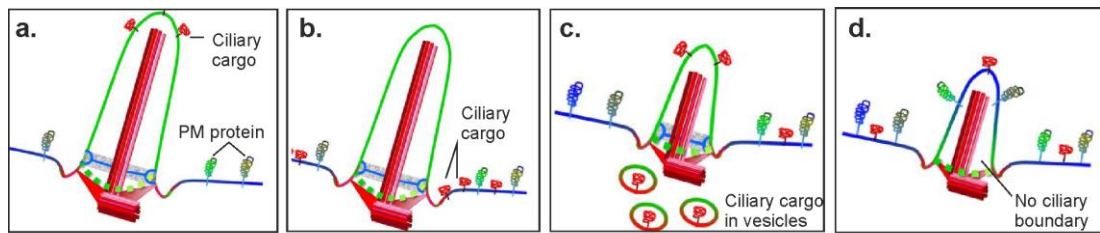


**Figure 1.14: Modes of trafficking defects in ciliopathies:** (a) Normal primary cilium showing normal trafficking of ciliary cargo to the tip of the cilium. PM is Plasma membrane protein. (b) Normal primary cilium, defects in transport of specific ciliary proteins. (c) Defects in ciliogenesis due to defective transport of proteins required for ciliogenesis. (d) Defects in ciliogenesis due to loss of transition zone (TZ) components leading to loss of ciliary boundary. Figure modified from [148].

It can be understood that mutation in *OCRL1* might disrupt trafficking of proteins required for ciliogenesis therefore disrupting cilia formation and function. Joubert Syndrome (JBTS) includes symptoms like cystic kidney, photoreceptor degeneration and brain malfunction; caused due to mutations in several genes involved in ciliary trafficking [148]. For instance, mutation in *Ahi1* disrupts delivery and fusion of ciliary cargo carrying vesicles to the primary cilium via its interaction with Rab8 [154]. It results in reduced number or absence of cilia since trafficking of essential proteins required for ciliogenesis is disrupted (figure 1.14, c). A severe form of multi-organ ciliopathy called Meckel-Gruber syndrome (MKS) is caused due to mutations in genes coding for proteins involved in transition zone (TZ) formation [155]. Loss of function of MKS proteins leads to loss of ciliary boundary formation resulting in stunted cilia growth and abnormal membrane composition (figure 1.14, d).

Taken together it can be understood that formation and maintenance of cilia are vital for normal development and functioning of various organs. Since cilia do not synthesise proteins on their own therefore it depends on proper sorting and trafficking of ciliary cargo from the cytoplasm [143]. The mechanism of transport of several important receptors to cilia, and the function of many identified ciliary proteins still remains elusive. As *SDCCAG3* has been implicated in endocytic trafficking and has been shown to co-localize with centrosomal marker [123], its role in ciliogenesis was examined in the current study.

## **AIMS**

### **Primary AIM**

Several lines of evidence suggest the role of PTPN13 in negative regulation of Fas receptor trafficking, however, it is still not clear which trafficking pathways and molecular machineries are exactly involved in this regulation. Cell surface trafficking of transmembrane receptors is often described as a function of secretory or recycling pathways. Since SDCCAG3 was implicated in regulation of surface levels of TNF and Glut-1 receptors therefore it appeared to be an ideal candidate which could be involved in mediating Fas receptor trafficking along with PTPN13. Hence, the main goals of this study were-

- I. To examine if SDCCAG3 was involved in mediating Fas receptor trafficking.
- II. To understand the molecular mechanism behind it
- III. To determine if SDCCAG3 and PTPN13 were involved together as a complex to regulate trafficking of Fas receptors and apoptotic signalling.

### **Secondary AIM**

Another part of this thesis examined if SDCCAG3 affected trafficking to other specialized areas of plasma membrane like cilia. This study draws on the research conducted by Yu, Erdmann lab in which SDCCAG3 was found to localize to the cilium and its depletion affected the number of cilia in RPE cells. It was also found to interact with IFT88. Based on this unpublished data from the Erdmann laboratory, this study further examined the effect of SDCCAG3 depletion on ciliogenesis in another cell line-IMCD3 cells. It also aimed at rescuing the phenotype observed. Another aim was to examine localization of transiently expressed SDCCAG3 fusion protein in cilia which was not described before.

## 2 Materials and Methods

### 2.1 Materials

#### 2.1.1 Chemicals and reagents

3-Amino-1,2,4-triazole (A8056)	Sigma-Aldrich
Agarose NEEOLTRA	Carl Roth®
Acrylamide solution 40% (BP1402-1)	Fisher Scientific
Bovine Serum Albumin (BSA) ,Fraction V	Fisher Scientific
BSA ,Microbiological grade	Fisher scientific
Brilliant Blue G-250 (BP100-25)	Fisher Scientific
Caspase 6 (human) (recombinant, active)	Enzo® life sciences
ALX-201-060	(USA)
CD261/TRAIL-R1 Mouse Anti-human mAb (Clone DR-4-02) FITC conjugate	Molecular probes, Inc. (USA)
DAPI (4,'6-Diamidino-2-Phenylindole)	Thermo Fisher Scientific
EGF Alexa Fluor® 647 conjugated (E35351)	Thermo Fisher Scientific
Lipofectamine 2000	Life technologies
Leupeptin A	Sigma Aldrich
Diluted Bulk SUPERCRIPT II (91681)	Life technologies
Transferrin (from human serum)	Molecular Probes, Inc. (USA)
Alexa Fluor® 555 conjugate (T35352)	
Vectashield® hard set mounting media	Vector Laboratories
Vectashield® with DAPI hard set mounting	Vector Laboratories
z-VAD-fmk (CAS 187389-52-2)	Santa Cruz
Protease cocktail inhibitor EDTA free	Roche Diagnostics Deutschland GmbH
PageRuler Plus Pre Stained Protein Ladder	Thermo Fisher Scientific
Ponceau S (P3504)	Sigma-Aldrich

## 2.1.2 Commercial Kits

Mini Trans-Blot ®Electrophoresis and blotting	Bio-rad
Pierce Cell Surface Biotinylation kit (89881)	Thermo Fisher Scientific
Supersignal West Pico Chemiluminescent substrate	Thermo Fisher Scientific
Supersignal West Femto Chemiluminescent substrate	Thermo Fisher Scientific
GFP-Trap®	ChromoTek
Protino Glutathione Agarose 4B	Macherey-Nagel
Fast SYBR® Green master Mix	Applied Biosystems
GeneJET Gel Extraction Kit #K0692	Thermo Scientific
GeneJET Plasmid Miniprep Kit #K0503	Thermo Scientific
RNeasy® Plus Mini Kit	Qiagen
NucleoBond® Xtra Midi	Macherey-Nagel
Quick change II XL Site directed mutagenesis	Aligent technologies
Slyde-A-Lyzer™ dialysis cassette	Thermo Scientific

## 2.1.3 Primary Antibodies

Name	Supplier	Application
Acetyl- $\alpha$ -Tubulin (Lys40) (D20G3) XP® rabbit mAb	Cell Signaling Technology®	IF (1:800)
Anti-Gamma tubulin antibody [GTU-88] ab11316	Abcam®	IF (1:100)
Anti-Dysbindin antibody (ab124967)	Abcam®	WB (1:500)
Anti-Fas (human, activating) clone CH-11 #05-201	Millipore™	IF(1:300) FC (1:500)
Anti-Lamp-1 antibody ab24170	Abcam®	IF (1:800)
Anti-SDCCAG3 (HPA029303) (Atlas antibodies)	Sigma Life Science (Sweden)	WB (1:250) IF (1:25)
Anti-VPS35 antibody ab10099	Abcam®	WB (1:500)
Anti-GFP	Peden Lab	WB (1:2000)
Caspase 8 (1C12) mouse mAb	Cell Signaling	WB (1:1000)

CD71 (D7G9X) XP® Rabbit mAb	Cell Signaling	WB (1:2000)
EEA-1 (N-19):sc-6415	Santa Cruz Biotechnology,	IF (1:100)
EEA-1 (C45B10) Rabbit mAb	Cell Signaling	IF (1:200)
EGF Receptor Antibody	Cell Signaling	WB(1:1000)
FAP-1 (H-300):sc-15356	Santa Cruz Biotechnology,	WB (1:500)
Fas (C-20):sc-715	Santa Cruz Biotechnology,	WB (1:500)
Fas, mAb (ZB4)	Enzo® life sciences	IF (1:300) FC (1:500)
GM130	AP lab	IF
HA-Tag (6E2) Mouse mAb	Cell Signaling	WB (1:1000)
HRS antibody (14346)	Cell Signaling	WB (1:1000)
IFT88 polyclonal antibody	Proteintech	WB (1:750)
Monoclonal ANTI-FLAG®M2, Clone M2	Sigma-Aldrich	IF (1:1000) WB (1:500)
Monoclonal Anti-β-Tubulin	Sigma Aldrich®	WB (1:5000)
Myc-tag (9E10) mouse	Gentaur	WB (1:1000) IF (1:100)
N-Cadherin (13A9): sc-59987	Santa Cruz Biotechnology,	WB (1:500)
Purified Mouse Anti-EEA-1	BD Transduction laboratories™	IF (1:300)
Purified Mouse Anti-E-Cadherin	BD Transduction laboratories™ (USA)	WB (1:500)
Polycystin-2 (D-3) sc-28331	Santa Cruz Biotechnology,	WB (1:100)
PTPN13 Antibody NB100-56139	Novus Biologicals®	WB (1:500)
SDCCAG3 PolyAb	Proteintech™	IF (1:300)

IF- immunofluorescence; FC-Flow cytometry; WB-Western Blotting

#### 2.1.4 Secondary Antibodies

Name	Supplier	Application
Donkey anti-goat IgG-HRP (sc2020)	Santa Cruz Biotechnology, INC.	WB (1:5000)
Mouse IgG Peroxidase conjugate	Sigma	WB (1:5000)
Rabbit IgG	Sigma	WB (1:5000)

Peroxidase conjugate		
Alexa Fluor® 680 rabbit	Thermo Fisher Scientific	WB (1:10,000)
DyLight 800 mouse	Thermo Fisher Scientific	WB (1:10,000)
Alexa Fluor® 488 m/r	Thermo Fisher Scientific	IF (1:500)
Alexa Fluor® 594 m/r	Thermo Fisher Scientific	IF (1:500)
Alexa Fluor® 647 goat	Thermo Fisher Scientific	IF (1:500)

### 2.1.5 Biological Material

Plasmids were maintained and propagated in *E.coli* Nova Blue (XL1) form Stratagene GmbH, Heidelberg. Recombinant proteins were expressed in *E.coli* (Rosetta TM2) from Novagene, New Jersey (USA).

### 2.1.6 Buffers and Solutions

For Immunofluorescence-

- PBS (Phosphate-buffered Saline) 20X- Sodium Chloride (160g), potassium Chloride (4g), Potassium dihydrogen phosphate (4.8g), sodium phosphate dibasic (71.g) in 1L pH 7.4
- Blocking buffer-1% BSA in 1X PBS
- Permeabilisation buffer-0.5% TritonX in 1X PBS
- Paraformaldehyde- 4% PFA dissolved in PBS, pH 7.2-7.4

For Western Blotting-

- Laemmli Buffer (4X) - 40% (v/v) Glycerol, 1% (w/v) Bromophenol Blue, 8% (w/v) SDS, 250mM Tris-HCl pH 6.8, 20% β-mercaptoethanol
- Transfer Buffer (10X) - Tris (30.3g), Glycine (144.0g) pH8.3
- Running Buffer (10X) - Tris (30.3g), Glycine (144.0g), SDS (10g)
- PBST Buffer (1X) - PBS(1X), 0.05% Tween-20
- Lysis Buffer- 1% Triton-X in 1X PBS
- Wash Buffer- 0.5% Triton-X in 1X PBS

### 2.1.7 Primers

Name	Sequence	Application
SDCCAG3	F: GGCGAATTCGGCATGTCGGGCTACCAGCGC R: GGCAGATCTTCAAGAGTCTTCCTCCTCGTC	qRT-PCR
Fas	F: ACCCTCCTACCTCTGGTTCTTAC R: GACTGTGCAGTCCCTAGCTT	qRT-PCR
GAPDH	F: GGTGAAGGTCGGAGTCAACG R: ATCTCGCTCCTGGAAGATGG	qRT-PCR
A6 (Rescue 1)	F:ATAAGTTACGACGCGCTAAAGGATGAAAATTCT R:AGAATTTTCATCCTTTAGCGCGTCGTAACCTTATC	Site directed mutagenesis
A7 (Rescue 2)	F:GAGACACTGAACCTAGTAGCCGAAATCCTTAAATC R: GATTTAAGGATTTTCGGCTACTAGGTTCAAGTGTCTC	Site directed mutagenesis
A8 (Rescue 3)	F: GAAAACCACGTAGTCAAGCTAAAACAGGAA R: GATTTCCCTGTTTTAGCTTGACTACGTGGTT	Site directed mutagenesis

### 2.1.8 siRNA

Name	Sequence-Overhangs	Supplier
AllStar Negative Control	n/a	Qiagen
Fas siRNA (h) sc-29311	n/a	Santa Cruz
Hs_SDCCAG3_6 #SI04185888 (no.1)	CGACGCACUGAAAGAUGAATT	Qiagen
Hs_SDCCAG3_7 #SI04216499 (no.2)	ACUGAAUCUUGUUGCCGAATT	Qiagen
SDCCAG3 Silencer® #s21238 (no.3)	CCACGUCGUGAAACUAAAATT	Ambion® life technologies™
HRS	CGACAAGAACCCACACGUCTT	Dharmacon™
DTNBP1 Silencer® #s38427	CAGCAAUCUGACUCAUUUTT	Ambion® life technologies™
Mm_Sdccag3_1 #SI04945885	CGAUAGACUCACUGAUUUUATT	Qiagen
mIFT88 siRNA S101457792	AAGGCAUUAGAUACUUAUAAAATT	Qiagen

### **2.1.9 Constructs**

HA-EGFP-FAS and SDCCAG3 expression constructs were from Erdmann lab. RNAi resistant SDCCAG3 rescue constructs were created using site directed mutagenesis in pcDNA3-myc vector (Invitrogen, Life technologies, Germany). Rab5 Q79L expression construct was obtained from Andrew Peden. pCS2 HRS-RFP was a gift from Edward De Robertis (Addgene plasmid #29685). pCMV3-C-Flag human dysbindin gene was purchased from Sino Biological Inc. (HG15072-CF). pGex-6-P1 vector with glutathione-S-transferase was obtained from GE Healthcare (München).

## **2.2 Methods**

### **2.2.1 Bacteria procedures**

#### **2.2.1.1 Competent cell culture**

*E. Coli* XL1-Blue or BL21 bacteria were spread on a LB (Luria-Bertani) agar plate overnight at 37°C. Next day, a single colony was inoculated in 2 ml of LB media and incubated overnight at 37°C. Then, 1 ml of the overnight culture was inoculated in 100ml of LB medium followed by vigorous shaking at 37°C for 2 hours. The culture was then incubated on ice for 15 minutes and centrifuged at 3300 xg for 10 minutes at 4°C. The supernatant was discarded and pelleted cells were resuspended in ice cold 40 ml 0.1M CaCl<sub>2</sub>. Cells were then incubated on ice for 30 minutes and centrifuged again as described above. Supernatant was removed and cells were resuspended in 6 ml of ice cold 0.1M CaCl<sub>2</sub> containing 15% glycerol. 100 µl of freshly prepared competent cells were immediately aliquoted into sterile 1.5 ml Eppendorf tubes each and stored at -80°C.

#### **2.2.1.2 Transformation with DNA**

Competent cells (100 µl) were thawed on ice and mixed with 5 µl of plasmid DNA (from 1 µg/µl stock) or 7.5µl of ligation mix and swirled gently. The mixture was then incubated on ice for 20 minutes followed by a heat shock treatment at 42°C for 45 minutes with subsequent cooling on ice for 2 minutes. Transformed bacteria was then incubated with 900 µl of pre-warmed LB media and incubated at 37°C for 1 hour with constant shaking at 220 rpm. Bacterial cells were pelleted by centrifuging

briefly at 5000xg, 900 µl from the supernatant was removed and cells were suspended in the remaining 100 µl of media to spread on the antibiotic containing LB agar plates. XL10 Gold Ultracompetent cells were thawed on ice and mixed with 10 µl of DNA (ethanol precipitated) obtained from mutagenesis PCR and swirled gently. The mixture was treated in the same way as mentioned above.

### **2.2.2 Mammalian Cell Culture**

HeLa, HEK293 and HCT116 cell were maintained in DMEM supplemented with L-glutamine, 10% Fetal Bovine Serum (FBS), 1% Penicillin/streptomycin at 37°C in 5% CO<sub>2</sub> atmosphere. RPE and IMCD3 cells were maintained in DMEM/F-12 medium supplemented with L-glutamine, 10% FBS, 1% Penicillin/streptomycin, and 2.625 g/L sodium bicarbonate.

### **2.2.3 DNA manipulation**

#### **2.2.3.1 DNA transfection**

Cells were cultured in 35 mm dishes and transfected at 60-80% confluency with 1-2 µg of DNA using Lipofectamine™ 2000 according to the manufacturer's protocol. DNA was pre-diluted in 100 µl of opti-MEM along with Lipofectamine™ 2000 at a ratio of 1:3. The mixture was vortexed briefly and incubated for 15 minutes at room temperature. The volume of the mixture was then made up to 500 µl and applied to the dishes containing cells in 1.5 ml of DMEM without antibiotics. Then medium was replaced next day in the transfected dishes with DMEM containing antibiotics and cells were harvested after 48h of transfection.

#### **2.2.3.2 siRNA transfection**

Small interfering RNA (siRNA) duplexes were used to delete specific protein levels. RNA duplexes were either purchased commercially or custom made with a 19 nucleotide long core sequence towards a unique mRNA target and contained 3' dTdT overhangs. In 6-well plate format, cells were transfected at 30-50% confluency. 5 µl of 20 µmol siRNA was pre-diluted in 245 µl of Opti-MEM to obtain a final concentration of 100 pmol. 5 µl of Lipofectamine™ 2000 was also diluted in 245 µl of

Opti-MEM in a separate tube. After 5 min of incubation at room temperature, both pre-diluted siRNA and Lipofectamine™ 2000 were mixed together. After 15 min the mixture was applied to the dishes containing full DMEM supplemented with antibiotics and incubated for 72 hours. For 12-wells plate format, final concentration of 50pmol of siRNA was transfected using 2.5µl of Lipofectamine™ 2000 and for 60mm dishes final concentration of 200pm of siRNA was transfected with 10µl of Lipofectamine™ 2000.

### 2.2.3.3 Site directed mutagenesis

In order to introduce single point mutations, a commercial site directed mutagenesis kit was used. The mutagenic DNA primers were designed to contain three silent mutations with at least 10 nucleotides of DNA sequence flanking on either sides. 1.25 µl of primers were used from 100 ng/µl stock in a 50µl PCR reaction. 50 ng of plasmid DNA was amplified with 2.5 U/µl of *PfuUltra* HF DNA polymerase using dNTPs and double distilled water. PCR was carried out in a PCR machine from peQlab, Germany with the following conditions:

Segment	Cycles	Temperature	Time
1	1	95°C	1 minute
2	18	95°C	50 seconds
		60°C	50 seconds
		68°C	variable
3	1	68°C	7 minutes

After PCR, 1 µl of *Dpn* 1 restriction enzyme (10U/µl) was added directly to the PCR reaction and incubated at 37°C for 3 hours to digest the parental supercoiled dsDNA. Digested DNA was then precipitated in the following manner- 1/10 volume of 3 M sodium acetate (pH 5.2) was added to DNA and mixed well. Then 2.5 volume of cold 100% ethanol was added and DNA was incubated at -80°C for 20 minutes. DNA was then centrifuged at maximum speed for 15 minutes to obtain a transparent pellet which was washed with 300µl of 70% ethanol once and the supernatant was discarded by another centrifugation for 5 minutes. DNA pellet was air-dried and re-suspended in 10µl of double-distilled water. 5µl of DNA was used for transforming XL gold bacteria using the same protocol as described above

## 2.2.4 Polymerase Chain reaction

### 2.2.4.1 PCR

Coding sequences were cloned from original plasmid constructs into target plasmid constructs via a polymerase chain reaction. Primers with restriction sites were designed with at least 15 nucleotides binding to the target sequence. Following scheme was used PCR-

Ingredient	Final Concentration	Volume ( $\mu$ l)
ddH <sub>2</sub> O	-	up to 50
5X Phusion HF Buffer	1X	10
dNTP mix	200 $\mu$ M	1
Forward Primer	0.5 $\mu$ M	1
Reverse Primer	0.5 $\mu$ M	1
Template	up to 100 ng	
Phusion polymerase	1U	0.5

### 2.2.4.2 RT-PCR

HeLa cells were used to extract RNA by using TRIzol for cell lysis and homogenization. Phase separation was achieved by adding 0.2ml of chloroform/1ml of TRIzol. After 15 minutes of centrifugation at x12000g, only aqueous phase was separated by angling the microcentrifuge tubes. RNA was isolated by adding 0.5 ml of 100% isopropanol to the aqueous phase followed by 10 minutes incubation at room temperature and centrifugation at x12000g for 10 minutes. RNA pellet was then treated to remove any RNAases and gDNA contaminants by using RNAeasy Plus minikit according to the manufacturer's protocol. RNA concentration measured with the NanoDrop spectrophotometer.

2 $\mu$ g of RNA was used to prepare cDNA by using superscriptase II in the following scheme based on the manufacturer's instructions-

Segment	Components	Volume	Final Conc.
Denature	Total RNA	8.6µl	2 µg
	Oligo dT <sub>15</sub>	1 µl	1.25µM
	dNTP mix	1 µl	0.5mM
	RNase free H <sub>2</sub> O	1.9 µl	-
	Mixture was heated at 65°		
Anneal	5X buffer	4 µl	1X
	DTT 0.1M	2 µl	0.01M
	RNase inhibitor	0.5 µl	-
cDNA synthesis	Heated at 42°C for 2 minutes		
	Superscriptase II	1 µl	-
	Heated at 42°C for 50 minutes		
Terminate reaction	Reaction inactivated at 70°C for 15 minutes		

Undiluted synthesized cDNA was used to amplify specific genes by PCR. The final PCR products were electrophoresed on 2% gel containing Syber safe stain along with 100bp ladder and observed with a Gel Dock™ EZ gel documentation system.

#### 2.2.4.3 Real-Time quantitative PCR

Relative mRNA levels were quantified using SYBR® Green chemistry on a CFX96™ Real-Time detection system by Bio-Rad. In a 10µl reaction volume, 1µl of undiluted cDNA template, 5µl of Fast SYBR® Green master mix (1X) was used along with 0.4 µl each of forward and reverse primers (0.2 µM) plus 3.2 µl of RNAase free water. Samples were prepared in triplicates in a 96 wells plate format along with control wells that had no template. Cycling parameters have been described below:

Segment	Temperature	Time
Initial denaturation	95°C	3 min
40 cycles:		
Step 1	95°C	30s
Step 2	60°C	30s
Step 3	72°C	30s

In order to test the dynamic range of reverse transcription reaction, RNA dilution curves were generated by preparing serial dilutions of RNA. Next, each of these dilutions was converted via RT in a 20µl reaction volume as described above. Once the reaction was over then all the samples were amplified in real-time to obtain 'ct' values and generate a standard curve. In the end, regression analysis was performed to obtain correlation coefficients.

In order to test the amplification efficiencies of the target and normalizer in this assay, a cDNA dilution series was amplified in real time PCR and slope of the resulting regression line was examined. Now the 'ct' values of normalizer were subtracted from the ct values of target for each dilution point to obtain  $\Delta Ct$  values. The cartoon below depicts each of the dilution points as alphabets. These  $\Delta Ct$  values were then plotted in a graph to obtain a regression line.

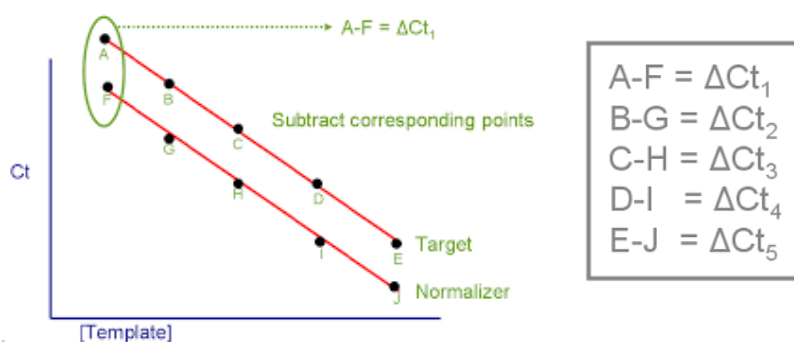


**Figure2.1:** A Cartoon depicting calculation of  $\Delta Ct$  value. (Figure adopted from appliedbiosystems.com)

## **2.2.5 Protein Methods**

### **2.2.5.1 Protein Estimation**

Protein concentration was measured using DC Assay kit's micro-assay plate method according to the manufacturer's instructions. 5µl of protein lysate was mixed with 25µl of reagent A and 200µl of reagent B, incubated in dark and at room temperature. After 15 minutes of incubation, absorbance was read at 680 nm with a spectrophotometer. For each experiment, protein samples were equalized by equalizing their relative absorbance in the following manner-

$$x \mu\text{l} = (\text{Smallest } A_{680} \text{ in the experimental set} / A_{680} \text{ sample}) * \text{Total volume } (\mu\text{l})$$

### **2.2.5.2 Western blotting**

Cells were lysed with 1% Triton X-100 in PBS supplemented with protease inhibitors. Post-nuclear supernatant was obtained by centrifuging the cells at 15,000xg for 15 minutes followed by boiling the samples with 1X Laemmli buffer for 5 minutes. Samples were separated using polyacrylamide gels (SDS-PAGE) composed of stacking gel (5% (v/v) acrylamide in 0.25M Tris (pH 6.8), 0.2% (w/v) SDS) and a separating gel (10% acrylamide in 0.75M Tris (pH 8.8), 0.2% (w/v) SDS). Samples were resolved and transferred using nitrocellulose membrane in 1X Towbin transfer (20% Methanol) at 250mA for 90 minutes. Resolved proteins were visualized with Ponceau S to confirm transfer of proteins on to the membrane followed by blocking with 5% non-fat dry skimmed milk for 1 hour. After blocking, samples were then incubated with primary antibodies in 0.5% milk at 4°C overnight. Either HRP or fluorescently tagged secondary antibodies were used to stain the membranes. HRP conjugated secondary antibodies were used at a concentration of 1:5000 in 0.5% milk for 1 hour at room temperature and blots were developed using X-ray films. Fluorescently conjugated secondary antibodies were used at a concentration of 1:10,000 in 0.5% milk for 1 hour at room temperature. Licor machine was used to develop the blots after washing and drying the membrane completely.

### **2.2.5.3 Protein expression and purification**

SDCCAG3 with N-terminal GST fusion protein was produced using pGEX expression system. Gene encoding full length SDCCAG3 in pGEX vector was

obtained from Erdmann lab. This expression construct was transformed into BL21 strain of *E.coli* and a single colony was inoculated into 100 ml of LB *amp*<sup>+</sup> medium for overnight culture at 37°C at 180 rpm. Next day, this culture was distributed equally into 450ml of LB *amp*<sup>+</sup> medium and incubated further at 37°C until desired optical density was obtained (OD<sub>600</sub> in the range of 0.6-0.8). To induce the expression of the recombinant protein, culture was further incubated with 0.5mM Isopropyl β-D-1thiogalactopyranoside (IPTG) for 6 hours at 25°C or overnight at 18°C. Next, bacteria was harvested from the medium by centrifugation at 4000xg for 20 minutes and resuspended in 20ml ice-cold lysis buffer (0.5% Triton-X in 1X PBS supplemented with protease cocktail inhibitors). Resuspended bacterial pellet was also sonicated to aid cell lysis. This suspension was centrifuged further for 30 minutes at 10,000xg and 4°C. Recombinant protein was recovered from the supernatant by incubating it with the pre-washed 400µl of glutathione agarose beads 4B (to pre-wash the beads, they were washed three times with the lysis buffer at 1800 rpm for 4 minutes each) at 4°C for 3-4 hours. Glutathione beads with bound GST fusion protein were washed and stored at -20°C or eluted further.

Fusion protein was eluted from the beads by incubating them with glutathione containing elution buffer (50mM glutathione and 50mM Tris-HCl (pH 7.9) in water, pH 8.0). The beads were incubated in this buffer for 30 minutes at room temperature under constant rotation. The process was repeated three times. Purified protein was then recovered through dialysis by using Slide-A-Lyzer™ dialysis cassette according to the manufacturer's instructions and measured for protein concentration.

#### **2.2.5.4 Cell surface biotinylation**

HeLa or HCT116 cells were cultured on 60mm dishes and treated with control or three different SDCCAG3 siRNA for 72 hours. On the day of the experiment, confluent cell culture dishes were washed once with ice-cold PBS (0.1M disodium phosphate, 0.15M sodium chloride; pH 7.2 in ultrapure water). EZ-Link Sulfo-NHS-SS-Biotin was weighed accordingly and solubilised in ice-cold PBS at a concentration 0.25mg/ml. At least 2 ml of biotin solution was applied to each culture dish to cover the entire surface area. After 1 hour of incubation on ice, cells were washed with 1% BSA/PBS twice in order to remove any unbound biotin. Then cells were washed again with 1X cold PBS to remove any remaining labelling (biotin) or

quenching (BSA) solution. Dishes were then incubated at a slanted position to collect and remove any remaining solution before cell lysis. 1% Triton X-100 in PBS supplemented with protease cocktail inhibitors was used for lysing cells and obtaining post nuclear supernatant. Cells were maintained on ice throughout the labelling and cell lysis process. Following sub-cellular fractionation, relative protein concentration was measured using DC Assay kit. 10% of the inputs were kept aside as 'total lysate' and equal amount of protein was incubated with 10µl of NeutrAvidin agarose bead/sample for 1 hour at 4°C under constant rotation.

Samples were then washed thrice at 3000xg with cold 1X PBS supplemented with protease cocktail inhibitor to remove any total lysate solution. After the last wash, beads were resuspended in 2X Laemmli buffer and boiled at 95°C for 5 min followed by immunoblotting.

### **2.2.6 Flow cytometry**

Cells were cultured in 6 well plates and after 72 hours of treatment with specific siRNA, confluent dishes were harvested using 500µl of Trypsin-EDTA/well. In order to remove the trypsin completely, cells were centrifuged at 166xg for 5 minutes and resuspended in 500µl of pre chilled 1% BSA/PBS. Hereafter, cell suspensions were maintained on ice throughout the labelling process. 100µl aliquots were prepared for labelling various surface antigens from each experimental condition. Concentration of the primary antibodies used has been described before. Samples were mixed with appropriate primary antibodies and incubated at 4°C for 1 hour under constant rotation. Following incubation, samples were washed thrice with 1% BSA/PBS by centrifuging at 166xg for 2 minutes. After each wash, cells pellets were resuspended by pipetting them up and down gently. In cases where secondary antibody labelling was required, samples were incubated with Alexa-488 conjugated secondary antibody at 1:500 dilution in 1% BSA/PBS for 1 hour at 4°C under constant rotation. Samples were immediately analysed by BD LSR II or FACSCalibur flow cytometer. Untreated wild type cells were used as controls wherein unlabelled sample cells were used for instrument settings and adjusting the background auto fluorescence and secondary only labelled cells were used as a negative control for the labelling.

### **2.2.7 Immunocytochemistry**

Coverslips containing cells were washed once with 1X PBS in a 6 well plate and fixed with 1.5 ml of 4% PFA /well at room temperature for 20 minutes. Excess PFA was removed by extensive washing with 1X PBS three to five times. Cells were then permeabilized with 0.5% Triton X-100 in PBS for 10 minutes followed by blocking with 1% BSA/PBS at room temperature for 1 hour. Labelling solution containing primary antibodies at appropriate dilutions was prepared in 1% BSA/PBS. A humidified chamber was prepared for antibody incubation where 60µl of labelling solution was used per coverslip on a parafilm.

### **2.2.8 Statistical analysis**

Statistical analysis was performed using Prism (Graph Pad software) for data obtained from multiple independent experiments as specified in the figure legends. The statistical significance was calculated using student t-test or analysis of variance (ANOVA). Multiple tests and corrections were applied where required.

### **2.2.9 Assays**

#### **2.2.9.1 Rescue of protein levels**

RNAi resistant SDCCAG3 constructs were generated using site directed mutagenesis kit according to the manufacturer's protocol. HeLa cells were transfected with siRNA against SDCCAG3 along with 500ng of siRNA resistant DNA in 245 µl of OptiMEM. Lipofectamine™ 2000 was also diluted in 245 µl of OptiMEM and incubated for 5 minutes at room temperature. The pre-diluted reagents were then mixed together and incubated for 15 minutes at room temperature before applying them to 1.5 ml of media. The transfected samples were incubated for 72 hours and biotinylated as described above. The surface fraction was purified using NeutrAvidin beads before processing them for immunoblotting.

#### **2.2.9.2 Endocytic trafficking**

HeLa cells were treated with control or SDCCAG3 siRNAs for 72 hours. On the day of the experiment, cells were harvested from the dishes by using trypsin-EDTA. Only surface population of Fas receptors was labelled using 1µg/ml of Anti-Fas CH-

11 or ZB4 antibody in ice-cold 1% BSA/PBS solution for 1 hour at 4°C with constant rotation. Unbound primary antibody was removed by washing the cells three times with 1% cold BSA/PBS at 166xg for 2 minutes. Washed cells were resuspended in pre-warmed DMEM media and incubated at 37°C for various time points. At the end of each time point, endocytosis was stopped by incubating the cells on ice. In the end, cells were labelled with Alexa 488 conjugated secondary antibody for 1 hour at 4°C with constant rotation and washed thrice to remove any unbound labelling antibody. Samples were analysed immediately using BD LSR II Flow cytometer or BD FACSCalibur™. Unstained and secondary only labelled HeLa cells were also analysed as negative controls.

#### **2.2.9.3 Degradation assay**

HeLa cells were treated with control or SDCCAG3 siRNA duplex and transfected with HA-EGFP-FAS construct in a 12-wells plate format. After 48 hours of transfection, medium in each well was replaced with DMEM supplemented with 500ng/ml Anti-Fas (CH-11) antibody and cycloheximide (50µg/ml) for various periods of time. Cells were then washed with 1X PBS once and lysed with 1% Triton X-100. The lysates were equalized and processed for immunoblotting in a similar manner as described above.

#### **2.2.9.4 Antibody chase**

HeLa cells were treated with control or SDCCAG3 siRNA for 24 hours and split on to coverslips. After 48 hours of further incubation, cells were washed once with ice-cold 1X PBS and shifted to 0°C on ice to halt trafficking. Live cells were then labelled with 1µg/ml of agonistic Anti-Fas (CH-11) antibody for 1 hour on ice in 1% BSA/PBS. Unbound antibody was washed away and cells were shifted to 37°C for various time points in full DMEM supplemented with 100nM leupeptin. Internalization was halted by shifting the cells back to 0°C and fixing them immediately in ice-cold 4% PFA. Cells were washed and permeabilized shortly followed by blocking with 1% BSA/PBS. Samples were then stained with endocytic markers such as EEA-1 or Lamp-1 accordingly. Images were acquired with a confocal microscope as described above.

### **2.2.9.5 Antibody uptake**

HeLa cells were treated with control or SDCCAG3 siRNAs. After 24 hours of incubation, cells were split on to coverslips and incubated for a further 48 hours. On the day of the experiment, cells were pre-incubated with 100  $\mu$ M leupeptin for 2 hours and then bathed with 1  $\mu$ g/ml of non-agonistic Anti-Fas (DX-2) antibody in the presence of leupeptin. Continuous uptake of antibody was allowed for 6 hours after which cells were washed once with ice-cold 1X PBS and fixed with 4% PFA for 20 minutes. Cells were then permeabilized for staining with Lamp-1 or EEA-1 antibodies. In the end, cells were stained with Alexa Fluor conjugated secondary antibodies and images were acquired using a confocal microscope. Confocal cross sections were analysed for co-localization as described below.

### **2.2.9.6 Co-localization analysis**

Co-localization analysis was performed on the confocal sections showing maximum intensity for Lamp-1 or EEA-1 and Fas antigens using JACoP plugin in Image J software. Threshold levels were adjusted uniformly across the conditions to reduce background noise from the analysis. Occurrence of co-localization was calculated using Pearson's correlation coefficient (PCC) and quantification of the co-localization was obtained using overlap coefficients ( $k_1$  &  $k_2$ ).

### **2.2.9.7 Endosomal lumen localization of Fas receptors**

HeLa cells were split, seeded on to coverslips (super-resolution grade) and co-transfected with GFP tagged constitutively active Rab 5 (1  $\mu$ g/ $\mu$ l) along with specific siRNA. After 48 hours of transfection, cells were pre incubated with 100 nm of Leupeptin in full DMEM medium. Following short pre-treatment, cells were stimulated with 1  $\mu$ g/ $\mu$ l of Anti-Fas (CH-11) antibody at 37°C for 1 hour in leupeptin supplemented DMEM to induce trafficking. Following incubation, coverslips were washed once with ice-cold 1X PBS at room temperature and fixed with 4% PFA. After 20 minutes of fixation at room temperature, coverslips were washed three times with 1X PBS to remove any remaining PFA solution from the coverslips. Cells were then permeabilized with 0.5% Triton X-100 in PBS for 10 minutes followed by 30 minutes of blocking with 1% BSA/PBS. Finally, cells were incubated with Alexa 594 conjugated anti-mouse secondary antibody for 1 hour and mounted using

vectashield after washing the coverslips three times with 1X PBS and once with water. Images were acquired using spinning disc confocal microscope or super-resolution microscope.

**Line scale analysis** was performed in order to quantify the levels of Fas receptors present in the lumen of enlarged endosomes. Confocal cross sections of individual endosomes were analysed by using Image J exactly as described before [59]. “A straight line was drawn across each endosome to measure the fluorescence intensity across their diameter. This intensity was then normalized to account for varying sizes of the endosomes analysed. The first and second maximum pixel intensities across the diameter were normalized to 0 and 100, respectively, to represent the boundaries of the limiting membrane. The location across the line of pixel 0 was then subtracted from each pixel situated on the line, and this value was divided by the total diameter (in pixels) of the endosomes. Thus normalized pixel distances were generated which corresponded to the distance across the line occupied by each pixel and was expressed as a percentage. Then for each pixel number, pixel intensities were normalized to 0 and 100, respectively, generating normalized fluorescence across the line. Pixel values that lay between 40-60% across the diameter were averaged to obtain middle fluorescence value for each endosome.” A Microsoft Excel VBA (Visual Basic for Applications) program was written to calculate the middle fluorescence (40-60) values automatically from the raw pixel intensities obtained from line scale analysis as described above. The code has been shown and explained in detail in appendix I.

#### **2.2.9.8 Caspase 8 cleavage**

Cells were treated with control or SDCCAG3 siRNA in 12 wells plate format. After 72 hours of transfection, normal media was replaced with media supplemented with 500ng/ $\mu$ l of Anti-Fas (CH-11) antibody and cycloheximide (50 $\mu$ g/ml) for various time points. At the end of incubation, cells were washed with 1X PBS once and lysed with 1% Triton X-100 in PBS. Post-nuclear supernatant was obtained and all the samples were equalized before boiling with 1X Laemmli buffer. Samples were then resolved on a 15% acrylamide gel and transferred to a PVDF membrane using Trans-Blot<sup>®</sup> Turbo<sup>™</sup> transfer system according to the manufacturer's instructions.

The transferred proteins were blocked with 1% BSA/PBS for 1 hour and blotted for Caspase 8 and  $\beta$ -tubulin.

#### **2.2.9.9 *In-vitro* Caspase cleavage**

Purified SDCCAG3 protein with N-terminus GST tag was assessed for its cleavage by recombinant active caspase 6 enzyme. Up to 1 $\mu$ g of purified protein was incubated with or without Caspase 6 enzyme (1 U) in a 25  $\mu$ l reaction mix in caspase assay buffer (50mM HEPES, 50mM NaCl, 0.1% CHAPS, 10mM EDTA, 5% Glycerol, 10mM DTT, pH 7.2) for 2 hours at 37°C. Caspase inhibitor Z-VAD-FMK (10 $\mu$ M) was also added to the reaction to test the specificity of the cleavage activity. The reaction was terminated by adding 1 X Laemmli buffer and boiling the samples at 95°C for 5 minutes. Samples were then separated on a 10% acrylamide gel and stained with coomassie dye. Samples were also analysed by western blotting with SDCCAG3 antibody.

#### **2.2.9.10 Ciliogenesis**

IMCD3 cells were split on to coverslips and treated with specific siRNA or transfected with DNA as required in a 12 well plate format. After 48 hours of transfection, cells were incubated in low serum containing media for 16 hours in order to induce ciliogenesis.

For RPE cells, they were split on to coverslips and treated with specific siRNA for 24 hours after which cells were shifted to low serum environment for 48 hours. At the end of serum starvation, cells were incubated on ice for 20 minutes in order to dissociate any intracellular tubulin and then fixed with 4% PFA for 20 minutes at room temperature.

#### **2.2.9.11 Rescue of Ciliogenesis defect**

IMCD3 cells were seeded on coverslips in a 12 well plate and transfected with control or mSDCCAG3 siRNA along with 1.5 $\mu$ g of human EGFP-SDCCAG3 constructs or EGFP-vector using Lipofectamine 2000. After 48 hours of transfection, cells were incubated in low serum to induce ciliogenesis and further processes for immunofluorescence analysis.

### **3 Role of SDCCAG3 in Fas receptor trafficking**

#### **3.1 Introduction**

Fas receptors are type I transmembrane proteins that are expressed on the cell surface exposing their extracellular domain to interact with its ligand and mediate apoptotic signalling via its cytoplasmic domain [64]. Therefore, surface presentation of Fas receptors is a crucial regulatory event for determining the apoptotic activity of cells. It is a complex and a multilevel process that can be regulated at various stages such as (i) the transcriptional activity of *Fas* gene; (ii) rate of internalization of the receptors; (iii) rate of constitutive turnover or degradation of the receptors. This is not an exhaustive list of the events that can influence FasR surface levels but highlights the factors discussed in this chapter. As described before, PTPN13 has been implicated in down-regulation of Fas receptor surface levels and regulation of its transport to the surface. Reduced expression levels of PTPN13 correlated with increased surface levels of Fas receptors in many cancer cell lines [72, 73, 105-108]. Therefore, expression levels of SDCCAG3 were also perturbed to determine any effect on trafficking. HeLa and HCT116 cells were used as a model in this study as they were easy to transfect and manipulate, and they were shown to express detectable levels of intracellular PTPN13, SDCCAG3 and Fas receptors on the surface. RNAi against SDCCAG3 was used to silence its expression levels in these cell lines.

#### **3.2 Aim**

The main aim of this chapter is to establish if SDCCAG3 plays a role in regulating the intracellular trafficking of Fas receptors or not. The Following approaches were considered for answering this question:

- (i) To investigate changes in the surface levels of Fas receptors upon silencing SDCCAG3
- (ii) To examine an effect on the transcriptional activity of *Fas* gene upon silencing SDCCAG3
- (iii) Monitor changes in the rate of internalization and degradation upon knockdown of SDCCAG3
- (iv) To observe the effect on the intracellular trafficking of internalized Fas receptors upon silencing SDCCAG3

### 3.3 Results

#### 3.3.1 Knockdown of SDCCAG3 increased cell surface levels of FasR

Three different approaches were used in order to investigate changes in Fas receptor surface levels upon transient knockdown of SDCCAG3:

- (i) Semi-quantitative fluorescent confocal microscopy to stain only surface population of FasR by using a specific antibody against an extracellular epitope
- (ii) Flow cytometry based measurement of only the surface population by fluorescent labelling of a primary antibody targeting an extracellular epitope on Fas receptors
- (iii) Cells surface biotinylation and purification of the surface fraction by streptavidin pulldown. Quantitative fluorescent western blotting was performed to measure only the surface population of Fas receptors

All the approaches demonstrated an increase in the cell surface levels of Fas receptors specifically upon knockdown of SDCCAG3.

The antibodies used in these assays were validated for their specificity and assays were optimized using appropriate controls.

In addition, the increased cell surface phenotype was rescued by restoring the levels of SDCCAG3 in siRNA treated samples and transcriptional activity of *Fas* was monitored to rule out that increase in the surface levels of Fas receptors was due to an overall increased expression of *Fas* gene.

### 3.3.1.1 Validation of Anti-Fas antibodies for immunofluorescence

Three of the antibodies against Fas receptor were validated for immunofluorescence analysis- Anti-Fas (CH-11), anti-Fas (ZB4) that recognize the extracellular epitope and anti-Fas (C-20) that recognizes the intracellular epitope on Fas receptors. Therefore, both Anti-Fas (CH-11 and ZB4) antibodies stained only the surface population of Fas receptors in the case of control siRNA treated cells. This surface staining was lost in the case of Fas siRNA treated cells demonstrating the specificity of the antibodies. Similarly, Anti-Fas (C-20) antibody stained the intracellular pool of Fas receptors in control siRNA treated cells which diminished in the case of Fas siRNA treated cells as shown in Figure 3.1. Therefore, antibodies targeting the extracellular epitopes of Fas receptors were used for microscopic analysis of cell surface levels of Fas receptors.

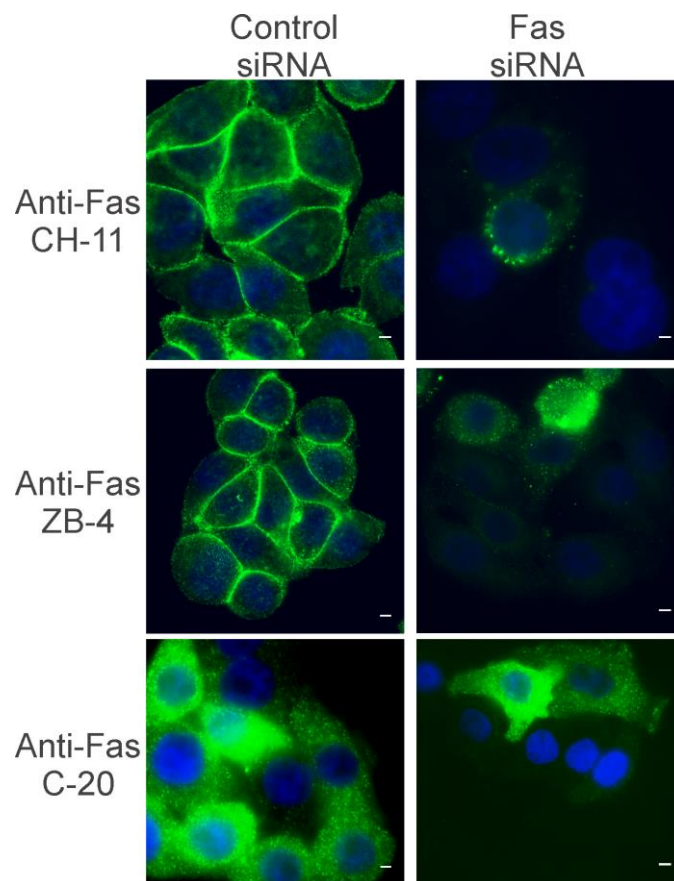
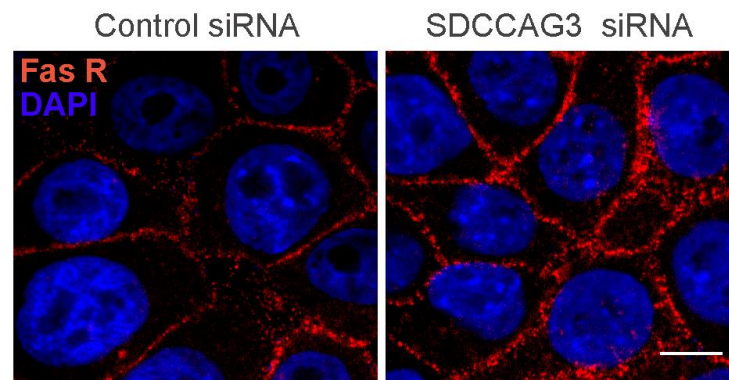


**Figure 3.1: Immunofluorescence analysis of antibodies against Fas receptors in HeLa cells.** Cells were permeabilized only in case of Anti-Fas (C-20) labelling. Alexa 488 conjugated secondary antibodies was used for labelling the cells. The nucleus was stained with DAPI in blue. Images were obtained using wide field epifluorescent microscope and scale bar represents 5 $\mu$ m.

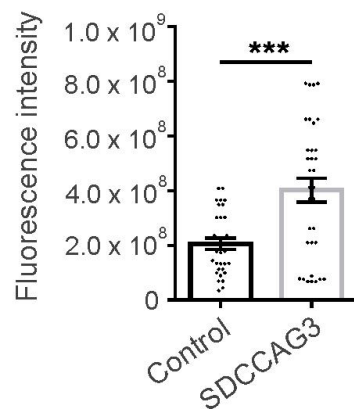
### 3.3.1.2 Microscopic analysis of Fas R cell surface levels

Figure 3.2 shows representative confocal images of HeLa cells treated with siRNA against SDCCAG3 or with control siRNA and stained for Fas receptors using an antibody that recognizes the extracellular domain of Fas receptors (Anti-Fas CH-11). Depletion of SDCCAG3 led to increased cell surface levels of Fas receptors as shown in figure 3.2. Quantitative analysis of corrected total cell fluorescence (CTCF) was calculated as Integrated density-(Area of selected region x Mean fluorescence of background). It revealed that increase in cell surface fluorescence in SDCCAG3 depleted cells was significantly higher than in control cells as shown in panel b of Figure 3.2.

a.



b.



c.

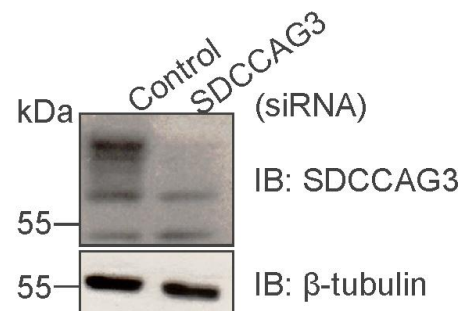


**Figure 3.2: Microscopic analysis of FasR surface levels upon SDCCAG3 knockdown.**

(a) Immunofluorescence analysis of cell surface levels of Fas receptors upon SDCCAG3 and control knockdown in HeLa cells. Non permeabilized HeLa cells were stained with Anti-Fas (CH-11) followed by incubation with Alexa 594 conjugated secondary antibody. Images were obtained using a confocal microscope. Scale bar, 5µm. (b) Quantitative analysis of CTCF (corrected total cell fluorescence) represented as scatter plot with bars. Student's t-test, n=3, \*\* (p< 0.05), p = 0.0073, error bars represent ±s.e.m. (c) Immunoblot analysis of knockdown efficiency of SDCCAG3. Anti β-tubulin was used as a loading control.

### 3.3.1.3 Validation of Anti-Fas antibodies for flow cytometry

Antibodies against Fas receptors were used for flow cytometry based surface staining. As shown in figure 3.3, Anti-Fas CH-11 (a) and DX-2 (b) showed positive staining for Fas receptors (red) on the surface however upon treatment with Fas siRNA, the staining reduced considerably as indicated by a shift in the peak (green). Alexa 488 conjugated secondary antibody alone served as a negative control (black). Unstained HeLa cells (grey) were used as a control for background staining. Figure 3.3 (c) shows positive staining for Anti-Fas (DX-2) increased upon overexpression of Fas (population shown in green) as compared to the empty vector in HeLa cells. Unstained and secondary alone did not show any positive staining for Fas receptors (population in red).

Therefore, Anti-Fas CH-11 and DX-2 staining was found to be specific for Fas receptors and was used in subsequent experiments for measuring surface Fas population via flow cytometry.

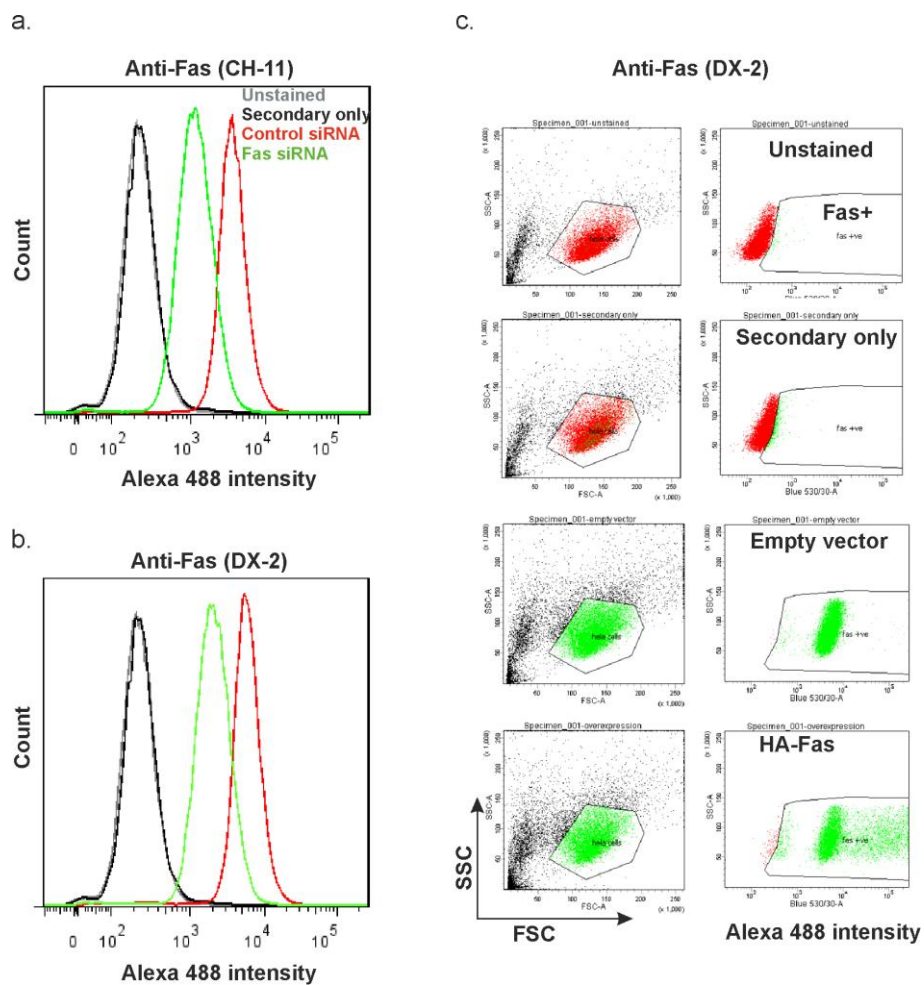


**Figure 3.3: Validation of Fas antibodies for Flow cytometry.** Analysis of surface levels of Fas receptors with Anti- Fas CH-11 (a) or DX-2 (b) antibody upon treatment with control or Fas siRNA. Cells were stained with Alexa 488 conjugated secondary antibodies. The histograms represent Alexa 488 intensity of the indicated samples on the x-axis and the total number of cells analysed on the y-axis. (c) Analysis of Anti-Fas (DX-2) antibody specificity upon staining HeLa cells expressing empty vector or HA-Fas. The left panel shows SSC (side) vs FSC (forward) scatter. Scatter plot in the right panel shows SSC on the y-axis and Alexa 488 intensity on the x-axis for the indicated samples. Analysed cells were gated to show Fas negative population in red and Fas positive population in green.

### 3.3.1.4 Flow cytometry analysis of FasR surface levels

Live HeLa cells were analysed for the surface levels of Fas and other receptors via flow cytometry. Cells were treated with three different siRNA against SDCCAG3 and control siRNA. All three siRNA were able to reduce expression levels of SDCCAG3 efficiently as shown in figure 3.4. In agreement with the previous results, elevated levels of Fas receptors were found on the surface of SDCCAG3 treated cells as compared to the control while other receptors such as EGF and Transferrin were not affected (Figure 3.5, a). In addition, another family member of TNF receptor family called TRAIL-R1 was tested. SDCCAG3 knockdown did not affect surface levels of TRAIL-R1 receptors. Figure 3.5 (b) shows quantification of median fluorescence intensities expressed as a percentage where control was 100%. The difference between the mean intensities of Fas surface levels upon SDCCAG3 and control samples was found to be significant. This data demonstrates that surface levels of Fas receptors increase upon knockdown of SDCCAG3 in HeLa cells.

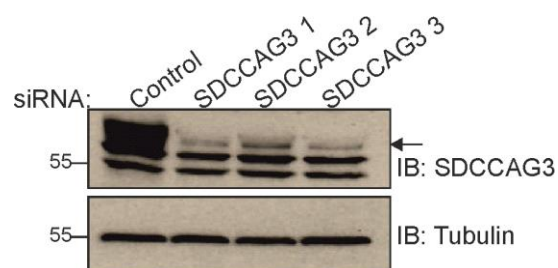


**Figure 3.4: Immunoblot analysis of the knockdown efficiency of SDCCAG3** upon treatment with SDCCAG3 and control siRNA.  $\beta$ -tubulin was used as a loading control.

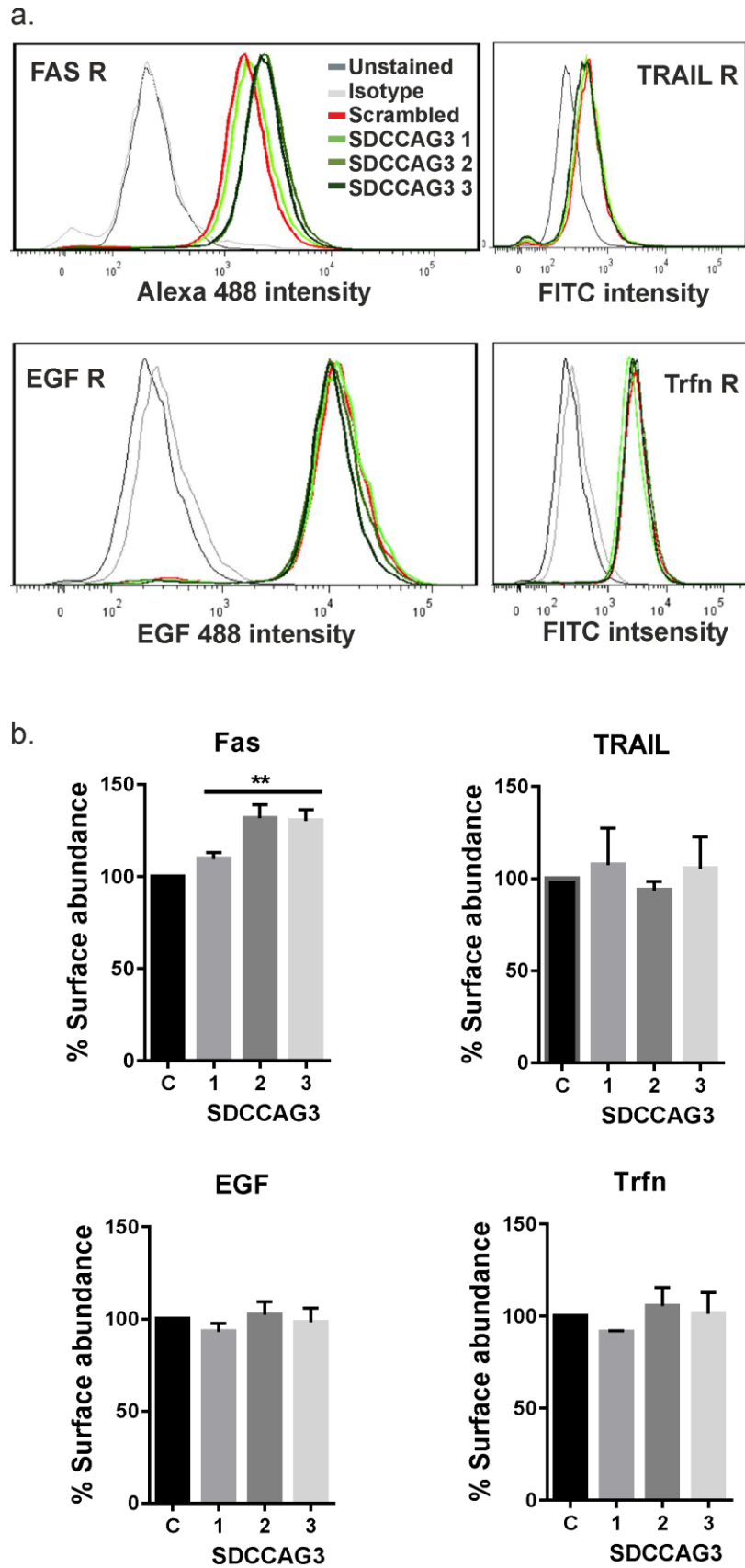


**Figure 3.5: Flow cytometry analysis of cell surface levels.** (a) Analysis of surface levels of the indicated receptors in SDCCAG3 and control siRNA treated HeLa cells. Live cells were

stained with specific primaries followed by Alexa 488 conjugated secondary antibody in some cases and observed via BD LSRII flow cytometer. (b) Bar graphs represent mean intensities from at least three independent experiments (n=3, \*\*p<0.05, p=0.0015 for Fas, one way ANOVA, Dunnett's multiple comparisons test). Error bars represent  $\pm$  s.e.m.

### 3.3.1.5 Validation of Cell Surface Biotinylation assay

HeLa cells were biotinylated according to the protocol described before. The biotinylated surface fraction was detected with an anti-biotin antibody to demonstrate efficient labelling by biotin reagents and streptavidin mediated pulldown (figure 3.6). Immunoblotting with anti- $\beta$ -tubulin antibody confirmed that only surface fraction was labelled in the optimized protocol and that the streptavidin purified fraction was free of any intracellular contaminants. The experiment was performed in triplicates labelled as samples 1, 2 and 3. Hence, this blot validated the experimental procedure for isolating the cell surface fraction only.

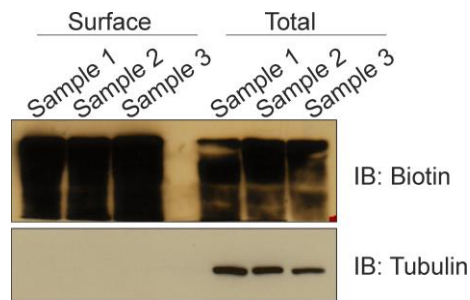


**Figure 3.6: Immunoblot analysis of biotinylated surface and total fraction of HeLa cells.** Samples 1, 2 and 3 represent triplicates. Anti-Biotin antibody was used as a positive control in order to verify the labelling reaction with biotin reagents. Anti- $\beta$ -tubulin antibody was used as a negative control for surface labelling.

Anti-Fas (C-20) antibody was validated for its specificity by siRNA against Fas receptors. The immunoblot below confirmed the correct band of 42 kDa that represents Fas receptors as indicated by the arrow in the figure below. Therefore, Anti-Fas (C-20) antibody was used to detect Fas receptors in the subsequent immunoblots.

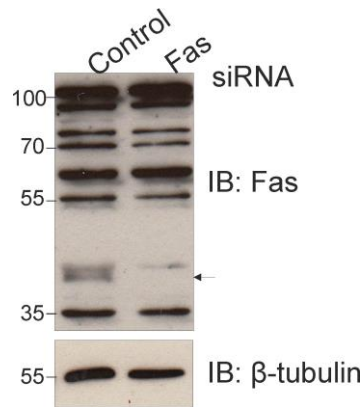


**Figure 3.7: Immunoblot analysis of Fas receptors upon control or Fas siRNA treatment in HeLa cells.** Anti-Fas (C-20) antibody was used to detect Fas receptors (indicated by an arrow). Anti- $\beta$ -tubulin antibody was used as a loading control.

### 3.3.1.6 Biotinylation assay to measure surface levels of FasR

Effect on the surface levels of Fas receptors upon depletion of SDCCAG3 was assessed by cell surface biotinylation. Three independent siRNAs against SDCCAG3 were tested in order to confirm that the observed phenotype was not due to ‘off-target’ effects of the siRNA treatment. Figure 3.8 below demonstrates that all three siRNAs against SDCCAG3 showed similar efficiency of the knockdown for an equal amount of lysate loaded in all the samples (as shown by the  $\beta$ -tubulin blot). Surface expression of Fas receptor was found to be elevated upon treatment with all three SDCCAG3 siRNA as compared to the control siRNA. No changes in the total levels of Fas receptors were observed in case of SDCCAG3 siRNA no.1 and 2 as compared to the control. However, a slight increase in total levels of Fas receptor was observed in case of SDCCAG3 no.3 siRNA as compared to the control. Fluorescence based quantitative immunoblotting allowed quantification of the protein levels as shown in panel b. The increase in the surface levels of Fas receptor was found to be significantly higher in SDCCAG3 treated samples as compared to the control. The extent of the phenotype observed was similar in case of SDCCAG3 no.2 and 3 siRNAs but lesser in the case of no.1 siRNA.

Furthermore, an increase in the surface levels of Fas receptors upon SDCCAG3 knockdown was specific as the similar effect was not observed in case of other receptors such as Transferrin, EGF, and N-cadherin in HeLa cells. Quantification of the surface levels of these receptors showed no significant difference between

SDCCAG3 and control siRNAs treated cells as shown in panel b. Therefore, it can be concluded that SDCCAG3 knockdown elevated surface levels of Fas receptors specifically.

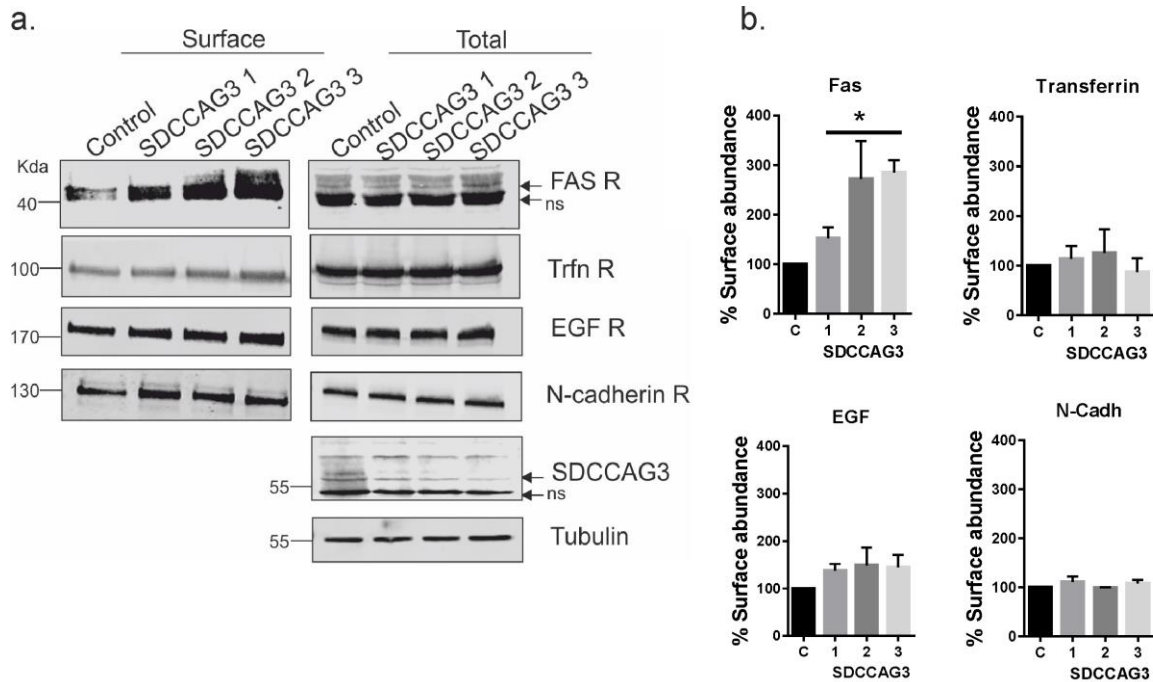
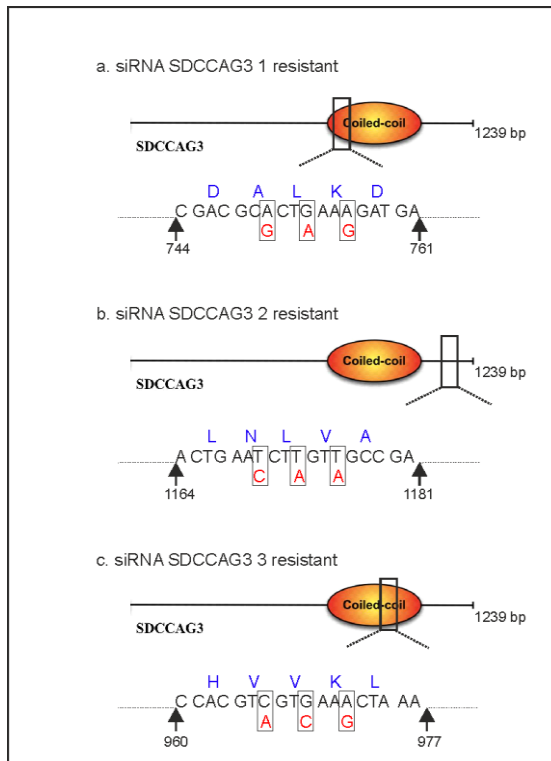


**Figure 3.8: Analysis of FasR levels by cell surface biotinylation upon SDCCAG3 knockdown.** (a) Immunoblot analysis of biotinylated cell surface fraction and total lysate of HeLa cells treated with three independent siRNA against SDCCAG3 and control. Fluorescence based immunoblots were developed using LI-COR scanner. Fas receptors were detected using anti-Fas (C-20) antibody; endogenous levels of other mentioned receptors were detected using their specific antibodies; arrow indicates staining specific for SDCCAG3, ns stands for non-specific;  $\beta$ -tubulin was used as a loading control. (b) Quantitative analysis of cell surface levels of the indicated receptors represented as bar graphs. On x-axis, 'C' stands for control siRNA and 1-3 stands for three siRNAs against SDCCAG3. The y-axis represents relative abundance of receptors expressed as a percentage when control is 100%. The quantification shows mean of at least three independent experiments (n=3), error bars represent  $\pm$ s.e.m; one-way ANOVA was performed to determine the p-value;  $** < 0.05$ ;  $p = 0.0340$  for Fas receptors.

### **3.3.1.7 Rescue of the surface levels of Fas receptors upon SDCCAG3 knockdown**

In order to exclude that the transfection procedure using siRNA against SDCCAG3 affected surface levels of Fas receptors by off-target effects, siRNA resistant versions of SDCCAG3 were generated by site directed mutagenesis. Three consecutive silent mutations were introduced to generate mutants that were resistant to their respective SDCCAG3 siRNAs. Box 1 displays the schematic representation of the three rescue constructs generated. The base pairs that were mutated are highlighted in red and arrows indicate the position of the siRNA targeted region in full length SDCCAG3. Co-transfection of siRNAs against SDCCAG3 with their respective mutant constructs revealed overexpression of SDCCAG3 even in the presence of siRNA (Figure 3.9, a). Samples showing knockdown of SDCCAG3 with three different siRNAs showed an increase in Fas receptor surface levels as shown in the previous result. However, restoration of SDCCAG3 levels with mutant constructs in siRNA knockdown samples rescued the surface phenotype i.e. surface levels of Fas receptors in the rescue samples were comparable to the control sample as shown in the figure. In line with the previous result, surface levels of transferrin receptors were unaffected in both knockdown and rescue samples for all three siRNA.

The bar graph represents surface levels of Fas receptors expressed as a percentage where control is 100%. Consistent with the previous result, knockdown of SDCCAG3 elevated surface levels of Fas receptors significantly as compared to the control. However, the difference between the surface levels of Fas receptor in rescue samples and control was not significant (Figure 3.9, b) This data confirmed that the increase in surface levels of Fas receptors is specific to SDCCAG3 knockdown and can be rescued by restoring the intracellular levels of SDCCAG3.



**Box1: Schematic representation of the construct designs used for rescuing the surface phenotype of Fas receptors upon SDCCAG3 knockdown.**

(a-c) Three silent mutations (red) were introduced by site directed mutagenesis PCR which did not affect the protein sequence (blue). Arrows indicate the beginning and end of the sequence targeted by siRNAs which is also shown as a boxed region on the modular structure of SDCCAG3.

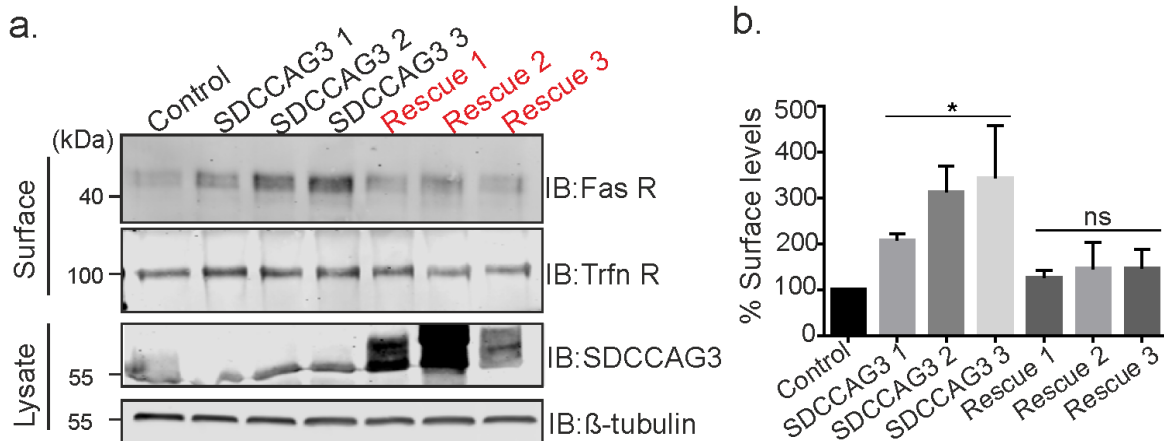


**Figure 3.9: Rescue of cell surface levels of FasR upon SDCCAG3 knockdown.** (a) Immunoblot analysis of surface levels of Fas receptor upon transfection with SDCCAG3 siRNA alone or co-transfection with siRNAs and siRNA resistant SDCCAG3 constructs (labelled as Rescue 1-3) in HeLa cells. (b) Quantification of surface levels of Fas receptors normalized to  $\beta$ -tubulin and expressed as a percentage. Data was collected from three independent experiments (n=3, One way ANOVA, Sidak's multiple comparisons, \*p<0.05, p=0.045, ns-not significant). Error bars represent  $\pm$ s.e.m.

### 3.3.1.8 Fas levels were elevated upon SDCCAG3 knockdown in HCT116 cell

The effect of SDCCAG3 depletion on Fas levels was also examined in another epithelial cell line called HCT116. Cell surface biotinylation analysis in these cells revealed an increase in both the surface and total levels of Fas receptors upon depletion of SDCCAG3 siRNA as compared to the control as shown in figure 3.10 (a). Quantification of the surface and total levels revealed a significant increase upon SDCCAG3 depletion (b). This data supported the previous data obtained in HeLa cells where an increase in surface population of FasR was observed upon knockdown of SDCCAG3. However, the total population of FasR did not change as dramatically in HeLa cells as compared to HCT116. The reason for this discrepancy could not be explained. Whether or not depletion of SDCCAG3 affected total basal levels of FasR required further experimentation described later.

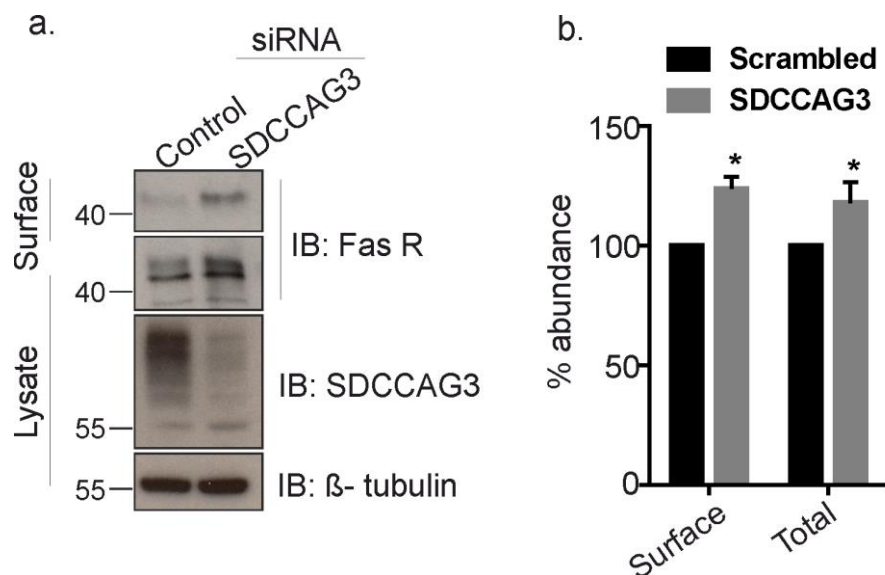


**Figure 3.10: Analysis of FasR levels upon SDCCAG3 knockdown in HCT116 cells.** (a) Immunoblot analysis of HCT116 cells treated with control or SDCCAG3 no.1 siRNA. The surface fraction was isolated by cell surface biotinylation and purified with streptavidin coated beads. Total lysate was tested for SDCCAG3 knockdown efficiency and tubulin acted as a loading control. (b) Quantification of immunoblots for surface and total levels of Fas receptors was performed using Image J. Receptor levels were normalized to their respective tubulin controls and expressed as a percentage. Data was collected from three independent experiments (n=3, multiple t-tests, \*p<0.05, p=0.0100 for surface levels and p=0.0355 for total levels).

Surface levels of Fas receptors in HCT116 cells were also analysed using flow cytometry as described before. Figure 3.11 (a) shows that treatment with SDCCAG3

siRNA led to an increase in the fluorescence intensity of Fas receptors (in red) as compared to the control siRNA treated cells (in blue). Alexa 488 conjugated secondary antibody staining was used as a negative control (in black). Quantification of the median fluorescence intensities expressed as percentage revealed that difference in the two samples was significant (b). Knockdown efficiency of the SDCCAG3 siRNA in HCT116 cells was confirmed in (c).

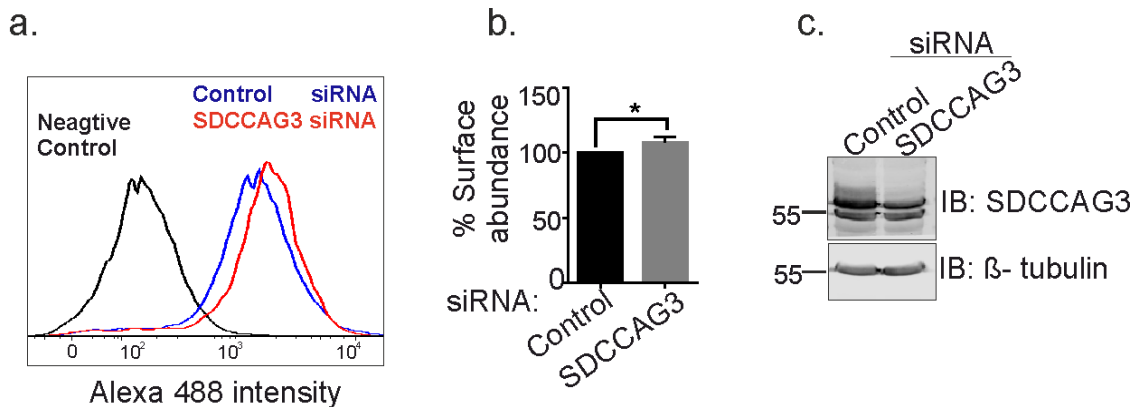


**Figure 3.11: Flow cytometry analysis for Fas receptor levels in HCT116 cells treated with SDCCAG3 no.3 siRNA and control siRNA.** (a) Histograms representing intensity levels of Fas receptors in siRNA treated cells (red and blue) and negative control (black) as indicated. X-axis represents intensity of Alexa 488 conjugated antibody signal in the samples. Y-axis represents cell count. (b) Bar graphs representing changes in surface levels of Fas receptors in percentage where control is 100%. Data represent n=3, \*p<0.05, p=0.0314, unpaired t-test, two-tailed, error bars represents ±s.e.m. (c) Immunoblot analysis of the knockdown efficiency of SDCCAG3 in control or SDCCAG3 siRNA treated cells. β-tubulin was used as a loading control.

### 3.3.2 SDCCAG3 knockdown did not affect the transcriptional activity of FasR

In order to investigate if the increase in the surface levels of Fas receptors was an effect of an increased transcriptional activity or not, mRNA levels of Fas receptors were measured in control or SDCCAG3 knockdown samples. HeLa cells were

transfected with control or three different siRNA against SDCCAG3. After 72 hours of transfection, RNA was isolated and cDNA were prepared from each sample. A PCR reaction was set up using cDNA from different experimental conditions to amplify genes such as *Fas*, *GAPDH*, and *SDCCAG3*. The amplified genes were run on 2% agarose gel for semi-quantitative analysis of the *Fas* mRNA levels as shown in figure 3.12. Quantification of the relative gene expression revealed no substantial differences in the expression levels of *Fas* upon silencing SDCCAG3 with three different siRNA. *GAPDH* was used as a negative control. Expression levels of *Fas* were normalized to *GAPDH*. The blot also reveals a decrease in the expression of *SDCCAG3* upon its knockdown as expected. However, this approach was semi-quantitative in nature and required further validation from a more rigorous method of quantification.

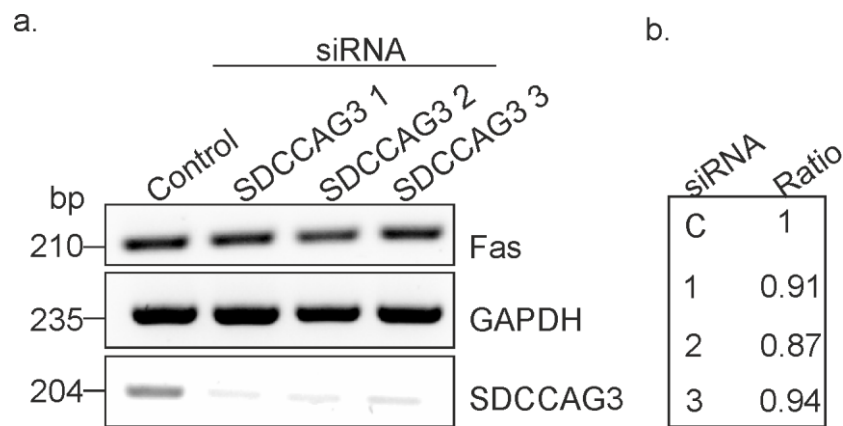


**Figure 3.12: Analysis of mRNA levels of *Fas* upon SDCCAG3 depletion** (a) Semi-quantitative analysis of the changes in gene expressions of *Fas* in HeLa cells treated with control or three different siRNA against SDCCAG3. (b) Band intensities for *Fas* in SDCCAG3 knockdown samples were compared to the control and the relative expression ratio was normalized with *GAPDH*.

In order to measure the changes in the mRNA levels of *Fas* more accurately, quantitative real-time PCR was performed. Firstly, RNA dilution curves were generated in order to assess the efficiency of reverse transcriptase reaction (RT). Figure 3.13 shows that for different concentrations of RNA, RT efficiency is consistent for both *Fas* (a) and *GAPDH* (b) across all concentrations as all the dilution points were in the same line. Secondly, amplification efficiencies for the target and normalizer genes were assessed by generating their cDNA dilution curves.

Then slope of these dilution curves was generated in order to evaluate the difference between the two curves (i.e. their efficiencies). Figure 3.13 (c) shows the slope of 0.6. The amplification efficiencies are considered similar only if the slope is between -0.1 to 0.1. Therefore, this data showed that *Fas* and *GAPDH* were not being amplified with similar efficiencies in this assay and hence their expression levels were compared using the Pfaffl method.

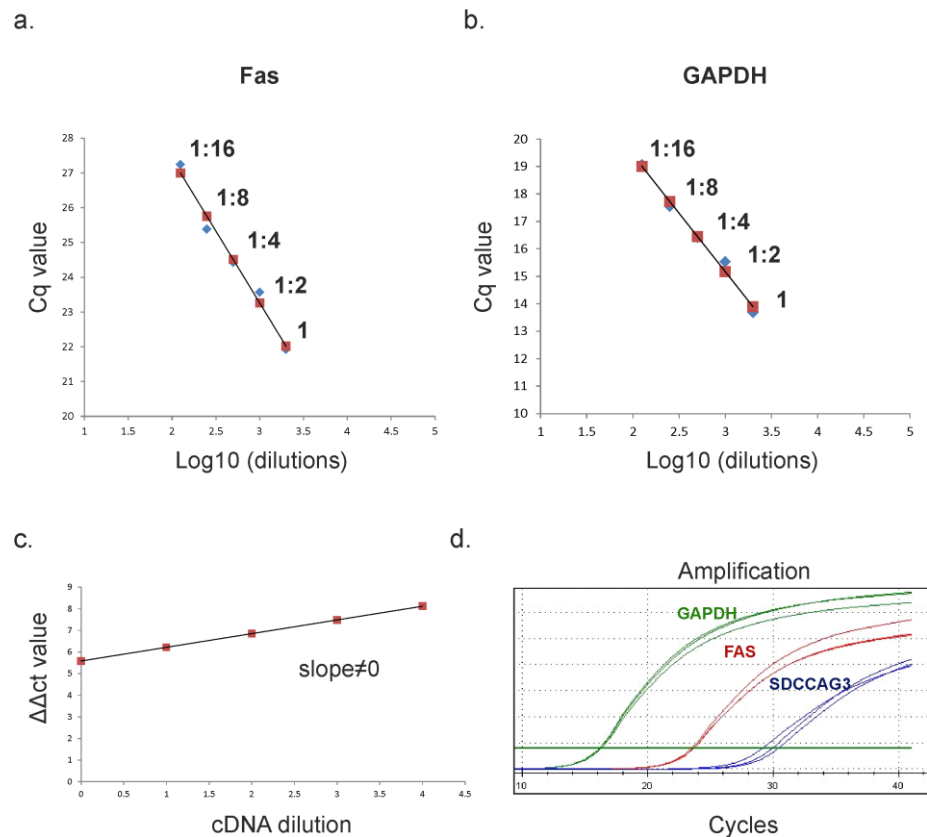


**Figure 3.13: Optimization of qRT-PCR.** Dynamic range of reverse transcription for *Fas*-  $R^2$  0.98 (a) and *GAPDH*-  $R^2$  0.98 (b) was determined. RNA was serially diluted and Cq values obtained from the amplification of the genes were plotted on y-axis corresponding to the amount of RNA described on the x-axis. (c) Slope generated from the  $\Delta\Delta C_t$  values of the two genes (y-axis) against the varying amounts of cDNA used (x-axis). (d) Representative amplification curves of the indicated genes.

Relative expression level of *Fas* mRNA was determined from three independent repeats. cDNAs from control or SDCCAG3 siRNA treated HeLa cells were isolated to amplify *Fas* and *GAPDH* in real time. Triplicates for each experimental condition were prepared. Figure 3.14 shows a graphical representation of the relative fold changes in the mRNA levels of *Fas* in SDCCAG3 knockdown samples as compared

to the control. Expression levels of *GAPDH* were used to normalize the levels of *Fas* in this assay. The data clearly shows that relative changes in the mRNA levels of *Fas* upon treatment with SDCCAG3 were minimal and not statistically significant.

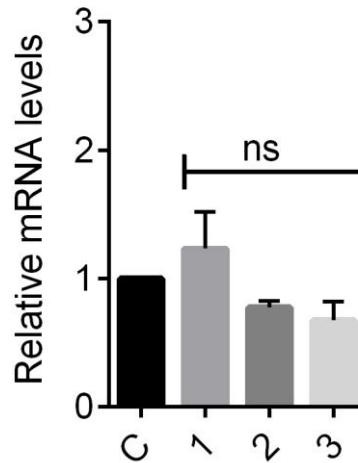


**Figure 3.14: Graphical representation of the relative mRNA levels of *Fas* receptors in SDCCAG3 knockdown samples (three different siRNA against SDCCAG3 represented as 1, 2 and 3) as compared to the control siRNA knockdown sample (C).  $\Delta\Delta Ct$  (Pfaffl) method was used to calculate the relative gene expression where *GAPDH* was used as the normalizer. Data was collected from three independent experiments (N=3) with internal triplicates. Ordinary One-way ANOVA was performed to test if the differences among the means were significant ( $p=0.1480$ ; ns= not significant).**

### 3.3.3 SDCCAG3 knockdown did not alter the rate of internalization of FasR

#### 3.3.3.1 Rate of internalization upon stimulation with an agonistic antibody

Surface levels of transmembrane proteins are partly a function of the rate of intracellular trafficking. Therefore, the rate of trafficking of Fas receptors was determined by flow cytometry. Surface population of Fas receptors was stained using an agonistic Anti-Fas (CH-11) antibody and incubating the cells for various time points at 37°C. Loss of receptors from the surface over a period of time represented the event of internalization. Figure 3.15 below shows histograms obtained from the flow cytometry analysis of internalized Fas receptors in control or SDCCAG3 treated HeLa cells (a). Median fluoresce intensity (MFI) obtained was used to calculate the amount of receptors remaining on the surface relative to 0 time point.

This amount was expressed as a percentage and represented as % Endocytosis (b). The graph below demonstrates no significant difference between the rate of trafficking in case of SDCCAG3 knockdown cells as compared to the control. Therefore, an increase in the surface levels of Fas receptors was not due to the inhibition of its internalization upon silencing SDCCAG3.

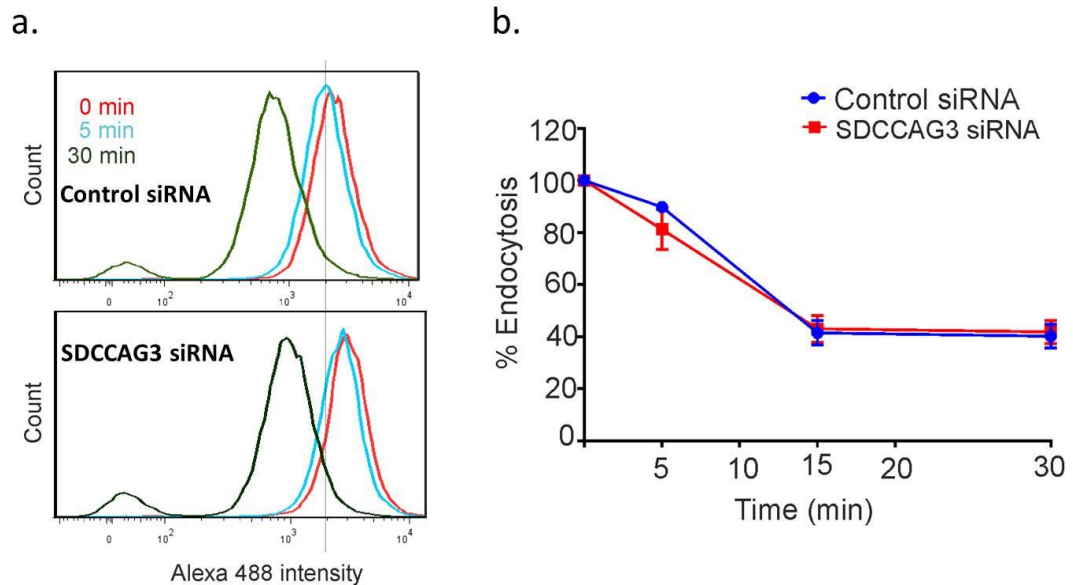


**Figure 3.15: Flow cytometry analysis of the rate of trafficking of Fas receptors.** (a) Histograms representing surface levels of Fas receptors at indicated time point in control or SDCCAG3 no.3 siRNA treated cells upon activation with agonistic Anti-Fas (CH-11) antibody (1 $\mu$ g/ml). (b) Quantification of the receptors levels remaining on the surface after various time points represented as % endocytosis. Data was obtained from three independent experiments (n=3) and analysed using Tukey's multiple comparisons test. Data was not found to be significantly different. Error bars represent  $\pm$ s.e.m

### 3.3.3.2 Rate of internalization upon stimulation with a non-agonistic antibody

HeLa cells treated with control or SDCCAG3 no. 3 siRNA were stimulated with a non-agonistic Anti-Fas (ZB4) antibody for various time points to observe changes in the surface levels of Fas receptors. As expected, no substantial internalization was induced upon activation with a non-agonistic antibody even after 30 minutes of incubation. Therefore, this data proved that loss of surface population of FasR upon stimulation with an agonistic antibody was specifically due to internalization induced and not due to antibody diffusion. Although both the antibodies bind to the same target, ZB4 is an IgG molecule and so it is incapable of inducing receptor

oligomerization which is essential for internalizing FasR. In contrast, Anti-Fas (CH-11) is an IgM molecule that is able to cluster FasR quickly and efficiently to induce internalization.

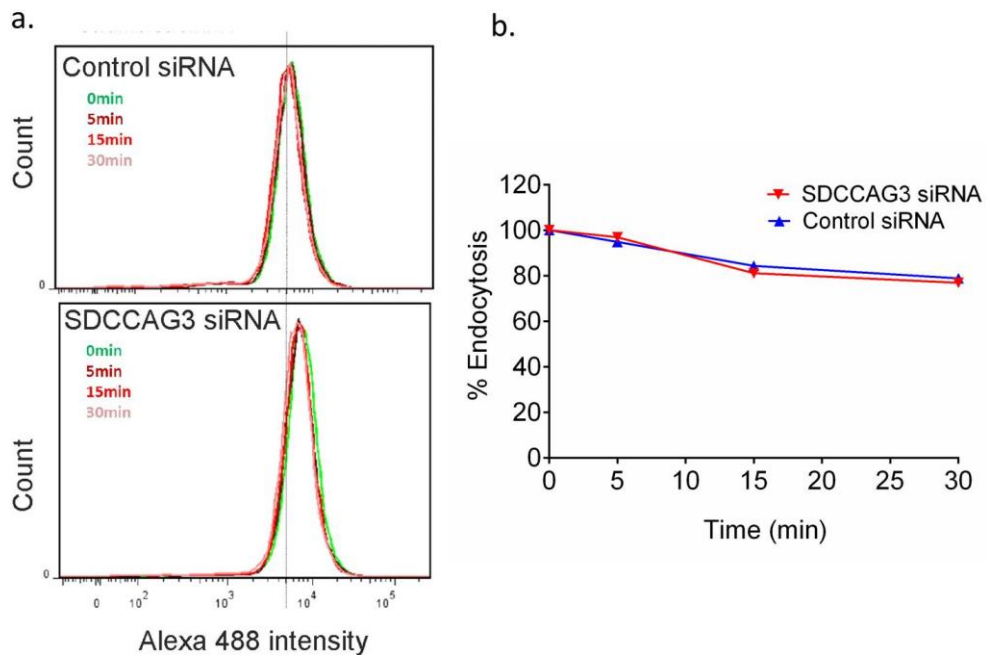


**Figure 3.16 Trafficking of FasR upon stimulation with a non-agonistic antibody.** (a) Flow cytometry analysis of HeLa cells upon stimulation with Anti-Fas (ZB4) antibody under different experimental conditions as indicated. Histograms represent surface level intensity. (b) Quantification of the histograms obtained in a. Changes in the levels of the surface population of Fas receptors were not significant. Tukey's multiple comparison tests, n=3, error bars represent  $\pm$ s.e.m.

### 3.3.4 Effect on the basal level of overexpressed Fas receptors upon SDCCAG3 knockdown

For transient overexpression of Fas receptors in HeLa cells, a construct was generated containing an N-terminus HA tag and an extracellular EGFP tag placed before the transmembrane domain. The modular structure of the construct used has been described below in Figure 3.17.

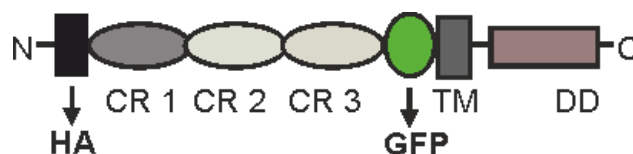


**Figure 3.17 The modular structure of Fas receptor construct.** The construct design displaying N-terminus HA tag (black) and EGFP tag (green) placed before the transmembrane domain (TM). Three cysteine rich regions on the extracellular domain are labelled are CR 1, 2 and 3. Cytoplasmic death domain (DD) is at the C-terminus end.

Transient transfection of HA-EGFP-Fas construct revealed localization of overexpressed Fas on the surface after 72 hours of transfection along with control or SDCCAG3 siRNA and no co-localization with the golgi marker GM130 (Figure 3.18). Depletion of SDCCAG3 did not affect the plasma membrane localization of overexpressed Fas receptors. Qualitative analysis of the confocal images with overexpressed FAS also revealed an increased expression level of Fas upon depletion of SDCCAG3. Therefore, it can be concluded that overexpressed Fas retained its correct localization and function.

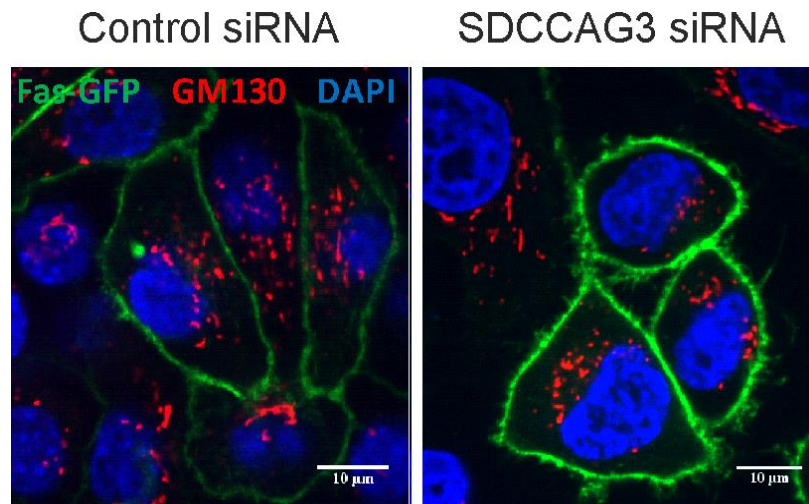


**Figure 3.18: Surface expression of FasR construct.** Representative confocal images showing surface localization of overexpressed HA-EGFP-FAS in control or SDCCAG3 no.3 siRNA treated HeLa cells. Scale bar represents 10μm.

#### **3.3.4.1 Depletion of SDCCAG3 increases basal expression of transiently expressed FAS receptors**

Effect of SDCCAG3 depletion on the basal levels of Fas receptors was examined by overexpressing tagged Fas receptors in HeLa cells in the presence of SDCCAG3 or control siRNA. Quantitative fluorescent microscopy was used to analyse the results. HeLa cells that overexpressed Fas receptors in the presence of SDCCAG3 siRNA

had increased expression levels of Fas as compared to control siRNA treated cells as shown in Figure 3.19 (a). However, levels of untagged overexpressed E-cadherin were unaffected by the knockdown of SDCCAG3. This was quantified in (b) which confirmed that the increased expression levels of Fas were significant. In case of E-cadherin, there was a tendency for increased expression levels upon SDCCAG3 depletion but it was not found to be significant. This data confirmed that SDCCAG3 depletion affected steady-state levels of transiently expressed Fas receptors suggesting its role in regulating constitutive trafficking and turnover of Fas receptors.

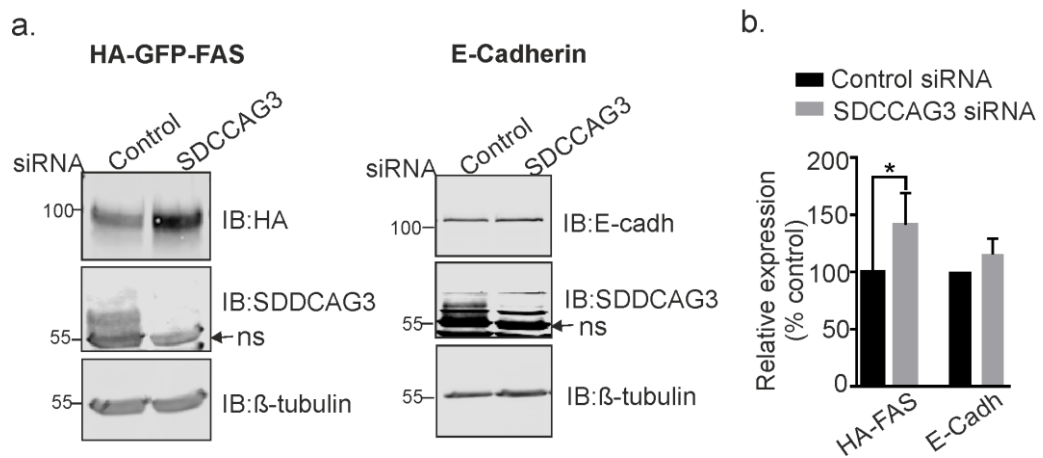


**Figure 3.19: Effect of SDCCAG3 depletion on basal levels of EGFP-SDCCAG3.** (a) Representative Immunoblots of the steady-state levels of tagged Fas receptors and untagged E-cadherin receptors transiently expressed in HeLa cells treated with SDCCAG3 no. 3 or control siRNA. SDCCAG3 was blotted to confirm the knockdown efficiency and β-tubulin was used as a loading control. ns stands for non-specific. (b) Quantification of the expression levels in (a). Unpaired student's t-test, n=3, \*p<0.05, p=0.0246 for HA-Fas and p=0.1132 for E-cadherin, error bars represent ±s.e.m.

### 3.3.4.2 Depletion of SDCCAG3 delays rate of degradation of HA-GFP-FAS

Rate of turnover of transiently expressed Fas was analysed in HeLa cells treated with control or SDCCAG3 siRNA. Cells were stimulated with an agonistic Anti-Fas (CH-11) antibody (500 ng/ml) for various time points in the presence of cycloheximide (100 μM). Activated HA-GFP-Fas receptors were internalized and their kinetics of turnover was analysed by quantitative fluorescent western blotting. Quantification of the percentage of receptors remaining revealed that within 30 minutes of stimulation, Fas receptors were down-regulated and then upregulated again after 1 hour even in

the presence of cycloheximide as shown in figure 3.20 (b). After 2 hours, only 56% receptors were remaining in control siRNA treated samples but in case of SDCCAG3 knockdown, at least 80% receptors were remaining. Differences in the amount of receptors after 1 hour and 2 hours of stimulation were found to be significant. This delay in the rate of Fas receptor turnover upon stimulation indicated a requirement for SDCCAG3 in post-endocytic trafficking of Fas receptors.

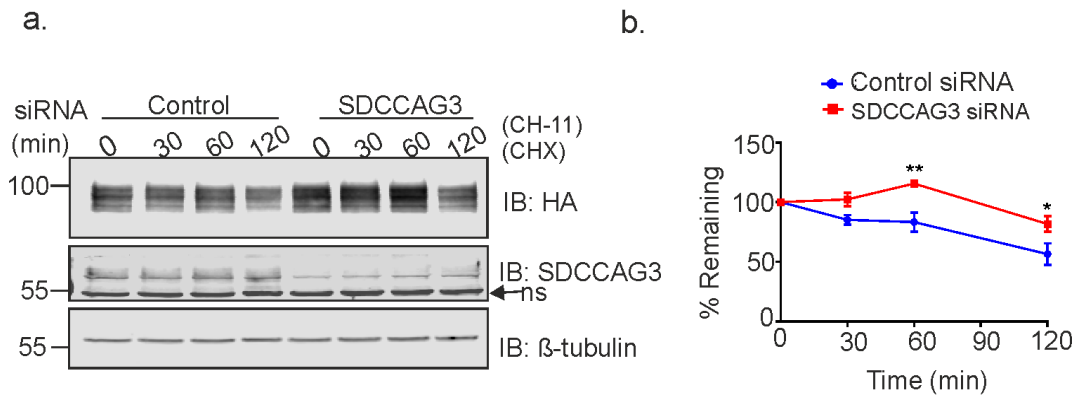


**Figure 3.20: Rate of degradation of EGFP-SDCCAG3.** (a) Immunoblot analysis of the kinetics of HA-GFP-FAS degradation following agonist stimulation in control or SDCCAG3 no.3 siRNA treated HeLa cells. SDCCAG3 was analysed for its knockdown efficiency and  $\beta$ -tubulin was used as a loading control. ns stands for non-specific. (b) Quantification of remaining surface receptors expressed as a percentage in terms of control and normalized with  $\beta$ -tubulin. Sidak's multiple comparisons test was used,  $n=3$ , error bars represent  $\pm$ s.e.m.

### 3.3.5 SDCCAG3 co-localizes with internalized Fas receptors and sorts them into Late Endosomes/Lysosomes.

#### 3.3.5.1 SDCCAG3 co-localizes with internalized Fas receptors

In order to investigate the role of SDCCAG3 in the regulation of Fas receptor trafficking more closely, internalized Fas receptors were examined for co-localization with SDCCAG3. Surface Fas receptors were labelled with the agonistic anti-Fas (CH-11) antibody in HeLa cells and chased for various time points. At 0 minutes, only the surface population of Fas receptor was labelled and hence no co-localization was observed between endogenous puncta of SDCCAG3 and surface Fas (Figure 3.21,a). Multiple studies have shown Fas receptor to undergo fast internalization (within 2 to 5 minutes) in some cell lines while no internalization has been reported for some cell lines upon stimulation. However, in this study,

intracellular puncta of Fas receptors could be seen inside the cells after 5, 15 and 30 minutes of stimulation in contrast with 0 minutes. Therefore, HeLa cells used in this study showed internalization of Fas receptors upon their stimulation. In consistence with the previous literature, SDCCAG3 also showed intracellular punctate staining. A fraction of internalized Fas receptors co-localized with SDCCAG3 as shown below. Partial overlap could be seen between Fas receptors (green) and SDCCAG3 (red).

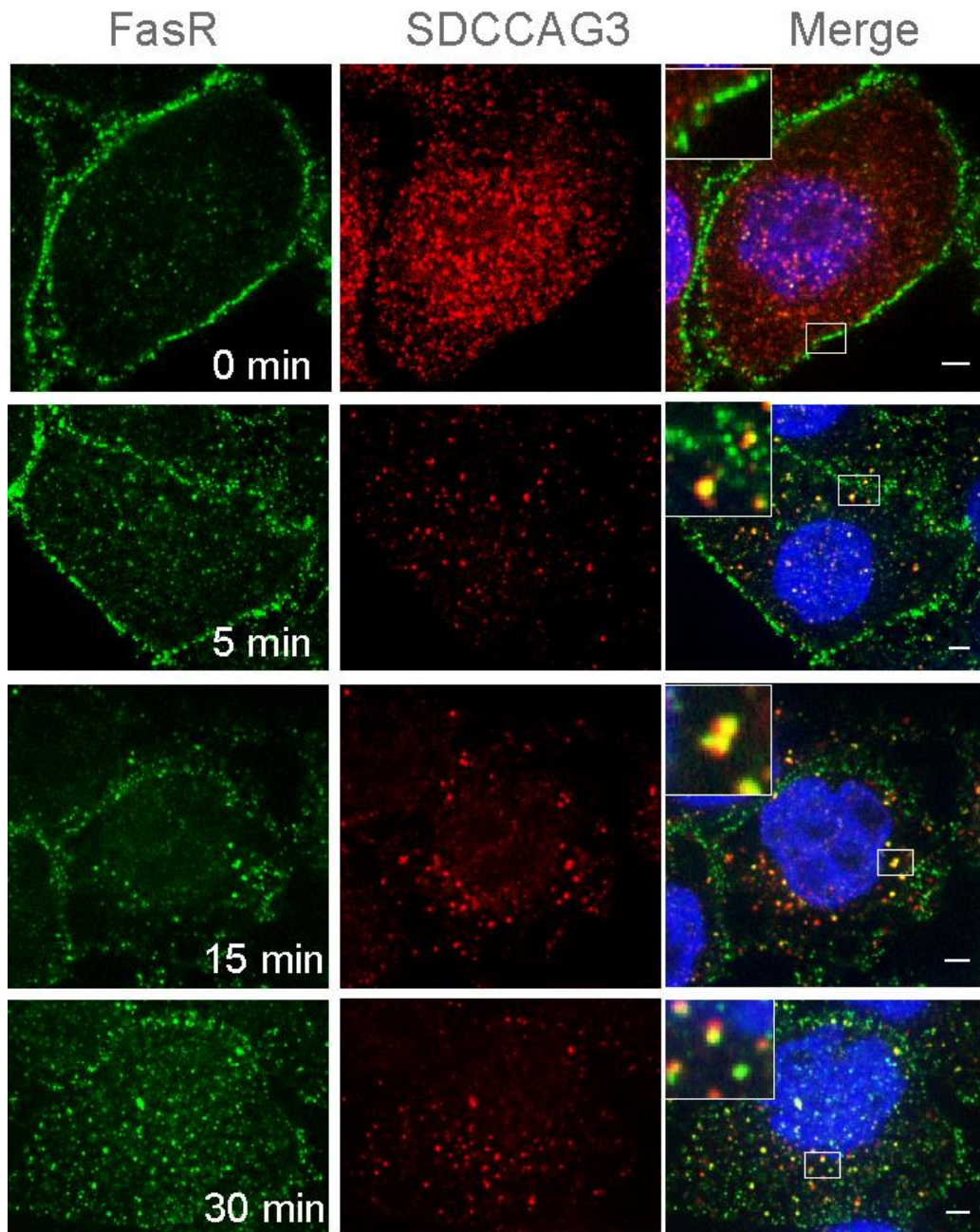


**Figure 3.21: Analysis of co-localization between internalized FasR and SDCCAG3.** (a) Immunofluorescence analysis of co-localization between Fas receptors (green) and

SDCCAG3 (red). Fas receptors were surface labelled with Anti-Fas (CH-11) antibody (1µg/ml) and were allowed to internalize for the indicated time points. Cropped inset panels show examples of non-existent (0 min) or existent co-localization. Images were acquired with a confocal microscope. Scale bars, 5µm.

Quantification of the correlation coefficient from at least five to eight cells revealed an increase in the incident of co-localization between FasR and SDCCAG3 after stimulation as compared to 0 minutes. (i), Figure 3.22. The extent of co-localization increased constantly up to 15 minutes after which it decreased again (ii). The increase was due to the presence of more internalized receptors after 5 minutes in SDCCAG3 positive compartment. Correlation coefficient value represents the correlation between the two intensities and does not quantify the degree of overlap.

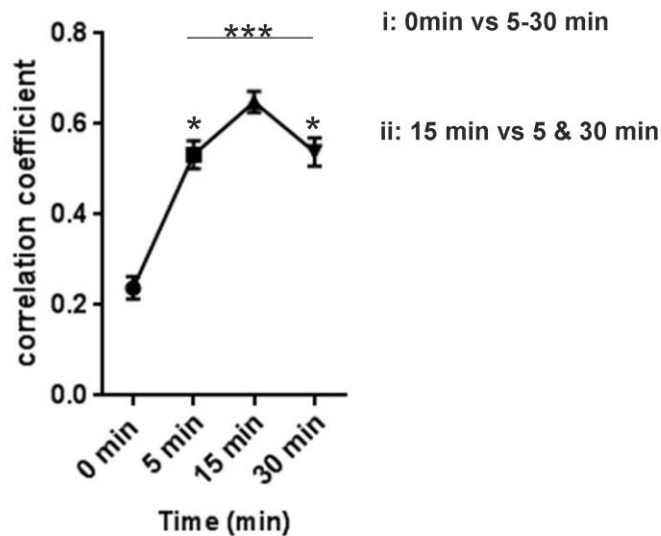


**Figure 3.22: Quantification of co-localization between internalized FasR and SDCCAG3.** Data obtained in figure 3.21 was analysed for co-localization by using Just another co-localization plugin (JACoP) in image J to calculate correlation coefficients. Data was analysed from 5-8 cell using Tukey's multiple comparison tests, \* $p < 0.05$ , \*\*\* $p < 0.01$ .

### 3.3.5.2 Sub-cellular localization of SDCCAG3 and internalized Fas receptors

Previous studies have shown that SDCCAG3 co-localizes with EEA-1 and transferrin positive compartments. It also co-localized with Vps35 which is known to be present in early/sorting endosomes. Therefore, sub-cellular localization of internalized FasR and SDCCAG3 in early endosomes was confirmed by staining for early endosomal compartments with anti-EEA-1, a classic marker for early

endosomes. As expected, after 5 minutes of internalization, puncta positive for FasR and SDCCAG3 were shown to be present in EEA-1 positive compartments. Two examples have been highlighted below in insets 1 and 2 (figure 3.23). Partial overlap was observed between SDCCAG3 and internalized FasR in the EEA-1 positive compartments as indicated in the previous data as well. This data indicates that SDCCAG3 might regulate trafficking of Fas receptor soon after its internalization into early endosomes. Since SDCCAG3 depletion did not alter the rate of internalization of FasR, therefore, it raises a possibility that SDCCAG3 might be regulating post-endocytic sorting of Fas receptors in the early endosomes.

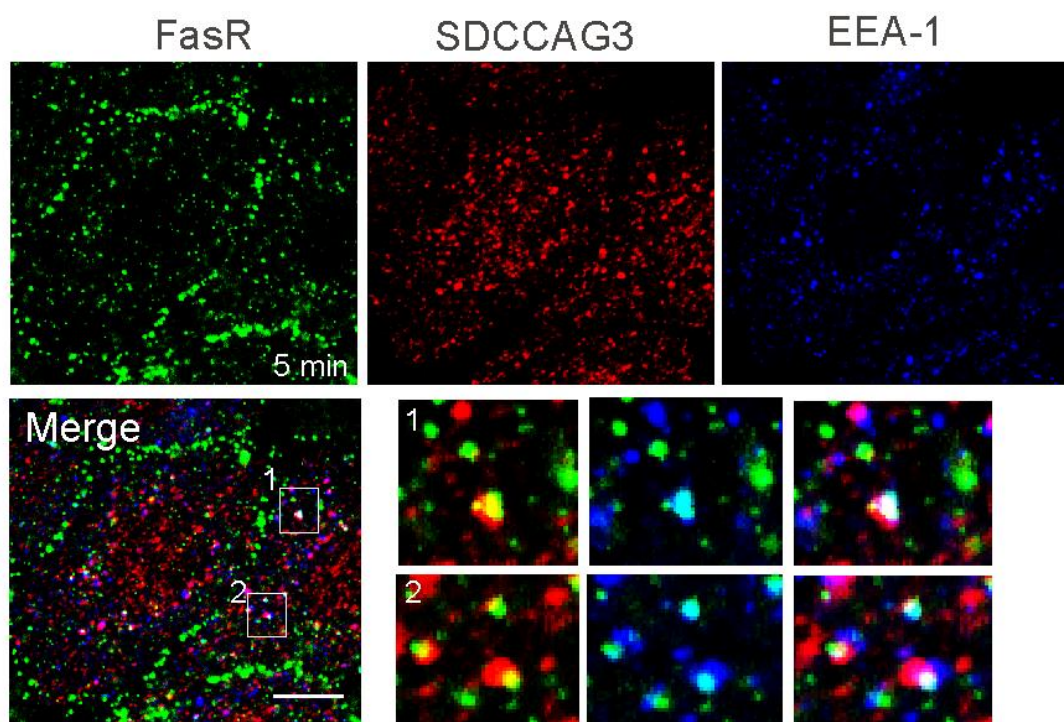


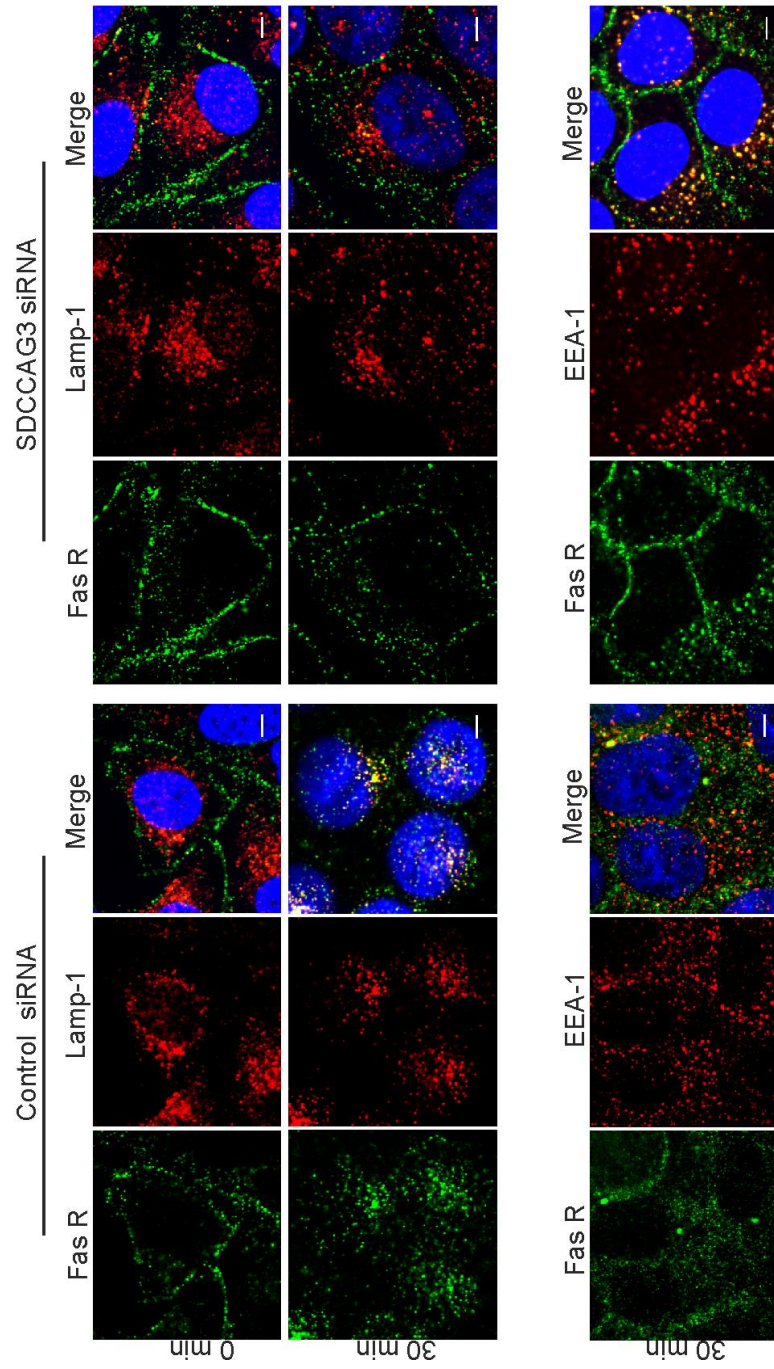
**Figure 3.23: Subcellular localization of internalized FasR and SDCCAG3:** HeLa cells were incubated with anti-Fas (CH-11) at 0°C to label only the surface population of FasR. The cells were then incubated at 37°C and chased for 5 minutes. Localization between endogenous FasR (green), SDCCAG3 (red) and EEA-1 (blue) was observed with a confocal microscope. Scale bar, 5µm.

### 3.3.5.3 SDCCAG3 sorts Fas receptors into Late endosomes/Lysosomes

To investigate if SDCCAG3 was involved in post-endocytic sorting of internalized Fas receptors in the early endosomes, intracellular distribution of FasR was examined under both stimulated and steady-state conditions. Two distinct intracellular markers -for early endosomes (EEA-1) and for late endosomes/lysosomes (Lamp-1) were used. Figure 3.24 (a) shows the distribution of internalized Fas receptors upon stimulation with agonistic Anti- Fas (CH-11) antibody in HeLa cells treated with control or SDCCAG3 siRNA. Only the surface population of Fas receptors was labelled and chased for 30 minutes in the presence of leupeptin. In control siRNA treated cells, quantitative analysis shows significant co-localization between Fas receptors and Lamp-1 after 30 minutes in contrast to 0 minutes. However, in case of SDCCAG3 knockdown, minimum co-localization was observed between Fas receptor and Lamp-1 after 30 minutes. In contrast with control siRNA treated cells where only internalized pool of Fas receptors was observed, SDCCAG3 depleted cells had both internalized and a surface pool of Fas receptors after 30 min. Co-localization analysis revealed that both the extent of co-localization and correlation between Lamp-1 and Fas receptors was significantly higher in control cells than SDCCAG3 depleted cells after 30 min as shown in the upper panel of figure 3.24 (b).

Further analysis of co-localization with EEA-1 revealed that the internalized Fas receptors in SDCCAG3 depleted cells were present in EEA-1 positive compartments as compared to control cells after 30 minutes (Figure 3.24. a) Quantification of this co-localization confirmed that a significant population of Fas receptors co-localized with EEA-1 in SDCCAG3 depleted cells as compared to control. These results suggested that SDCCAG3 is involved in sorting of Fas receptors from early endosomes to lysosomes. In the absence of SDCCAG3, Fas receptors were trapped inside the early endosomes and did not enter the late endosomes/lysosomal compartments efficiently.

a.



b.

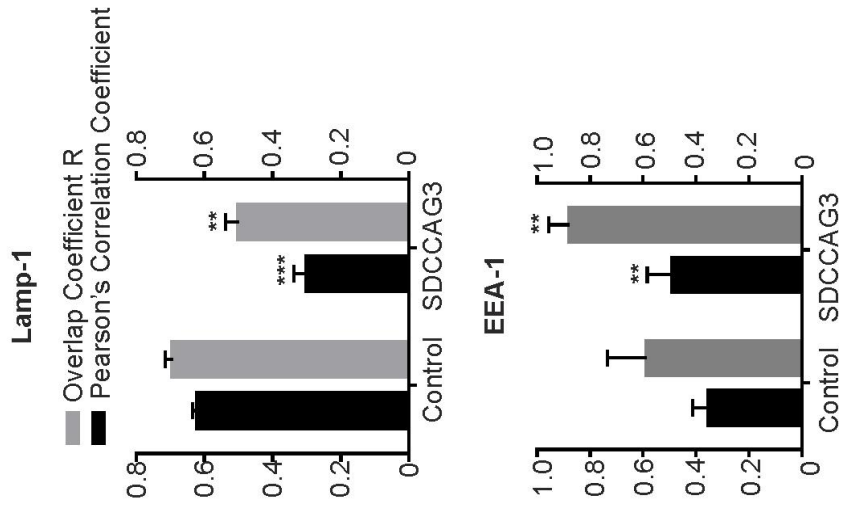


**Figure 3.24** (a) Immunofluorescence analysis of the sub-cellular localization of Fas receptors in HeLa cells upon stimulation with agonistic Anti-Fas (CH-11) antibody (1 $\mu$ g/ml) in the presence of Leupeptin (100nM) for the indicated time points. Upon internalization, Fas receptors (green) co-localized with Lamp-1 positive vesicles (red) in control siRNA treated cells in contrast with SDCCAG3 no.2 siRNA treated cells after 30 minutes of antibody chase. Additionally, Fas receptors in control cells (green) did not co-localize with EEA-1 (red) substantially as compared to the SDCCAG3 depleted cells after 30 minutes of antibody chase. Images were acquired using a confocal microscope. Scale bar represents 5 $\mu$ m. (b) Quantification of the extent of correlation (Pearson's correlation coefficient, PCC) and co-localization (Mander's overlap coefficient R) between Fas receptors and endosomal markers such as Lamp-1 and EEA-1. Co-localization analysis was performed on confocal cross-sections using JACoP (*Just another co-localization plugin*) in ImageJ. Data was collected from three independent experiments n=3, unpaired student's t-test, \*\*p<0.01, \*\*\*p<0.001, error bars represent  $\pm$ s.e.m.

Under steady-state conditions, the fate of Fas receptors was similar as compared to agonist stimulated receptors in SDCCAG3 depleted cells. A non-agonistic antibody Anti-Fas (DX-2) was fed to control or SDCCAG3 siRNA treated HeLa cells for 6 hours in the presence of leupeptin and stained for intracellular markers like EEA-1 and Lamp-1. Figure 3.25 (a) shows that internalized Fas receptors co-localized in Lamp-1 positive vesicles after 6 hours in control cells but not in SDCCAG3 depleted cells. In line with the previous result, quantification of the co-localization analysis revealed that amount of Fas receptors in Lamp-1 positive compartments was significantly higher in control cells than SDCCAG3 depleted cells (Figure 3.25.b).

In line with the previous results, steady-state distribution of internalized Fas receptors also revealed that depletion of SDCCAG3 increased co-localization between EEA-1 and Fas receptors as shown in Figure 3.25 (c) and quantified in (d).

Above described figures demonstrates that depletion of SDCCAG3 affects trafficking of Fas receptors from EEA-1 to Lamp-1 in line with the notion that during endocytic trafficking, receptors are sorted towards late endosomes/lysosomes from the early endosomes.

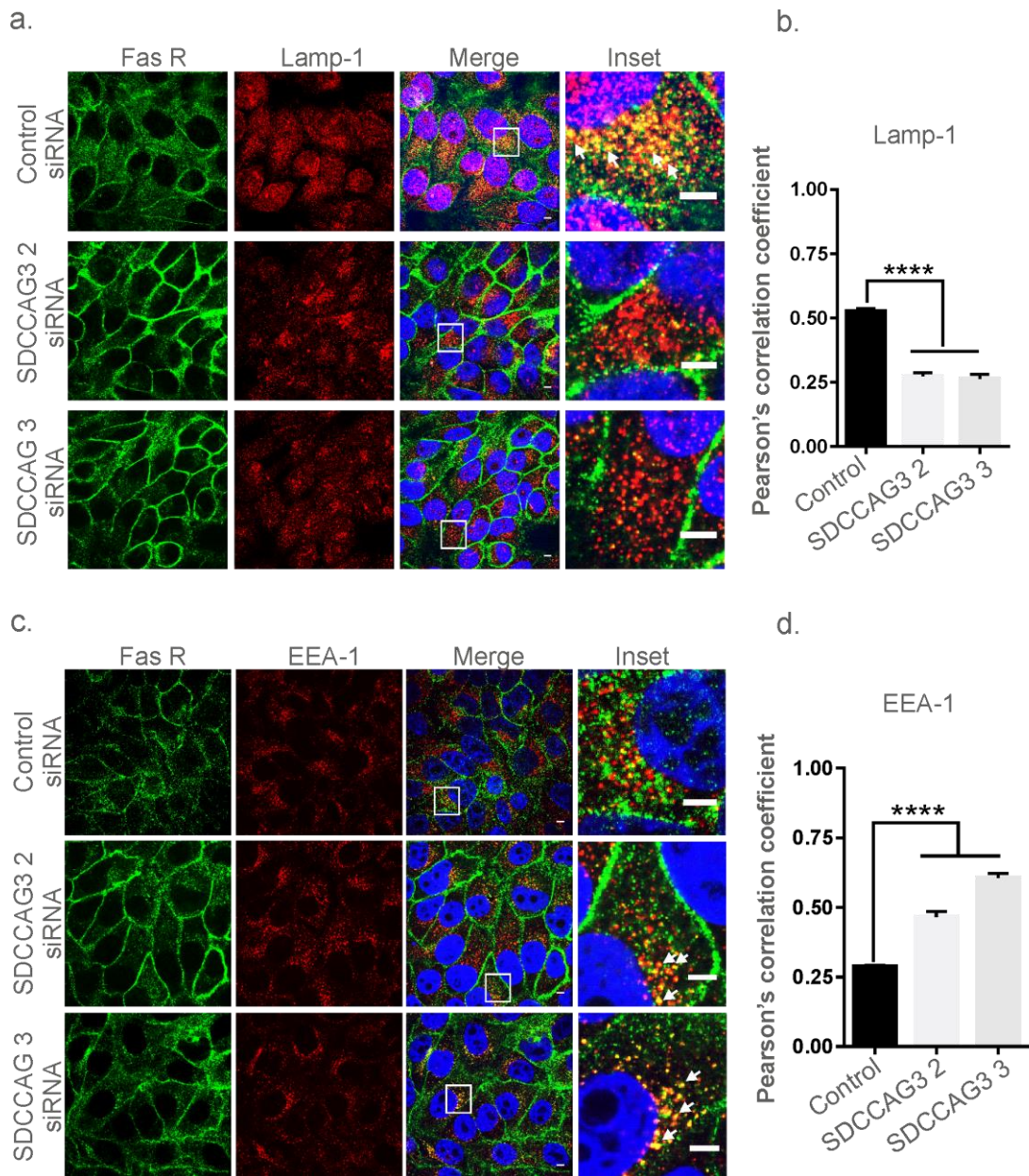


**Figure 3.25:** HeLa cells treated with control or SDCCAG3 no.2 and 3 siRNA were subjected to bath application of non-agonistic Anti-Fas (DX-2) antibody (1 $\mu$ g/ml) in the presence of Leupeptin (100nM). After 6 hours of antibody feeding, cells were fixed and stained for endosomal markers such as Lamp-1 (a) and EEA-1 (c). Arrows indicate co-localization between Fas R and Lamp-1 (a) or EEA-1 (c). Images were acquired using a confocal microscope. Scale bars represent 5 $\mu$ m (a,c). Quantification of Pearson's correlation coefficient observed between Fas receptors and Lamp-1 (b) or EEA-1 (c) under different treatment conditions. Co-localization was analysed using JACoP (*Just another co-localization plugin*) in ImageJ. At least 300 cells were analysed from three independent experiments. One way ANOVA (Dunnett's multiple comparisons test) was performed, \*\*\*\*p<0.0001, error bars represent  $\pm$ s.e.m.

## **4 Molecular mechanism of FasR sorting by SDCCAG3**

### **4.1 Introduction**

Previous data suggested a defect in the early endosome-to-lysosome transitioning of FasR upon depletion of SDCCAG3. Early endosomes act as the sorting stations that differentiate the recycling cargo from the cargo destined for degradation. The membrane of the early endosomes, populated with ubiquitinated receptors, bends and invaginates to form intraluminal vesicles (ILVs) to give rise to the multivesicular bodies enriched with cargo destined for lysosomal degradation [13]. Protein machinery involved in the sorting process to MVBs has been characterized and described extensively-the ESCRT complexes. A component of the ESCRT-0 complex, HRS, is known to be involved in sorting a wide variety of surface receptors like EGFR [39]. An ESCRT binding accessory protein called dysbindin has been described previously to connect receptors or cytoplasmic adaptor proteins to the ESCRT machinery for sorting into ILVs [59]. It mediates sorting via its interaction with HRS. Perturbations in the expression levels of dysbindin have been linked to an increased surface expression of transmembrane receptors, a phenotype similar to the one observed upon depletion of SDCCAG3 in the current study [58, 59]. Furthermore, two independent studies suggested dysbindin as an interacting partner of SDCCAG3 through proteomic screenings [156, 157]. Therefore, it was hypothesised that SDCCAG3 might be mediating ILV sorting of Fas receptors via its interaction with dysbindin and HRS.

### **4.2 Aim**

Based on the hypothesis above, the main goal of this chapter was to demonstrate if SDCCAG3 regulated sorting of Fas receptors into ILVs or not. If yes, then another aim was to examine if Dysbindin and HRS were involved in mediating this sorting.

## 4.3 Results

### 4.3.1 Depletion of SDCCAG3 delays sorting of Fas receptors into ILVs

#### 4.3.1.1 Constitutively active Rab5-GFP to create enlarged endosomal lumen

The small GTPase Rab5 has been described as the switch involved in the process of endosomal maturation from early endosomes to late endosomes/lysosomes. It mediates homotypic fusion of early endosomes through GTP-dependent recruitment and activation of various effector proteins [158]. Overexpression of GTPase defective mutant, Rab5 (Q79L), leads to the formation of enlarged endosomes as compared to the wild type Rab5 expression, shown below in figure 4.1. These enlarged endosomes have been characterised in many studies and shown to contain markers for both early and late endosomes/lysosomes. They were also described to be similar to MVEs (multivesicular endosomes) with internal vesicles [159]. The enlarged size of these endosomes defines the limiting membrane and internal vesicles distinctly which has been useful in studying sorting of various receptors into the intraluminal vesicles (ILVs). They are also useful for studying the localization of proteins in different microdomains on the endosomes [158, 159]. Therefore, enlarged endosomes were used in this study to dissect the molecular mechanism of Fas receptor sorting in detail.

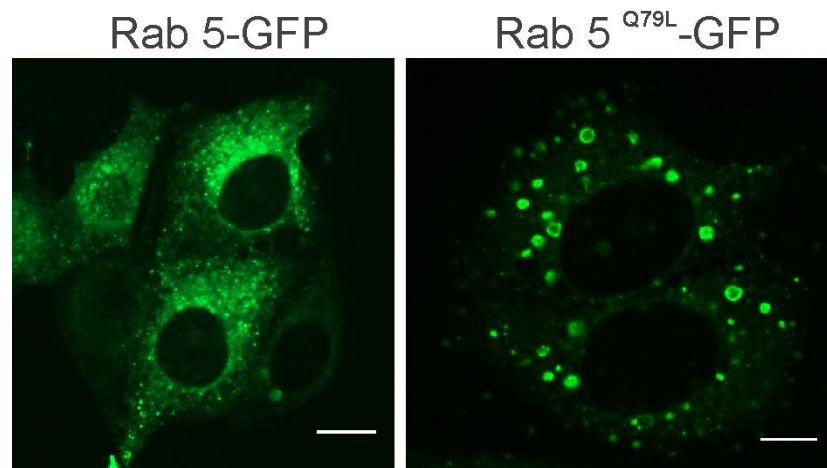


**Figure 4.1: The enlarged endosomes:** Immunofluorescence analysis of the intracellular punctate of transiently expressed Rab5-GFP as compared to the constitutively active Rab5<sup>Q79L</sup>-GFP. Images were acquired using a confocal microscope. Scale bars represent 5 $\mu$ m.

#### **4.3.1.2 SDCCAG3 promotes sorting of activated Fas receptors into Intraluminal vesicles**

Cell surface receptors that are destined for lysosomal degradation are transferred from the endosomal limiting membrane to the intraluminal vesicles (ILVs) of multivesicular bodies (MVBs). Based on the previous data, it can be concluded that Fas receptors are also destined for lysosomal degradation following internalization into early endosomes. Therefore, it was examined whether SDCCAG3 depletion affected the sorting of Fas receptors into ILVs. Constitutively active Rab5<sup>Q79L</sup> tagged with GFP was transiently expressed in HeLa cells treated with control or SDCCAG3 siRNA for 72 hours. Endogenous Fas receptors were stimulated with agonistic Anti-Fas (CH-11) antibody and examined for their intracellular localization by confocal microscopy. As shown in Figure 4.2 (a), after 2 hours of stimulation, Fas receptors (red) were present inside the lumen in case of control cells. In contrast, in SDCCAG3 depleted cells, Fas receptors localized predominantly to the limiting membranes of enlarged endosomes occupying distinct subdomains on it. Most of the endosomes exhibited minimal or no intraluminal fluorescence in SDCCAG3 depleted cells. In order to quantify the distribution of Fas receptors across the enlarged endosomes, a line scale analysis was performed on confocal cross-sections as described before. A representative line scale analysis of the endosomes highlighted in insets is shown in (b, c). The two peaks in green represent the boundary of the enlarged endosome indicating the limiting membrane. The shaded red area represents the distribution of fluorescence intensity inside the enlarged endosomes indicating Fas receptor distribution. The analysis clearly shows that in control cells Fas receptors are present inside the lumen indicated by a single peak in red in between the two peaks in green (b). In case of SDCCAG3 depleted cells, one of the peaks in green corresponded with the red peak indicating that Fas receptor was present on the boundary of the enlarged endosome (c). Figure 4.2 (d) shows a representative line scale analysis of the endosomes with normalized diameter and intensity. The peaks indicate limiting membrane and the hatched box indicates the central region of the endosomal lumen. The red line corresponding to SDCCAG3 depleted cells shows lower fluorescence in the middle region of the endosome as compared to the control cells (blue line). An analysis of ~100 endosomes from multiple cells and three different experiments revealed 45% reduction in the middle

fluorescence i.e. distribution of Fas receptors in the lumen of enlarged endosomes in case of SDCCAG3 depleted cells as compared to control cells. In conclusion, this data demonstrates the requirement of SDCCAG3 for sorting of Fas receptors into ILVs of MVBs. It is in line with the previous data and re-establishes the fact that absence of SDCCAG3 disrupts the trafficking of Fas receptors out of early endosomes to late endosomes/lysosomes.

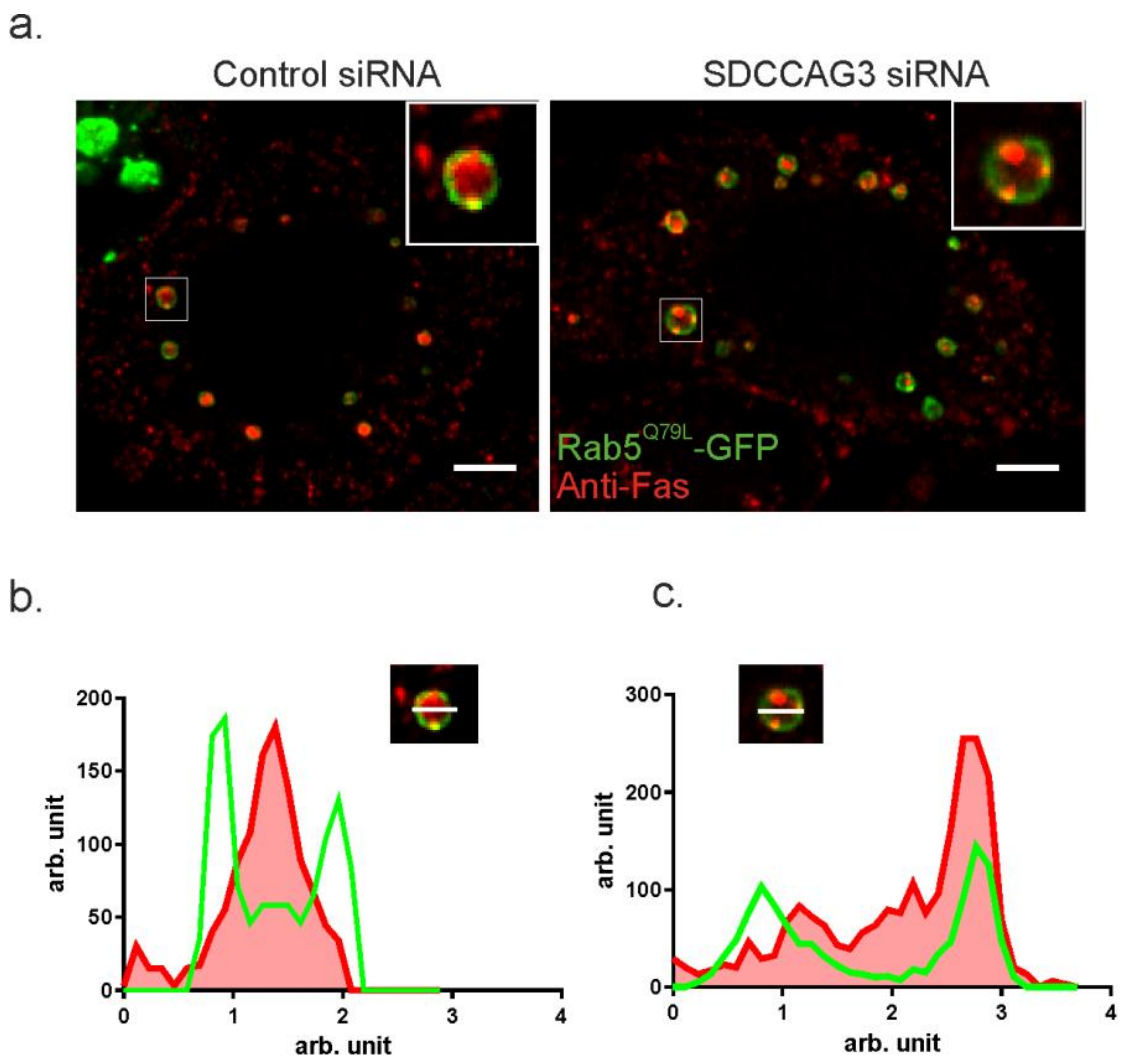
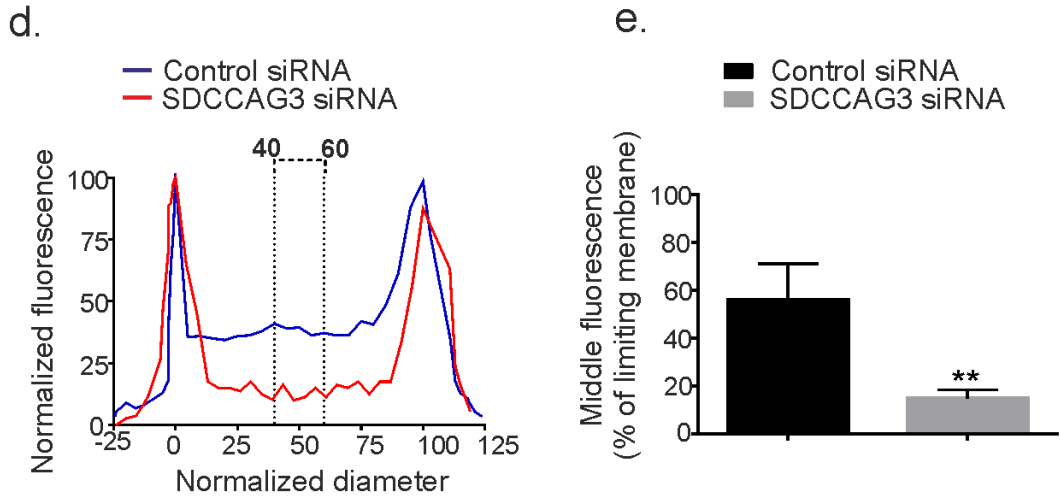


Figure 4.2 (a) Immunofluorescence analysis of re-distribution of Fas receptors from endosomal limiting membrane to intraluminal vesicles in constitutively active Rab5<sup>Q79L</sup> enlarged endosomes. Control or SDCCAG3 no.3 siRNA treated HeLa cells were transfected with Rab5 Q79L-GFP and stimulated with agonistic Anti-Fas (CH-11) antibody (1 $\mu$ g/ml) for 1 hour in the presence of Leupeptin (100nM). Cell were fixed and observed by a confocal microscope. Insets show representative expanded endosomes. Scale bar represents 5 $\mu$ m. (b, c) Representative line scale analysis of the enlarged endosomes highlighted in inset panels.



(d) Model of line scale analysis used for quantifying Fas receptors localized to intraluminal vesicles. To illustrate this model, two representative endosomes were picked randomly from the control and SDCCAG3 knockdown images. The normalized diameter represents the diameter of endosomes, where 0 and 100 correspond to the pixel distances with the highest and second highest pixel intensities, representing the limiting membranes of the endosomes. The blue and red traces represent the normalized fluorescence pixel intensity measured across the endosomes in control and SDCCAG3 depleted cells, respectively, with the maximum pixel intensity across the line normalized to 100. The region covered by a dotted line shows the normalized fluorescence values of pixels from 40-60% of the normalized diameter that was used to determine the mean intraluminal fluorescence for each endosome.

(e) Graphical representation of the compiled results of the line scale analysis for Fas receptors. Middle (40-60%) fluorescence value expressed as a percentage of the limiting membrane (normalized diameter). Unpaired student's t-test,  $n > 100$  endosomes from three independent experiments,  $**p < 0.01$ ,  $p = 0.0075$ , error bars represents  $\pm$ s.e.m.

#### 4.3.1.3 Analysis of FasR sorting with Structured Illumination Microscopy

Defects in the intraluminal sorting of FAS receptors upon depletion of SDCCAG3 was analysed further with three dimensional modelling (3D) together with ‘super-resolution’ structured illumination microscopy (SIM). Control or SDCCAG3 siRNA treated HeLa cells that also transiently expressed Rab5<sup>Q79L</sup>-GFP were processed in a similar manner as described previously. The 3D SIM characterisation of the distribution of Fas receptors in enlarged endosomal lumen further validated the previous results obtained from confocal microscopy. Qualitative analysis of the images obtained from super-resolution light microscopy revealed the distribution of Fas receptors both on the limiting membrane and inside the lumen of the enlarged endosomes in control cells. However, in SDCCAG3 depleted cells, Fas receptors were localized mostly to the limiting membrane (Figure 4.3.a)

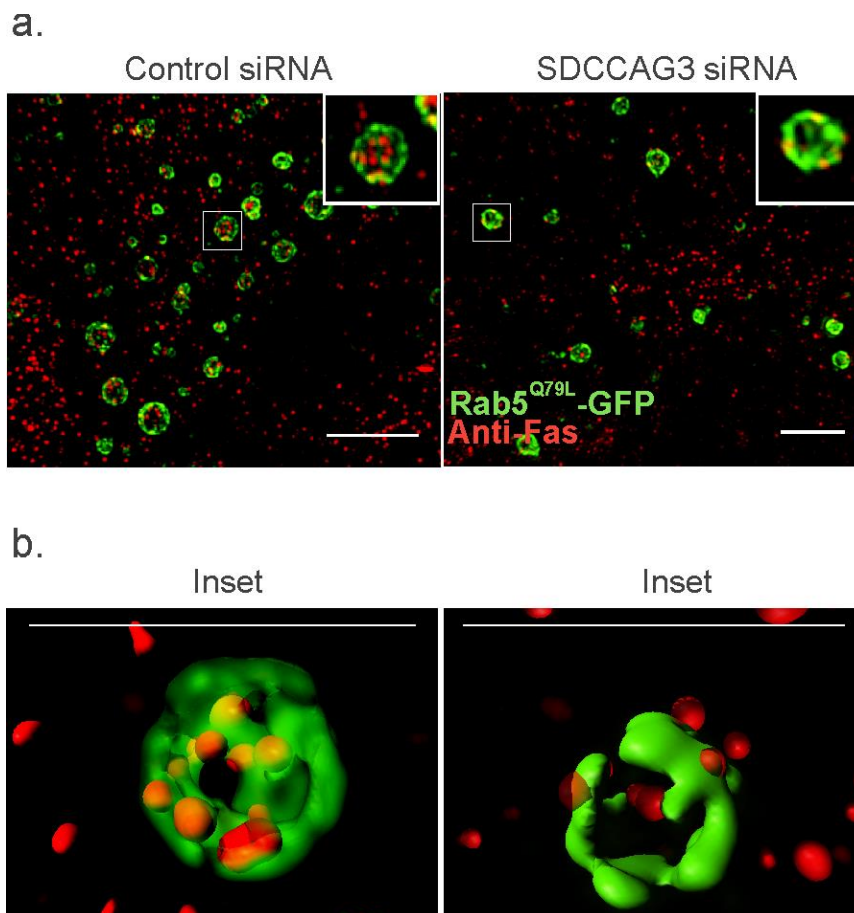


**Figure 4.3 3D-SIM analysis of FasR sorting.** (a) Immunofluorescence analysis of ILV sorting of Fas receptors in control or SDCCAG3 no.3 siRNA treated HeLa cells using 3D-Structured illumination microscopy. (b) Three-dimensional modelling of endosomes highlighted by the insets. Scale bars represent 5 $\mu$ m (a, b).

#### **4.3.1.4 SDCCAG3 knockdown delays sorting of Fas receptors into ILVs under steady-state**

Distribution of Fas receptor in enlarged endosomes under steady state was examined. Control or SDCCAG3 siRNA treated HeLa cells co-expressing Rab5<sup>Q79L</sup>GFP were fed with a non-agonistic Anti-Fas (DX-2) antibody (1µg/ml) for various time points. After 2 hours of antibody feeding, confocal cross-sections revealed that in control cells Fas receptors localized both on the limiting membrane and the lumen of the enlarged endosomes. In contrast, in SDCCAG3 depleted cells, Fas receptors localized mostly on the limiting membrane or near the periphery inside the enlarged endosomes (Figure 4.4 a). Line scale analysis of the representative endosomes highlighted in insets showed that in control cells a single peak of the red histogram indicating Fas receptors fluorescence was present in between the two green peaks indicating the limiting membrane (b). In SDCCAG3 depleted cells, the peak of the red histogram representing Fas receptor fluorescence corresponded with one of the green peak indicating that receptor is present on the limiting membrane (c). Line scale analysis from several endosomes was quantified and analysed for the distribution of Fas receptors across the enlarged endosomes. The graphical representation of the analysis shows that fluorescence intensity of Fas receptor in control cells was at least 30% higher than SDCCAG3 depleted cells. This difference was found to be statistically significant.

In conclusion, this data is in line with the previous data showing requirement of SDCCAG3 for intraluminal sorting of Fas receptors.

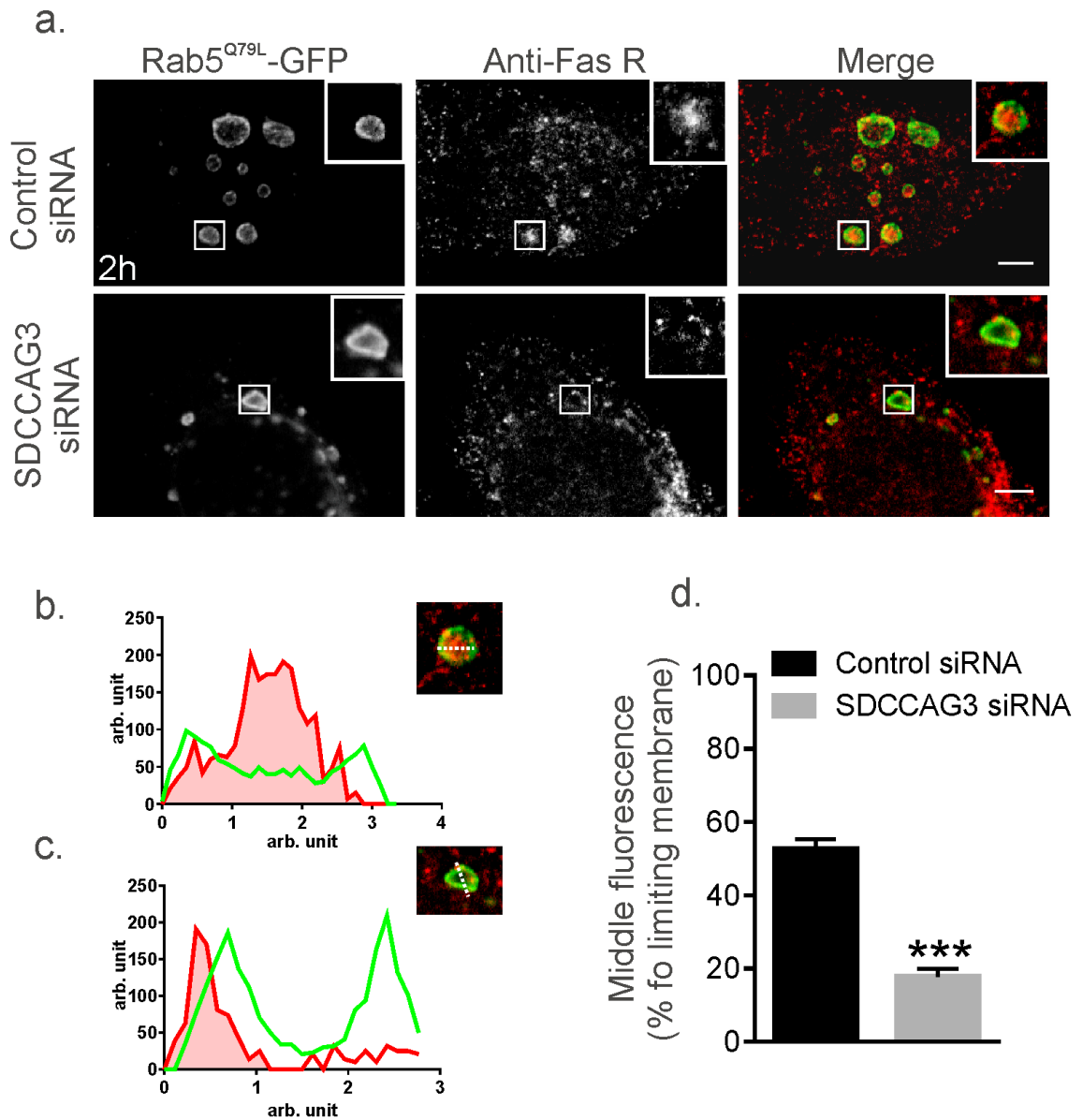


**Figure 4.4** (a) Representative confocal cross sections depicting the distribution of Fas receptors labelled by feeding Anti-Fas (DX-2) antibody for 2 hours in the presence of leupeptin (100 nM) to HeLa cells treated with control or SDCCAG3 no. 3 siRNA and co-expressing Rab5<sup>Q79L</sup>GFP. Examples of the enlarged endosomes have been cropped and shown in insets. Scale bars represent 5 $\mu$ m. (b, c) Line scale analysis of the enlarged endosomes highlighted in the insets. (d) Graphical representation of the quantification of fluorescence intensity of Fas receptor in the lumen of the enlarged endosomes expressed as a percentage. Data was collected from at least 50 endosomes from multiple cells and three different experiments (n=50, N=3). Unpaired student's t-test was performed, two-tailed, \*\*\*\*p<0.0001, error bars represent  $\pm$ s.e.m.

Additionally, ILV sorting of Fas receptors under steady state was analyzed at a later time point such as after 6 hours of antibody feeding. Qualitative analysis of the data shown in Figure 4.5 (a) revealed that in case of both control and SDCCAG3 siRNA, Fas receptors localized in the lumen of the enlarged endosomes predominantly. Quantification of this data confirmed that the difference between the mean fluorescence intensity of Fas receptors across the enlarged endosomes in control and SDCCAG3 knockdown samples was not statistically significant (b). This data demonstrates that depletion of SDCCAG3 only caused a delay in the distribution of Fas receptors from the limiting membrane to the endosome but did not inhibit the process completely. Therefore, it can be concluded that absence of SDCCAG3 was essential for sorting of Fas receptors into ILVs at a normal rate but not an absolute requirement for their sorting.

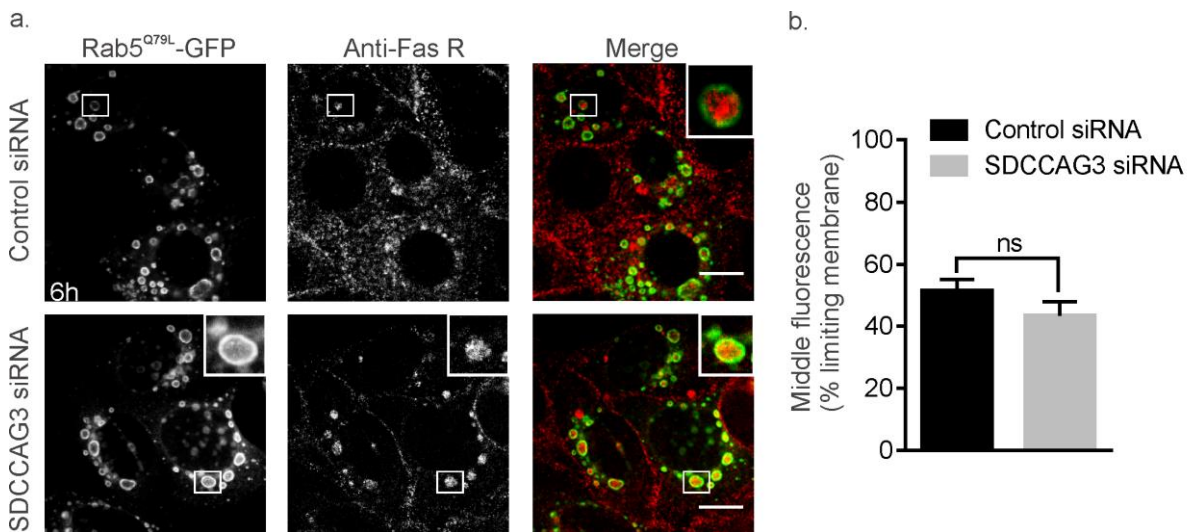


**Figure 4.5** (a) Representative confocal cross sections depicting distribution of Fas receptors labelled by feeding Anti-Fas (DX-2) antibody for 6 hours in the presence of leupeptin (100 nM) to HeLa cells treated with control or SDCCAG3 no. 3 siRNA and co-expressing Rab5<sup>Q79L</sup>GFP. Examples of the enlarged endosomes have been cropped and shown in insets. Scale bars represent 5 $\mu$ m. (b, c) Line scale analysis of the enlarged endosomes highlighted in the insets. (d) Graphical representation of the quantification of fluorescence intensity of Fas receptor in the lumen of the enlarged endosomes expressed as a percentage. Data was collected from at least 30 endosomes from multiple cells and three different experiments (n=30, N=3). Unpaired student's t-test was performed, two-tailed, p=0.15, error bars represent  $\pm$ s.e.m.

#### **4.3.1.5 SDCCAG3 knockdown does not affect sorting of Transferrin**

Transferrin (Tf) is an iron-binding protein which binds to its receptor called Tf receptor to undergo endocytic trafficking to early endosomes. It delivers iron and then is sorted to be recycled back to the cell surface. It represents an alternative trafficking fate than Fas receptors which were found to be entering late endosomes/lysosomes. Hence, Alexa Fluor 555 conjugated transferrin (Tf-555) was examined for any sorting defects upon depletion of SDCCAG3 in order to investigate whether its depletion affected other receptors following different endocytic pathways or not. HeLa cells treated with control or SDCCAG3 siRNA and co-expressing Rab5<sup>Q79L</sup>GFP were stimulated with recombinant Tf-555 for 1 hour in the presence of leupeptin (100nM). Figure 4.7 (a) shows that Tf-555 localized on the limiting membrane of the enlarged endosomes predominantly in case of both control and SDCCAG3 siRNA depleted cells. Line scale analysis of the representative endosomes highlighted in the insets also showed that peaks of the red histogram (indicating Tf-555 fluorescence) corresponded with the peaks of the green histogram (indicating the limiting membrane) in both control (b) and SDCCAG3 siRNA treated cells (c). Quantification of the middle fluorescence for several endosomes from multiple cells and different experiments also confirmed that there was no significant difference between the mean middle fluorescence of Tf-555 in control and SDCCAG3 siRNA treated cells (d).

In conclusion, depletion of SDCCAG3 did not alter the post-endocytic trafficking route of transferrin receptors. This data was consistent with the previous observation in the current study which stated that depletion of SDCCAG3 did not affect cell surface or total levels of transferrin receptors in HeLa cells.

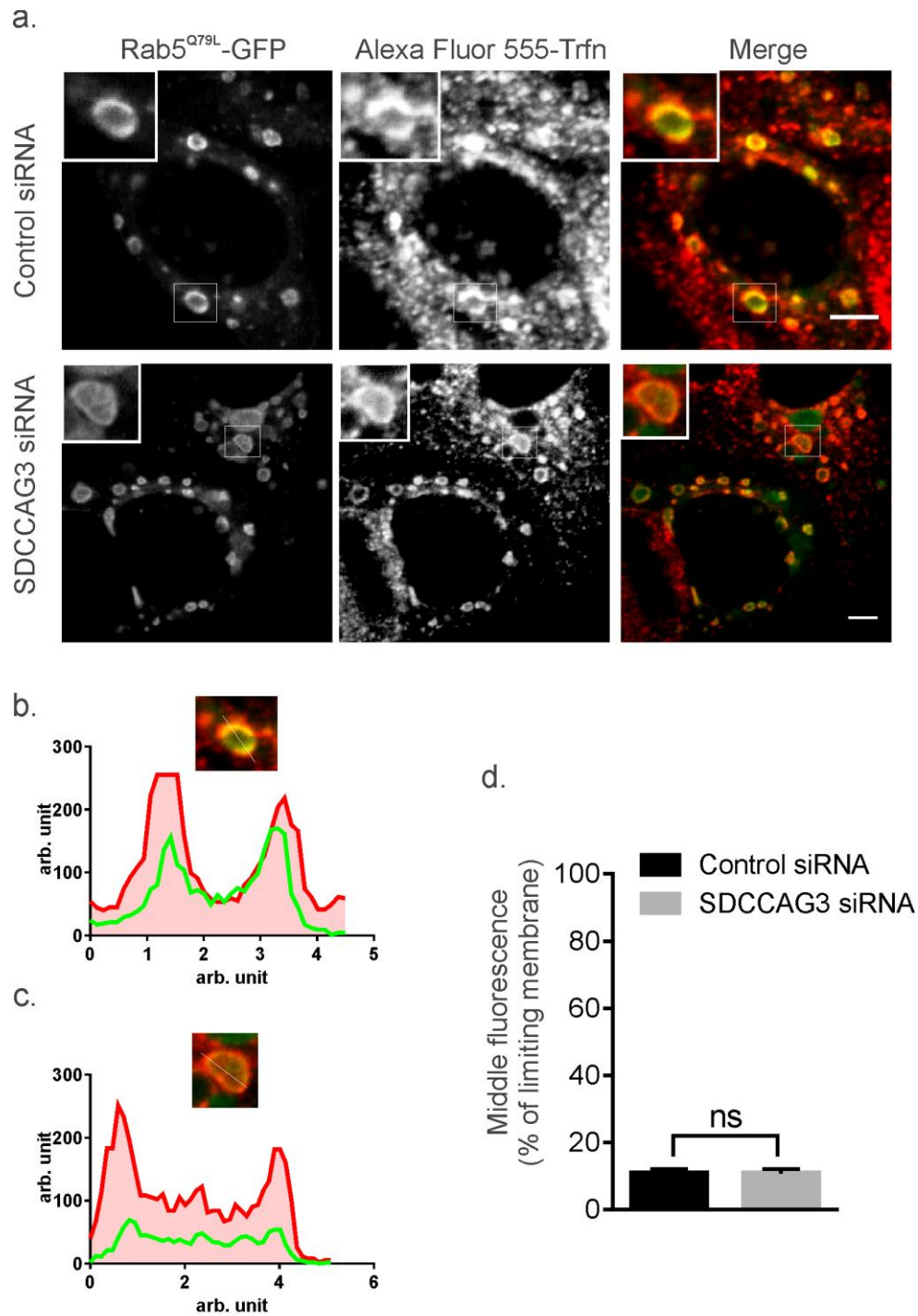


**Figure 4.6** (a) Confocal cross sections depicting distribution of Alexa Fluor 555 conjugated Transferrin after 1 hour of stimulation in the presence of leupeptin (100 nM) in HeLa cells treated with control or SDCCAG3 no. 3 siRNA and co-expressing Rab5<sup>Q79L</sup>GFP. Scale bars represent 5 $\mu$ m. (b, c) Line scale analysis of the enlarged endosomes highlighted in the insets. (d) Graphical representation of the quantification of middle fluorescence intensity of Trfn-555 expressed as a percentage. Unpaired student's t-test (n=50,N=3), two-tailed, \*p<0.05, p=0.98, ns stands for not significant, error bars represent  $\pm$ s.e.m.

#### **4.3.1.6 SDCCAG3 knockdown does not affect sorting of EGF receptor**

Endocytic trafficking of EGF receptors has been characterized extensively. These receptors internalize upon stimulation with their ligand and enter into tubulovesicular compartments known as sorting endosomes from where they can be either recycled back to the plasma membrane or sorted via MVBs into lysosomes for degradation. Downregulation of EGF receptor is also important for negatively regulating anti-apoptotic signalling mediated by it. Therefore, the effect of SDCCAG3 depletion on the lysosomal sorting of EGFR was analysed. Alexa 647 conjugated recombinant EGF was used to stimulate the internalization of EGFR. After 1 hour of stimulation of HeLa cell co-expressing Rab5<sup>Q79L</sup>GFP and treated with control or SDCCAG3 siRNA, distribution of EGF across the enlarged endosomes was analysed. Figure 4.7 (a) shows that in case of both control and SDCCAG3 siRNA, EGF was localized either inside the lumen or on the limiting membrane of the enlarged endosomes. Line scale analysis of the representative endosomes shows that peaks of the red histogram indicating fluorescence intensity of EGF was in between the peaks of the green histogram (indicating the limiting membrane) and also corresponded with the peaks in both control (b) and SDCCAG3 depleted cells (c). Quantification of the distribution of mean fluorescence intensity for EGF was not found to be significantly different in case of control or SDCCAG3 knockdown cells (d). At the given time point and concentration of the EGF used for this experiment, only ~20% of the total EGF fluorescence was found to localize to the middle of the enlarged endosomal lumen.

In conclusion, EGFR sorting was not affected by the absence of SDCCAG3. This data was in line with the previous observation in the current study that depletion of SDCCAG3 had no effect on the surface or total levels of EGFR.

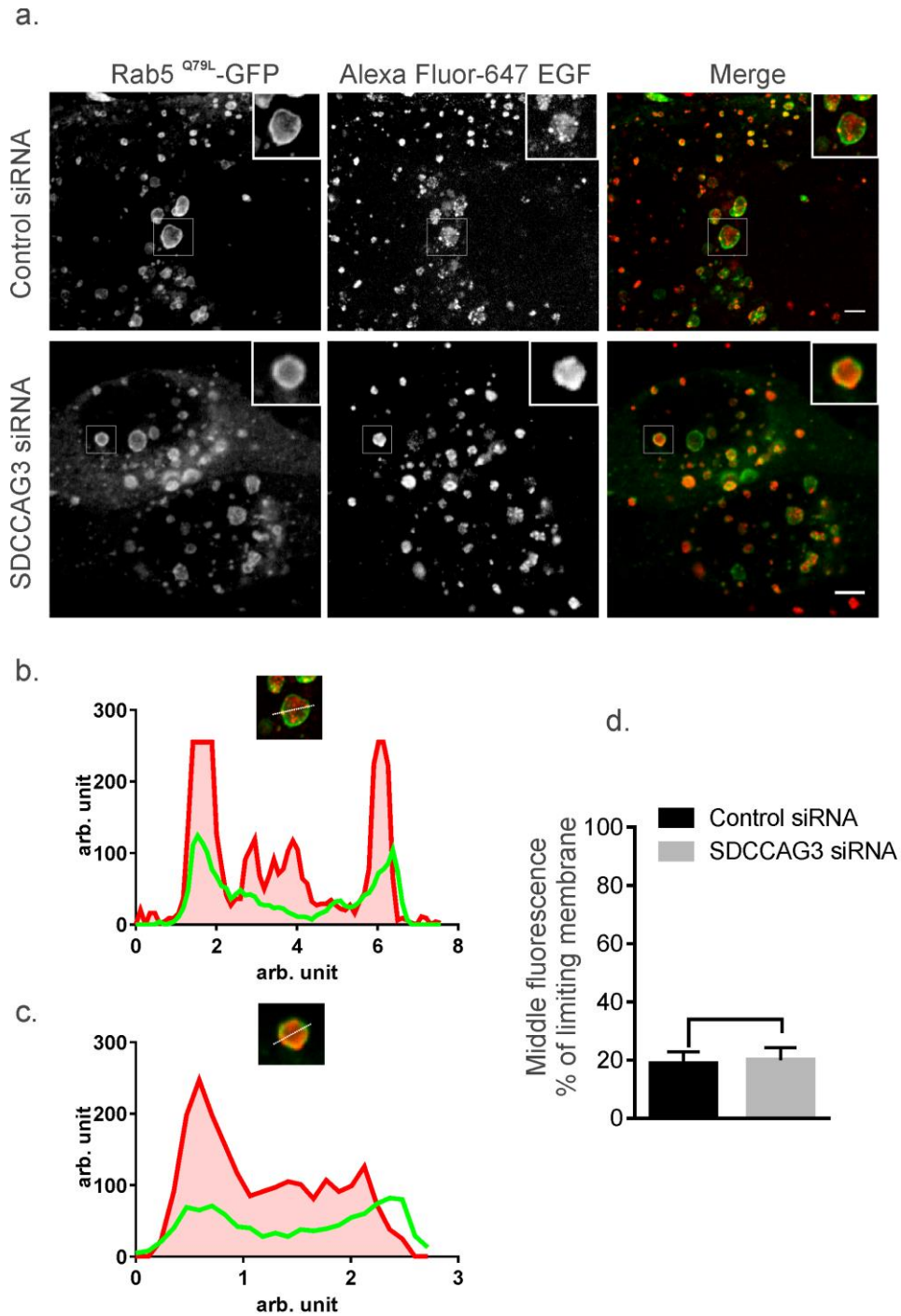


**Figure 4.7** (a) Confocal cross sections depicting distribution of Alexa Fluor 647 conjugated EGF after 1 hour of stimulation in the presence of leupeptin (100 nM) in HeLa cells treated with control or SDCCAG3 no. 3 siRNA and co-expressing Rab5<sup>Q79L</sup>-GFP. Scale bars represent 5 $\mu$ m. (b, c) Line scale analysis of the enlarged endosomes highlighted in the insets. (d) Graphical representation of the quantification of middle fluorescence intensity of EGF-647 expressed as a percentage. Unpaired student's t-test (n=33, N=3), two-tailed, \*p<0.05, p=0.829, ns stands for not significant, error bars represent  $\pm$ s.e.m.

### 4.3.2 Molecular machinery involved in sorting Fas receptors

#### 4.3.2.1 SDCCAG3 interacts with Dysbindin

To decipher the molecular mechanism by which SDCCAG3 regulates sorting of Fas receptors, an association of SDCCAG3 with endosomal sorting machinery was examined. Two studies employing proteomic approaches, immunoprecipitation, and affinity capture-mass spectrometry, identified dysbindin as the interaction partner of SDCCAG3 [156, 157]. Dysbindin drew our attention as it interacts directly with the core sorting machinery component HRS (ESCRT-0). It has been described previously as an accessory protein linking GPCRs to ESCRT machinery [58, 59]. Therefore, the interaction between SDCCAG3 and Dysbindin was tested. Lysate from HeLa cells was incubated with GST tagged SDCCAG3 protein on glutathione agarose beads. Endogenous dysbindin was affinity precipitated as a 50 kDa band with GST-SDCCAG3 pulldown only and not with GST on beads alone. Therefore, this data confirmed the interaction between SDCCAG3 and dysbindin as suggested previously.

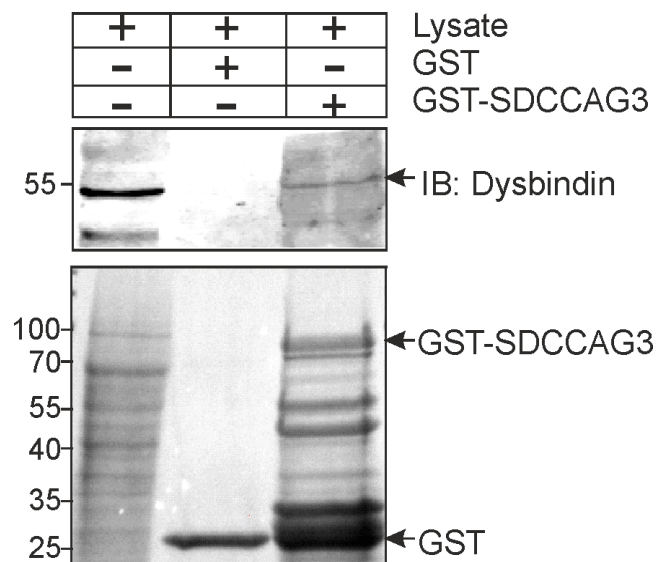


**Figure 4.8:** Immunoblot analysis of affinity precipitation of endogenous Dysbindin with GST-SDCCAG3 immobilized on glutathione sepharose beads in HeLa cells. Input represent 10% of the total lysate. GST and GST-SDCCAG3 bands were stained with Ponceau S and labelled with an arrow.

#### 4.3.2.2 Localization of SDCCAG3 and Dysbindin on endosomes

Next, it was examined whether SDCCAG3 and dysbindin co-localize together to form a complex as suggested by the above data. To visualize the distribution of SDCCAG3 and dysbindin on endosomes easily, constitutively active Rab5<sup>Q79L</sup>GFP was used to create enlarged endosomes. These endosomes enabled localization of SDCCAG3, dysbindin, and HRS on the limiting membrane easily. Intracellular localization of endogenous SDCCAG3 was examined in HeLa cells treated with control or SDCCAG3 siRNA and co-expressing Rab5<sup>Q79L</sup>GFP. SDCCAG3 localized to the limiting membrane of the enlarged endosomes only in control cells and not in SDCCAG3 depleted cells (Figure 4.9). Therefore, the staining pattern observed for endogenous SDCCAG3 was specific.

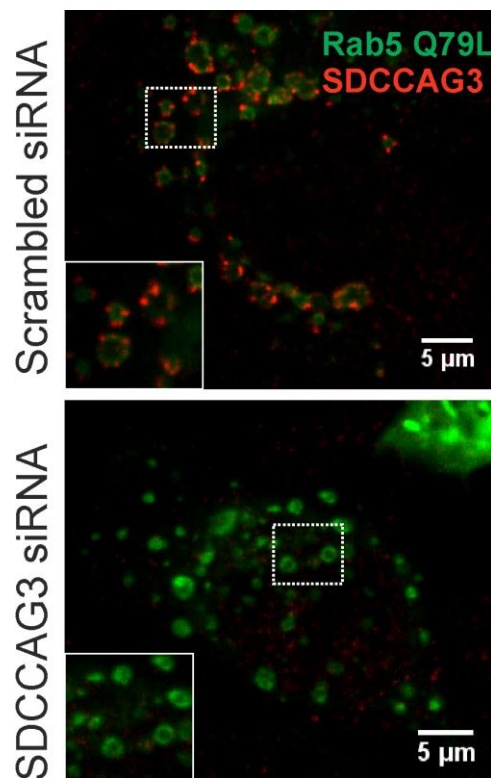


**Figure 4.9:** Immunofluorescence analysis of localization of endogenous SDCCAG3 on Rab5<sup>Q79L</sup> mediated enlarged endosomes in HeLa cells treated with control or SDCCAG3 no.3 siRNA. Endosomes were labelled with GFP and SDCCAG3 was labelled with Alexa 594 secondary antibody. Confocal cross sections show localization of SDCCAG3 (red) on the enlarged endosomes in control cells only. Cropped panels highlight the representative examples. Scale bars, 5μm.

Furthermore, localization of dysbindin and HRS was also examined. HeLa cells co-expressing Rab5<sup>Q79L</sup>GFP and dysbindin-flag were imaged using a confocal microscope. Qualitative analysis of the cross-sections revealed that dysbindin occupied distinct microdomains on these enlarged endosomes (Figure 4.10.a). In line with the previous studies, HeLa cells transiently expressing HRS showed uniform staining all over the boundary of the endosomes (b). Next, co-localization between SDCCAG3 and dysbindin or HRS was analysed by confocal microscopy. Representative cross-sections showed that puncta of endogenous SDCCAG3 co-localized with the puncta of transiently expressed dysbindin-flag on the enlarged endosomes (c). Since HRS-RFP localized evenly on the surface of the endosomes therefore, it was present in the SDCCAG3 containing microdomains of the endosomes as well (d).

Thus, this data suggest that the complex formed between SDCCAG3 and dysbindin might be present in the HRS positive endosomes. Additionally, the presence of HRS confirmed the early endosomal origin of the artificially created enlarged endosomes. Taken together, this data supports the hypothesis that SDCCAG3 might form a complex with dysbindin in the early/sorting endosomes in order to regulate ESCRT mediated sorting of Fas receptors into ILVs. However, further analysis of the role of dysbindin and HRS in mediating sorting of Fas receptors was required to support this hypothesis.

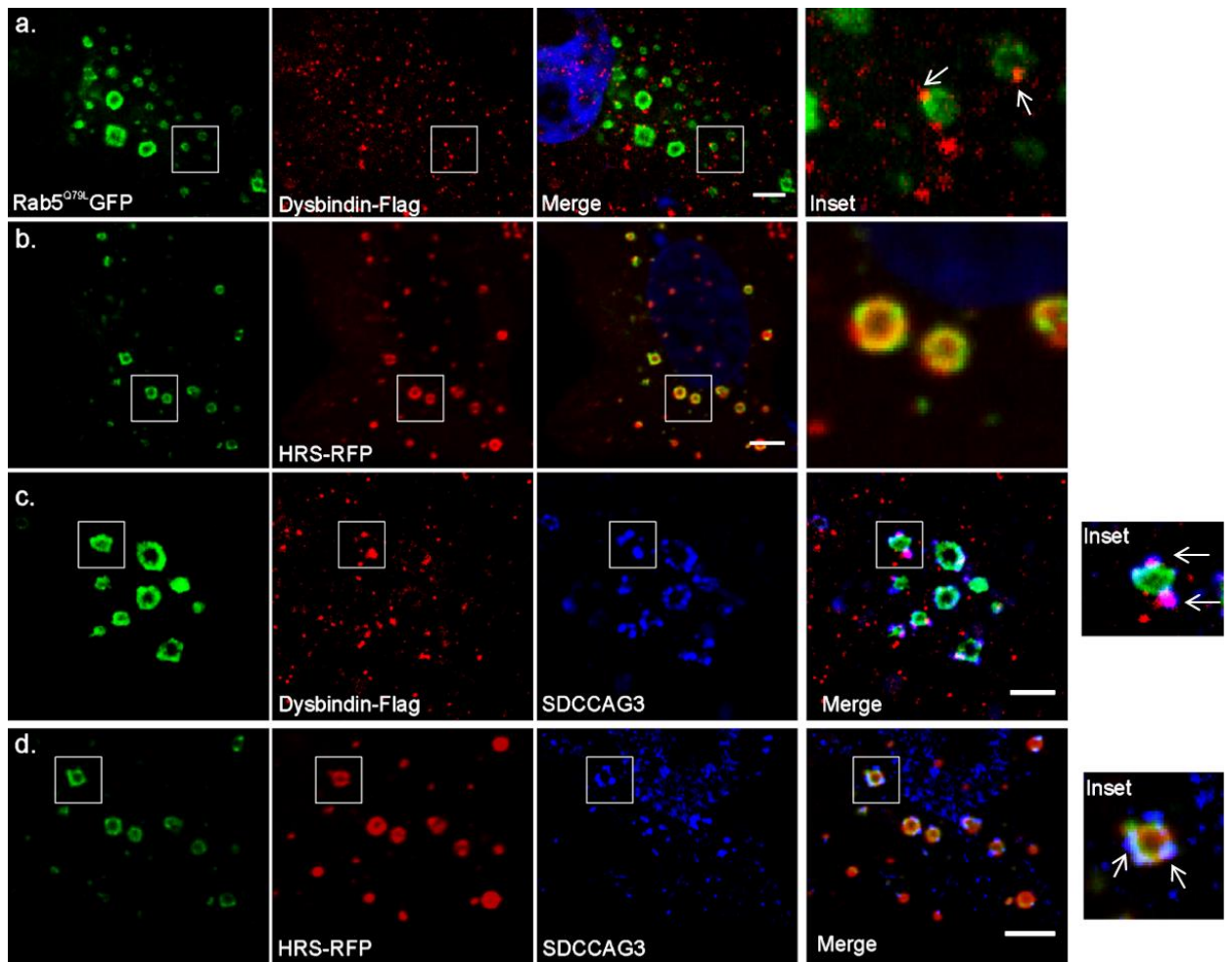


**Figure 4.10:** Immunofluorescence analysis of intracellular localization of SDCCAG3, Dysbindin and HRS. (a) Confocal cross sections of HeLa cells co-expressing Rab5<sup>Q79L</sup> GFP (green) and Dysbindin-Flag (red) show localization of Dysbindin on the boundary of the enlarged endosomes (inset) as indicated by the arrows in inset panel. (b) Representative confocal image showing presence of HRS on the enlarged endosomes in HeLa cells co-expressing Rab5<sup>Q79L</sup>GFP (green) and HRS-RFP (red). (c) Triple labelling in HeLa cells co-expressing Rab5<sup>Q79L</sup>GFP (green) and Dysbindin-Flag (red), and stained for endogenous SDCCAG3 (blue). SDCCAG3 co-localized with Dysbindin on the enlarged endosomes as indicated by the arrows in inset panel. (d) Triple labelling in HeLa cells co-expressing Rab5<sup>Q79L</sup>GFP (green) and HRS-RFP (red), and stained for endogenous SDCCAG3 (blue). Arrows indicate locations on the enlarged endosomes where SDCCAG3 co-localized with HRS. Scale bars represent 5 $\mu$ m.

#### **4.3.2.3 SDCCAG3 regulates sorting of Fas receptors via Dysbindin-HRS endocytic sorting machinery**

To further investigate the association of SDCCAG3 with dysbindin and HRS, surface levels of Fas receptors were examined upon their depletion. It was hypothesised that if dysbindin and HRS are forming a complex to regulate Fas R trafficking then their depletion should have an effect on its trafficking. HeLa cells were treated with control, dysbindin and HRS siRNA and surface levels were observed via flow cytometry. Figure 4.11 (a) shows histograms representing fluorescence intensity of the surface Fas receptors under different treatment conditions as indicated. As compared to the control siRNA treated cells, levels of surface Fas receptors increased upon depletion of dysbindin and HRS. Double knockdown of dysbindin and SDCCAG3 also showed elevated levels of Fas receptors as expected. However, the amount of increase in Fas R surface levels upon double knockdown was comparable to dysbindin only knockdown suggesting that SDCCAG3 and dysbindin act along the same pathway in regulating intracellular trafficking of Fas R. Quantification of the surface levels confirmed that the increase in the surface levels of Fas R was significantly higher in dysbindin, HRS and double knockdown of SDCCAG3 + dysbindin as compared to the control siRNA treated cells (b). Efficiency of the knockdown was also confirmed in all the treated cells (c).

This data strongly suggest that SDCCAG3 forms an endocytic complex with dysbindin and HRS to regulate intracellular trafficking of Fas receptors which in turn affects its surface presentation in HeLa cells.

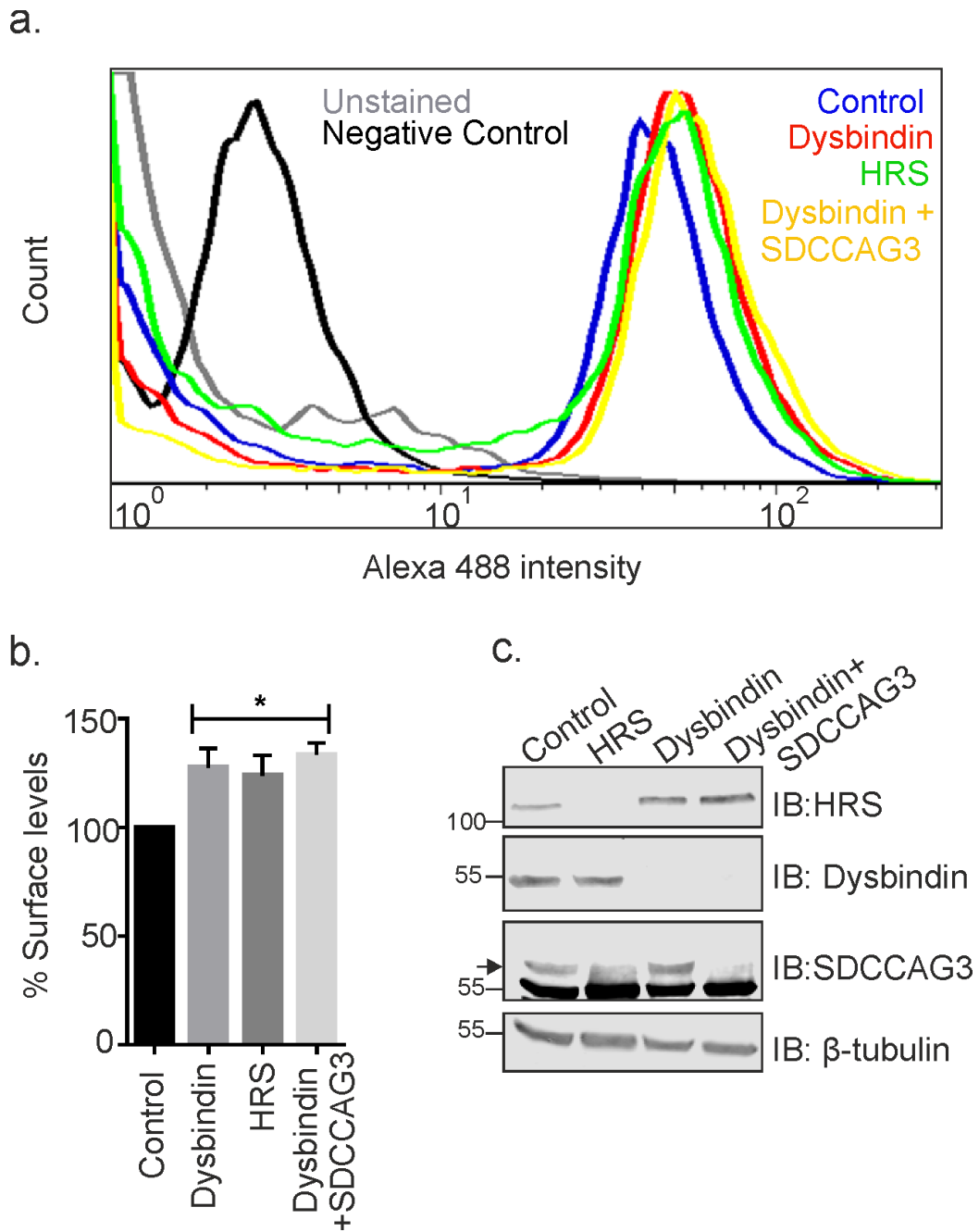


**Figure 4.11:** (a) Flow cytometry analysis of the surface levels of Fas R in dysbindin, HRS and dysbindin + SDCCAG3 siRNA treated HeLa cells. Surface Fas R were labelled with Anti-FAS (DX-2) antibody for 1 hour on ice. Alexa-488 conjugated secondary antibody was used to analyse the surface intensity via FACSCalibur™. Only secondary antibody staining was used as the negative control. (b) Quantification of the fluorescence intensity of labelled surface Fas R in HeLa cells. One way-ANOVA, Dunnett's multiple comparisons test from three independent experiments (n=3), \*p<0.05, p=0.0254, error bars represent  $\pm$ s.e.m. (c) Immunoblot analysis of the knockdown efficiency of the indicated proteins. The arrow indicates endogenous SDCCAG3 band.  $\beta$ -tubulin was used as a loading control.

#### **4.3.2.4 Dysbindin and Hrs are involved in the same pathway as SDCCAG3 to regulate intracellular trafficking of Fas receptors**

Since depletion of dysbindin and HRS affected intracellular trafficking of Fas R therefore, it was hypothesised that they might be involved in intraluminal sorting of Fas R into MVBs in the same manner as SDCCAG3. To monitor any such ILV sorting defect, HeLa cells that transiently expressed Rab5<sup>Q79L</sup>GFP were treated with control, dysbindin and HRS siRNA. Cells were then stimulated with agonistic Anti-Fas (CH-11) antibody for 1 hour in the presence of leupeptin as described before. Qualitative analysis of the immunofluorescence data in Figure 4.12 (a) showed that after 1 hour of stimulation Fas receptors in the lumen of the enlarged endosomes in case of control cells. In contrast, dysbindin siRNA treated cells showed localization of Fas R mostly on the limiting membrane but some amount of fluorescence was also observed inside the lumen. Consistent with the previous literature, depletion of HRS led to a redistribution of Fas receptors in the limiting membrane of the enlarged endosomes predominantly. Fas receptors that localized on the limiting membrane occupied discrete subdomains on them and did not stain the limiting membrane uniformly. More than 50 endosomes were quantified from three independent experiments for each sample and line scale analysis was performed to calculate the fluorescence intensity of Fas receptors in the middle of the lumen that was expressed as % middle fluorescence. Quantification of the middle fluorescence as shown in (b) confirmed that depletion of dysbindin and HRS led to defects in intraluminal sorting of Fas receptor as compared to the control significantly. Depletion of HRS had a larger impact on the sorting of Fas receptors into MVBs as compared to dysbindin depletion.

This data proves that Fas receptor sorting is affected by dysbindin and HRS which act together as a sorting complex. It also strongly support the hypothesis that SDCCAG3 mediates Fas R sorting via dysbindin-HRS endocytic machinery.

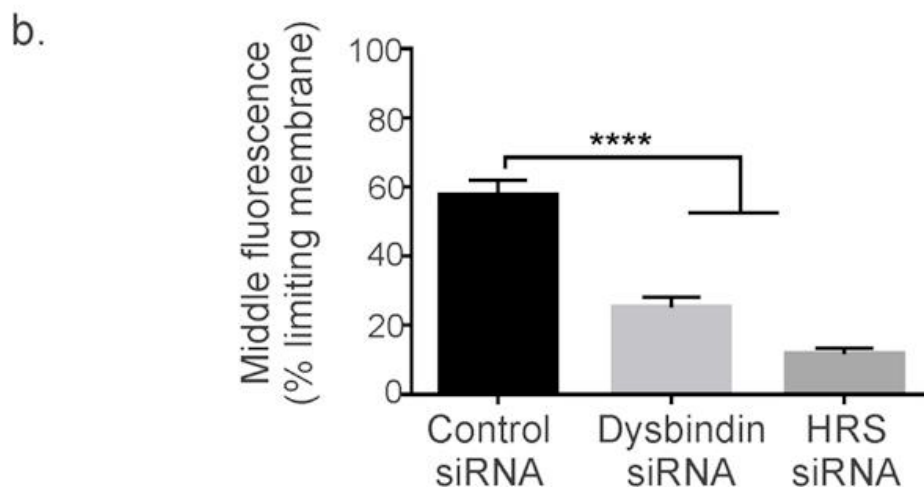
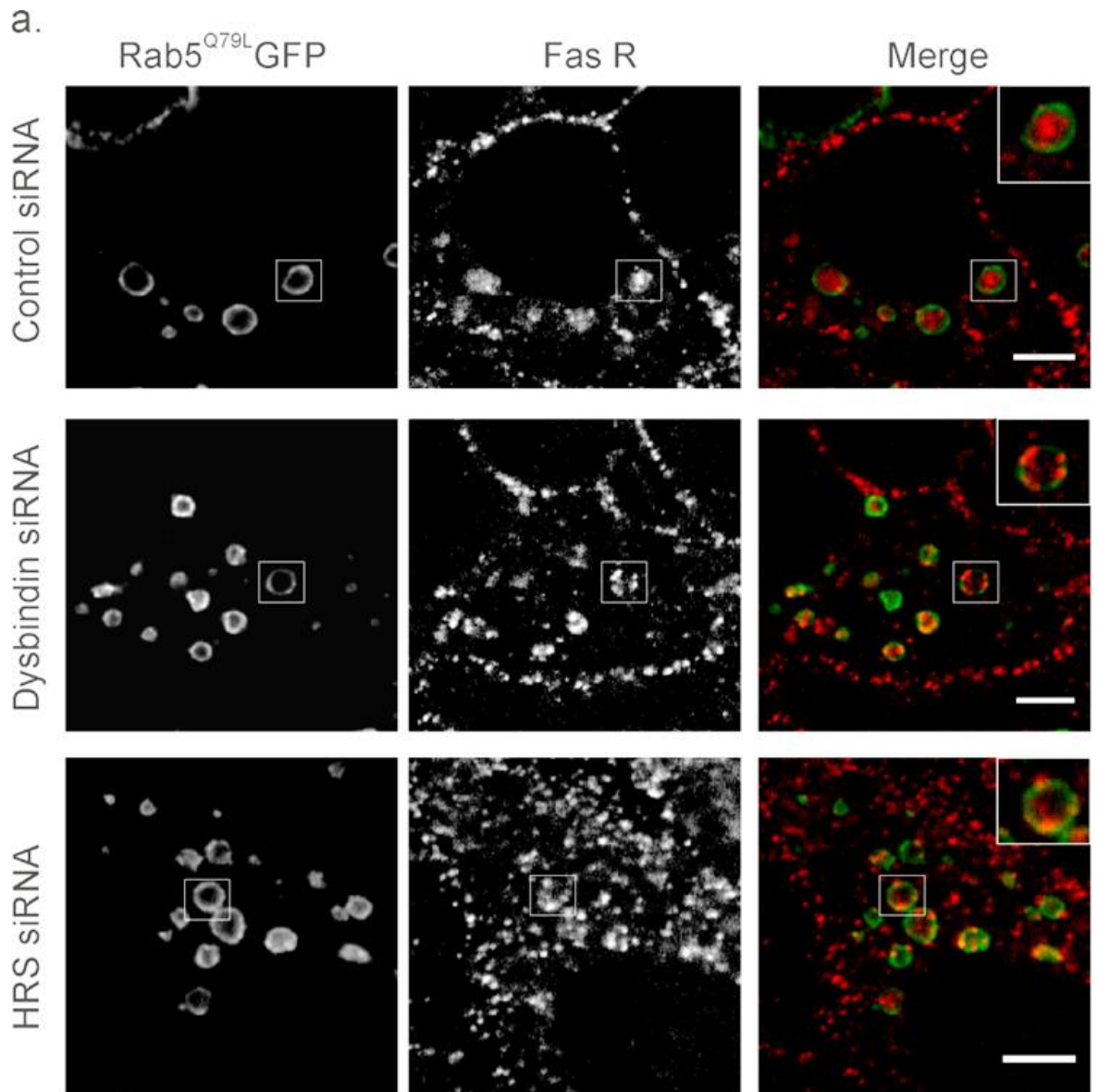


**Figure 4.12:** (a) Immunofluorescence analysis of ILV sorting of Fas receptors into MVBs in control, dysbindin and HRS siRNA treated HeLa cells co-expressing Rab5<sup>Q79L</sup>GFP. Cells

were stimulated with agonistic Anti-Fas (CH-11) antibody (1 $\mu$ g/ml) for 1 hour in the presence of leupeptin (100nM) and stained with Alexa-594 conjugated secondary antibody. Images were acquired using a confocal microscope. Representative confocal cross sections have been displayed for each treatment condition as indicated. Examples of the cropped endosomes have been highlighted in insets. Scale bars represent 5 $\mu$ m in all the panels. (b) Graphical representation of the fluorescence intensity of Fas receptors found in the lumen of the enlarged endosomes and expressed as a percentage. Quantification was done using line scale analysis in Image J as described before. Data was collected from three independent experiments and analysed using One way ANOVA, Dunnett's multiple comparisons test, n=52, \*\*\*\*p<0.0001, error bars represent  $\pm$ s.e.m.

## 5 Role of SDCCAG3 in apoptotic signalling

### 5.1 Introduction

Once stimulated by its ligand, Fas receptors cluster together on the surface to initiate downstream apoptotic signalling. Therefore, surface levels of Fas receptors greatly influence the downstream signalling events i.e. higher expression of Fas receptors can lead to faster onset, increased rate of signalling and vice versa. Previous data in this study has shown that knockdown of SDCCAG3 increased surface levels of Fas receptors in HeLa and HCT116 cells as well as increased their resident time in the early endosomes. Death receptors from TNF superfamily have been implicated in mediating apoptotic signalling from early endosomes by assembling DISC. Therefore, it could be hypothesised that increased levels of surface receptor and delay in their transition from early-to late endosomes or lysosomes would increase the rate of apoptotic signalling as well. This hypothesis was supported by the unpublished data from Erdmann laboratory which showed that HeLa cells subjected to different concentrations of agonistic anti-FAS (CH-11) antibody for 6 hours had significantly lower amount of viable cells in SDCCAG3 knockdown sample as compared to the control. The levels of non-viable cells in SDCCAG3 knockdown samples were comparable to PTPN13 knockdown samples. Since PTPN13 has been

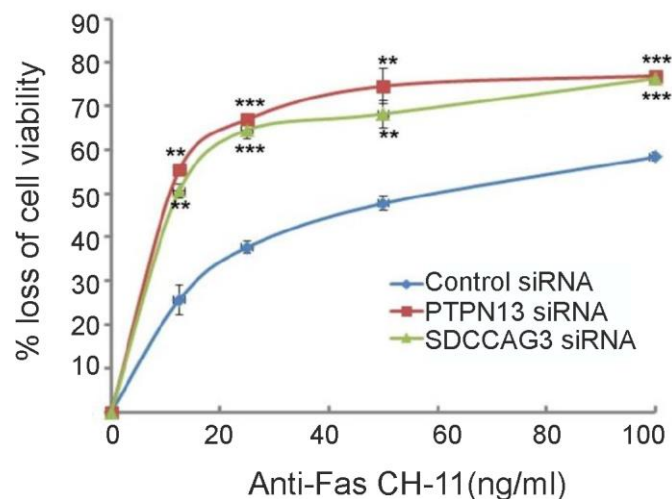


**Figure 5.1:** Cell viability measured by MTT assay. HeLa cells treated with SDCCAG3 no.1, PTPN13 or control siRNA were subjected to stimulation with agonistic anti-FAS (CH-11) antibody at different concentrations in the presence of 2 $\mu$ g/ml of cycloheximide for 6 hours. A dose response curve was generated to measure the amount of dead cells expressed

as % loss of cell viability. Data was obtained from three independent experiments (n=3), \*\*p<0.01, \*\*\*p<0.001, ± s.e.m. *Unpublished data by Fangyan Yu, Erdmann lab.*

shown to negatively regulate the surface levels and apoptotic signalling of FasR, therefore, it was hypothesised that SDCCAG3 and PTPN13 might act together in the same pathway to regulate FasR trafficking.

As mentioned before in chapter 1, caspases play a pivotal role in carrying out programmed cell death or apoptosis. They cleave their substrates in a specific manner by using cysteine residue in their catalytic site [95]. Upon stimulation, Fas receptors activate caspase 8 that in turn activates executioner caspases like caspase 3. Several lines of evidence suggest that in Fas activated apoptosis, caspase 3 cleaves pro-caspase 6 to produce active caspase 6 [94]. Recently, a study identified SDCCAG3 as a substrate of caspase 6 [160]. 2-dimensional electrophoresis/MALDI-TOF was performed to identify new substrates of caspase 6 and the analysis revealed that recombinant caspase 6 was able to cleave SDCCAG3 in HepG2 cell extracts. The study also subjected HeLa cells to staurosporine (STS) treatment to induce apoptosis in the presence or absence of caspase inhibitors. The immunoblot analysis showed an intact 48kDa band corresponding to endogenous SDCCAG3 in untreated and STS + caspase 6 inhibitors treated cells. In contrast, this 48kDa band disappeared in STS treated cells suggesting cleavage of SDCCAG3. Therefore, levels of SDCCAG3 were being affected upon STS treatment and required further analysis. Unpublished data from Erdmann lab showed that transiently expressed SDCCAG3 was cleaved during stimulation with an agonistic anti-Fas antibody. This cleavage was only observed upon stimulation and not in the absence of stimulation or in the presence of caspase inhibitors suggesting the SDCCAG3 was specifically cleaved by active caspases only (figure 5.2). Increased surface levels of FasR and decreased cell viability upon treatment with SDCCAG3 siRNA along with cleavage of SDCCAG3 by an executioner caspase provided compelling pieces of evidence to hypothesise that SDCCAG3 negatively regulated apoptosis.

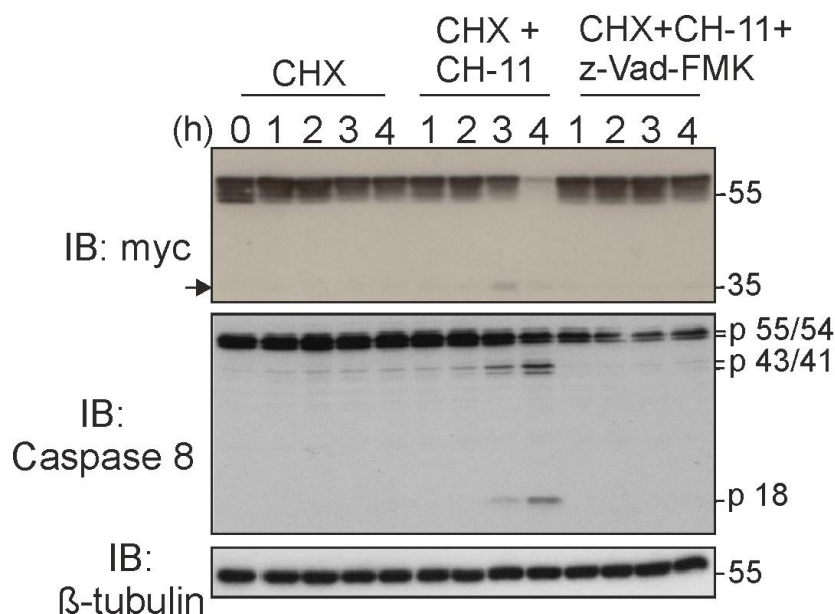


**Figure 5.2: SDCCAG3 is cleaved upon activation of FasR.** Overexpressed SDCCAG3-myc (55kDa) was cleaved upon activation of Fas mediated apoptotic signalling to produce a 35 kDa band after 3 hours of treatment (indicated by an arrow) with Anti-Fas (CH-11) and cycloheximide. In contrast, SDCCAG3-myc by cycloheximide alone or in the presence of pan caspase inhibitor (z-vad-fmk). *Unpublished data by Fangyan Yu, Erdmann lab.*

## 5.2 Aim

On the basis of the hypothesis that SDCCAG3 acted along the same pathway as PTPN13 for regulating Fas mediated apoptotic signalling, changes in the expression levels of SDCCAG3 would affect the rate of apoptosis. Therefore this chapter focussed on-

- (i) Determining the rate of apoptotic signalling upon depletion of SDCCAG3
- (ii) To confirm that SDCCAG3 is a substrate of caspase 6
- (iii) To analyse if PTPN13 and SDCCAG3 acted together as a complex to mediate trafficking of FasR

## 5.3 Results

### 5.3.1 Depletion of SDCCAG3 increases the rate of caspase 8 cleavage

HeLa cells were treated with control or SDCCAG3 siRNA and subjected to stimulation by agonistic anti-Fas (CH-11) antibody. As a result of stimulation, full length caspase 8 (p55/54) was cleaved into a larger fragment (p43/41) and a smaller fragment (p18). The smaller fragment represents the active caspase enzyme of 18 kDa as shown by the arrow in figure 5.3 (a) below. No detectable amount of caspase 8 cleavage occurred after 1 hour of stimulation with 500ng/ml of agonistic antibody but after two hours more amount of cleaved caspase 8 fragments were present in SDCCAG3 depleted cells. Quantification of the cleaved fragment revealed that the difference between the amount of active caspase 8 enzyme present in SDCCAG3 depleted and control cells was statistically significant (b). Since caspase 8 is the initiator caspase therefore more active caspase 8 implies increased and faster apoptotic signalling in SDCCAG3 depleted cells.

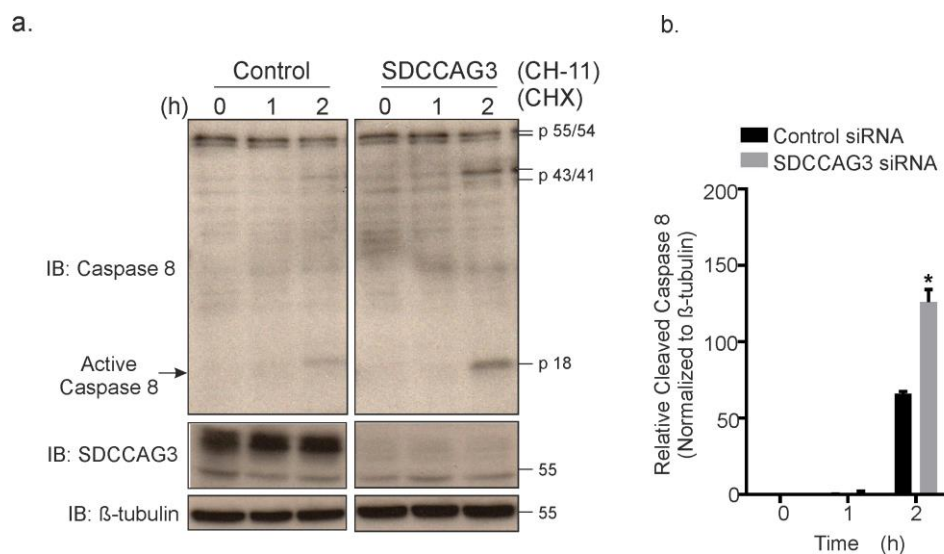


**Figure 5.3: Caspase 8 cleavage upon FasR activation in HeLa cells.** Immunoblot analysis of HeLa cells treated with control or SDCCAG3 no. 3 siRNA. Cells were activated with 500ng/ml Anti-Fas (CH-11) and 50  $\mu$ g/m of cycloheximide for indicated time points. Active caspase 8 fragment of 18kDa was detected by anti-caspase 8 antibody. (b) Quantification of active caspase 8 fragment (p18) normalized to  $\beta$ -tubulin in the treated samples. Blots were quantified using ImageJ. Data was collected from three independent experiments (n=3), Sidak's multiple comparisons test was performed, \* $p < 0.05$ , error bars represent  $\pm$ s.e.m.

Similar results were obtained in HCT116 cells as well. As compared to the control cells, SDCCAG3 depleted HCT116 cells showed accumulation of more active

caspase 8 enzyme (p18 fragment) after 2 and 3 hours of stimulation with agonistic anti-Fas (CH-11) antibody (a). It can be seen that accumulation of active caspase 8 fragments increased with time. The difference in the amount of cleaved caspase 8 was found to be statically significant (b) suggesting that SDCCAG3 negatively regulates apoptotic signalling in HCT116 cells.

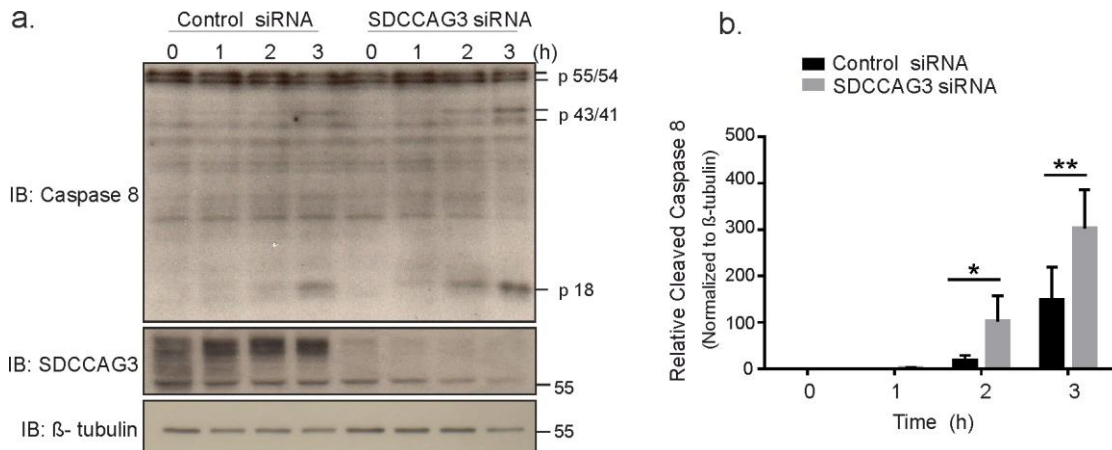


**Figure 5.4 Immunoblot analysis of caspase 8 cleavage in HCT116 cells.** Cells were treated with control or SDCCAG3 no.2 siRNA and incubated with 500 ng/ml of Anti-Fas (CH-11) antibody and 50 µg/ml of cycloheximide for the indicated time points. β-tubulin was used as negative control. (b) Quantification of cleaved caspase 8 fragments (p18) in control and SDCCAG3 knockdown samples normalized to β-tubulin. X-ray films were scanned and quantified with ImageJ. Sidak's multiple comparisons (n=3), \*p<0.05, \*\*p<0.01 error bars represent ±s.e.m.

### 5.3.2 SDCCAG3 is cleaved upon activation of Fas mediated apoptosis

Based on the evidence from the literature, recombinant SDCCAG3 was examined as a substrate of caspase 6. Since the unpublished data from Erdmann lab indicated cleavage of exogenously expressed SDCCAG3, therefore, recombinant SDCCAG3 was analysed to show its cleavage by caspase 6. N-terminus GST tag version of SDCCAG3 was produced and purified from a bacterial strain as shown below in figure 5.5. The coomassie staining revealed the presence of non-specific bands along with the purified GST tagged SDCCAG3 of the correct molecular weight as indicated by the arrow. The presence of these non-specific bands could be attributed to bacterial proteins binding non-specifically to GST beads apart from the GST

tagged protein or it could be due to degradation of the purified product during production.

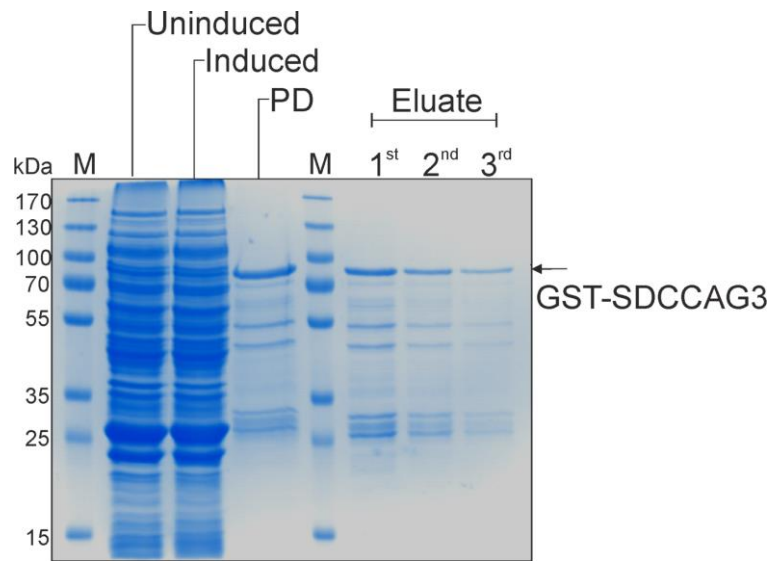


**Figure 5.5: Coomassie Blue staining for recombinant SDCCAG3.** GST-SDCCAG3 expression construct was transformed and purified from *E.Coli*. The staining shows fractions before and after induction with IPTG, and pull down fraction with GST beads. Recombinant SDCCAG3 (marked by an arrow) was then eluted from the beads and used for further analysis.

Recombinant GST tagged SDCCAG3 was incubated with active caspase 6 obtained commercially. The reaction was carried out in a caspase buffer either in the presence or in the absence of pan-caspase inhibitor z-VAD-fmk. As shown in below in figure 5.6, GST-SDCCAG3 could be detected as a band of ~90kDa which was cleaved only in the presence of caspase 6 to produce a smaller band of ~60kDa (highlighted by an asterisk). This band was not observed in the samples containing no caspase 6 enzyme or caspase 6 enzyme in the presence of z-VAD-fmk. The data is in line with both aforementioned literature and unpublished data from Erdmann lab. On logical grounds, cleavage of recombinant SDCCAG3 should produce at least two additional fragments-larger and a smaller fragment. However, coomassie staining in the data above revealed only one additional band (~60kDa) apart from the parent SDCCAG3 band (~90kDa). It could be due to the limitation of the detection method or the

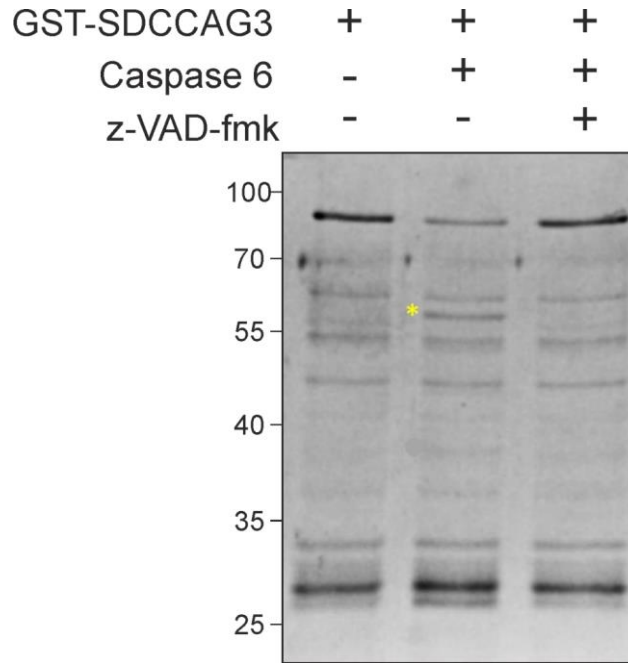


**Figure 5.6: Coomassie Blue staining of GST-SDCCAG3 cleavage by Caspase 6.** Recombinant SDCCAG3 alone, with active caspase 6 enzyme or with caspase 6 in the presence of z-VAD-fmk was incubated at 37°C for 1 hour in the caspase assay buffer. GST-SDCCAG3 was cleaved by caspase6 specifically to produce a ~60kDa band indicated by the asterisk. (N=3)

presence of non-specific bands that could interfere with the detection of cleaved fragments. Therefore, anti-SDCCAG3 antibody which recognises its C-terminus was used to examine the presence of cleaved bands upon incubation with active caspase 6 enzyme. Recombinant SDCCAG3 was incubated alone or with active caspase 6 enzyme in the presence or absence of a pan-caspase inhibitor. Immunoblot analysis with anti-SDCCAG3 revealed the presence of a ~25kDa band only in the lane containing the active enzyme and not in the other two lanes (figure 5.7). This indicated that the observed band is a specific cleavage product.

Taken together, these observations suggest that recombinant GST tagged SDCCAG3 (~90kDa) is cleaved by caspase 6 enzyme possibly to produce a larger fragment of around 60kDa and a smaller fragment of approximately 30kDa. This data also suggests that most likely that caspase 6 cleavage site might be in the C-terminus region of SDCCAG3. However, this data alone cannot exclude the possibility of the existence of more than one caspase 6 cleavage site on SDCCAG3.

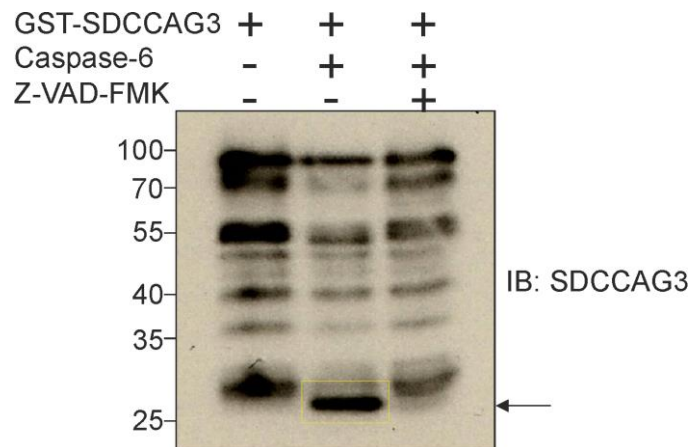


**Figure 5.7: Analysis of the caspase 6 cleavage site on SDCCAG3.** Immunoblot analysis of the recombinant SDCCAG3 under indicated treatments conditions showing a unique cleaved product of 30kDa in the middle lane only as indicated by the arrow and highlighted in a yellow box.

#### 5.4 Analysis of PTPN13 localization with Fas receptors

Data obtained in chapter 3 showed co-localization between SDCCAG3 and internalized FasR in the early/sorting endosomes. It was also hypothesised that SDCCAG3 might be forming a complex with PTPN13 to regulate FasR trafficking. However, the available antibodies against SDCCAG3 and PTPN13 were from the same species which prevented any examination of direct co-localization between them. Hence, co-localization between PTPN13 and internalized FasR in early/sorting endosomes was examined.

##### 5.4.1 PTPN13 co-localized with internalized Fas receptors

Fas receptors in HeLa cells were stimulated with the agonistic CH-11 antibody as described before. Before internalization, at 0 minute, receptors can be seen on the surface of HeLa cells but after 5 minutes of stimulation they could be observed as intracellular punctae. In case of PTPN13, mostly intracellular punctate staining was observed at 0 minutes with occasional instance of co-localization with Fas receptors on the surface. However, after 5 minutes of stimulation of Fas receptors, PTPN13 appeared to change its intracellular distribution and co-localize with internalized Fas receptors (figure 5.8, a).

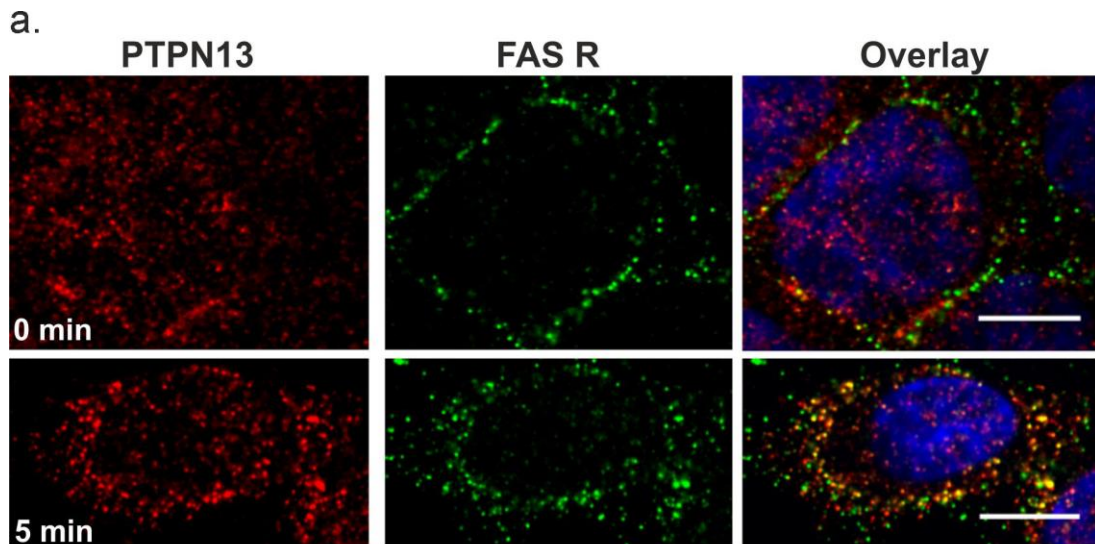
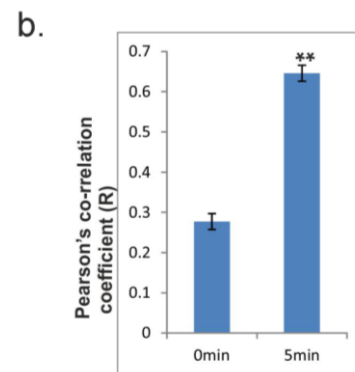


**Figure 5.8: Analysis of co-localization between PTPN13 and FasR.** (a) Immunofluorescence analyses of the co-localization between endogenous PTPN13 and Fas receptors. HeLa cells were stimulated with 1 $\mu$ g/ml of anti-Fas (CH-11) antibody (green) for the indicated time points. Cells were fixed and stained for PTPN13 (red). Scale bar represents 5 $\mu$ m. (b) Quantification of the co-localization observed in (a). Pearson's correlation coefficient was calculated using JACoP tool in image J. Data represents average from three independent experiments (N=3) from at least (n>30 cells). Student's t-test, \*\*p<0.05, error bars represent  $\pm$ s.e.m.

Quantification of the correlation coefficient of co-localization between PTPN13 and FasR revealed a significant difference between 0 and 5 minutes (b). This data suggests that PTPN13 mainly co-localizes with the internalized FasR population. This data is also in line with previous studies that suggested co-localization between PTPN13 and FasR at the cell surface.



#### 5.4.2 PTPN13 and Fas receptors co-localize in the early endosomes

Next, it was examined if PTPN13 co-localized with internalized FasR in early endosomes or not. It was hypothesised that PTPN13 might form a complex with SDCCAG3 at early endosomes which might serve as a possible link between SDCCAG3 and FasR. On the basis of this idea, sub-cellular compartment where PTPN13 and internalized FasR co-localised was examined. For this triple labelling,

EEA-1, a marker for early endosomes was used since internalized FasR were previously shown to enter the EEA-1 positive compartments. At 0 minute time point, intracellular staining of PTPN13 and EEA-1 receptors were observed and FasR were seen on the surface. However, after 5 minutes of internalization FasR and PTPN13 were seen in EEA-1 positive compartments. Thus, this data supports the hypothesis that PTPN13 might be forming a complex with SDCCAG3 at early endosomes to regulate FasR trafficking.

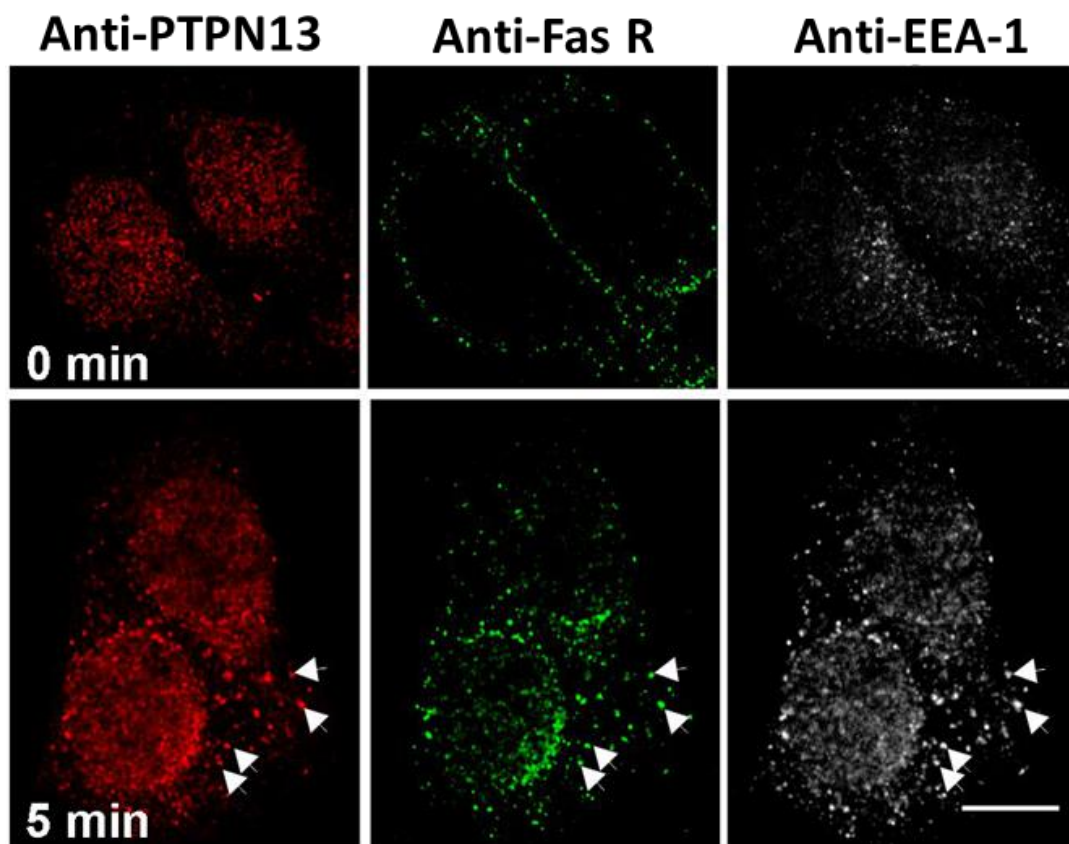


**Figure 5.9: Sub-cellular localisation of FasR and PTPN13.** Immunofluorescence analysis of PTPN13 (red), FasR(green) and EEA-1 (white) in HeLa cells stimulated with 1 $\mu$ g/ml anti Fas CH-11 antibody for the indicated time points. Arrows highlight the puncta that co-localized in all three channels. Scale bar represents 5 $\mu$ m.

## 6 Discussion

### 6.1 SDCCAG3 regulates post-endocytic trafficking of FasR

The current study demonstrates that SDCCAG3 is a novel player in apoptotic signalling such that it negatively regulates Fas mediated apoptosis by sorting Fas receptors towards lysosomal degradation. Expression levels of SDCCAG3 were shown to affect the surface presentation of Fas receptors, which was investigated using three different approaches. Firstly, semi-quantitative fluorescent microscopy showed that depletion of SDCCAG3 expression levels led to increased surface levels of FasR in HeLa cells. Quantification of the images revealed an almost 2-fold increase in the surface intensity of FasR in SDCCAG3 siRNA treated cells (figure 3.2). This data was further validated as the antibody used for detecting Fas receptors was shown to be specific (did not produce any surface staining in the Fas siRNA treated cells), and the efficacy of the siRNA was proved by western blotting. The antibody detection of endogenous SDCCAG3 produced multiple bands between 70 and 55kda which disappeared upon treatment with SDCCAG3 siRNA except two non-specific bands at the bottom of the multiple bands of SDCCAG3. These multiple bands were seen due to phosphorylation as demonstrated previously [123].

Secondly, data obtained from the microscopic analysis was confirmed with flow cytometry that allowed precise quantification of the surface levels. Analysis of the histograms obtained in HeLa cells showed statistically significant increases in the surface intensity of Fas receptors in the absence of SDCCAG3 expression levels (figure 3.5). Three different siRNA against SDCCAG3 showed consistent phenotype which supported the specificity of the phenotype observed with individual siRNA. However, the reason for difference in the extent of the phenotype observed between SDCCAG3 siRNA no.1 and 2 or 3 is not clear since due the knockdown efficiency of three siRNA used was comparable. Another TNF receptor superfamily member, TRAIL R1 was not affected by the expression levels of SDCCAG3. This data was consistent with a previous study which used a custom made siRNA against SDCCAG3 and observed no difference in the surface levels of TRAIL R1 upon knockdown of SDCCAG3 via flow cytometry [35]. Regulation of TNFR1 surface

levels by SDCCAG3 has also been implicated before in a study which showed that transient expression of a truncated version of SDCCAG3 containing only the coiled-coil domain led to decreased surface levels of TNFR1 [124]. The study claimed that an expression construct containing only coiled-coil domain represented a dominant negative version of SDCCAG3. However, data gathered in the current study does not lend support to the view that loss-of-function of SDCCAG3 reduces surface levels of the receptors in the TNF family; on the contrary, it could be suggested that overexpression of the coiled-coil domain might instead lead to the gain-of-function phenotype. Two other receptors that follow distinct endocytic routes like EGFR and Transferrin were also not affected by SDCCAG3 expression levels suggesting that regulation of FasR surface levels by SDCCAG3 was highly specific.

Thirdly, cell surface biotinylation data was consistent with the previous results i.e. depletion of SDCCAG3 increased surface levels of FasR specifically and had no effect on other receptors like EGFR, transferrin, and N-cadherin (figure 3.8). Independent use of more than two or more siRNA against the same target helps in differentiating true phenotype in comparison to the 'off-target' effects as well as increases confidence in the data obtained. Hence, three different siRNA against SDCCAG3 were tested. A similar phenotype was observed upon knockdown of SDCCAG3 with these three different siRNA; however, the severity of the phenotype between SDCCAG3 no.1 and 2 or 3 siRNA knockdown samples was different. A gold standard in validating the phenotype observed upon siRNA treatment is the rescue of the effect by expression of a siRNA-resistant version of the gene. Increased surface levels of FasR could be rescued upon restoring the expression levels of SDCCAG3 by introducing siRNA resistant constructs (figure 3.9). These results provided confirmatory evidence that SDCCAG3 expression levels affected surface levels of FasR.

Cell surface biotinylation allowed analysis of both the surface and total pool of the receptors. SDCCAG3 expression levels only affected surface levels of FasR and not the total levels in case of SDCCAG3 no.1 and 2 siRNA however, a slight increase in case of SDCCAG3 no.3 siRNA was observed in HeLa cells (figure 3.8). The effect of SDCCAG3 expression levels on the surface presentation of FasR were tested in

another epithelial cell line called HCT116. The data obtained in HCT116 cells showed an increase in both the surface and total levels of FasR upon depletion of SDCCAG3 via cell surface biotinylation (figure 3.10) and flow cytometry (figure 3.11). Often increase in the total levels of proteins could be attributed to an increased transcriptional activity (mRNA levels) of the protein. In order to rule out any transcriptional effect on Fas receptors upon depletion of SDCCAG3, mRNA levels of Fas receptors were measured. The knockdown of SDCCAG3 had no effect on the transcriptional activity of FasR as no significant difference was observed in the mRNA levels of *Fas* upon depletion of SDCCAG3 with three different siRNA (figure 3.14). This data further corroborated the notion that SDCCAG3 affects the surface presentation of FasR.

It was hypothesised that an increase in the surface levels could be a consequence of the altered trafficking and so the rate of endocytosis of FasR was analysed by flow cytometry. However, depletion of SDCCAG3 did not appear to affect the rate of FasR endocytosis (figure 3.15). In type I and not in type II cells, activation of FasR is often described to be preceded by internalization. In this study, around 60% of FasR were internalized rapidly within 15 minutes of stimulation leaving a smaller fraction of FasR on the surface. On the basis of this data, it could be speculated that HeLa cells in this study had a tendency to behave more like type I cells. Instead of altered trafficking, SDCCAG3 was found to be rather involved in regulating the basal turnover and degradation of internalized Fas receptors (figure 3.19). In steady-state cells, SDCCAG3 depleted sample showed an increased expression of exogenous FasR specifically as it had no effect on the overexpressed E-cadherin receptors. This upregulation in the expression levels could be explained due to defects in the degradation of internalized FasR as SDCCAG3 depletion slowed down the rate of degradation upon stimulation with an agonistic antibody (figure 3.20). It is not clear as to why total levels of endogenous FasR did not change upon SDCCAG3 depletion in HeLa cells, although increased expression was found in HCT116 cells. In summary, depletion of SDCCAG3 increased surface levels of Fas receptor without inhibiting its rate of endocytosis but delaying the rate of degradation of exogenous Fas receptors suggesting that SDCCAG3 might interfere in the endosomal sorting of FasR.

## **6.2 SDCCAG3 co-localizes with FasR in early endosomes and regulates their sorting towards late endosome/lysosome**

SDCCAG3 has been shown to localize to early endosomes and partially co-localize with EEA-1 before [123]. Microscopic analysis data in the current study showed that SDCCAG3 co-localizes with internalized FasR in EEA-1 positive endosomes (figure 3.23). The instance of co-localization measured as correlation coefficient decreased after 15 minutes of internalization suggesting that co-localization was rather transient, giving insight into the molecular events following internalization of FasR in HeLa cells (figure 3.22). Systematic analysis of the localization with different endosomal markers (EEA-1 and Lamp-1) revealed that depletion of SDCCAG3 traps FasR into early endosomes that are internalized following stimulation with an agonistic antibody (figure 3.24). Since depletion of SDCCAG3 only delayed the rate of degradation and did not inhibit it completely, therefore, it can be understood that depletion of SDCCAG3 might be causing only a delay in transitioning of FasR from early to late endosomes (figure 3.20). Similarly, continuous uptake of a non-agonistic antibody against FasR also revealed the accumulation of FasR in early endosomes in SDCCAG3 depleted cells (figure 3.25). Similar studies have been performed that tested free uptake of an antibody to reveal intracellular localization of receptors under different treatment conditions [161]. The current data is not consistent with a previous study that showed depletion of SDCCAG3 mislocalized receptors like Glut1 and CD97 to lysosomes and reduced their surface as well as total levels in HeLa cells [35]. Although authors of that study showed depletion of SDCCAG3 reduced levels of Glut1 (which could be rescued by bafilomycin, a lysosomal blocker) but no accumulation of Glut-1 in Lamp-1 positive vesicles was shown in that study. Furthermore, only a minor phenotype was observed by them in case of CD97 receptor which showed a slight but significant reduction in the surface level upon depletion of SDCCAG3 along with mild phenotype of mislocalization to lamp-1 that was not analysed statistically. The authors used a different siRNA (custom made) against SDCCAG3 as compared to the current study to knockdown SDCCAG3. It is not clear if use of a different siRNA could be the reason for the discrepancy observed between their data and the current study.

As described before, surface receptors destined for degradation are sorted into the intraluminal vesicles of the multi-vesicular bodies that mature into late endosomes and fuse with the lysosomal bodies where the protein degradation is executed [17]. Clathrin mediated internalization of FasR to form signalling platforms in the early endosomes has been described before [86]. It can be speculated that this pathway might lead to sorting of Fas receptors towards lysosomes in order to attenuate apoptotic signalling. However, endolysosomal pathway of Fas receptors has not been described yet. Therefore, the current study explored the mechanism behind post-endocytic trafficking of Fas receptors. Enlarged endosomes created by constitutive expression of Rab5 was used as the main tool in this study to examine the transport of Fas receptors into ILVs. This approach has been used in many other studies in the past to demonstrate sorting of receptors in to ILVs [33, 59, 162-164].

In-depth analysis of the molecular mechanism of sorting of FasR into lysosomes in the current study lends firm support to the claim that SDCCAG3 is involved in sorting of FasR to the lysosomes. Depletion of SDCCAG3 increased accumulation of FasR in the limiting membrane of the enlarged endosomes suggesting a defect in sorting of FasR into intraluminal vesicles of MVBs (figure 4.2). This data was consistent with the previous observations and provided an explanation as to why depletion of SDCCAG3 led to an accumulation of FasR in early endosomes ultimately leading to a delay in degradation. Super resolution microscopy also confirmed these observations and three dimensional reconstructions of the images enabled clear localization of FasR at the limiting membrane in SDCCAG3 depleted cells in contrast with localization inside intraluminal vesicle in control cells (figure 4.3). Since depletion of SDCCAG3 affected trafficking of FasR not only after stimulation but at steady-state levels as well, therefore, sorting of FasR into ILVs was analysed using a non-agonistic antibody. Continuous uptake of a non-agonistic antibody against FasR showed accumulation inside the intraluminal vesicle only in case of control cells and not in SDCCAG3 depleted cells (figure 4.4). This data was consistent with the previous results and established the requirement for SDCCAG3 in sorting of FasR under steady-state conditions. However, it should be noted that SDCCAG3 depletion did not inhibit the entry of FasR into the intraluminal vesicle but caused merely a delay in sorting as longer time points for antibody feeding

showed no significant difference in the intraluminal localization of FasR between control and SDCCAG3 depleted cells (figure 4.5). This observation could be due to either impartial knockdown of SDCCAG3 or due to involvement of other molecular components, compensatory pathways mediating sorting of FasR under steady-state.

Defects in FasR sorting were found to be specific as depletion of SDCCAG3 did not affect sorting of EGF (figure 4.6) and transferrin receptors (figure 4.7). The current data about transferrin receptor sorting is in agreement with the literature as an overwhelming amount of evidence supports that transferrin receptors are sorted towards the recycling pathway and not into the intraluminal vesicle [20, 159]. Previous studies have shown that EGFR is ubiquitinated using ubiquitin ligase called Cbl which has been implicated in facilitating its clathrin mediated endocytosis and sorting into MVBs [39].

SDCCAG3 was described as a retromer-WASH complex associated protein [51] and as a part of the retromer-SNX27 complex, it was implicated in endosome-to-PM sorting as mentioned above [35]. Hence, the current study describes a function of SDCCAG3 that is inconsistent with its role as a retromer associated protein. However, on logical grounds, there is no compelling reason to argue that retromer associated proteins cannot be involved in opposing or multiple intracellular trafficking pathways. In fact, some sorting nexins like SNX5 and SNX1 which are a part of the core retromer machinery have been shown previously to mediate endosome-to-lysosomal trafficking of some surface receptors. For example, a study highlighted the role of PIPKI $\gamma$ 5 (type 1 gamma phosphatidylinositol phosphate 5-kinase) in collaborating with SNX5 to facilitate interaction between HRS and ubiquitinated EGFR. SNX5 is a known retromer associated protein. While loss of other retromer components such VPS35 or VPS26 did not have any effect on the lysosomal degradation of EGFR, loss of SNX5 prevented sorting of EGFR into ILVs resulting in a prolonged EGFR signalling [165]. These observations demonstrate a retromer independent function of SNX-5 in the lysosomal sorting. Similarly, SNX-1 was also shown to mediate sorting of a GPCR called protease-activated receptor-1 (PAR-1) independently of the retromer complex [166]. Furthermore, role of SNX-1 and 2 in Rho-GTPase modelling has been described to be independent of retromer

[167]. Therefore, it can be understood that proteins involved in the retromer mediated endosome-to-TGN trafficking can operate on different trafficking pathways also like endosome-to-lysosome independently of retromer. On the basis of the evidence collected in this study, it can be argued that SDCCAG3 might also be involved in the endosome-to-lysosomal targeting of FasR conceivably independently of retromer.

### **6.3 SDCCAG3 mediates endosome-to-lysosome sorting of Fas receptors via Dysbindin-HRS axis**

The current research provides molecular insight into the mechanism by which SDCCAG3 regulates lysosomal sorting of FasR. SDCCAG3 has been implicated as an interacting partner of dysbindin in two independent proteomic studies previously [156, 157]. This interaction was demonstrated in the current study as endogenous dysbindin was detected in the pull down fraction of GST tagged SDCCAG3 (figure 4.8). However, this interaction was not characterized completely in this study; therefore on the basis of the available data, the nature of this interaction cannot be defined. SDCCAG3 was shown to be localized in the limiting membrane of the enlarged endosomes specifically as the siRNA mediated knockdown of SDCCAG3 abolished the punctate staining from the limiting membrane (figure 4.9). Similarly, overexpression of dysbindin also showed punctate staining on the limiting membrane of enlarged endosomes. These puncta co-localized with the endogenous SDCCAG3 which further strengthened the possibility of a complex formation between SDCCAG3 and dysbindin in the subdomains of the sorting endosomes (figure 4.10). Recent studies have shown that dysbindin is involved in the lysosomal sorting of G-protein coupled receptors (GPCRs) like  $\delta$ -opioid receptor (DOP) and dopamine-2 receptor (D2R), chemokine receptor type 4 (CXCR4) [58, 59]. The phenotype observed upon depletion of SDCCAG3 in the current study resembled that of dysbindin depleted cells shown in other studies. For instance, surface levels of the aforementioned receptors were upregulated in dysbindin depleted cells. No effect was observed on the rate of endocytic trafficking instead the rate of proteolysis was perturbed due to intraluminal sorting defects. Additionally, depletion of dysbindin did not affect lysosomal degradation of EGFR [58] suggesting that

SDCCAG3 and dysbindin might act in a similar endosome-to-lysosomal route which is distinct from the route taken up by EGF receptors. Furthermore, dysbindin was implicated as an accessory sorting protein that linked cellular regulators of GPCRs sorting like  $G\alpha_s$  and GASP-1 (GPCR-associated binding protein-1) to HRS, a component of the ESCRT-0 machinery [59]. Evidence of an interaction between dysbindin and HRS was demonstrated by co-immunoprecipitation [58] and yeast-two hybrid screening [168] suggesting that there is a direct interaction between them. Based on the available evidence so far, it can be understood that dysbindin is an accessory protein of the ESCRT-0 sorting machinery that acts in the early steps of the endolysosomal sorting such that it facilitates the connection between cellular regulators and the ESCRT machinery.

Next, it was hypothesised that SDCCAG3 might be executing its sorting activity by forming a complex with dysbindin which would connect it to HRS and therefore the ESCRT machinery. In other words, depletion of dysbindin and HRS should affect the intracellular trafficking of FasR in a similar manner as SDCCAG3 if they all act in the similar pathway. This was indeed true as HeLa cells with dysbindin and HRS knockdown showed upregulated cell surface levels of FasR suggesting that they acted in a similar pathway as SDCCAG3 (figure 4.11). Additionally, co-transfection of siRNA against SDCCAG3 and dysbindin did not increase the levels of FasR any further as compared to only SDCCAG3 or only dysbindin depleted cells. Therefore, this data provided confirmatory evidence that dysbindin and HRS might be involved with SDCCAG3 in the same pathway to regulate FasR trafficking. Apart from the surface levels, sorting of FasR into intraluminal vesicles of MVBs upon silencing of HRS and dysbindin revealed a defect in the sorting as less FasR accumulated inside the lumen of the enlarged endosomes (figure 4.12). This data was consistent with the previous literature, as mentioned earlier, that sorting of some GPCRs and dopamine receptors were shown to be perturbed by silencing of dysbindin. Similarly, depletion of HRS was also shown to produce defects in the ILV sorting of receptors [169]. However, it is not clear whether FasR sorting by SDCCAG3 is ubiquitination dependent or independent. Nevertheless, HRS has been implicated in the sorting of receptors in both ubiquitination dependent and independent manner. The presence of an adaptor protein has often been implicated in mediating sorting of non-

ubiquitinated cargo by HRS. Taken together, current data appears to suggest strongly that SDCCAG3 regulates endo-lysosomal sorting of FasR by mediating its ILV sorting via dysbindin thereby connecting it to the ESCRT machinery which mediates the sorting of FasR into ILVs. The model below depicts the molecular machinery involved with SDCCAG3 in ILV sorting of the internalized Fas receptors as suggested by the current study. It is currently not known how SDCCAG3 might access FasR at the early endosomes. But it can be speculated that PTPN13 might be the most likely candidate to connect FasR with the SDCCAG3 at the endosomes.

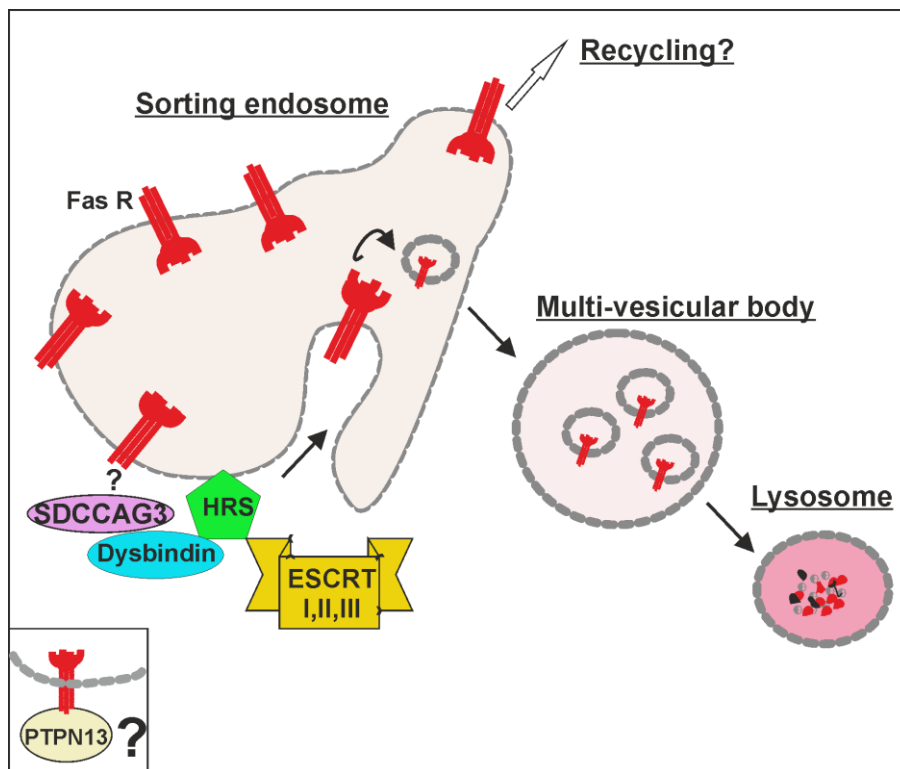


**Figure 6.1: Predicted model for SDCCAG3 mediated sorting of FasR into ILVs.** SDCCAG3 was shown to regulate sorting of FasR into ILVs via dysbindin and ESCRT machinery. It was shown to interact and co-localize with dysbindin. siRNA mediated depletion of both dysbindin and HRS resulted in an increased surface levels of FasR and defective sorting of FasR into ILVs.

#### **6.4 SDCCAG3 is a novel negative regulator of Fas mediated apoptosis**

Since SDCCAG3 was shown to regulate FasR trafficking, therefore, the effect of its depletion on apoptotic signalling was analysed. FasR mediated apoptotic signalling has been studied extensively in the past. The overwhelming amount of literature supports the idea that cleavage of procaspase 8 into active caspase 8 is one of the hallmarks of apoptotic signalling. Hence, levels of cleaved fragments of caspase 8 representing active caspase 8 were analysed by immunoblotting. The data observed in figure 5.3) revealed that depletion of SDCCAG3 led to an increased accumulation of active caspase 8 after stimulation of FasR with an agonistic antibody. Higher levels of active caspase 8 were due to enhanced cleavage of procaspase 8 since the cytosolic levels of procaspase 8 (p55/54 fragment) did not appear to be more in SDCCAG3 depleted cells. This observation clearly reflects that larger quantity of procaspase 8 was being cleaved thus the larger quantity of DISC complex was being assembled in SDCCAG3 depleted cells. It is not surprising since SDCCAG3 depleted cells had higher levels of FasR on the surface which would have enabled engagement and oligomerisation of more FasR leading to more homotypic interactions between death domains (DD) of FasR and FADD to form a larger DISC platform. It could be imagined that higher amount of FADD would automatically lead to recruitment of more procaspase 8 via homotypic interaction between their death effector domains (DED). On the basis of this data, it can be concluded that SDCCAG3 is a negative regulator of apoptotic signalling.

However, data obtained from agonistic monoclonal antibodies cannot be extrapolated directly to the natural Fas ligand due to subtle differences in the mechanism of triggering apoptosis by them. Firstly, based on molecular modelling it was predicted that CH-11 binds to the same domains (CRD 2 and 3) on FasR as the ligand but on the opposite side such that binding of Fas ligand brings two hydrophobic patches together with the ligand on the inside and receptors clustered on the outside. In contrast, an IgM antibody like CH-11 clusters multiple Fas receptors back-to-back rather than in a face-to-face configuration. [170] Secondly, stimulation with agonistic antibodies triggered microaggregates formation of FasR in both Fas sensitive and insensitive cell lines which was not found to be the case upon stimulation with the soluble Fas ligand. This microaggregation, however, did not

affect the kinetics of apoptosis induction by the ligand and the antibody as they were found to be comparable [87]. Therefore, it can be understood that aggregation of FasR by agonistic antibodies cannot be correlated with the ability to induce Fas mediated apoptosis and that the induction of apoptosis by the Fas ligand versus antibodies is comparable but might employ slightly different mechanisms. Nevertheless, agonistic antibodies have been used in various studies in the past to induce apoptotic signalling. O' Reilly et al., 2009 propounded the view that it is only the membrane bound Fas ligand that is required for mediating apoptosis in lymphocytes and not the soluble Fas ligand [171]. They demonstrated that at physiological levels, soluble Fas ligand was indeed involved in non-apoptotic signalling like NF $\kappa$ -B signalling for survival. On the basis of these arguments, it can be concluded that use of agonistic antibodies for inducing apoptosis in cultured cells can be viewed as a justifiable alternative to soluble Fas ligand because they can efficiently induce apoptosis in all cell types as compared to the soluble Fas ligand.

Increased levels of active caspase 8 were observed in both HeLa and HCT116 cells in the current study. As mentioned before, HeLa cells appeared to behave like type I while HCT116 cell line has been characterised as type II in the previous studies [172]. Since depletion of SDCCAG3 upregulated surface levels of FasR in both the cell lines, therefore, enhanced caspase 8 cleavage was also observed in both. The consensus view seems to be that type I and II cell lines vary in the downstream signalling mechanisms after receptor stimulation (i.e. the mitochondrial pathway is either involved or not) and not in the initial signalling events like DISC assembly and recruitment of pro-caspase 8 to DISC. This might explain why SDCCAG3 might affect apoptotic signalling in a type II cell line like HCT116 which do not even internalize FasR into endosomes upon stimulation [64].

Caspases are crucial components of the apoptotic signalling. Data obtained in this study confirmed that SDCCAG3 is a substrate of caspase 6 and also demonstrated its cleavage in vitro (figure 5.6). Recombinant caspase 6 enzyme cleaved GST-tagged SDCCAG3 specifically and the cleaved SDCCAG3 was detectable via coomassie blue staining. However, the available data is not sufficient to judge if SDCCAG3 had one or multiple cleavage sites and where the cleavage site might be located on

SDCCAG3. However, unpublished data from Erdmann lab showed that overexpressed N-terminus myc tagged SDCCAG3 (55 kDa) was cleaved upon stimulation with an agonistic anti-Fas antibody (figure 5.2). Immunoblot analysis revealed that anti-myc antibody was able to recognize a cleaved fragment of around 35 kDa suggesting that caspase 6 cleavage sites might be located near C-terminus region since the larger fragment contained an intact N-terminus myc tag. To complement this data, an antibody against the C-terminus region of SDCCAG3 was used to identify the smaller fragment predicted to contain the intact C-terminus region of SDCCAG3. As expected, anti-SDCCAG3 antibody identified a fragment close to 25 kDa which matched with the predicted size of the smaller fragment based on the previous data (figure 5.7). To conclude, this data is sufficient to demonstrate that SDCCAG3 is a substrate of caspase 6. Identifying the exact cleavage sites of caspase 6 on SDCCAG3 was outside the scope of this study. Furthermore, caspase 6 has been implicated in Alzheimer and other neurodegenerative diseases [173]. Association of SDCCAG3 with dysbindin also points towards plausible roles of SDCCAG3 in neurodegenerative disorders [174]. Therefore, it could be hypothesised that SDCCAG3 might play a role in neuronal apoptosis as well.

### **6.5 Does SDCCAG3 form a complex with PTPN13 to regulate trafficking of Fas receptors and apoptotic signalling?**

The current study demonstrated that SDCCAG3 was involved in the post-endocytic sorting of FasR towards lysosomal degradation such that its depletion led to an accumulation of these receptors on the surface and increased sensitivity towards apoptosis. Similarly, depletion of PTPN13 has also been shown to increase cell surface levels of FasR and sensitivity towards Fas mediated apoptosis in the past suggesting that PTPN13 and SDCCG3 might act together to mediate regulation of FasR trafficking and signalling. Following arguments can be advanced to support the hypothesis that SDCCAG3 forms a complex with PTPN13; firstly, SDCCAG3 was shown to interact directly with the FERM domain of PTPN13 via yeast two hybrid screening and co-immunoprecipitation [123]. Secondly, PTPN13 were also shown in this study to co-localize with FasR in the early endosomes like SDCCAG3 (figure 5.9). It is the first time that PTPN13 has been shown to co-localize to the early

endosomes. However, co-localization between FasR and PTPN13 has been shown before [108]. Hence, localization of both SDCCAG3 and PTPN13 with FasR in the early endosomes place them in the correct location for regulating sorting of FasR. However, these observations require further experimentation to judge the specificity of the anti-PTPN13 antibody staining. Thirdly, PTPN13 can localize to the plasma membrane via its interaction with PI[4,5]P2 and bind to the cytoplasmic tail of FasR via its PDZ 2 domain [109]. Therefore, it can be convincingly hypothesised that most likely PTPN13 connects FasR with SDCCAG3 in order to regulate endocytic trafficking of FasR.

## **6.6 Proposed model for SDCCAG3 mediated regulation of apoptosis**

Taken together, this study describes a novel function of SDCCAG3 in Fas mediated apoptotic signalling where it regulates intracellular sorting of FasR towards lysosomal degradation and shuts off the apoptotic signalling.

Further research is required to explain the exact mechanism behind elevated surface levels of FasR. Increase in the surface levels of FasR can be a function of the following aspects that have not been explored in this study-firstly, enhanced recycling by an unknown mechanism can explain the increase in the surface population of FasR; secondly, increased trafficking of the Golgi pool of Fas receptor to the plasma membrane can also contribute to the increased surface population. However, increased synthesis of FasR can be ruled out since SDCCAG3 depletion was shown not to affect the mRNA levels of *Fas*.

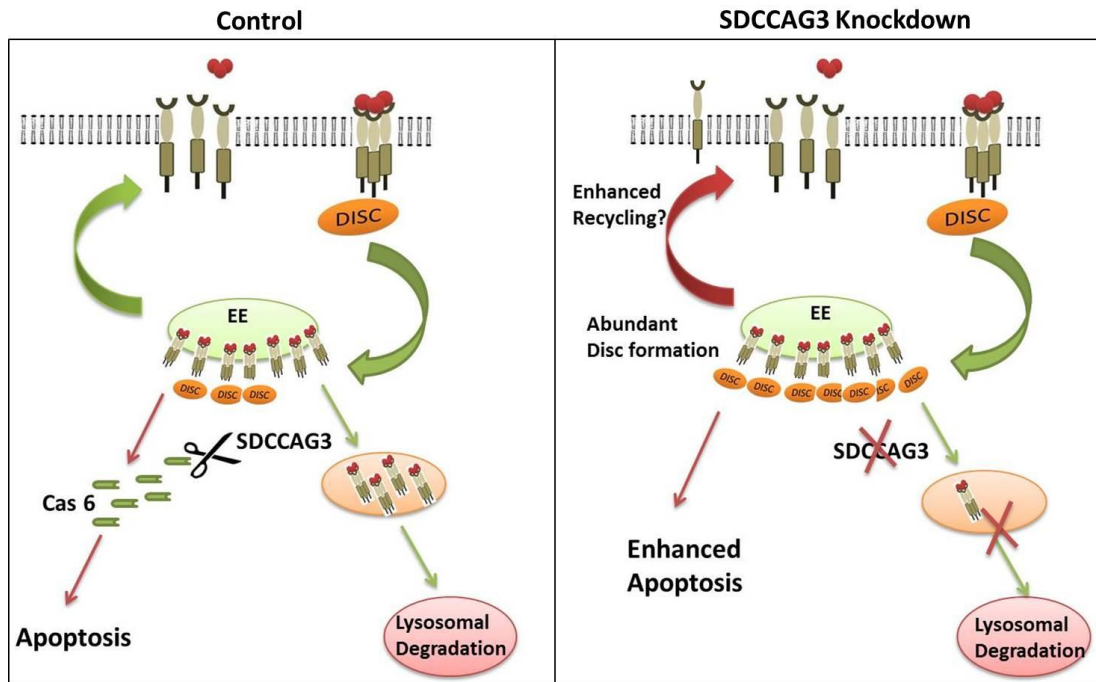


**Figure 6.2: Hypothetical model of negative regulation of apoptotic signalling by SDCCAG3.**

The above model summarises the main findings of the current study. In case of control cells, stimulated FasR internalize and assemble DISC complex in the early endosomes. It is tempting to speculate that once DISC is assembled then it would cleave the executioner caspases including caspase 6 which might cleave SDCCAG3 and prevent sorting of FasR towards lysosomes to sustain apoptotic signalling by a positive feedback loop. In this scenario, sorting of FasR by SDCCAG3 might act as a checkpoint for sustaining or blocking apoptotic signalling further. In case of SDCCAG3 depleted cells, externally stimulated Fas receptors internalize into early endosomes and sustain apoptotic signalling for a longer period due to delayed transitioning from early to late endosomes. This enables assembly of a large amount of DISC complex as shown by faster and more accumulation of active caspase 8 in SDCCAG3 depleted cells (figure 5.3, 5.4) leading to a higher rate of cell death in these cells as shown in the unpublished data from the Erdmann lab (figure 5.1). Thus, this model explains the suggested anti-apoptotic role of SDCCAG3 in the current study.

## 7 SDCCAG3 in ciliogenesis

### 7.1 Introduction

A yeast-two hybrid screening performed in Dr. Kai Erdmann's laboratory identified intraflagellar transport protein-88 (IFT88) as one of the potential binding partner of SDCCAG3 by using its first N-terminal one hundred amino acids as a bait. This interaction was found to be specific as SDCCAG3 (1-100aa) did not interact with FERM domain of PTPN13, C-terminus FRMPD4 or empty pGBT9 vector used as controls (figure 7.1, a). IFT88 belongs to intraflagellar complex B (IFT B) which is involved in anterograde trafficking of proteins, formation and maintenance of cilia [129]. Therefore, IFT88 was a suitable candidate to characterise its interaction with SDCCAG3 further and understand the functional relevance of this interaction. Transiently expressed myc-SDCCAG3 (full length) was pulled down with EGFP-IFT88 specifically and not with EGFP-Rab8 thereby confirming the interaction (b).

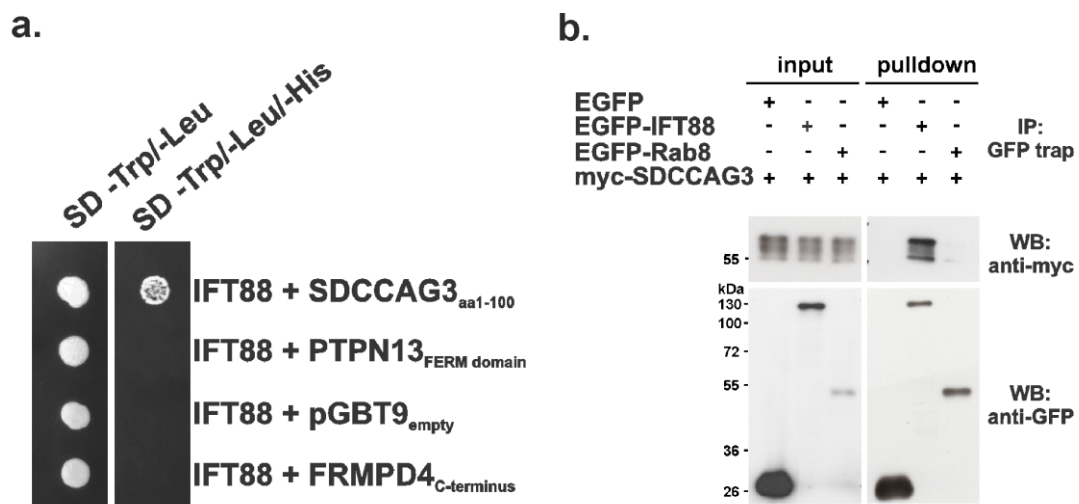


**Figure 7.1: SDCCAG3 interacts with intraflagellar transport protein-88:** (a) Yeast-two hybrid analysis of interaction between SDCCAG3 (1-100) amino acids (used as bait) with full length IFT88, FERM domain of PTPN13, C-terminus FRMPD4 (FERM and PDZ containing protein 4) and empty pGBT9 vector. Interaction was tested by monitoring the growth of yeast in tryptophan (Trp), leucine (Leu) and histidine (His) deficient media. A positive interaction was observed only in case of IFT88 and SDCCAG3 (aa1-100) as compared to the negative control. (b) Full length myc tagged SDCCAG3 was transiently expressed in Cos7 cells and analysed for its presence detected by anti-myc antibody in the lysate pulled down EGFP-IFT88 coated beads. EGFP alone and EGFP-Rab8 were used as negative control. (*Unpublished data- Fangyan Yu, Erdmann lab*)

IFT88 is involved in the polarized vesicle trafficking of proteins in cilia which is the foundation of functional cilia. Disruption of normal ciliary trafficking results in improper ciliogenesis and many ciliopathies in humans. Although bioinformatics and proteomic screenings have identified a large number of proteins to be associated with cilia but their functional relevance still remains elusive. Our understanding of polarized trafficking pathways in cilia is limited. Many molecular machinery and pathways such as recycling of cargo back to the cilium remain to be identified. As SDCCAG3 has been localized to the early endosomes [123], retromer positive vesicles [35] and has been implicated in trafficking pathways [124] before therefore localization and function of SDCCAG3 in cilia was studied further in detail.

## **7.2 Aim**

Based on its interaction with IFT88, SDCCAG3 was hypothesised to act along with IFT88 in the process of ciliogenesis and trafficking of ciliary cargo. The primary aims of this study was-

1. To identify localization of exogenously expressed SDCCAG3 in the primary cilium
2. To investigate the role of SDCCAG3 in formation and maintenance of cilia in IMCD3 cells
3. To explore ciliary cargo dependent on SDCCAG3 for their trafficking in cilia

## 7.3 Results

### 7.3.1 Localization of transiently expressed SDCCAG3 in cilia

In order to examine the localization of SDCCAG3 in the primary cilium, an expression construct of SDCCAG3 was used and cells were labelled with antibodies against cilia markers such as acetylated- $\alpha$ -tubulin ( a marker for axoneme) and  $\gamma$ -tubulin ( a marker for the basal body). Human EGFP-SDCCAG3 was transiently overexpressed in the inner medullary collecting duct-3 (IMCD3) cells and co-stained with ciliary markers such as acetylated- $\alpha$ -tubulin and  $\gamma$ -tubulin to investigate the localization of SDCCAG3 in cilia. Full length SDCCAG3 showed punctate staining in the cytoplasm of the IMCD3 cell and co-localized predominantly with  $\gamma$ -tubulin in the basal body. No co-localization was observed with the acetylated  $\alpha$ -tubulin in the axoneme (figure 7.2, a). Yeast-two hybrid analysis and biochemical data from the Erdmann lab showed that N-terminal 1-100 amino acids of SDCCAG3 were sufficient for mediating its interaction with IFT88, therefore, localization of SDCCAG3 to the basal body without first 1-100aa was analysed. As shown in figure (b), SDCCAG3 expression construct without 1-100aa region failed to accumulate in the basal body anymore. Furthermore, only 1-100aa region of SDCCAG3 was also analysed for its localization in cilia and as expected, just 1-100aa N-terminal region was sufficient for its recruitment to the basal body (c).

Thus, the above data demonstrated that transiently expressed SDCCAG3 localized to the basal body in cilia. The first N-terminal region of SDCCAG3 (1-100aa) was both necessary and sufficient for its localization to the basal body. This region contains an IFT88 binding site and therefore it was hypothesised that molecular interaction with IFT88 might be necessary for localization of SDCCAG3 to the basal body.

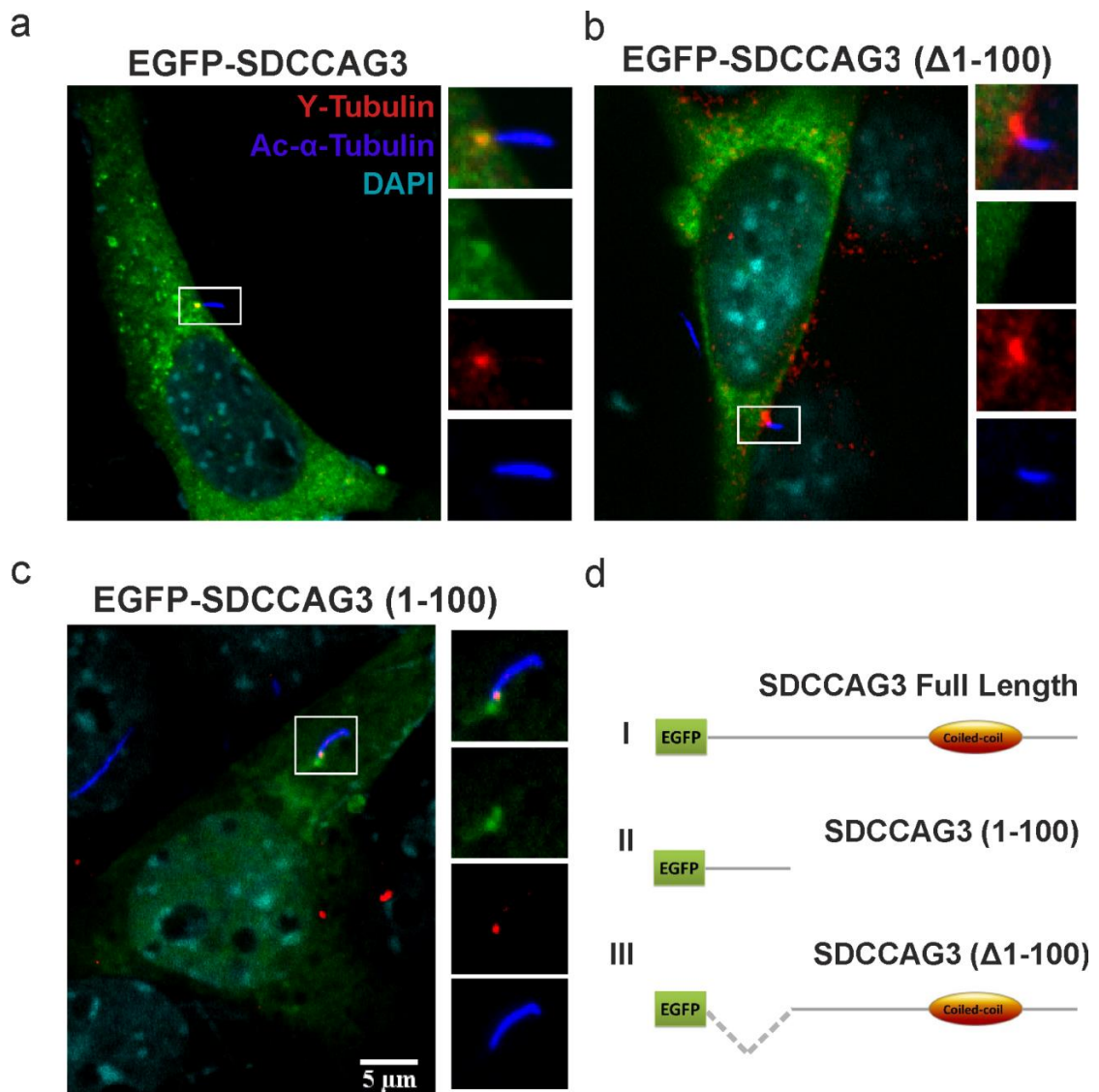


**Figure 7.2: Localization of transiently expression EGFP-SDCCAG3 expression constructs in IMCD3 cells.** Human SDCCAG3 expression constructs with N-terminal EGFP tags were transfected into inner medullary collecting duct-3 (IMCD3) cells. After 48 hours of transfection, cells were serum starved to induce ciliogenesis and stained for markers like acetylated- $\alpha$ -tubulin (blue),  $\gamma$ -tubulin (red). Full length SDCCAG3 accumulated in the basal body (a). While the deletion construct of SDCCAG3 lacking the first 100 amino acids ( $\Delta$ 1-100aa) failed to localize at the basal body (b). A truncated version of SDCCAG3 containing only 1-100 amino acids was sufficient for localization of SDCCAG3 into basal body (c). DAPI was stained in cyan and SDCCAG3 is shown in green. Images are representative of three independent experiments. Scale bar represents 5 $\mu$ m.

(d) Schematic representation of the various SDCCAG3 expressions constructs used in the experiment- Full length (I), truncated construct containing only N-terminal 1-100aa (II) and a shorter version lacking first 1-100aa region (III).

### 7.3.2 SDCCAG3 localization to centrosome is not dependent on IFT88

Gamma-tubulin was used as the centrosomal/basal body marker to assess the localization of SDCCAG3. IMCD3 cells, transiently expressing wild-type SDCCAG3, were treated with non-specific scrambled or mouse IFT88 siRNA. Cells were serum starved to induce ciliogenesis and stained to analyse SDCCAG3 localization. As shown in figure 7.3 (a), wild-type EGFP-SDCCAG3 accumulated with  $\gamma$ -tubulin in both scrambled or mIFT88 treated cells. Therefore, localization of SDCCAG3 did not depend upon IFT88 as it was recruited to centrosome/basal body even in the absence of IFT88. Quantification of the percentage of co-localization between SDCCAG3 and  $\gamma$ -tubulin in cells collected from three independent experiments also confirmed that SDCCAG3 was present at centrosomes independently of IFT88 (b). However, immunoblot analysis of the knockdown efficiency of IFT88 revealed that the knockdown was not complete and that the remaining amount of IFT88 could be sufficient for recruiting SDCCAG3 to the centrosomes.

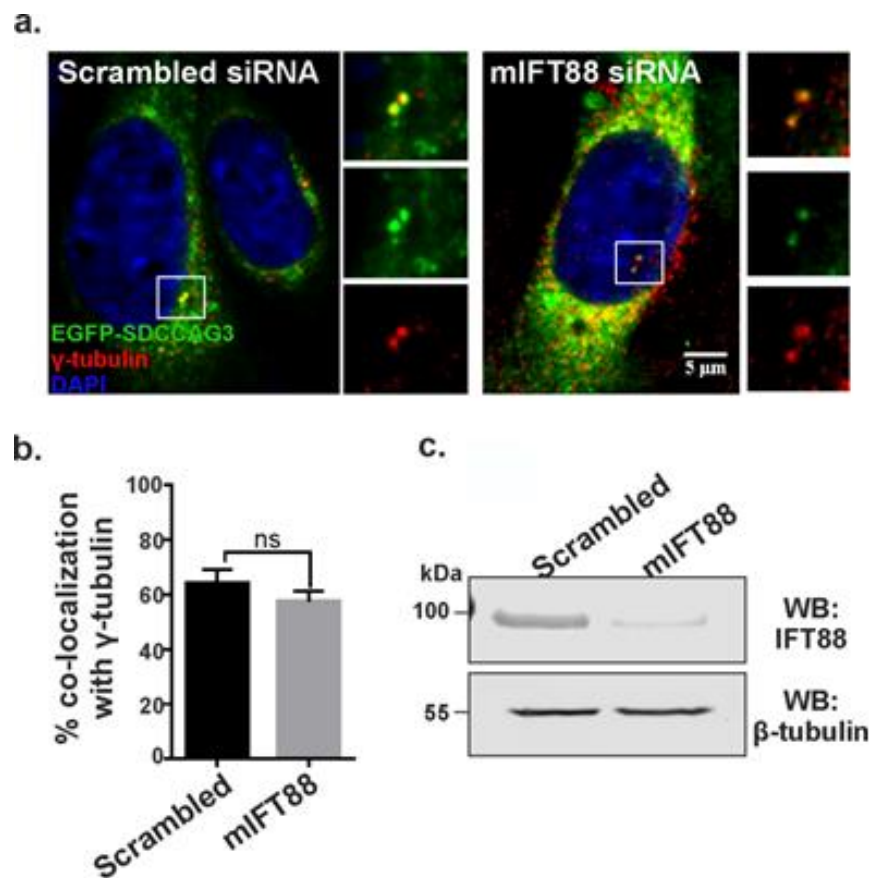


**Figure 7.3: SDCCAG3 is recruited to centrosomes independently of IFT88.** (a) IMCD3 cells expressing wild-type SDCCAG3 (green) were treated scrambled or mIFT88 siRNA and

stained with  $\gamma$ -tubulin (red). DAPI was stained in blue. Inserted panels show co-localization between EGFP-SDCCAG3 and  $\gamma$ -tubulin from the representative cells in both the cases. Scale bar represents 5 $\mu$ m. (b) Extent of co-localization between SDCCAG3 and  $\gamma$ -tubulin was analysed from cells collected from three independent experiments (N=3). Student's t-test was used to analyse the statistical significance of the data, ns-not significant ( $p=0.231$ ). (c) Immunoblot analysis of the knockdown efficiency of IFT88 in IMCD3 cells using scrambled or mIFT88 siRNA.  $\beta$ -tubulin was used as a loading control.

### 7.3.3 SDCCAG3 depletion impairs ciliogenesis

Next, it was analysed if SDCCAG3 was involved in the formation of cilia since IFT88 is a well-established protein to be involved in ciliogenesis. IMCD3 cells were treated with scrambled or mouse SDCCAG3 siRNA.

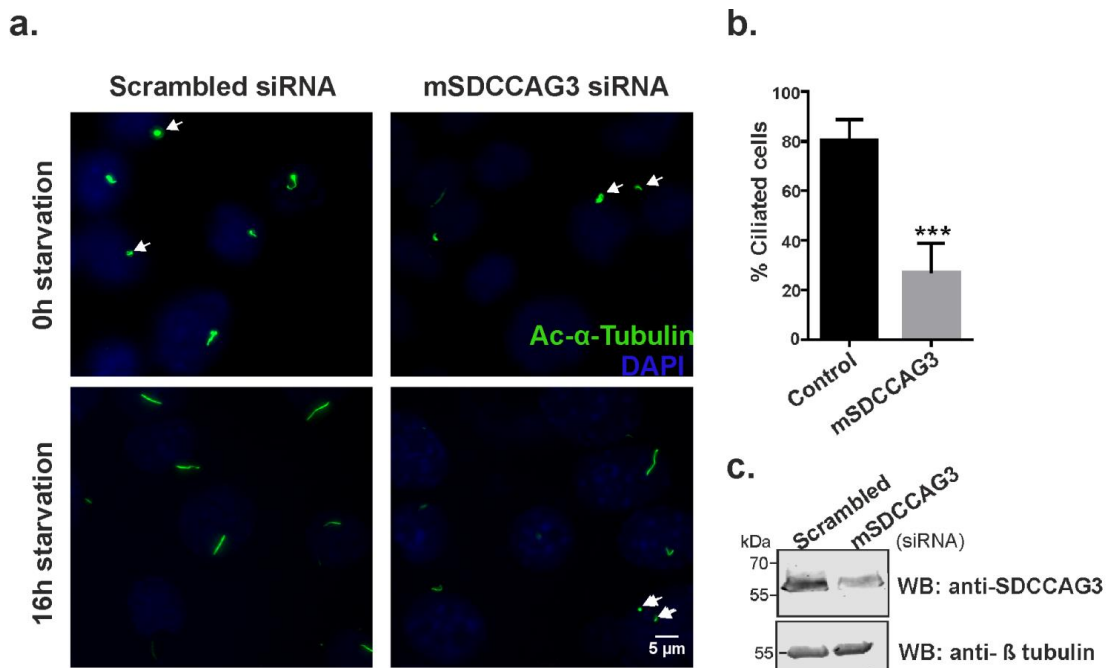


**Figure 7.4: Depletion of SDCCAG3 impairs ciliogenesis.** (a) IMCD3 cells, treated with scrambled or mouse SDCCAG3 siRNA, were serum starved for the indicated time points in order to induce ciliogenesis. Cells were stained with acetylated-tubulin (green) and DAPI (blue). Arrow indicate nascent cilia. Scale bars represent 5 $\mu$ m. (b) Quantification of ciliated cells expressed as a percentage and analysed using student's t-test (N=3,\*\*\* $p<0.001$ , error bars represent  $\pm$ s.e.m). (c) Immunoblot analysis of knockdown efficiency of SDCCAG3 upon treatment with scrambled or mSDCCAG3 siRNA.  $\beta$ -tubulin used as a loading control.

Cells were serum starved for 0 or 16 hours to induce ciliogenesis. As shown in figure 7.4 (a), at 0 hours mostly nascent cilia was observed in case of both scrambled and mSDCCAG3 siRNA treated cells as indicated by the arrows.

However after 16 hours, more cells had mature cilia in scrambled sample as compared to mSDCCAG3 cells which still showed the presence of nascent cilia. (b) Quantification of the number of ciliated cells present in both the samples revealed that there were at least 50% less ciliated cell in mSDCCAG3 siRNA samples as compared to the scrambled.

Furthermore, length of the cilia was also quantified and compared between the two samples. As shown in figure 7.5, depletion of SDCCAG3 led to a significant decrease in the average length of cilia. Based on the data above, it could be concluded that SDCCAG3 is involved in the formation of cilia and also controls cilia length.

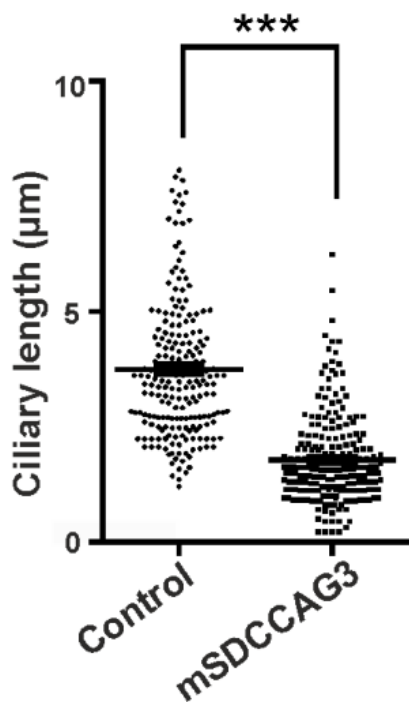


**Figure 7.5: Depletion of SDCCAG3 decreases length of cilia.** Quantification of the length of cilia from the data shown in figure 7.4. The average length of cilia decreased significantly upon depletion of SDCCAG3 (N=3, F-test, \*\*\*p<0.001, error bars represent  $\pm$ s.e.m). Cilia length was measure using ImgaeJ analytical tools.

#### 7.3.4 Rescue of ciliogenesis defect upon SDCCAG3 re-expression

Next, it was analysed whether defects in ciliogenesis and cilia length observed upon depletion of SDCCAG3 could be rescued upon restoring the levels of SDCCAG3. Human SDCCAG3 expression construct was introduced in IMCD3 cells treated with mouse SDCCAG3 siRNA since it targeted only the endogenous SDCCAG3 and did not affect the human expression construct. IMCD3 cells treated with scrambled or mSDCCAG3 siRNA and transfected with human wild type EGFP SDCCAG3 showed localization of SDCCAG3 at the base of the cilium (figure 7.6, a) as

observed before. Quantification of the data revealed that expression of EGFP-SDCCAG3 in mSDCCAG3 siRNA treated cells restored the percentage of ciliated cells completely such that they were comparable to the scrambled sample. The phenotype could not be rescued upon expression of EGFP alone (b). Expression of EGFP-SDCCAG3 ( $\Delta 1-100$ ) was also analysed but it did not restore the levels of ciliated cells. In contrast, it reduced the percentage of ciliated cells in scrambled siRNA treated cells as well suggesting that this mutation exerted a dominant negative effect and disrupted the normal functioning of endogenous SDCCAG3.

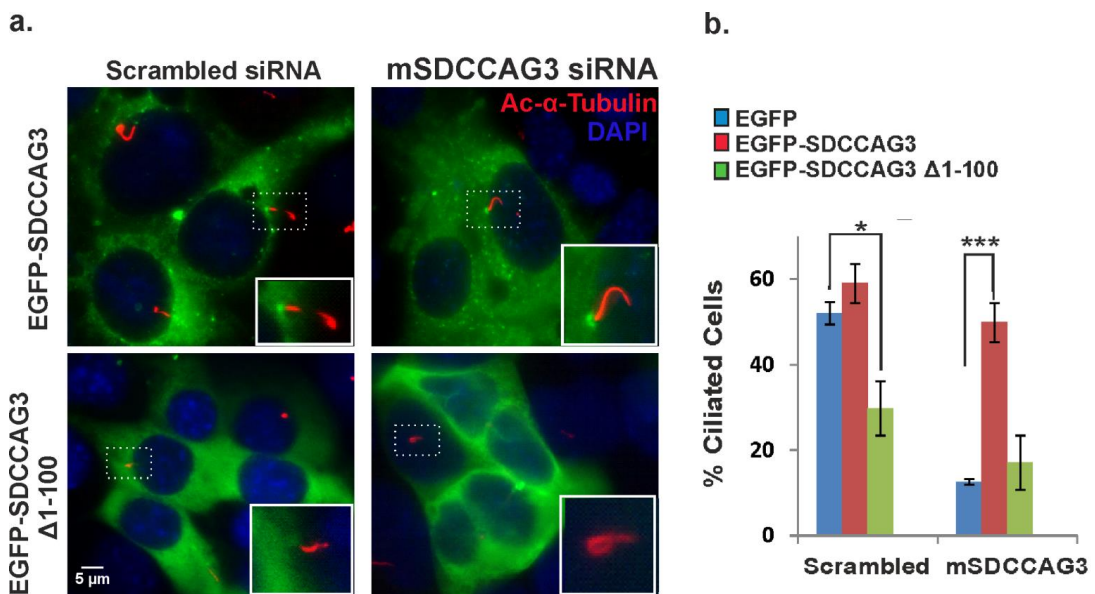


**Figure 7.6: Rescue of ciliogenesis defect by transient expression of SDCCAG3.** (a) IMCD3 cells were transfected with scrambled or mouse SDCCAG3 siRNA along with wild type human EGFP-SDCCAG3, mutant EGFP-SDCCAG3 ( $\Delta 1-100$ ) or EGFP alone. Only wild type SDCCAG3 and not the mutant, accumulated at the base of the cilium stained with acetylated-tubulin (red) in case of both scrambled and mSDCCAG3 siRNA. Insets show representative cilium. Scale bars represent 5  $\mu$ m. (b) Quantification of ciliated cells expressed as a percentage in samples transfected with the indicated constructs (N=3, unpaired t-test, \* $p < 0.05$ , \*\*\* $p < 0.001$ , error bars represent  $\pm$ s.e.m).

Additionally, Cilia length was also observed in the above mentioned experiment. Expression of wild type human EGFP-SDCCAG3 was able to rescue the average length of cilia in mouse SDCCAG3 siRNA treated cells in contrast with EGFP expression alone (figure 7.7)

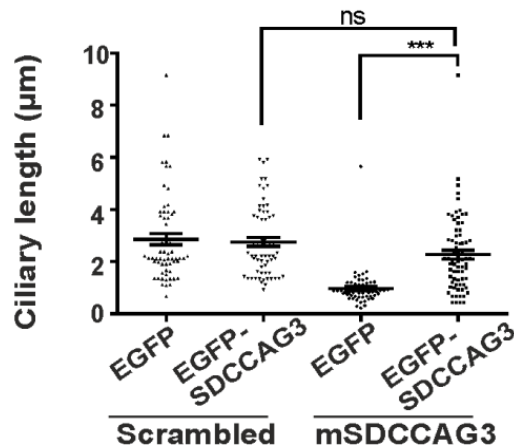


**Figure 7.7: Rescue of cilia length upon expression EGFP-SDCCAG3.** Samples from figure 7.6 were used to quantify the length of cilia upon expression of wild type human EGFP-SDCCAG3 construct to rescue shortened cilia phenotype in mSDCCAG3 siRNA treated cells. In contrast to EGFP alone, EGFP-SDCCAG3 restored the length of cilia in mSDCCAG3 sample such that the cilia length in both scrambled and mSDCCAG3 siRNA treated cells was comparable. (N=3, F-test, \*\*\*p<0.001, ns-not significant, error bars represent  $\pm$ s.e.m).

### 7.3.5 SDCCAG3 and IFT88 function in the same pathway

Role of IFT88 in the formation and maintenance of cilia has been described before. Depletion of IFT88 and SDCCAG3 in RPE cells reduced the number of ciliated cells; however, simultaneous transfection of both SDCCAG3 and IFT88 siRNA together did not reduce the number of ciliated cells any further. Statistical analysis of the data revealed that the difference between the percentage of ciliated cells in IFT88 alone or with SDCCAG3 depleted cells was not significant. This data suggested that SDCCAG3 and IFT88 might coordinate together in the same pathway for ciliogenesis (figure 7.7 a). The efficiency of the knockdown was confirmed using specific antibodies (b).

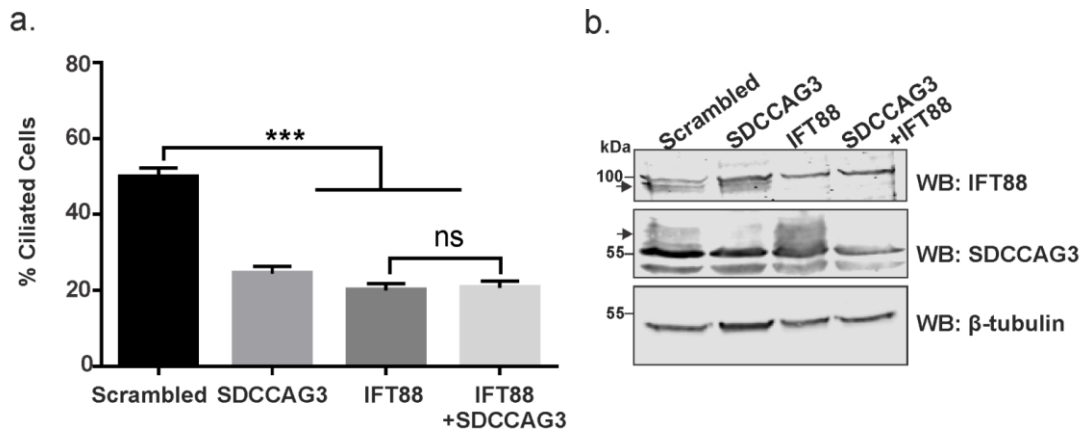
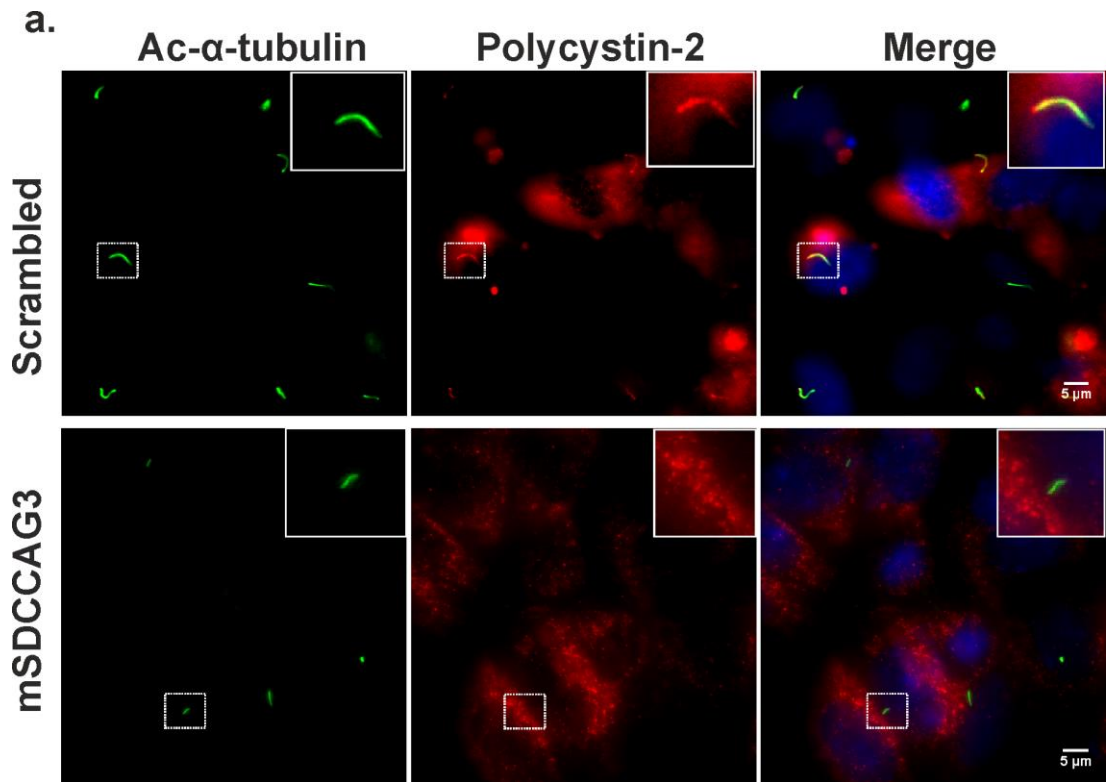


**Figure 7.8: SDCCAG3 coordinate with IFT88 in the same pathway.** (a) A number of ciliated cells were analysed and expressed as a percentage in RPE cells treated with indicated siRNA (N=3, unpaired t-test, \*\*\*p<0.01, ns-not significant, error bars represent  $\pm$ s.e.m). (b) Immunoblot analysis of the knockdown efficiency of IFT88 or SDCCAG3.  $\beta$ -tubulin was used as a loading control.

### 7.3.6 Depletion of SDCCAG3 impairs trafficking of Polycystin-2 to cilia

Polycystin-2 (PC-2) is a ciliary membrane receptor which is transported to the mature cilium via polarised trafficking pathways. Loss of IFT88 has been shown to disrupt trafficking of PC-2 before. Since SDCCAG3 appeared to act in the same pathway as IFT88, therefore, ciliary trafficking of PC-2 was examined upon depletion of SDCCAG3. IMCD3 cells were serum starved for 16 hours and stained for endogenous PC-2 with an established antibody along with a cilia marker. Immunofluorescence analysis revealed a defect in the transport of cytoplasmic PC-2 to the cilia in the absence of SDCCAG3. PC-2 could be seen co-localizing along the length of the axoneme stained with anti-acetylated tubulin in case of the scrambled siRNA transfected cells only and not SDCCAG3 depleted cells (Figure 7.9,a). Quantification of the above data revealed a significant reduction in the percentage of PC-2 receptors transported to the cilium upon silencing SDCCAG3 (b). Thus, this data suggests that SDCCAG3 might be involved in transport of a transmembrane receptor, PC-2, into cilia.



b.

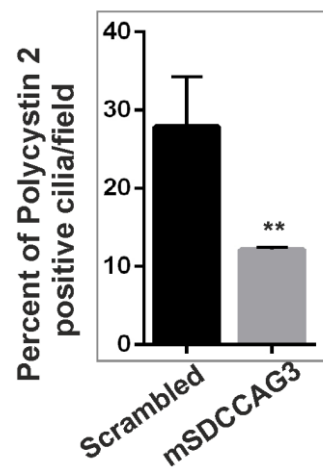


**Figure 7.9: Depletion of SDCCAG3 disrupts trafficking of Polycystin-2 to cilia.** (a) Immunofluorescence analysis of ciliary localization of Polycystin-2 in IMCD3 cells treated with scrambled or mSDCCAG3 siRNA and serum starved for 16 hours. Cilia were stained with anti-acetylated tubulin antibody (red) and anti-polycystin-2 antibody (green). DAPI was stained in blue. Scale bars represent 5 $\mu$ m. (b) Quantification of Polycystin-2 localization to cilia under different treatment conditions expressed as a percentage (N=3, unpaired t-test, \*\*p<0.05, error bars represent  $\pm$ s.e.m). (*Data obtained in collaboration with Yu, Erdmann lab*)

### 7.3.7 Rescue of Polycystin-2 trafficking defect with EGFP-SDCCAG3

The phenotype observed upon depletion of SDCCAG3 i.e. defect in PC-2 trafficking to cilia was confirmed by a rescue experiment. A human SDCCAG3 expression construct was co-transfected with a mouse siRNA against SDCCAG3 in IMCD3 cells. As mentioned before, this expression construct was resistant to the mouse siRNA and was able to restore the expression levels of SDCCAG3 successfully as the phenotype could be rescued upon transfection (figure 7.10, a). EGFP-SDCCAG3 showed accumulation at the base of the ciliary axoneme and rescued the localization of PC-2 to cilia. While overexpression of EGFP alone showed diffused cytoplasmic staining and failed to rescue the ciliary localization of PC-2. Quantification of this

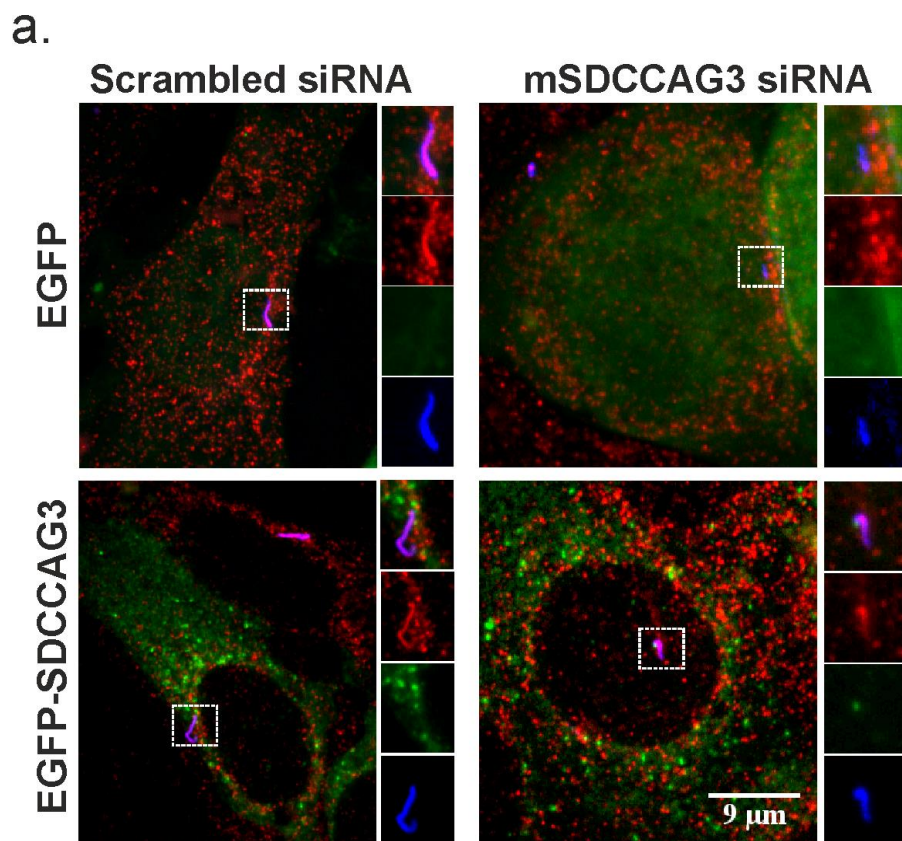
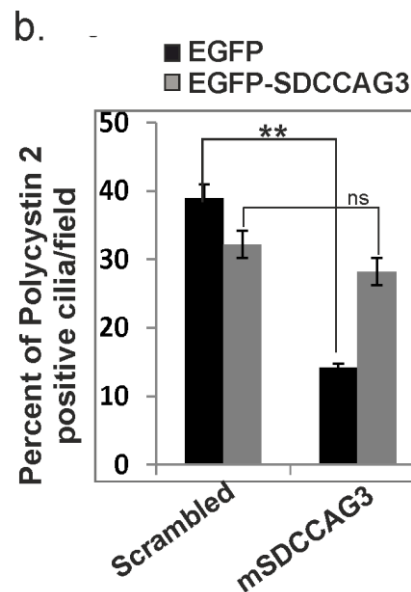


**Figure 7.10: Defect in Polycystin-2 localization to cilia was rescued upon restoring SDCCAG3 levels.** IMCD3 cells treated with scrambled or mouse SDCCAG3 siRNA were transfected with human EGFP-SDCCAG3 expression construct that was not targeted by mouse siRNA. (a) Representative immunofluorescence images showing localization of PC-2 (red) to the axoneme (blue) in control and mSDCCAG3 cells transfected with EGFP-SDCCAG3. While no co-localization could be observed in case of EGFP treated cells. Scale bar, 9 $\mu$ m. (b) Quantification of the above data showing percentage of PC-2 localization in

ciliated cells under indicated treatment conditions. Data obtained from three independent studies, n=3, t-test, \*\*p<0.01, ns-not significant, ±s.e.m



Quantification of this data revealed that difference between the percentage of co-localization between PC-2 and cilia was significantly different for scrambled and mSDCCAG3 siRNA treated cells overexpressing EGFP alone. However, no significant difference could be observed between scrambled and mSDCCAG3 treated cells overexpressing EGFP-SDCCAG3. Therefore, it can be concluded that localization of SDCCAG3 into cilia is crucial for the transport of PC-2 to cilia.

### 7.3.8 Depletion of SDCAAG3 does not alter Rab8 trafficking to cilia

Rab8 has been implicated in the process of cilia formation and trafficking such that it localizes to the developing cilia and exits from the mature cilia. Therefore, trafficking of Rab8 to cilia upon depletion of SDCCAG3 was observed in order to examine if SDCCAG3 regulated ciliogenesis via regulating trafficking of Rab8. Immunofluorescence analysis revealed that in contrast to PC-2, depletion of SDCCAG3 did not have any effect on the localization of Rab8 to cilia. Since Rab8 has been shown to localize to the cilium during initial phases of the ciliogenesis, therefore, its localization was examined 8 hours (figure 7.11) after serum starvation. Quantification in (b) revealed no significant difference in the percentage of

localization between Rab8 and ciliary marker acetylated- $\alpha$ -tubulin. Hence, it can be concluded that absence of SDCCAG3 does not disrupt Rab8 transport to cilia.

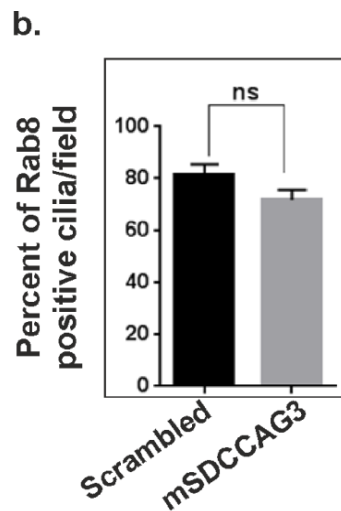
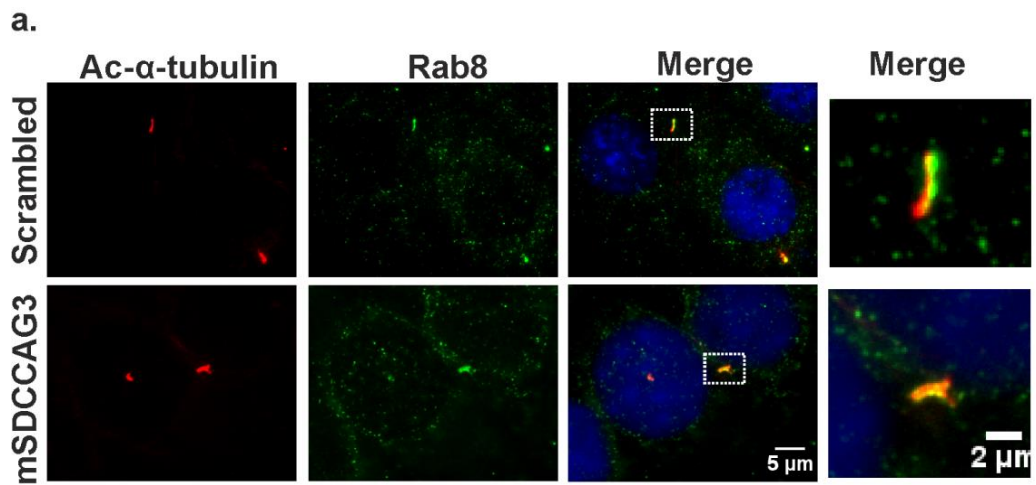


**Figure 7.11: SDCCAG3 does not regulate Rab 8 localization to cilia.** (a) IMCD3 cells were treated with scrambled or mSDCCAG3 siRNA and subjected to serum starvation for 8 hours. Cilia were stained with anti-acetylated tubulin (red) and Rab8 was stained with anti-Rab8 (green). DAPI was stained in blue. Insets have been magnified in the separate panels. (b) Quantification of the co-localization between cilia and Rab8 expressed as a percentage (N=3, unpaired t-test, ns-not significant, error bars represent  $\pm$ s.e.m).

## **7.4 Discussion**

This study was based on the previous data collected in the Erdmann lab that identified SDCCAG3 as a novel interaction partner of a well-known ciliary protein called IFT88. The current study demonstrated that SDCCAG3 is required for ciliogenesis and trafficking to the cilium.

### **7.4.1 SDCCAG3 localizes to cilia**

It was shown to localize to the basal body upon overexpression in IMCD3 cells (figure 7.2). The wild type EGFP tagged SDCCAG3 co-localized with  $\gamma$ -tubulin which is a known marker for the basal body. It was also shown that N-terminal 1-100 amino acids of SDCCAG3 were both sufficient and necessary for localizing SDCCAG3 to the base of the cilium as the mutant SDCCAG3 expression construct lacking 1-100 amino acids failed to localize to the basal body. A recently published large scale proteomics study by Gupta *et. al.*, 2015 characterized protein-protein interactions in the centrosome and cilium interface by using in vivo proximity dependent biotinylation (BioID) analysis [175]. They identified SDCCAG3 to be in the proximity of centrosomal proteins. Previous unpublished data from Erdmann lab also showed that first 1-100 amino acids of SDCCAG3 were sufficient to mediate its interaction with intraflagellar transport protein 88 (IFT88). Therefore, localization of SDCCAG3 to cilia and its association with an important ciliary transport component formed the basis of further investigation into the role of SDCCAG3 in ciliogenesis.

### **7.4.2 Regulation of cilia formation and length by SDCCAG3**

In this study, IMCD3 cells were used as a model to understand the effect of SDCCAG3 depletion on ciliogenesis. Endogenous SDCCAG3 was depleted by using siRNA which was shown to knockdown SDCCAG3 efficiently. Depletion of SDCCAG3 was found to reduce the number (figure 7.4) and the average length of the cilia (figure 7.5). This phenotype was generated specifically due to the depletion of endogenous SDCCAG3 as it could be rescued upon introducing a siRNA resistant SDCCAG3 expression construct (figure 7.6). In consistence with the unpublished data from the Erdmann lab (figure 7.1), mutant SDCCAG3 construct lacking 1-100 amino acids failed to rescue the ciliogenesis defects. It rather acted as a dominant

negative and its introduction reduced the number of cilia further (figure 7.6). This data proves that N-terminus 1-100aa region of SDCCAG3 is responsible for its localization to cilia. This region also contains the IFT88 binding site in SDCCAG3. However, interaction with IFT88 was not found to be the exclusive event responsible for ciliary localization of SDCCAG3 as partial knockdown of IFT88 in IMCD3 cells did not prevent localization of SDCCAG3 to cilia (figure 7.3). Nevertheless, SDCCAG3 and IFT88 act together in the same pathway for promoting ciliogenesis as simultaneous depletion of both SDCCAG3 and IFT88 in RPE cells showed no additional reduction in the number of cilia when compared to the samples with their individual knockdowns.

The current data provides strong evidence to support the claim that SDCCAG3 promotes ciliogenesis but it is still unclear how exactly SDCCAG3 is involved in controlling the formation and length of cilia. It can be speculated that SDCCAG3 might be involved in the early stages of ciliogenesis such as centrosome maturation or membrane docking or IFT docking and transport. Since SDCCAG3 has been shown to be associated with the early/recycling endocytic compartments [35, 123] and with the retromer-WASH complex [51] therefore it is tempting to speculate its role in the regulation of endocytic trafficking to support ciliogenesis. The role of endocytic trafficking during early stages of ciliogenesis has been described in many studies suggesting an interplay between vesicular trafficking and ciliogenesis [129]. For example, IFT20 has been localized to both Golgi and cilia. It was suggested to be involved in the transport of ciliary protein from Golgi to cilia as its depletion reduced the amount of polycystin-2 localization to cilia [147]. Some IFT proteins (which are a part of ciliary transport system) have been implicated in regulating recycling of CD3 complex in a polarized manner in non-ciliated cells also, therefore, suggesting that cellular endocytic transport machinery might serve a role in ciliogenesis as well [176]. Another set of player involved in both vesicular and ciliary trafficking are Rab proteins such as Rab8 that are involved in Golgi to cilia transport and Rab11 in the endocytic recycling compartment (ERC) that has been associated with the initial stages of cilia formation [177] Small GTPase, ARF-like 6 (Arl6), has been implicated in both vesicle transport and sorting of receptors, like SSTR3, to cilia [129] and in regulation of Wnt signalling [178].

IFT88 has been shown previously to promote growth and maintenance of ciliary length [143]. It accumulates at the base of the cilium from where it regulates the trafficking of particles in to the developing axoneme as a part of a bigger complex called IFT-B. IFT particles are involved in ‘in’ and ‘out’ trafficking of materials from the cilia continuously; and so it can be speculated how they maintain the length of the cilium. Theoretical model proposed for ciliary length states that it is a result of the balance between the rates of assembly and disassembly of cilia [143]. Thus it can be hypothesised that since IFT88 is known to affect the rate of assembly of the cilium, therefore, its loss can result in a stunted axoneme. While it is easy to understand how trafficking by IFT particles control the length of the cilium, it is difficult to imagine how SDCCAG3- a centrosomal protein localized at the base of the cilium would control its length. Other modes of ciliary length regulation that have been described previously include regulation by actin modulation, axoneme modifications or intracellular signalling [179]. Therefore, mechanism of regulation of ciliary length remains to be determined in the future. It should be noted that current data does not suggest a failure in maintaining the length of the mature cilium upon loss of SDCCAG3; instead, it suggests stunted growth of the axoneme.

#### **7.4.3 SDCCAG3 regulates trafficking of ciliary cargo**

This study also demonstrated a role of SDCCAG3 in the trafficking of transmembrane receptors like polycystin-2 to cilia (figure 7.9). Defects in the polycystin-2 trafficking could be rescued upon restoring the expression levels of SDCCAG3 (figure 7.10). In contrast, it had no effect on the trafficking of Rab8 during very early stages of ciliogenesis (figure 7.11). IFT88 has been implicated in the transport of polycystin-2 to cilia before. Given the localization of SDCCAG3 at the base of the cilia, it can be hypothesised that it might be involved in either fusion of Golgi-derived vesicle laden with polycystin-2 or docking of these vesicles or both. Interestingly, a recent proteomic data has identified SDCCAG3 in the interactome of proteins involved in vesicle docking and fusion at the ciliary base [175]. On the basis of this data, a more general role of SDCCAG3 can be proposed in regulating trafficking into the primary cilium. Moreover, a defect in the transport of polycystin-2 to cilia has been associated with the pathogenesis of polycystic kidney disease.

Therefore, in-depth analysis of the mechanism by which SDCCAG3 regulated ciliary trafficking of polycystin-2 can open new avenues into ciliopathy research.

## **7.5 SDCCAG3 at the crossroads**

### **7.5.1 Cell cycle and ciliogenesis**

Centrosomes play a crucial role in both cell cycle and ciliogenesis which are tightly connected. Several pieces of evidence have been presented to support the notion of bidirectional crosstalk between cell cycle and ciliogenesis. Cells that undergo improper or defective cell divisions often result in abnormal cilia formation. Similarly, cells with improper ciliogenesis show defects in cell division [131, 133]. For instance, some overproliferative cancer cell lines fail to form proper cilia and undergo unchecked cell division [133]. IFT88 has also been described to restrain cell cycle progression and promote ciliogenesis. It was shown that loss of IFT88 promoted cell cycle progression and overexpression of IFT88 suppressed G1/S phase transition along with inducing apoptotic cell death [180]. Since SDCCAG3 has been implicated in both cell division [123] and ciliogenesis (current study) therefore it can be speculated that SDCCAG3 might have a role in this bidirectional signalling.

### **7.5.2 Endocytic trafficking and ciliogenesis**

Association of SDCCAG3 with an active form of Arf6 i.e. GTP-Arf6 [125] can also account for multiple functions mediated by SDCCAG3 like endocytic trafficking of surface receptors and cytokinesis. Arf6 is an endocytic recycling protein that has been implicated in surface trafficking of various receptors and regulating the transport of endocytic cargo during cytokinesis at the midbody and intercellular bridge [24]. Interestingly, a cilium localizing protein called Arl13b was implicated in endocytic recycling and surface expression of CD1a receptor. It was shown to co-localize with the recycling compartment residents such as Arf6 and Rab22a [181]. Mutations in Arl13b have been associated with disrupted sonic hedgehog signalling possibly due to improper cilia functioning [182]. On the basis of such pieces of evidence, it can be argued that SDCCAG3 might be a link mediating endocytic trafficking and ciliogenesis through Arf6.

### **7.5.3 Ciliogenesis and Apoptosis**

Signalling pathways involved in ciliogenesis and cell cycle regulation such as hedgehog (Hh) signalling was shown to negatively regulate the surface levels of Fas receptors and inhibit apoptosis [183]. It has been implicated in promoting cell proliferation by inducing G1-S phase transition. Many components of Hh signalling pathways localize to cilia to regulate cellular functions [184]. The view that inhibition of apoptosis can be mediated by ciliary and cell cycle regulatory proteins, is in line with the fact that cell death, proliferation and ciliogenesis are can influence each other dynamically. Future research on the functions of SDCCAG3 can be helpful in understanding the complex nature of the interplay between these pathways.

## **8 Summary and future perspectives**

The current study demonstrated two novel functions of SDCCAG3 in the regulation of Fas receptor trafficking and ciliogenesis. The advent of proteomic approaches enabled identification of new interacting partners and cellular functions of SDCCAG3 in the recent past. Taken together, most of these studies suggested a role of SDCCAG3 in the regulation of intracellular trafficking. It could be speculated that SDCCAG3 might be acting at the intersection of multiple cellular pathways such as cytokinesis, ciliogenesis, and apoptosis by regulating vesicular trafficking involved in these pathways. Although, current study and other studies have identified associations of SDCCAG3 with different endocytic machineries but the exact function of SDCCAG3 in trafficking remains elusive.

### **8.1 Overview of the role of SDCCAG3 in FasR trafficking and apoptosis**

In summary, the negative regulation of Fas mediated apoptosis by PTPN13 had been described in several studies previously but the exact mechanism of how PTPN13 controlled the surface presentation of Fas receptors was not known. Therefore, it was hypothesised that interaction with SDCCAG3 might provide the missing link between PTPN13 and regulation of surface trafficking of Fas receptors. Data provided in this study demonstrated that expression levels of SDCCAG3 indeed affected the surface presentation of Fas receptors. Surface levels of FasR increased in both HeLa and HCT116 cells upon depletion of SDCCAG3. In this case, the effect on the surface presentation of FasR was not due to any defects in their internalization but rather due to an altered rate of their proteolysis. Overexpression of Fas receptors in SDCCAG3 depleted cells resulted in an increase in their basal expression levels and a slight reduction in the rate of degradation. Given the fact that SDCCAG3 were found to localize on the early endosomes, it was further hypothesised that SDCCAG3 might be involved in the post-endocytic sorting of Fas receptors. This idea was examined by analysing the subcellular localization of internalized Fas receptors which revealed an accumulation in the early endosomes and a concomitant decrease in late endosome/lysosome localization upon depletion of SDCCAG3. This defect was observed under both stimulated and steady-state trafficking of FasR. As expected, endogenous staining against SDCCAG3 showed a

partial overlap with the internalized Fas receptors upon stimulation. Additionally, internalized FasR co-localized with SDCCAG3 possibly in the sorting endosomes. In-depth analysis revealed the mechanism behind the SDCCAG3 mediated regulation of Fas receptor trafficking. Depletion of SDCCAG3 led to a delay in sorting of internalized Fas receptors from the limiting membrane of the enlarged endosomes into the lumen. Therefore, it could be concluded that SDCCAG3 is involved in the endo-lysosomal sorting of Fas receptors. Furthermore, this study described the molecular mechanism behind sorting by SDCCAG3. Dysbindin, which was shown before to connect cytoplasmic adaptors of GPCRs to the ESCRT machinery via its interaction with HRS[59], was found to interact with SDCCAG3. In this study, both dysbindin and HRS were shown to act in the same pathway and coordinate with SDCCAG3 in mediating the intraluminal sorting of Fas receptors.

Effect on the surface presentation of FasR upon depletion of SDCCAG3 also translated into altered apoptotic signalling as demonstrated by increased active caspase 8 accumulation. It was also suggested to be cleaved during Fas mediated apoptotic signalling (Yu, Erdmann lab). This work demonstrated its cleavage by caspase 6 as shown earlier in a study. Thus, SDCCAG3 was shown to be a negative regulator of apoptosis. To conclude, this study established (a) a new role of SDCCAG3 in lysosomal sorting involving dysbindin and HRS mediated pathway (b) a new mode of regulation of Fas mediated apoptosis, and (c) suggested a possible mechanism that PTPN13 might employ to regulate FasR surface expression.

## **8.2 SDCCAG3 and PTPN13 in apoptosis: future perspectives**

This work lays the foundation for future research into understanding the details of the molecular mechanism of Fas trafficking and signalling by PTPN13. A complex formation between PTPN13 and SDCCAG3 at the early endosomes was suggested to be involved in the regulation of FasR trafficking in this study. In order to support this claim, more detailed analysis is required such as (a) analysing the significance of the interaction between SDCCAG3 and PTPN13 for FasR trafficking. A mutant expression construct of SDCCAG3 lacking PTPN13 binding site or containing point mutations that disrupt the binding should not have any effect on the surface levels of FasR if they act together as a complex to regulate trafficking. The binding region and the point mutation affecting the interaction between SDCCAG3 and PTPN13 have

been elucidated previously in a study [123]. (b) Surface levels of transmembrane receptors can also be a function of the secretory pathway. Therefore, analysis of this complex in TGN-to-PM trafficking of Fas receptor should also be examined. (c) PTPN13 was shown to be degraded by autophagy in p62 (an autophagosomes cargo protein) dependent manner in order to promote Fas mediated apoptosis [121]. Recently, WASH was implicated in inhibiting autophagy by suppressing Beclin-1 ubiquitination. It was also shown to co-localize with p62 in autophagosomes [185]. An interaction between SDCCAG3 and WASH has been identified in a proteomic screen as well [186]. Could SDCCAG3 be also involved in preventing the autophagic degradation of PTPN13 via WASH mediated inhibition of autophagy? This model could explain how SDCCAG3 might be involved in negative regulation of Fas mediated apoptosis along with PTPN13.

### **8.3 Overview of the role of SDCCAG3 in ciliogenesis**

This study was premised on the data collected previously in the Erdmann lab which showed that SDCCAG3 interacts directly with IFT88 via its first 100 N-terminal amino acids (Yu, unpublished data). Subsequently, it was found to localize at the basal body upon transfection of SDCCAG3 expression construct in the current study. This study also showed that depletion of SDCCAG3 led to reduced formation and length of cilia in IMCD3 which could be rescued upon transient expression of SDCCAG3 construct. It acted along the same pathway as IFT88 to regulate ciliogenesis. However, its localization to the centrosome was independent of IFT88. SDCCAG3 was also shown to regulate trafficking of a receptor, polycystin-2, that is also regulated by IFT88. Depletion of SDCCAG3 did not affect the trafficking of Rab8, an essential player in cilia formation and trafficking. Therefore, this study demonstrated SDCCAG3 in the control of ciliogenesis but the underlying mechanism remains unknown.

### **8.4 Concluding remarks**

SDCCAG3 can shed a new light into the regulation of Fas mediated apoptosis which is exploited by cancer cells to avoid cell death by natural defence system and chemotherapeutic drugs. Further research is required to examine if there is any correlation between the expression levels of SDCCAG3 and surface levels of Fas

receptors in various cancer cells, a phenomenon that has been reported for PTPN13. Data from this study can also be extended to further study the role of SDCCAG3 in regulating Fas mediated apoptosis upon stimulation with its physiological ligands and intracellular trafficking of other death receptors from the TNF receptor superfamily. Therefore, future research should be directed towards establishing the physiological relevance for control of SDCCAG3 in apoptosis which will also help in identifying a novel therapeutic target. For instance, the lower efficacy of the drug called Oxaliplatin, which is used for treatment of colon cancer, could be improved upon silencing PTPN13 [118]. Lowering the expression levels of PTPN13 led to increased cellular toxicity and reduced proliferation. PTPN13 is expressed at abnormally high levels in most forms of colon cancer and surgery or chemotherapy are the only available forms of treatments that are partly effective due to high resistance against apoptosis in these cancer cells. Also, a peptide targeting PTPN13 was used as a novel therapeutic tool against Fas resistant cancer cells to treat chronic myeloid leukemia in *in vivo* murine model [187]. Deeper understanding of the regulator pathways for Fas receptors such as the one described in this study lays the foundation for the development of novel therapeutics against cancer.

Growing number of ciliopathies identified recently indicates the importance of proper formation and functioning of cilia. SDCCAG3 has been implicated in trafficking of a polycystin-2 receptor that is involved in the pathogenesis of polycystic kidney disease. Therefore, further elucidation of its role in ciliary trafficking can open new avenues of research into the trafficking of polycystin-2 or other ciliary receptors involved in ciliopathies.

To conclude, SDCCAG3 is emerging as an important regulatory protein involved in disease related trafficking pathways, a notion supported by previous studies and corroborated in the current study.

## Appendix I

### *MS Excel VBA code for calculation of middle fluorescence intensity in ILVs*

```
Sub main()
    'For multiple data sets (x-y coordinates) of pixel vs intensity we identify last column / last
    row for normalization
    lastColumn = Sheet1.Cells(1, Columns.Count).End(xlToLeft).Column
    For colNum = 1 To lastColumn
        lastRow = Columns(colNum).SpecialCells(xlCellTypeConstants, 23).Cells.Count
        minVal = Application.WorksheetFunction.Min(Range(Cells(1, colNum),
        Cells(lastRow, colNum)))
        maxVal = Application.WorksheetFunction.Max(Range(Cells(1, colNum),
        Cells(lastRow, colNum)))
        For rowNum = 1 To lastRow
            'Normalized value for pixel or intensity is set
            Cells(rowNum, colNum) = (Cells(rowNum, colNum).Value - minVal) * 100 /
            (maxVal - minVal)
        Next rowNum
    Next colNum

    For colNum = 1 To lastColumn
        'For all odd columns i.e. pixel columns identify the 40 to 60 pixel range and color them
        If colNum Mod 2 <> 0 Then
            Set fortySixtyIntensitiesColl = New Collection
            lastRow = Columns(colNum).SpecialCells(xlCellTypeConstants, 23).Cells.Count
            For rowNum = 1 To lastRow
                If Cells(rowNum, colNum).Value >= 40 And Cells(rowNum, colNum).Value <=
                60 Then
                    fortySixtyIntensitiesColl.Add Cells(rowNum, colNum + 1).Value
                    Cells(rowNum, colNum).Interior.ColorIndex = 37
                    Cells(rowNum, colNum).Interior.ColorIndex = 37
                    Cells(rowNum, colNum + 1).Interior.ColorIndex = 37
                    Cells(rowNum, colNum + 1).Interior.ColorIndex = 37
                End If
            Next rowNum

            Dim fortySixtyIntensities() As Variant
            ReDim fortySixtyIntensities(fortySixtyIntensitiesColl.Count)
            Dim i As Integer
            For i = 1 To fortySixtyIntensitiesColl.Count
                fortySixtyIntensities(i - 1) = fortySixtyIntensitiesColl.Item(i)
            Next i

            'Calculate avg. intensity within 40 to 60 pixel range
```

```

Dim lCounter As Long
Dim dTotal As Double
Dim dAverage As Double

dTotal = 0
For lCounter = 0 To UBound(fortySixtyIntensities)
    dTotal = dTotal + fortySixtyIntensities(lCounter)
Next
dAverage = dTotal / UBound(fortySixtyIntensities)
Cells(lastRow + 1, colNum) = "Avg. Intensity"
Cells(lastRow + 1, colNum + 1).Interior.ColorIndex = 27
Cells(lastRow + 1, colNum + 1) = dAverage
Cells(lastRow + 1, colNum + 1).Interior.ColorIndex = 27
End If
Next colNum
Cells.Select
Cells.EntireColumn.AutoFit
End Sub

```

## Bibliography

1. Schlessinger, J., *Cell signaling by receptor tyrosine kinases*. Cell, 2000. **103**(2): p. 211-25.
2. Trott, J.F., et al., *Triennial Lactation Symposium: Prolactin: The multifaceted potentiator of mammary growth and function*. J Anim Sci, 2012. **90**(5): p. 1674-86.
3. Appenzeller-Herzog, C. and H.P. Hauri, *The ER-Golgi intermediate compartment (ERGIC): in search of its identity and function*. J Cell Sci, 2006. **119**(Pt 11): p. 2173-83.
4. Simon, S.M., *Golgi governance: the third way*. Cell, 2008. **133**(6): p. 951-3.
5. Bonifacino, J.S. and L.M. Traub, *Signals for sorting of transmembrane proteins to endosomes and lysosomes*. Annu Rev Biochem, 2003. **72**: p. 395-447.
6. De Matteis, M.A. and A. Luini, *Exiting the Golgi complex*. Nat Rev Mol Cell Biol, 2008. **9**(4): p. 273-84.
7. Sorkin, A. and M. von Zastrow, *Endocytosis and signalling: intertwining molecular networks*. Nat Rev Mol Cell Biol, 2009. **10**(9): p. 609-22.
8. Sorkin, A., *Cargo recognition during clathrin-mediated endocytosis: a team effort*. Curr Opin Cell Biol, 2004. **16**(4): p. 392-9.
9. McMahon, H.T. and E. Boucrot, *Molecular mechanism and physiological functions of clathrin-mediated endocytosis*. Nat Rev Mol Cell Biol, 2011. **12**(8): p. 517-33.
10. Haugh, J.M. and T. Meyer, *Active EGF receptors have limited access to PtdIns(4,5)P(2) in endosomes: implications for phospholipase C and PI 3-kinase signaling*. J Cell Sci, 2002. **115**(Pt 2): p. 303-10.
11. Sorkin, A. and M. Von Zastrow, *Signal transduction and endocytosis: close encounters of many kinds*. Nat Rev Mol Cell Biol, 2002. **3**(8): p. 600-14.
12. Nada, S., et al., *The novel lipid raft adaptor p18 controls endosome dynamics by anchoring the MEK-ERK pathway to late endosomes*. EMBO J, 2009. **28**(5): p. 477-89.
13. Jovic, M., et al., *The early endosome: a busy sorting station for proteins at the crossroads*. Histo Histopathol, 2010. **25**(1): p. 99-112.
14. Brandhorst, D., et al., *Homotypic fusion of early endosomes: SNAREs do not determine fusion specificity*. Proc Natl Acad Sci U S A, 2006. **103**(8): p. 2701-6.
15. McBride, H.M., et al., *Oligomeric complexes link Rab5 effectors with NSF and drive membrane fusion via interactions between EEA1 and syntaxin 13*. Cell, 1999. **98**(3): p. 377-86.
16. Simonsen, A., et al., *The Rab5 effector EEA1 interacts directly with syntaxin-6*. J Biol Chem, 1999. **274**(41): p. 28857-60.
17. Huotari, J. and A. Helenius, *Endosome maturation*. EMBO J, 2011. **30**(17): p. 3481-500.
18. Bonifacino, J.S. and R. Rojas, *Retrograde transport from endosomes to the trans-Golgi network*. Nat Rev Mol Cell Biol, 2006. **7**(8): p. 568-79.
19. Maxfield, F.R. and T.E. McGraw, *Endocytic recycling*. Nat Rev Mol Cell Biol, 2004. **5**(2): p. 121-32.
20. Mayle, K.M., A.M. Le, and D.T. Kamei, *The intracellular trafficking pathway of transferrin*. Biochim Biophys Acta, 2012. **1820**(3): p. 264-81.
21. Sonnichsen, B., et al., *Distinct membrane domains on endosomes in the recycling pathway visualized by multicolor imaging of Rab4, Rab5, and Rab11*. J Cell Biol, 2000. **149**(4): p. 901-14.
22. Deneka, M., et al., *Rabaptin-5alpha/rabaptin-4 serves as a linker between rab4 and gamma(1)-adaptin in membrane recycling from endosomes*. EMBO J, 2003. **22**(11): p. 2645-57.

23. Naslavsky, N., et al., *Rabenosyn-5 and EHD1 interact and sequentially regulate protein recycling to the plasma membrane*. Mol Biol Cell, 2004. **15**(5): p. 2410-22.
24. Schweitzer, J.K., A.E. Sedgwick, and C. D'Souza-Schorey, *ARF6-mediated endocytic recycling impacts cell movement, cell division and lipid homeostasis*. Semin Cell Dev Biol, 2011. **22**(1): p. 39-47.
25. Grant, B.D. and J.G. Donaldson, *Pathways and mechanisms of endocytic recycling*. Nat Rev Mol Cell Biol, 2009. **10**(9): p. 597-608.
26. Traer, C.J., et al., *SNX4 coordinates endosomal sorting of TfnR with dynein-mediated transport into the endocytic recycling compartment*. Nat Cell Biol, 2007. **9**(12): p. 1370-80.
27. Cullen, P.J., *Endosomal sorting and signalling: an emerging role for sorting nexins*. Nat Rev Mol Cell Biol, 2008. **9**(7): p. 574-82.
28. Cozier, G.E., et al., *The phox homology (PX) domain-dependent, 3-phosphoinositide-mediated association of sorting nexin-1 with an early sorting endosomal compartment is required for its ability to regulate epidermal growth factor receptor degradation*. J Biol Chem, 2002. **277**(50): p. 48730-6.
29. Seaman, M.N., *The retromer complex - endosomal protein recycling and beyond*. J Cell Sci, 2012. **125**(Pt 20): p. 4693-702.
30. Harbour, M.E., S.Y. Breusegem, and M.N. Seaman, *Recruitment of the endosomal WASH complex is mediated by the extended 'tail' of Fam21 binding to the retromer protein Vps35*. Biochem J, 2012. **442**(1): p. 209-20.
31. Jia, D., et al., *Multiple repeat elements within the FAM21 tail link the WASH actin regulatory complex to the retromer*. Mol Biol Cell, 2012. **23**(12): p. 2352-61.
32. Derivery, E., et al., *The Arp2/3 activator WASH controls the fission of endosomes through a large multiprotein complex*. Dev Cell, 2009. **17**(5): p. 712-23.
33. Tomas, A., et al., *WASH and Tsg101/ALIX-dependent diversion of stress-internalized EGFR from the canonical endocytic pathway*. Nat Commun, 2015. **6**: p. 7324.
34. Piotrowski, J.T., et al., *WASH knockout T cells demonstrate defective receptor trafficking, proliferation, and effector function*. Mol Cell Biol, 2013. **33**(5): p. 958-73.
35. McGough, I.J., et al., *Identification of molecular heterogeneity in SNX27-retromer-mediated endosome-to-plasma-membrane recycling*. J Cell Sci, 2014. **127**(Pt 22): p. 4940-53.
36. Zech, T., et al., *The Arp2/3 activator WASH regulates alpha5beta1-integrin-mediated invasive migration*. J Cell Sci, 2011. **124**(Pt 22): p. 3753-9.
37. Haglund, K. and I. Dikic, *The role of ubiquitylation in receptor endocytosis and endosomal sorting*. J Cell Sci, 2012. **125**(Pt 2): p. 265-75.
38. Schmidt, O. and D. Teis, *The ESCRT machinery*. Curr Biol, 2012. **22**(4): p. R116-20.
39. Madshus, I.H. and E. Stang, *Internalization and intracellular sorting of the EGF receptor: a model for understanding the mechanisms of receptor trafficking*. J Cell Sci, 2009. **122**(Pt 19): p. 3433-9.
40. Yamashita, Y., et al., *Ubiquitin-independent binding of Hrs mediates endosomal sorting of the interleukin-2 receptor beta-chain*. J Cell Sci, 2008. **121**(Pt 10): p. 1727-38.
41. Raiborg, C. and H. Stenmark, *The ESCRT machinery in endosomal sorting of ubiquitylated membrane proteins*. Nature, 2009. **458**(7237): p. 445-52.
42. Hanson, P.I. and A. Cashikar, *Multivesicular body morphogenesis*. Annu Rev Cell Dev Biol, 2012. **28**: p. 337-62.
43. Marshansky, V. and M. Futai, *The V-type H<sup>+</sup>-ATPase in vesicular trafficking: targeting, regulation and function*. Curr Opin Cell Biol, 2008. **20**(4): p. 415-26.

44. Maxfield, F.R. and D.J. Yamashiro, *Endosome acidification and the pathways of receptor-mediated endocytosis*. Adv Exp Med Biol, 1987. **225**: p. 189-98.
45. Aniento, F., et al., *Cytoplasmic dynein-dependent vesicular transport from early to late endosomes*. J Cell Biol, 1993. **123**(6 Pt 1): p. 1373-87.
46. Li, C., et al., *Role of the Retromer Complex in Neurodegenerative Diseases*. Front Aging Neurosci, 2016. **8**: p. 42.
47. Wen, L., et al., *VPS35 haploinsufficiency increases Alzheimer's disease neuropathology*. J Cell Biol, 2011. **195**(5): p. 765-79.
48. Bhalla, A., et al., *The location and trafficking routes of the neuronal retromer and its role in amyloid precursor protein transport*. Neurobiol Dis, 2012. **47**(1): p. 126-34.
49. Small, S.A. and K. Duff, *Linking Abeta and tau in late-onset Alzheimer's disease: a dual pathway hypothesis*. Neuron, 2008. **60**(4): p. 534-42.
50. Vilarino-Guell, C., et al., *VPS35 mutations in Parkinson disease*. Am J Hum Genet, 2011. **89**(1): p. 162-7.
51. McGough, I.J., et al., *Retromer binding to FAM21 and the WASH complex is perturbed by the Parkinson disease-linked VPS35(D620N) mutation*. Curr Biol, 2014. **24**(14): p. 1670-6.
52. Wang, C., et al., *VPS35 regulates cell surface recycling and signaling of dopamine receptor D1*. Neurobiol Aging, 2016. **46**: p. 22-31.
53. Spillantini, M.G., et al., *Alpha-synuclein in Lewy bodies*. Nature, 1997. **388**(6645): p. 839-40.
54. Wei, A.H. and W. Li, *Hermansky-Pudlak syndrome: pigmentary and non-pigmentary defects and their pathogenesis*. Pigment Cell Melanoma Res, 2013. **26**(2): p. 176-92.
55. Raposo, G. and M.S. Marks, *Melanosomes--dark organelles enlighten endosomal membrane transport*. Nat Rev Mol Cell Biol, 2007. **8**(10): p. 786-97.
56. Huizing, M., et al., *Disorders of lysosome-related organelle biogenesis: clinical and molecular genetics*. Annu Rev Genomics Hum Genet, 2008. **9**: p. 359-86.
57. Dell'Angelica, E.C., *AP-3-dependent trafficking and disease: the first decade*. Curr Opin Cell Biol, 2009. **21**(4): p. 552-9.
58. Marley, A. and M. von Zastrow, *Dysbindin promotes the post-endocytic sorting of G protein-coupled receptors to lysosomes*. PLoS One, 2010. **5**(2): p. e9325.
59. Rosciglione, S., et al., *Galphas regulates the post-endocytic sorting of G protein-coupled receptors*. Nat Commun, 2014. **5**: p. 4556.
60. Strasser, A., P.J. Jost, and S. Nagata, *The many roles of FAS receptor signaling in the immune system*. Immunity, 2009. **30**(2): p. 180-92.
61. Krammer, P.H., *CD95's deadly mission in the immune system*. Nature, 2000. **407**(6805): p. 789-95.
62. Nagata, S., *Apoptosis by death factor*. Cell, 1997. **88**(3): p. 355-65.
63. Peter, M.E. and P.H. Krammer, *The CD95(APO-1/Fas) DISC and beyond*. Cell Death Differ, 2003. **10**(1): p. 26-35.
64. Scaffidi, C., et al., *Two CD95 (APO-1/Fas) signaling pathways*. EMBO J, 1998. **17**(6): p. 1675-87.
65. Barnhart, B.C., E.C. Alappat, and M.E. Peter, *The CD95 type I/type II model*. Semin Immunol, 2003. **15**(3): p. 185-93.
66. Elmore, S., *Apoptosis: a review of programmed cell death*. Toxicol Pathol, 2007. **35**(4): p. 495-516.
67. Pan, G., et al., *Identification and functional characterization of DR6, a novel death domain-containing TNF receptor*. FEBS Lett, 1998. **431**(3): p. 351-6.
68. Sanséau D, L.P., *FAS (Fas cell surface death receptor)*, in *Atlas Genet Cytogenet Oncol Haematol. in press*.

69. Huang, B., et al., *NMR structure and mutagenesis of the Fas (APO-1/CD95) death domain*. Nature, 1996. **384**(6610): p. 638-41.
70. Chan, F.K., *The pre-ligand binding assembly domain: a potential target of inhibition of tumour necrosis factor receptor function*. Ann Rheum Dis, 2000. **59 Suppl 1**: p. i50-3.
71. Fu, Q., et al., *Structural Basis and Functional Role of Intramembrane Trimerization of the Fas/CD95 Death Receptor*. Mol Cell, 2016. **61**(4): p. 602-13.
72. Sato, T., et al., *FAP-1: a protein tyrosine phosphatase that associates with Fas*. Science, 1995. **268**(5209): p. 411-5.
73. Yanagisawa, J., et al., *The molecular interaction of Fas and FAP-1. A tripeptide blocker of human Fas interaction with FAP-1 promotes Fas-induced apoptosis*. J Biol Chem, 1997. **272**(13): p. 8539-45.
74. Shatnyeva, O.M., et al., *Modulation of the CD95-induced apoptosis: the role of CD95 N-glycosylation*. PLoS One, 2011. **6**(5): p. e19927.
75. Peter, M.E., et al., *Cell surface sialylation plays a role in modulating sensitivity towards APO-1-mediated apoptotic cell death*. Cell Death Differ, 1995. **2**(3): p. 163-71.
76. Dorrie, J., K. Sapala, and S.J. Zunino, *Interferon-gamma increases the expression of glycosylated CD95 in B-leukemic cells: an inducible model to study the role of glycosylation in CD95-signalling and trafficking*. Cytokine, 2002. **18**(2): p. 98-107.
77. Chakrabandhu, K., et al., *Palmitoylation is required for efficient Fas cell death signaling*. EMBO J, 2007. **26**(1): p. 209-20.
78. Feig, C., et al., *Palmitoylation of CD95 facilitates formation of SDS-stable receptor aggregates that initiate apoptosis signaling*. EMBO J, 2007. **26**(1): p. 221-31.
79. Rossin, A., et al., *Fas palmitoylation by the palmitoyl acyltransferase DHHC7 regulates Fas stability*. Cell Death Differ, 2015. **22**(4): p. 643-53.
80. Lautrette, C., et al., *Increase of Fas-induced apoptosis by inhibition of extracellular phosphorylation of Fas receptor in Jurkat cell line*. Apoptosis, 2006. **11**(7): p. 1195-204.
81. Kamitani, T., H.P. Nguyen, and E.T. Yeh, *Activation-induced aggregation and processing of the human Fas antigen. Detection with cytoplasmic domain-specific antibodies*. J Biol Chem, 1997. **272**(35): p. 22307-14.
82. Schutze, S. and W. Schneider-Brachert, *Impact of TNF-R1 and CD95 internalization on apoptotic and antiapoptotic signaling*. Results Probl Cell Differ, 2009. **49**: p. 63-85.
83. Schutze, S., V. Tchikov, and W. Schneider-Brachert, *Regulation of TNFR1 and CD95 signalling by receptor compartmentalization*. Nat Rev Mol Cell Biol, 2008. **9**(8): p. 655-62.
84. Koncz, G., et al., *Regulating Vav1 phosphorylation by the SHP-1 tyrosine phosphatase is a fine-tuning mechanism for the negative regulation of DISC formation and Fas-mediated cell death signaling*. Cell Death Differ, 2008. **15**(3): p. 494-503.
85. Siegel, R.M., et al., *SPOTS: signaling protein oligomeric transduction structures are early mediators of death receptor-induced apoptosis at the plasma membrane*. J Cell Biol, 2004. **167**(4): p. 735-44.
86. Lee, K.H., et al., *The role of receptor internalization in CD95 signaling*. EMBO J, 2006. **25**(5): p. 1009-23.
87. Legembre, P., et al., *Cutting edge: SDS-stable Fas microaggregates: an early event of Fas activation occurring with agonistic anti-Fas antibody but not with Fas ligand*. J Immunol, 2003. **171**(11): p. 5659-62.

88. Huang, D.C., J. Tschopp, and A. Strasser, *Bcl-2 does not inhibit cell death induced by the physiological Fas ligand: implications for the existence of type I and type II cells*. *Cell Death Differ*, 2000. **7**(8): p. 754-5.
89. Rodriguez, I., et al., *A bcl-2 transgene expressed in hepatocytes protects mice from fulminant liver destruction but not from rapid death induced by anti-Fas antibody injection*. *J Exp Med*, 1996. **183**(3): p. 1031-6.
90. Yin, X.M., et al., *Bid-deficient mice are resistant to Fas-induced hepatocellular apoptosis*. *Nature*, 1999. **400**(6747): p. 886-91.
91. Tchikov, V., et al., *Subcellular compartmentalization of TNF receptor-1 and CD95 signaling pathways*. *Eur J Cell Biol*, 2011. **90**(6-7): p. 467-75.
92. Chaigne-Delalande, B., et al., *CD95 engagement mediates actin-independent and -dependent apoptotic signals*. *Cell Death Differ*, 2009. **16**(12): p. 1654-64.
93. Li, J. and J. Yuan, *Caspases in apoptosis and beyond*. *Oncogene*, 2008. **27**(48): p. 6194-206.
94. Hirata, H., et al., *Caspases are activated in a branched protease cascade and control distinct downstream processes in Fas-induced apoptosis*. *J Exp Med*, 1998. **187**(4): p. 587-600.
95. Cohen, G.M., *Caspases: the executioners of apoptosis*. *Biochem J*, 1997. **326 ( Pt 1)**: p. 1-16.
96. Lavrik, I., et al., *The active caspase-8 heterotetramer is formed at the CD95 DISC*. *Cell Death Differ*, 2003. **10**(1): p. 144-5.
97. Lavrik, I.N., A. Golks, and P.H. Krammer, *Caspases: pharmacological manipulation of cell death*. *J Clin Invest*, 2005. **115**(10): p. 2665-72.
98. Liu, X., et al., *DFF, a heterodimeric protein that functions downstream of caspase-3 to trigger DNA fragmentation during apoptosis*. *Cell*, 1997. **89**(2): p. 175-84.
99. Lakhani, S.A., et al., *Caspases 3 and 7: key mediators of mitochondrial events of apoptosis*. *Science*, 2006. **311**(5762): p. 847-51.
100. Peter, M.E., et al., *The role of CD95 and CD95 ligand in cancer*. *Cell Death Differ*, 2015. **22**(4): p. 549-59.
101. Fulda, S., et al., *Sensitization for death receptor- or drug-induced apoptosis by re-expression of caspase-8 through demethylation or gene transfer*. *Oncogene*, 2001. **20**(41): p. 5865-77.
102. Tourneur, L., et al., *Loss of FADD protein expression results in a biased Fas-signaling pathway and correlates with the development of tumoral status in thyroid follicular cells*. *Oncogene*, 2003. **22**(18): p. 2795-804.
103. Irmeler, M., et al., *Inhibition of death receptor signals by cellular FLIP*. *Nature*, 1997. **388**(6638): p. 190-5.
104. Igney, F.H. and P.H. Krammer, *Death and anti-death: tumour resistance to apoptosis*. *Nat Rev Cancer*, 2002. **2**(4): p. 277-88.
105. Ivanov, V.N., et al., *FAP-1 association with Fas (Apo-1) inhibits Fas expression on the cell surface*. *Mol Cell Biol*, 2003. **23**(10): p. 3623-35.
106. Ivanov, V.N., Z. Ronai, and T.K. Hei, *Opposite roles of FAP-1 and dynamin in the regulation of Fas (CD95) translocation to the cell surface and susceptibility to Fas ligand-mediated apoptosis*. *J Biol Chem*, 2006. **281**(3): p. 1840-52.
107. Ungefroren, H., et al., *FAP-1 in pancreatic cancer cells: functional and mechanistic studies on its inhibitory role in CD95-mediated apoptosis*. *J Cell Sci*, 2001. **114**(Pt 15): p. 2735-46.
108. Winterhoff, B.J., et al., *Characterisation of FAP-1 expression and CD95 mediated apoptosis in the A818-6 pancreatic adenocarcinoma differentiation system*. *Differentiation*, 2012. **83**(3): p. 148-57.

109. Erdmann, K.S., *The protein tyrosine phosphatase PTP-Basophil/Basophil-like. Interacting proteins and molecular functions.* Eur J Biochem, 2003. **270**(24): p. 4789-98.
110. Abaan, O.D. and J.A. Toretsky, *PTPL1: a large phosphatase with a split personality.* Cancer Metastasis Rev, 2008. **27**(2): p. 205-14.
111. Ciccarelli, F.D., P. Bork, and E. Kerkhoff, *The KIND module: a putative signalling domain evolved from the C lobe of the protein kinase fold.* Trends Biochem Sci, 2003. **28**(7): p. 349-52.
112. Bompard, G., et al., *Membrane targeting of protein tyrosine phosphatase PTPL1 through its FERM domain via binding to phosphatidylinositol 4,5-biphosphate.* J Cell Sci, 2003. **116**(Pt 12): p. 2519-30.
113. Herrmann, L., T. Dittmar, and K.S. Erdmann, *The protein tyrosine phosphatase PTP-BL associates with the midbody and is involved in the regulation of cytokinesis.* Mol Biol Cell, 2003. **14**(1): p. 230-40.
114. Erdmann, K.S., et al., *The Adenomatous Polyposis Coli-protein (APC) interacts with the protein tyrosine phosphatase PTP-BL via an alternatively spliced PDZ domain.* Oncogene, 2000. **19**(34): p. 3894-901.
115. Gross, C., R. Heumann, and K.S. Erdmann, *The protein kinase C-related kinase PRK2 interacts with the protein tyrosine phosphatase PTP-BL via a novel PDZ domain binding motif.* FEBS Lett, 2001. **496**(2-3): p. 101-4.
116. Cuppen, E., et al., *No evidence for involvement of mouse protein-tyrosine phosphatase-BAS-like Fas-associated phosphatase-1 in Fas-mediated apoptosis.* J Biol Chem, 1997. **272**(48): p. 30215-20.
117. Schickel, R., et al., *miR-200c regulates induction of apoptosis through CD95 by targeting FAP-1.* Mol Cell, 2010. **38**(6): p. 908-15.
118. Xiao, Z.Y., et al., *Silencing Fas-associated phosphatase 1 expression enhances efficiency of chemotherapy for colon carcinoma with oxaliplatin.* World J Gastroenterol, 2010. **16**(1): p. 112-8.
119. Foehr, E.D., et al., *FAS associated phosphatase (FAP-1) blocks apoptosis of astrocytomas through dephosphorylation of FAS.* J Neurooncol, 2005. **74**(3): p. 241-8.
120. Joshi, S. and K.M. Ryan, *Autophagy chews Fap to promote apoptosis.* Nat Cell Biol, 2014. **16**(1): p. 23-5.
121. Gump, J.M., et al., *Autophagy variation within a cell population determines cell fate through selective degradation of Fap-1.* Nat Cell Biol, 2014. **16**(1): p. 47-54.
122. Scanlan, M.J., et al., *Characterization of human colon cancer antigens recognized by autologous antibodies.* Int J Cancer, 1998. **76**(5): p. 652-8.
123. Hagemann, N., et al., *The serologically defined colon cancer antigen-3 interacts with the protein tyrosine phosphatase PTPN13 and is involved in the regulation of cytokinesis.* Oncogene, 2013. **32**(39): p. 4602-13.
124. Neznanov, N., et al., *Serologically defined colon cancer antigen 3 is necessary for the presentation of TNF receptor 1 on cell surface.* DNA Cell Biol, 2005. **24**(12): p. 777-85.
125. Sakagami, H., Y. Hara, and M. Fukaya, *Interaction of serologically defined colon cancer antigen-3 with Arf6 and its predominant expression in the mouse testis.* Biochem Biophys Res Commun, 2016. **477**(4): p. 868-73.
126. Claing, A., et al., *beta-Arrestin-mediated ADP-ribosylation factor 6 activation and beta 2-adrenergic receptor endocytosis.* J Biol Chem, 2001. **276**(45): p. 42509-13.
127. D'Souza-Schorey, C., et al., *A regulatory role for ARF6 in receptor-mediated endocytosis.* Science, 1995. **267**(5201): p. 1175-8.

128. Sung, C.H. and M.R. Leroux, *The roles of evolutionarily conserved functional modules in cilia-related trafficking*. Nat Cell Biol, 2013. **15**(12): p. 1387-97.
129. Hsiao, Y.C., K. Tuz, and R.J. Ferland, *Trafficking in and to the primary cilium*. Cilia, 2012. **1**(1): p. 4.
130. Badano, J.L., et al., *The ciliopathies: an emerging class of human genetic disorders*. Annu Rev Genomics Hum Genet, 2006. **7**: p. 125-48.
131. Singla, V. and J.F. Reiter, *The primary cilium as the cell's antenna: signaling at a sensory organelle*. Science, 2006. **313**(5787): p. 629-33.
132. Satir, P. and S.T. Christensen, *Overview of structure and function of mammalian cilia*. Annu Rev Physiol, 2007. **69**: p. 377-400.
133. Ke, Y.N. and W.X. Yang, *Primary cilium: an elaborate structure that blocks cell division?* Gene, 2014. **547**(2): p. 175-85.
134. Craige, B., et al., *CEP290 tethers flagellar transition zone microtubules to the membrane and regulates flagellar protein content*. J Cell Biol, 2010. **190**(5): p. 927-40.
135. Gilula, N.B. and P. Satir, *The ciliary necklace. A ciliary membrane specialization*. J Cell Biol, 1972. **53**(2): p. 494-509.
136. Pazour, G.J. and R.A. Bloodgood, *Targeting proteins to the ciliary membrane*. Curr Top Dev Biol, 2008. **85**: p. 115-49.
137. Follit, J.A., et al., *The cytoplasmic tail of fibrocystin contains a ciliary targeting sequence*. J Cell Biol, 2010. **188**(1): p. 21-8.
138. Barr, F.A., *Rab GTPase function in Golgi trafficking*. Semin Cell Dev Biol, 2009. **20**(7): p. 780-3.
139. Nachury, M.V., et al., *A core complex of BBS proteins cooperates with the GTPase Rab8 to promote ciliary membrane biogenesis*. Cell, 2007. **129**(6): p. 1201-13.
140. Westlake, C.J., et al., *Primary cilia membrane assembly is initiated by Rab11 and transport protein particle II (TRAPP II) complex-dependent trafficking of Rabin8 to the centrosome*. Proc Natl Acad Sci U S A, 2011. **108**(7): p. 2759-64.
141. Kang, R.S. and H. Folsch, *An old dog learns new tricks: novel functions of the exocyst complex in polarized epithelia in animals*. F1000 Biol Rep, 2009. **1**: p. 83.
142. Zuo, X., W. Guo, and J.H. Lipschutz, *The exocyst protein Sec10 is necessary for primary ciliogenesis and cystogenesis in vitro*. Mol Biol Cell, 2009. **20**(10): p. 2522-9.
143. Ishikawa, H. and W.F. Marshall, *Ciliogenesis: building the cell's antenna*. Nat Rev Mol Cell Biol, 2011. **12**(4): p. 222-34.
144. Sukumaran, S. and B.D. Perkins, *Early defects in photoreceptor outer segment morphogenesis in zebrafish *ift57*, *ift88* and *ift172* Intraflagellar Transport mutants*. Vision Res, 2009. **49**(4): p. 479-89.
145. Pazour, G.J., et al., *Chlamydomonas IFT88 and its mouse homologue, polycystic kidney disease gene *tg737*, are required for assembly of cilia and flagella*. J Cell Biol, 2000. **151**(3): p. 709-18.
146. Haycraft, C.J., et al., *Intraflagellar transport is essential for endochondral bone formation*. Development, 2007. **134**(2): p. 307-16.
147. Follit, J.A., et al., *The intraflagellar transport protein IFT20 is associated with the Golgi complex and is required for cilia assembly*. Mol Biol Cell, 2006. **17**(9): p. 3781-92.
148. Madhivanan, K. and R.C. Aguilar, *Ciliopathies: the trafficking connection*. Traffic, 2014. **15**(10): p. 1031-56.
149. Nauli, S.M., et al., *Polycystins 1 and 2 mediate mechanosensation in the primary cilium of kidney cells*. Nat Genet, 2003. **33**(2): p. 129-37.

150. Hichri, H., et al., *From Lowe syndrome to Dent disease: correlations between mutations of the OCRL1 gene and clinical and biochemical phenotypes*. Hum Mutat, 2011. **32**(4): p. 379-88.
151. Coon, B.G., et al., *The Lowe syndrome protein OCRL1 is involved in primary cilia assembly*. Hum Mol Genet, 2012. **21**(8): p. 1835-47.
152. Hagemann, N., et al., *Crystal structure of the Rab binding domain of OCRL1 in complex with Rab8 and functional implications of the OCRL1/Rab8 module for Lowe syndrome*. Small GTPases, 2012. **3**(2): p. 107-10.
153. Madhivanan, K., D. Mukherjee, and R.C. Aguilar, *Lowe syndrome: Between primary cilia assembly and Rac1-mediated membrane remodeling*. Commun Integr Biol, 2012. **5**(6): p. 641-4.
154. Hsiao, Y.C., et al., *Ahi1, whose human ortholog is mutated in Joubert syndrome, is required for Rab8a localization, ciliogenesis and vesicle trafficking*. Hum Mol Genet, 2009. **18**(20): p. 3926-41.
155. Chih, B., et al., *A ciliopathy complex at the transition zone protects the cilia as a privileged membrane domain*. Nat Cell Biol, 2012. **14**(1): p. 61-72.
156. Huttlin, E.L., et al., *The BioPlex Network: A Systematic Exploration of the Human Interactome*. Cell, 2015. **162**(2): p. 425-40.
157. Mead, C.L., et al., *Cytosolic protein interactions of the schizophrenia susceptibility gene dysbindin*. J Neurochem, 2010. **113**(6): p. 1491-503.
158. Hirota, Y., et al., *A role for Rab5 activity in the biogenesis of endosomal and lysosomal compartments*. Biochem Biophys Res Commun, 2007. **364**(1): p. 40-7.
159. Wegner, C.S., et al., *Ultrastructural characterization of giant endosomes induced by GTPase-deficient Rab5*. Histochem Cell Biol, 2010. **133**(1): p. 41-55.
160. Cho, J.H., et al., *Identification of the novel substrates for caspase-6 in apoptosis using proteomic approaches*. BMB Rep, 2013. **46**(12): p. 588-93.
161. Steinberg, F., et al., *A global analysis of SNX27-retromer assembly and cargo specificity reveals a function in glucose and metal ion transport*. Nat Cell Biol, 2013. **15**(5): p. 461-71.
162. Morel, E., et al., *Phosphatidylinositol-3-phosphate regulates sorting and processing of amyloid precursor protein through the endosomal system*. Nat Commun, 2013. **4**: p. 2250.
163. Schroeder, B., et al., *CIN85 phosphorylation is essential for EGFR ubiquitination and sorting into multivesicular bodies*. Mol Biol Cell, 2012. **23**(18): p. 3602-11.
164. Tan, X., et al., *LAPTM4B is a PtdIns(4,5)P2 effector that regulates EGFR signaling, lysosomal sorting, and degradation*. EMBO J, 2015. **34**(4): p. 475-90.
165. Sun, Y., et al., *Endosomal type Igamma PIP 5-kinase controls EGF receptor lysosomal sorting*. Dev Cell, 2013. **25**(2): p. 144-55.
166. Gullapalli, A., et al., *An essential role for SNX1 in lysosomal sorting of protease-activated receptor-1: evidence for retromer-, Hrs-, and Tsg101-independent functions of sorting nexins*. Mol Biol Cell, 2006. **17**(3): p. 1228-38.
167. Prosser, D.C., et al., *A novel, retromer-independent role for sorting nexins 1 and 2 in RhoG-dependent membrane remodeling*. Traffic, 2010. **11**(10): p. 1347-62.
168. Formstecher, E., et al., *Protein interaction mapping: a Drosophila case study*. Genome Res, 2005. **15**(3): p. 376-84.
169. Razi, M. and C.E. Futter, *Distinct roles for Tsg101 and Hrs in multivesicular body formation and inward vesiculation*. Mol Biol Cell, 2006. **17**(8): p. 3469-83.
170. Hahne, M., et al., *Characterization of the non-functional Fas ligand of gld mice*. Int Immunol, 1995. **7**(9): p. 1381-6.

171. LA, O.R., et al., *Membrane-bound Fas ligand only is essential for Fas-induced apoptosis*. Nature, 2009. **461**(7264): p. 659-63.
172. Ozoren, N., et al., *The caspase 9 inhibitor Z-LEHD-FMK protects human liver cells while permitting death of cancer cells exposed to tumor necrosis factor-related apoptosis-inducing ligand*. Cancer Res, 2000. **60**(22): p. 6259-65.
173. LeBlanc, A., et al., *Caspase-6 role in apoptosis of human neurons, amyloidogenesis, and Alzheimer's disease*. J Biol Chem, 1999. **274**(33): p. 23426-36.
174. Larimore, J., et al., *The schizophrenia susceptibility factor dysbindin and its associated complex sort cargoes from cell bodies to the synapse*. Mol Biol Cell, 2011. **22**(24): p. 4854-67.
175. Gupta, G.D., et al., *A Dynamic Protein Interaction Landscape of the Human Centrosome-Cilium Interface*. Cell, 2015. **163**(6): p. 1484-99.
176. Finetti, F., et al., *Intraflagellar transport is required for polarized recycling of the TCR/CD3 complex to the immune synapse*. Nat Cell Biol, 2009. **11**(11): p. 1332-9.
177. Knodler, A., et al., *Coordination of Rab8 and Rab11 in primary ciliogenesis*. Proc Natl Acad Sci U S A, 2010. **107**(14): p. 6346-51.
178. Wiens, C.J., et al., *Bardet-Biedl syndrome-associated small GTPase ARL6 (BBS3) functions at or near the ciliary gate and modulates Wnt signaling*. J Biol Chem, 2010. **285**(21): p. 16218-30.
179. Keeling, J., L. Tsiokas, and D. Maskey, *Cellular Mechanisms of Ciliary Length Control*. Cells, 2016. **5**(1).
180. Robert, A., et al., *The intraflagellar transport component IFT88/polaris is a centrosomal protein regulating G1-S transition in non-ciliated cells*. J Cell Sci, 2007. **120**(Pt 4): p. 628-37.
181. Barral, D.C., et al., *Arl13b regulates endocytic recycling traffic*. Proc Natl Acad Sci U S A, 2012. **109**(52): p. 21354-9.
182. Larkins, C.E., et al., *Arl13b regulates ciliogenesis and the dynamic localization of Shh signaling proteins*. Mol Biol Cell, 2011. **22**(23): p. 4694-703.
183. Kenney, A.M. and D.H. Rowitch, *Sonic hedgehog promotes G(1) cyclin expression and sustained cell cycle progression in mammalian neuronal precursors*. Mol Cell Biol, 2000. **20**(23): p. 9055-67.
184. Fan, H. and P.A. Khavari, *Sonic hedgehog opposes epithelial cell cycle arrest*. J Cell Biol, 1999. **147**(1): p. 71-6.
185. Xia, P., et al., *WASH inhibits autophagy through suppression of Beclin 1 ubiquitination*. EMBO J, 2013. **32**(20): p. 2685-96.
186. Hein, M.Y., et al., *A human interactome in three quantitative dimensions organized by stoichiometries and abundances*. Cell, 2015. **163**(3): p. 712-23.
187. Huang, W., et al., *The role of Fas-associated phosphatase 1 in leukemia stem cell persistence during tyrosine kinase inhibitor treatment of chronic myeloid leukemia*. Leukemia, 2016. **30**(7): p. 1502-9.